An Investigation of Gas Lasers

Agnivesh Sharma Jugessur

Submitted in partial fulfillment of the requirements for the degree of
Master of Science,
in the School of Pure and Applied Physics,
University of Natal.

Durban
Republic of South Africa
June 1999

Preface

The experimental work described in this thesis was carried out in the Laser Group, School of Pure and Applied Physics, University of Natal under the supervision of Professor Max. M. Michaelis.

These studies represent original work by the author and have not otherwise been submitted in any form to another University. Where use has been made of the work of others, it has been duly acknowledged in the text.

13·09·99

ACKNOWLEDGEMENTS

The author would sincerely like to thank the following people for their great and generous co-operation in contributing to the success of this thesis:

Prof. Max Michaelis, my supervisor, for his enthusiasm, commitment, invaluable guidance, encouragement and for instilling in me the inspiration and passion for research in this field. His sense of humour, optimism and generosity helped me immensely during the difficult times,

Prof. M.A. Hellberg for his efficient administration and interest,

Mr Williem de Beer and all the members of the Physics Workshop for all their efforts with regard to the construction of several lasers and other constructional works undertaken during the course of this study,

Mr Aldo Conti for his great technical support and guidance in the experimental work,

Mr Robert Piasecki and the staff of the electronic workshop for their invaluable support and prompt solutions to problems,

Mr Derek Dixon for making the finance readily available for developing the photographs,

Mr. U. Panday for his co-operation in lending some of the Lab. equipment,

The members of the **Laser Group**, **South-African Atomic Energy Corporation,Pretoria** for their co-operation and for making my visit enjoyable and successful,

The **Durban Laser Group** Members for their support, encouragement and interesting discussions,

The staff of the **School of Pure and Applied Physics**, **University of Natal** for being kind and hospitable during the years of my study,

The **Space Physics Group** for their generosity in allowing me to use their computer software and hardware,

The **University of Natal** for the Graduate Award and the **FRD** for financial support.

Finally, I would like to thank my **parents** and **friends** for their love, support and belief in me.

Abstract

Pulsed lasers have a wide range of applications in industry, medicine and for scientific research. Many of these devices are expensive and have delicate optics. The nitrogen laser is robust and inexpensive to build and maintain. A short review of the experimental nitrogen lasers is given. A major part of this thesis covers work on increasing the energy output (from 30 μJ to 0.3 mJ). The one design of nitrogen laser consists of a pc board etched on the sides and at the centre for the laser discharge. The separated sections are rectangular in shape. However, in the new design the discharge section of the nitrogen laser has a parabolic shape and an inclined laser channel was used instead of a horizontal one to observe the effect on the energy output. Parameters such as the distance between the top and bottom plates, the area of the bottom plate, the area of the parabola and the flow velocity of nitrogen were varied. Both nitrogen gas and cold nitrogen vapour were used as the lasing medium. The substitution of vapour for gas increased the energy 2 fold. Liquid nitrogen was tried unsuccessfully as the medium in the discharge channel. Two large lasers were built giving increased laser energy. A multilayer nitrogen laser was also built increasing the output by a factor of 2.5. The multilayer idea was also tried on the large lasers. The multilayer laser behaves like a small capacitor bank, discharging in parallel into the laser channel. The low pressure electrodes which were used on the large parabolic laser consisted of a pair of flat copper electrodes enclosed in a plexiglass housing and the latter being connected to a vacuum pump. The effect of using the low pressure electrodes on the laser energy output was investigated. Three nitrogen lasers made of aluminium foil were also constructed where transparencies and mylar were used as the dielectric insulator. In addition, a multilayer parabolic N_2 laser was made using the same materials. A water wave simulation experiment of the parabolic laser was done which showed that due to the parabolic form, circular waves are converted into planes wave. The spark gap which acts as a fast nanosecond switch must be precisely located at the focus of the parabola. Otherwise the laser does not lase.

Michelson Interferometry was carried out to measure the coherence length of the laser which was found to be longer than that mentioned in the literature. The improved parabolic nitrogen laser was used to obtain fringes in a Mach Zehnder experiment. The laser is now being used by the Durban laser group as a diagnostic tool to measure the refractive index of the gas lens created in a Colliding Shock wire experiment.

Carbon dioxide lasers have numerous industrial applications. The Laser group at the Atomic Energy Corporation (AEC), Pretoria are looking into possible industrial applications such as carbon isotope separation, paint-stripping and de-rusting. The author spent some time at the centre to investigate how the beam quality and energy output of the laser can be improved since a near gaussian profile is very important for many applications. The carbon dioxide laser system basically consists of an oscillator and two amplifiers in series. Measurements of the beam parameters (waist size, pulse shape, divergence angle) along different sections of the laser chain were taken. The laser beam was double passed through one of the amplifiers to observe the effect on

the energy output. Burn patterns at several places were taken to observe the beam profile. An investigation into the optical energy losses along the laser chain was made. A device called the Three Element Detector invented by the Laser Group, AEC, was also used to analyse the laser beams.

TABLE OF CONTENTS

"If I have seen further than others, it is by standing upon the shoulders of giants.
On how he made discoveries
By always thinking unto them. I keep the subject constantly before me and wait till the first dawnings open little by little into the full light."

Newton, Isaac, (1642-1727)

CHAPTER ONE

1.0 LIGHT AND LASERS

1.1 Introduction

In almost every civilisation, light is considered to be the essence of life. Most living creatures depend on it to survive. Light has also many philosophical implications since for many it is the symbol of hope, happiness and prosperity. Light in its broader sense corresponds to the electromagnetic radiation in the range from approximately 10^{12} Hz to 10^{17} Hz and it can be viewed submicroscopically as a stream of photons where each photon has a specific energy given by $E = h\nu$, momentum given by $p = h/\lambda$ and a constant speed in vacuum given by $c = \nu\lambda$, where ν is the frequency and λ is the wavelength of light. Macroscopically, this stream of photon exhibits both wave and particle like behaviour. The most common mechanism for the emission of light is the excitation of an atom from its ground state to an excited state by the collision of the atom with either an atom, an electron or a photon. The excited state lasts for a period of the order of 10^{-9} s and on relaxation to the ground state, a photon is released. The energy of the photon is equal to the quantized energy change of the atom from the excited state to a lower level.

Mother nature has been generous enough not only to give us this source of energy for use in different ways but also to be able to use it in the form of laser light which nowadays has a wide range of technological and medical applications. Lasers generate or amplify coherent radiation at frequencies in the infrared, visible and the ultraviolet (and now there exist soft x-ray lasers) as a result of which the basic laser principle is now used in an enormous variety of devices operating in many parts of the electromagnetic spectrum. Practical laser devices in particular employ an extraordinary variety of materials, pumping methods and design approaches. The essential elements of most laser devices except some gas lasers where a mirror is not important are shown below in Figure (1.1) which consists of the following:

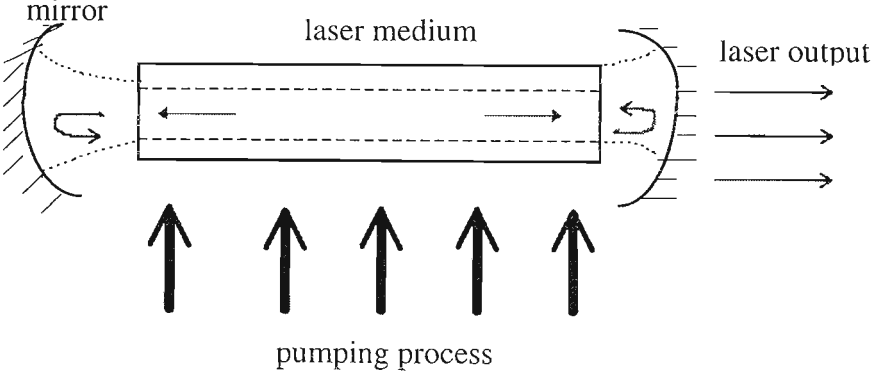

Figure (1.1): The essential elements of most laser devices.

(a) a laser medium consisting of an appropriate collection of atoms, molecules, ions or semiconducting crystal.

(b) a pumping process to excite these atoms into higher quantum energy levels.

(c) suitable optical feedback elements that allow a beam of radiation to either pass once through the laser medium or bounce back and forth repeatedly through the laser medium.

1.2 Historical review of lasers

Although the first laser was developed four decades ago, its roots go back long before physicists had developed the theoretical concepts behind the laser or its microwave emitting counterpart, the maser; an acronym for microwave amplification by stimulated emission of radiation. The thread of ideas leading to the laser can be traced back to a theory of light emission proposed by Albert Einstein before World War I. Einstein's ideas remained primarily of academic interest until the 1950's when Charles H.Townes conceived of and built the maser. The latter generated a wealth of ideas from physicists around the world. They were soon interested to extend the maser concepts to shorter wavelengths, particularly to infrared and visible light leading to the laser; acronym for light amplification by stimulated emission radiation. This triggered the rat race to build the first laser which was won by Theodore H. Maiman in May, 1960. He successfully applied the principles of the maser to achieve light amplification by stimulated emission of radiation. Shortly afterwards, Javan et al. (1961) demonstrated the first continuous wave(cw) laser, which used a He-Ne discharge. These inventions resulted in the search for the new laser transitions in various media: crystalline solids, gases, liquids, plastics and semiconductors.

1.3 Physical Principles

The principles underlying the laser operation are given in the framework of Quantum Mechanics.
Consider an atom having only two possible energy states: an upper state E_2 and a lower state E_1. If the atom is in the upper state and makes a transition to the lower state then energy can be emitted in the form of radiation of frequency given by the equation,

$$\nu = (E_2 - E_1)/h \qquad (1.3.1)$$

where h is the Planck constant.

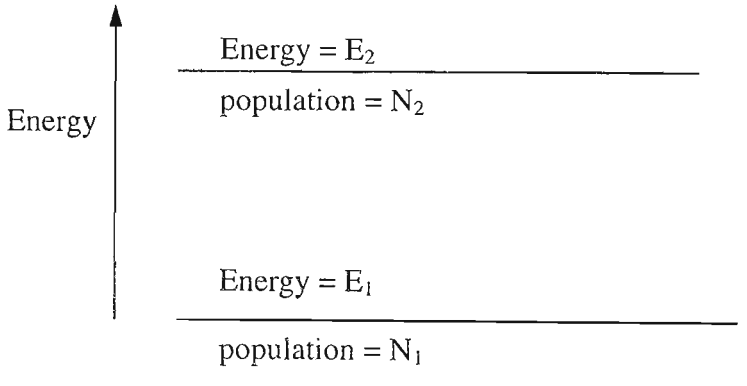

Figure (1.3.1): A two energy level system.

On the other hand, if the atom is initially in the lower energy state E_1 and makes a transition to the higher state E_2, radiation of frequency given by the above equation must be absorbed.

Emission can occur in two ways:

(a) the atom changing to the lower state at random, this is called **spontaneous emission**, contrasted with absorption (Figure 1.3.2).

(b) by a photon having an energy equal to the energy difference between the two levels interacting with the atom in the upper state and causing it to change to the lower state with the creation of a photon. It can be thought of, as the converse of absorption and is known as **stimulated emission** (Figure 1.3.3).

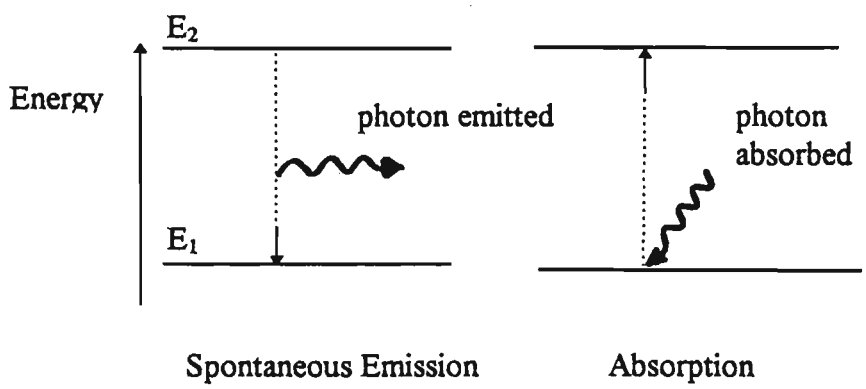

Figure (1.3.2): Spontaneous Emission and Absorption.

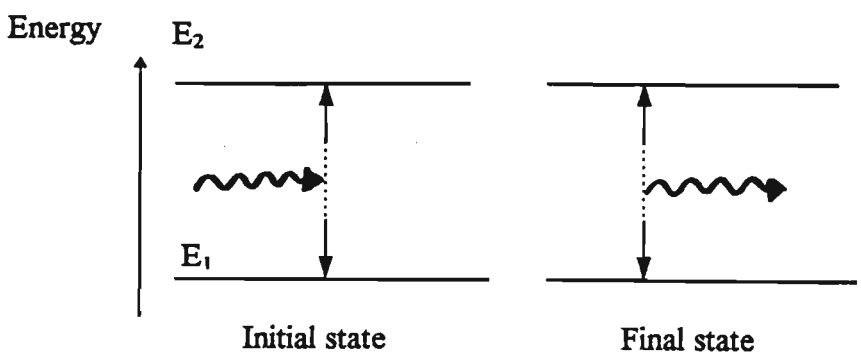

Figure (1.3.3): Stimulated Emission (Beesley, 1976).

There are two important points about stimulated emission upon which the properties of laser light depend. Firstly, the photon produced by stimulated emission and hence the light waves associated with them must be of nearly the same frequency. Secondly, the light waves associated with the two photons are in phase; they are said to be coherent. When several processes of spontaneous emission take place, the photons are incoherent, whereas they combine coherently (in phase) in stimulated emission. The concept of coherence may be simply illustrated by considering an electromagnetic wave in the medium (Figure 1.3.4). If the sinusoidal wave is produced in a spontaneous emission process lasting τ_{sp} seconds, the phase develops coherently in time for this period. Thereafter, the process terminates and another wave may be emitted with a random phase relationship to the first one. In this case, τ_{sp} denotes the coherence time and correspondingly the coherence length or distance traversed by the wave while phase coherence is preserved. It may be written as:

$$l_c = c\,\tau_{sp} \tag{1.3.2}$$

where l_c is the coherence length.

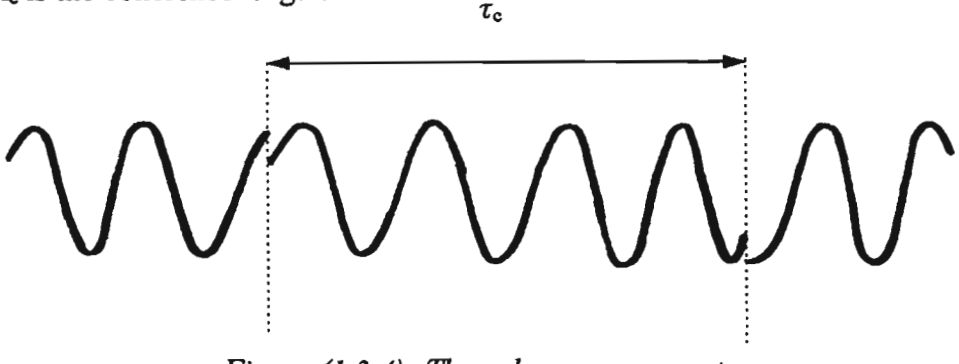

Figure (1.3.4): The coherence concept.

In a typical atomic transition which ranges from 10^6 to 10^9 Hz and therefore a coherence length of several metres is indicated by equation (1.3.2). In practice, however the coherence time may be considerably reduced by collisional processes (pressure broadening or lattice vibrations) which randomly interrupt the emission process at time interval τ_c much less than τ_{sp}. The above equation is then replaced by

$$l_c = c\,\tau_c \tag{1.3.3}$$

This yields coherence lengths of the order of a few centimetres or less for most sources of incoherent radiation such as lamps, discharges and plasmas. The existence of finite coherence time τ_c for a spectral line implies that the line cannot be infinitely sharp. When analysed, for example by means of a spectrometer, it will be found to have a finite spread in frequency, $\Delta\nu$, determined by the inverse of τ_c:

$$\Delta\nu = 1/2\pi\tau_c \tag{1.3.4}$$

The line may thus be described by a line profile $g(\nu)$, centred at ν_0, of width $\Delta\nu$.

Among other properties such as monochromaticity, directionality and brightness of laser beams, spatial or temporal coherence is one of them which is very important in many applications. The laser field at any point r and time t may be specified by a single quantity V(r,t), which may be taken to represent the magnitude of the electric and magnetic fields. The systematic relationship between the field quantities at two different spatial points r_1 and r_2, at times $t + \tau$ and t respectively may be represented by the mutual coherence function given by

$$\Gamma^{(1)}(r_1, r_2, \tau) = < V(r_1, t + \tau)\, V(r_2, \tau) > \tag{1.3.5}$$

and its normalised counterpart

$$\gamma^{(1)}(r_1, r_2, \tau) = \frac{\Gamma^{(1)}(r_1, r_2, \tau)}{[\Gamma^{(1)}(r_1, r_2, 0)\, \Gamma^{(1)}(r_2, r_2, 0)]^{1/2}} \tag{1.3..6}$$

The bracket < > represents the average energy over times long compared to the inverse of the oscillating bandwidth. The quantity $\gamma^{(1)}$ varies between the value 0, representing no correlation between the fields at points r_1 and r_2, and the value 1, representing perfect correlation. If we are interested in pure *spatial coherence* between two points, we may set the time interval $\tau = 0$ in equation (1.3.5); on the other hand, *temporal coherence* at a particular point may be represented by putting $r_1 = r_2$. The superscript 1 in equation (1.3.5) and (1.3.6) indicates that we are dealing with only first-order coherence.

Spatial and temporal coherence may be measured by means of suitable interferometers such as the Michelson interferometers. In the later chapters, an interferometry experiment was done to measure the coherence length of nitrogen lasers and also Mach-Zehnder interferometry was carried out with the same laser to observe the formation of fringe patterns. The skills acquired would then be used to observe density variations in gas-flow patterns of gas lenses formed during an experiment where wires generate colliding shock waves (see section 6.7). In those experiments, the spatial and temporal properties of the laser had to be considered and applied in order to find the interference fringes. In a Michelson experiment, a set of interference fringes is produced and the clarity or visibility of these provides a measure of the degree of temporal coherence at any point. If $\gamma^{(1)}(r_1, r_2, \tau)$ remains close to unity (clear fringes) at a certain point, while practically vanishing at another point (fringes practically invisible) and these two points are separated by distance l_c, then we have a coherence time again given by equation (1.3.3).

The coherence time can be related to the line width, in particular for a laser source to the oscillating bandwidth. Quantitatively, the product of τ_c and $\Delta\nu_{osc}$ must exceed a certain minimum value, independent of the form of the laser signal:

$$\tau_c \ \Delta\nu_{osc} > 1/4\pi \tag{1.3.7}$$

This result follows from the Fourier transform theory.

It is interesting to note that for a stabilised He-Ne laser with $\Delta\nu_{osc}$ in the range 50 - 500 Hz, values of l_c of the order of 100 km would be obtained. By contrast, the coherence length of a conventional lamp is at most a few cm whereas the coherence length of the parabolic nitrogen laser,as we should see later, is approximately 21 cm.

1.4 Population Inversion

For a two level energy system representing an atom in an upper and lower state, it is necessary to create a population inversion, i.e $N_2 > N_1$, thus building up the radiation field at frequency ν. The figures below illustrate the relative proportion in two energy levels before and after population inversion.

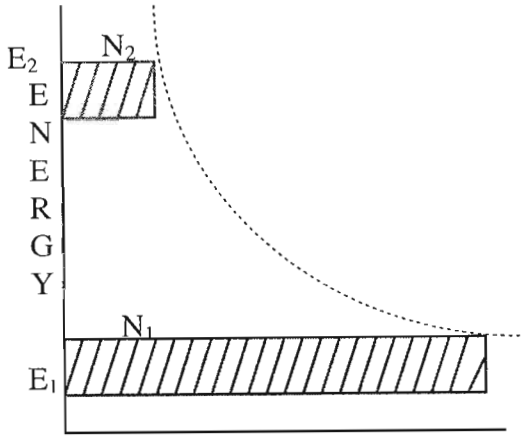

Figure (1.4.1a)

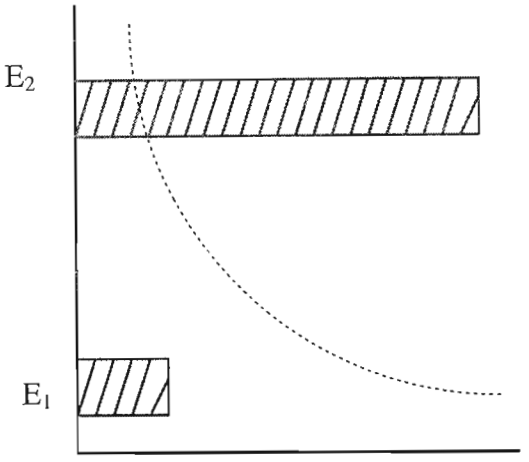

Figure (1.4.1b)

Figure (1.4.1a): Relative populations in two energy levels which satisfies the Boltzmann relation for thermal equilibrium.

Figure (1.4.1b): Inverted population difference required for optical amplification.

Consider again the two-level energy system (Figure1.3.1, p.2). Suppose that a photon of energy equal to the energy difference between the two levels approaches the two atoms , then absorption or stimulated emission processes are eqally probable under normal circumstances. In a system containing a very large number of atoms, the dominant process will depend on the relative number of atoms in the upper and lower states. A large population in the upper level will result in stimulated emission dominating while if there are more atoms in the lower level there will be more absorption than stimulated emission. The population of a number of energy levels obeys the Boltzmann distribution. For any two levels of energy E_1 and E_2 , the population ratio is

$$N_2/N_1 = \exp[-(E_2 - E_1)/kT] \qquad (1.4.1)$$

where k is the Boltzmann constant, T is the absolute temperature, $E_2 > E_1$. For stimulated emission to dominate it is necessary to increase the population of the upper energy level so that it is greater than that of the lower energy level; a

as population inversion. For stimulated emission to exceed absorption the temperature T in equation (1.4.1) would have to be negative. The Russian scientists Basov and Prokhorov considered the maser as a negative energy device due to this requirement of negative temperature necessary for population inversion. Population inversion can be achieved at ordinary temperatures but only under non-equilibrium conditions to which the Bolzmann Law does not apply. Population inversion is usually achieved by an external pump source. We take dye laser as an example, as dye laser pumping is one of the long term aims of this research. In dye lasers, population inversion can be achieved by using a nitrogen laser or a flash lamp as the pump source. The versatile dye laser is an indispensable tool in many areas of spectroscopy, where broad tunability is an essential requirement. Since the active medium is a liquid solution of organic dye, an almost infinite range of complex molecular structures cover any desired region of the spectrum (wavelength range roughly between 300 - 1500 nm).

Radiative processes whereby organic dyes are excited and de-excited are shown schematically in Figure (1.4.2). Excitation takes place from the ground state to a level within one of the systems of excited singlet states S_1, S_2. From S_1, radiative decay can take place directly to the ground state system G by fluorescence, with typical lifetime $\tau_{nr} \sim 1$ ns. Between the singlet systems, extremely rapid transitions take place non-radiatively by an electron tunelling process termed internal conversion, on a timescale $\tau_{nr} \sim 10^{-12}$ s. However, instead of a transition directly to the ground state, a non-radiative transition can also be induced by fields both inside and outside the molecule, from S_1 to the lowest excited triplet system T_1, on a timescale $\tau_{ir} \sim 10$ ns. From T_1, a radiative transition back to G takes place very slowly, by phosphorescence, with typical lifetime $\tau_{ph} \sim 1$ μs or longer. Being a transition between states of different spin, the phosphorescent emission is optically forbidden.

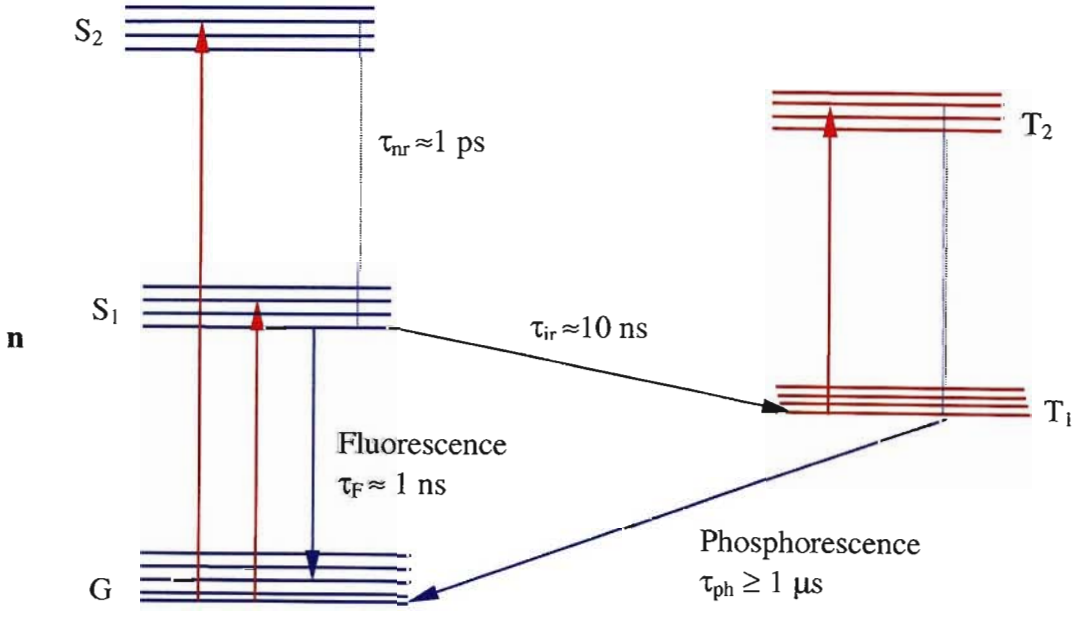

Figure (1.4.2): The radiative and nonradiative transitions in a dye molecule (Silfvast, 1996).

The phosphorescence process is too slow to be used for the purpose of laser action, requiring too high a dye concentration to be practically feasible. Hence, the fluorescent emission is always employed. Therefore, the existence of the triplet states constitutes an undesirable complication in a dye laser because of the high intersystem (singlet-triplet) crossing rate which reduces the fluorescence yield. Two processes are responsible for this: firstly, reduction of the first excited singlet state population and hence the amplification, and secondly enhancement of triplet-triplet absorption losses in the active medium. Circulation of the dye is thus essential.

Pumping of the dye can be done in two ways: transversely and longitudinally. In transverse pumping, a cylindrical lens may be used to focus the pump beam on the dye cuvette, at right angles to the direction of dye laser emission. In this configuration, very high gains are attainable. Longitudinal pumping has the advantage of spatial overlap between the pump and dye beams in the cuvette. Flashlamp-pumped (pulsed) and laser-pumped (continuous wave) dye lasers are in common use for different applications. The pumping source in a laser-pumped dye laser can be a nitrogen laser. The UV beam from the laser is focused on a thin line on the surface of a cell containing a dye solution. The dye lases and a beam emerges. The dye cell is made of quartz glass and it is 0.5 cm in diameter and 1 cm in length. Depending on the dyes used, mirror may be omitted and with a small 100 kW nitrogen laser, a solution of the common dye 7-diethylamino-4-methylcoumarin lases. This dye is used in fabric detergent as a whitening agent. The figure below shows a schematic diagram of the tunable dye laser.

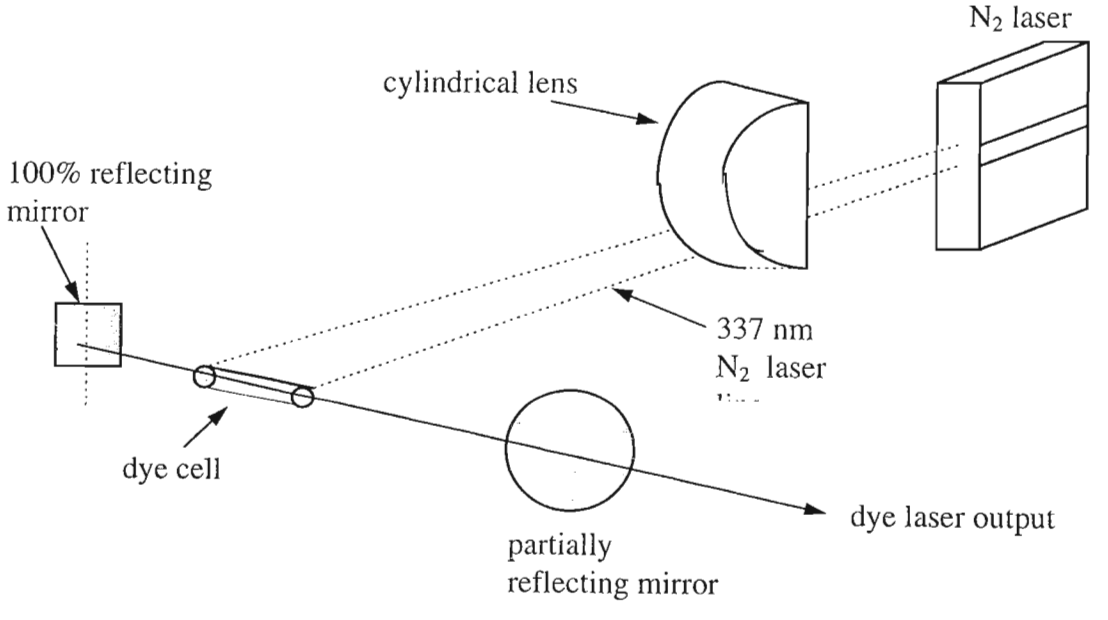

Figure (1.4.3): Schematic diagram of N_2 Laser-Pumped Dye Laser.

1.5 Laser Theory

The processes of spontaneous emission, absorption and stimulated emission are represented by the following equations:

$$\delta N_2/\delta t = -A_{21}N_2 \tag{1.5.1}$$

$$\delta N_2/\delta t = B_{12}\rho(\nu)N_1 \tag{1.5.2}$$

$$\delta N_2/\delta t = -B_{21}\rho(\nu)N_2 \tag{1.5.3}$$

where $\rho(\nu)$ is the radiation density of the interaction and A_{21},B_{12} and B_{21} are the Einstein coefficients.

If the system is in thermal equlibrium then the total energy of the system remains constant. Hence the number of photons absorbed equals the total number of photons emitted from the system by stimulated and spontaneous emission. It follows from equations (1.5.1),(1.5.2),(1.5.3) that

$$\delta N_2/\delta t = -A_{21}N_2 - B_{21}N_2\rho(\nu) + B_{12}N_1\rho(\nu) = 0 \tag{1.5.4}$$

Using the Boltzmann distribution,

$$N_2/N_1 = \exp(-h\nu/kT) \tag{1.5.5}$$

where k is the Boltzmann constant,

T is the absolute temperature of the system

it follows that

$$\rho(\nu) = A_{21}/(\exp(h\nu/kt)B_{12} - B_{21}) \tag{1.5.6}$$

$$= A_{21}/(\exp(h\nu/kt) - 1)B_{21} \qquad (B_{21} = B_{12})$$

The average energy of a black body radiation mode, ε, is obtained by dividing the total energy by the total number of oscillations and is given by

$$\varepsilon = h\nu/(\exp(h\nu/kT) - 1) \tag{1.5.7}$$

The number of modes per unit volume of cavity per unit fequency interval is $8\pi\nu^2/c^3$. Therefore, the energy density u_ν , i.e the energy per unit volume of cavity per unit frequency interval is given by

$$u_\nu = [8\pi\nu^2/c^3]h\nu/(\exp(h\nu/kT) - 1) \tag{1.5.8}$$

where c is the speed of light

A comparison of equation (1.5.6) and (1.5.8) shows that

$$B_{12} = B_{21} = B \tag{1.5.9}$$

and $$A_{21}/B = 8\pi h\nu^3/c^3. \tag{1.5.10}$$

If u_ν is plotted as a graph against frequency ν, then a curve similar to black body radiation is obtained and is as shown in Figure (1.5.1). A different curve is obtained for each temperature. Here, the radiation intensity represented by $I(\lambda, T)$ is plotted against the wavelength, λ.

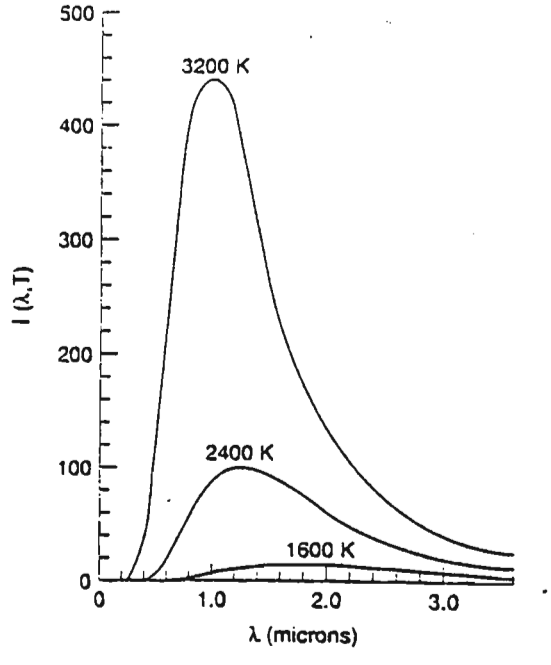

Figure (1.5.1): Black body radiation curve (Beesley, 1976).

Equation (1.5.9) shows that the probability of stimulation down is equal to the probability of absorption. Equation(1.5.10) has some important implications; the ratio R_e of the rate of spontaneous emission to the rate of stimulated emission under conditions of thermal equilibrium is given by

$$R_e = A_{21}/\rho(\nu)B \tag{1.5.11}$$

which on substituting equation (1.5.6) into equation (1.5.11) becomes

$$R_e = \exp(h\nu/kT) - 1 \tag{1.5.12}$$

The spontaneous emission dominates in the optical range and the stimulated emission dominates in the microwave range. The rate of spontaneous and stimulated emission becomes equal i.e $R_e = 1$ at $\lambda = 60$ μm in the far infra-red region of the spectrum.

1.6 The Threshold Condition

In order to achieve a good efficiency, laser materials must be chosen which require the minimum amount of energy to induce laser action. In practice this means finding out what population inversion must be achieved before all the losses in the system are overcome. A laser consists of an amplifying medium, usually a gas or a solid placed between two mirrors which form an optical resonator. The total loss is due to a number of different processes, the most important of which are:

(a) Transmission, absorption and scattering by mirrors.

(b) Absorption within the amplifying medium due to other energy levels.

(c) Scattering by optical inhomogeneities within the amplifying medium.

(d) Diffraction losses by the mirrors.

All these losses can be included in one parameter which can be expressed as the lifetime of a photon existing within the laser cavity. Such a lifetime is denoted by the symbol t_{photon}. The reciprocal of this will be the total rate of loss of photon from the laser per second as a result of the four processes outlined above. In Chapter 8, an investigation of optical energy losses was carried out on a carbon dioxide laser chain in order to find out ways by which these losses can be reduced to increase the laser energy output. In this case, most of the energy losses were from the transmission and diffractive losses at mirrors.

Consider a two-level energy system (Figure 1.3.1). Denoting the stimulated transition rate by

$$W' = \rho(\nu)B \tag{1.6.1}$$

From equation (1.5.10)

$$W'/A = \rho(\nu)c^3/8\pi h\nu^3 \tag{1.6.2}$$

The shape of the absorption curve denoted by $g(\nu)$ is also described an emission curve or frequency probability curve. $g(\nu)d\nu$ can be defined as the probability that a given transition between energy levels will result in an emission, or an absorption of a photon whose energy lies between $h\nu$ and $h(\nu + d\nu)$. The curve $g(\nu)$ is normalised so that the total area under it is always unity. Similar arguments apply to spontaneous emission, replace W' and A by $W'g(\nu)d\nu$ and $Ag(\nu)d\nu$ respectively. $W'g(\nu)d\nu$ is now the rate at which transitions take place resulting in photons of frequency lying between and ν and $\nu + d\nu$ due to radiation density $\rho(\nu)$. $Ag(\nu)d\nu$ is the rate of spontaneous emission into the frequency interval lying between ν and $\nu + d\nu$.

Equation (1.6.2) may be written as

$$W'g(\nu)d\nu = [\rho(\nu)c^3/8\pi h\nu^3\,]Ag(\nu)d\nu \tag{1.6.3}$$

The radiation density $\rho(\nu)$ is related to the radiation flux or intensity $I(\nu)$ by

$$I(\nu) = c\rho(\nu) \tag{1.6.4}$$

where c is the velocity of light in the laser medium

Using equation

$$A = 1/\tau_{spont.}$$

where τ_{spont} = spontaneous emission lifetime.

it then follows,

$$\int (W'g(\nu)d\nu) = \int [\rho(\nu)c^3/8\pi h\nu^3\,]Ag(\nu)d\nu$$

$$\Rightarrow \qquad W(\nu) = \{I(\nu)/c\}\{c^3/8\pi h\nu^3\}\{1/\tau_{spont.}\}\{g(\nu)\}$$

$$\Rightarrow \qquad W(\nu) = \{c^2/(8\pi h\nu^3\tau_{spont})\}\; g(\nu)I(\nu) \tag{1.6.5}$$

This is the total transition rate due to a monochromatic beam of radiation of frequency ν. Suppose a degeneracy g_1 is associated with the lower level E_1 and a degeneracy g_2 is associated with level E_2. The net rate of change of energy due to stimulated transitions (both up and down) is obtained by multiplying the transition rate by the net population inversion and the photon energy $h\nu$, i.e

$$h\nu(N_2 - N_1g_2/g_1)W(\nu) \tag{1.6.6}$$

Therefore the rate of increase in intensity may be expressed as

$$(dI/dt)_{GAIN} = h\nu(N_2 - N_1g_2/g_1)W(\nu)c \tag{1.6.7}$$

A gain or increase in intensity is assumed because a population inversion is also assumed i.e,

$$N_2 \geq N_1\, g_2/g_1 \tag{1.6.8}$$

The total loss rate is defined by means of the parameter t_{photon} discussed before, i.e

$$(dI/dt)_{LOSS} = I(\nu)/t_{photon} \tag{1.6.9}$$

The condition for lasing action to take place is

$$(dI/dt)_{GAIN} - (dI/dt)_{LOSS} \geq 0 \tag{1.6.10}$$

$$\Rightarrow \qquad h\nu(N_2 - N_1g_2/g_1)W(\nu)c - I(\nu)/t_{photon} \geq 0$$

$$\Rightarrow \qquad N_2 - N_1 g_2/g_1 \geq \{8\pi\nu^2 t_{spont.}\}/c^3 g(\nu) t_{photon}$$

For $\nu=\nu_0$

$$\Rightarrow \qquad N_2 - N_1 g_2/g_1 \geq \{8\pi\nu_0^2 t_{spont}\}/\{c^3 g(\nu) t_{photon}\} \qquad (1.6.11)$$

This is the threshold population inversion required for oscillation near the line $g(\nu_0)$.

The typical N_2 laser parameters such as the laser transition probability is 2.5×10^7/s, the upper laser lifetime is 40 ns, the inversion density is $2.5 \times 10^{17}/m^3$, the stimulated emission cross section is 4×10^{-17} m^2 and the small signal gain coefficient is 10/m. The threshold value which is a product of the stimulated emission cross section, the inversion density and the laser gain medium length is calculated to be 12 ± 5.

In the case of a dye laser, the laser transition probability is 2 to 5×10^8/s, the upper laser level lifetime is 2 to 5×10^{-9} s, the stimulated emission cross section is 1 to 4×10^{-20} m^2 and the small signal gain coefficient is 500/m.

The CO_2 laser has a laser transition probability of 0.25/s, an upper laser lifetime of 4 s, a stimulated emission cross section of 3×10^{-22} m^2 and a small signal gain coefficient of 0.9/m. The threshold value is calculated to be 1.6.

1.7 Resonators, Mirrors and Modes

The following theory may not all apply to Nitrogen lasers since like other lasers with high gain and without resonators, nitrogen lasers have poor beam quality, with output unpolarized, in multiple transverse and longitudinal modes. Virtually all nitrogen lasers can operate in supperradiant mode without cavity mirrors, but the output can be more than doubled with a simple cavity with 100 % reflective rear mirror and 4 % reflective front mirror. Such a cavity greatly reduces beam divergence. The theory given below is more relevant to lasers such as the Carbon dioxide laser. Chapter 8 gives the theory of its internal workings and some results on the investigation of its beam quality.

Gain in a laser is increased by placing the active medium between two mirrors which face each other. This arrangement of mirrors was familiar long before the advent of lasers and is known as the Fabry-Perot interferometer or Fabry-Perot etalon. Consider the laser gain medium inside the optical cavity of a dye laser (Figure 1.7.1). The active medium is the dye in its container surrounded by a helical flash lamp which is the pumping source. The mirrors are situated at the extreme sides. This dye laser is being used for lidar (light detection and ranging) experiments.

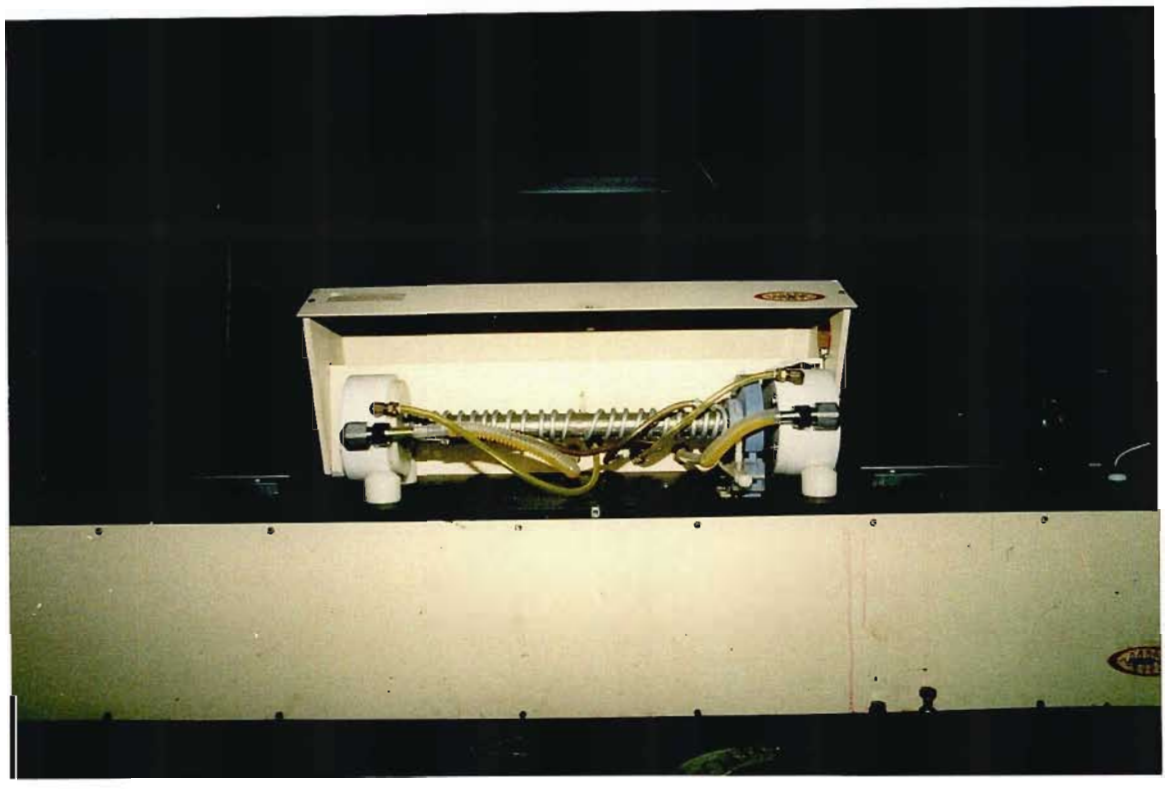

Figure (1.7.1): The optical cavity of a flash lamp dye laser.

When a population inversion exists within the active medium and a spontaneous emission produces a photon which travels along the axis of system, the photon interacts with an atom in an excited state to give stimulated emission and a wave which increases in amplitude passes through the active medium and out to one of the mirrors. The amplification or gain of the wave is further increased by reflection backward and forward within the laser cavity by means of the mirrors. A laser without any mirrors can act as an amplifier, with mirrors it becomes an oscillator.

The first c.w laser of Javan employed mirrors to actually seal off the ends of the tube containing the gas. This is not practised anymore as the discharge can cause damage to the mirrors. Instead the mirrors are mounted externally and the tube is sealed by attaching two optical flats at an angle to the optical axis. The angle is that which causes minimum reflection losses for light polarized normal to the plane of the flats and is known as the Brewster angle. The flats are referred to as Brewster windows. They are placed as shown, not parallel, to avoid beam displacements (Figure 1.7.2). The same technique is used in the CO_2 laser oscillator (see Chapter 8).

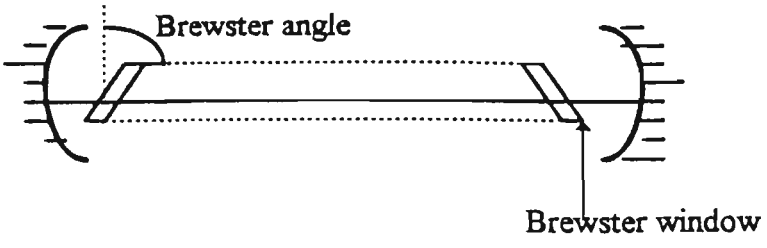

Figure (1.7.2): A laser cavity with Brewster windows.

In general, a photon travelling at right angles to the optical axis will not be amplified to form the laser beam although it may cause many stimulated emissions, there will not be a large enough number to overcome all losses, i.e the gain will be inadequate. However, when the wave is travelling only slightly off axis the wave may be able to 'zig-zag' between the mirrors a sufficient number of times to produce enough gain to overcome the losses (Beesley, 1976).The result of this is to produce an output which may consist of a variety of complicated patterns of light as shown below (Figure1.7.3). These patterns are the result of the laser operating in the TEM modes(transverse electromagnetic mode). These modes occur in a stable optical cavity such as in a CO_2 laser system.

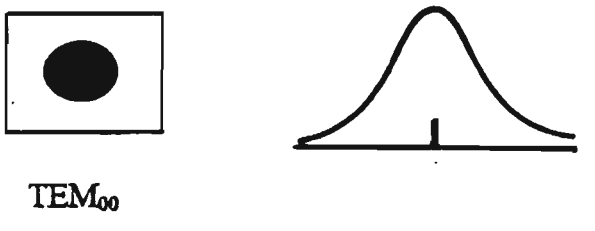

TEM_{00}

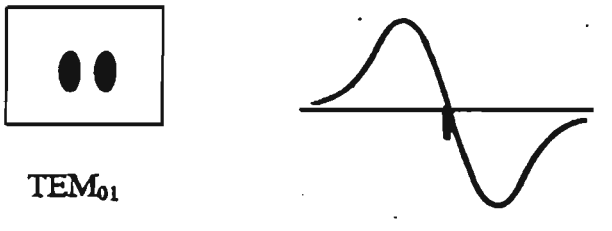

TEM_{01}

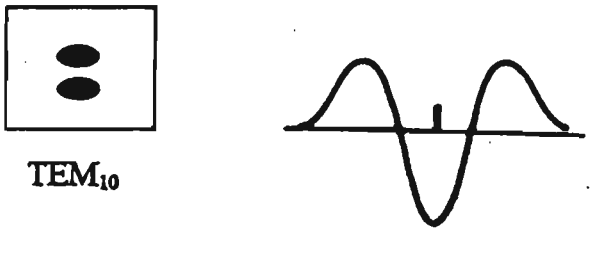

TEM_{10}

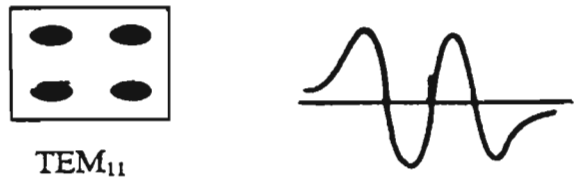

Figure (1.7.3): Transverse Electromagnetic Modes.

The most commonly used mode is the TEM_{00} or the uniphase mode. There are 3 factors to be considered to achieve oscillation in the TEM_{00} mode and the exclusion of higher order modes. They are cleanliness, laser tube diameter and the choice of mirrors having suitable radii of curvature. In the later chapter, a burn pattern from a carbon dioxide laser beam was obtained showing the TEM_{00} and TEM_{01} modes. Moreover, the dependence of gaussian modes on proper alignment and good quality optics was also investigated.

In order to keep as many modes as possible, the confocal resonator (Figure1.7.4) is used.

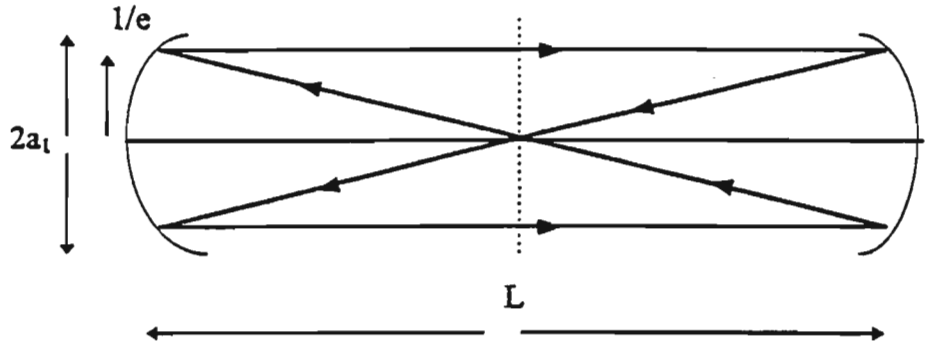

Figure (1.7.4): A confocal resonator.

If the radii (a_1) of the two mirrors are reduced until their foci coincide, or in case of mirrors having equal radii; their radii are both equal to the mirror separation, then the resonator is said to be confocal. At either mirror, the electric field amplitude drops to 1/e of its maximum value of a distance w_s from the central axis and this distance is termed the spot size at the mirror, usually of the order of a mm.

$$\text{Spot size, } w_s = (\lambda L/\pi)^{1/2} \qquad (1.7.1)$$

where L is the distance between the two mirrors.

Referring to the carbon dioxide laser beam (Chapter 8), the cavity length was about 1 m which gave a spot size of 1.8×10^{-3} m at either mirror.

The Fresnel number is an important parameter in the analysis of confocal resonator and is given by

$$N_f = (a_1)^2 / \lambda L \tag{1.7.2}$$

This number also provides information about the diffraction losses from the cavity. Using equation (1.7.1), (1.7.2) can be rewritten as

$$N_f = (1/\pi)\,(a_1)^2 / w_s^2 \tag{1.7.3}$$

The Fresnel number is therefore equal to the ratio of the mirror cross-section to the beam cross-section divided by π. In the mathematical analysis one usually requires the condition that this number should be large compared to unity, implying that diffractive energy losses should be small. The Fresnel number for the carbon dioxide laser system was calculated to be approximately 160, which implies that the laser system is an efficient one since diffractive losses are kept small. The Fresnel number for an excimer laser is approximately 130 and that of a copper vapour laser is about 100. The beam spot size at arbitrary positions z within the resonator is given by the formula:

$$w(z) = w_0[\, 1 + (2z/L)^2 \,]^{1/2} \tag{1.7.4}$$

where the beam waist at the centre is

$$w_0 = (\lambda L/2\pi)^{1/2} \tag{1.7.5}$$

From the above relation, the beam waist at the centre of the carbon dioxide laser cavity was approximately 1.3×10^{-3} m for a 1 m length cavity. This is therefore $\sqrt{2}$ times smaller than the spot size at either mirror, showing that the mirrors serve to focus the beam at the centre of the resonator. The formulae (1.7.1)-(1.7.5) are special cases of the general result applicable to a gaussian beam sustained within a cavity consisting of a pair of mirrors of arbitrary radii of curvature R_1 and R_2, separated by distance L. The beam waist at the axial position is:

$$w(z) = w_0[\, 1 + (\lambda z / \pi w_0^2)^2 \,]^{1/2} \tag{1.7.6}$$

while the surfaces of constant phase in the beam radii of curvature:

$$R = z[\, 1 + \{(\pi w_0^2)/(\lambda z)\}^2] \tag{1.7.7}$$

The distance over which the beam waist increases by a factor $\sqrt{2}$ is termed the Rayleigh range and is given by:

$$z_R = (\pi w_0^2)/\lambda \tag{1.7.8}$$

The Rayleigh range for the carbon dioxide laser beam was therefore approximately 0.5 m.

Since the electric field in the beam varies as w_0/w on axis, this is also the distance over which the beam energy on the axis is halved. For the confocal resonator, the Rayleigh range is exactly one half of the mirror separation as calculated and shown above. Hence, the carbon dioxide laser system described in Chapter 8 used a confocal resonator. As for nitrogen lasers, the gain is quite high (10/m) such that optical resonators become impractical.

CHAPTER TWO

2.0 THE NITROGEN GAS LASER

2.1 Introduction

This molecular gas laser utilises transitions between vibrational levels of different electronic states. It is termed a 'vibronic laser' from the combination of the words 'vibrational' and 'electronic'. Oscillation occurs primarily on the 337nm band of the second positive system ($C\ ^3\Pi_u \rightarrow B\ ^3\Pi_g$), which is a transition between the lowest pair of vibrational levels of two electronic states (Figure 2.1.1). The total spontaneous lifetime of the upper level is 44 ns and that of the lower level is 11μs. Consequently,cw laser operation is not possible. However, the system can operate very successfully as a self-terminating laser if excited by a sufficiently rapid current pulse (risetime of a few nanoseconds).

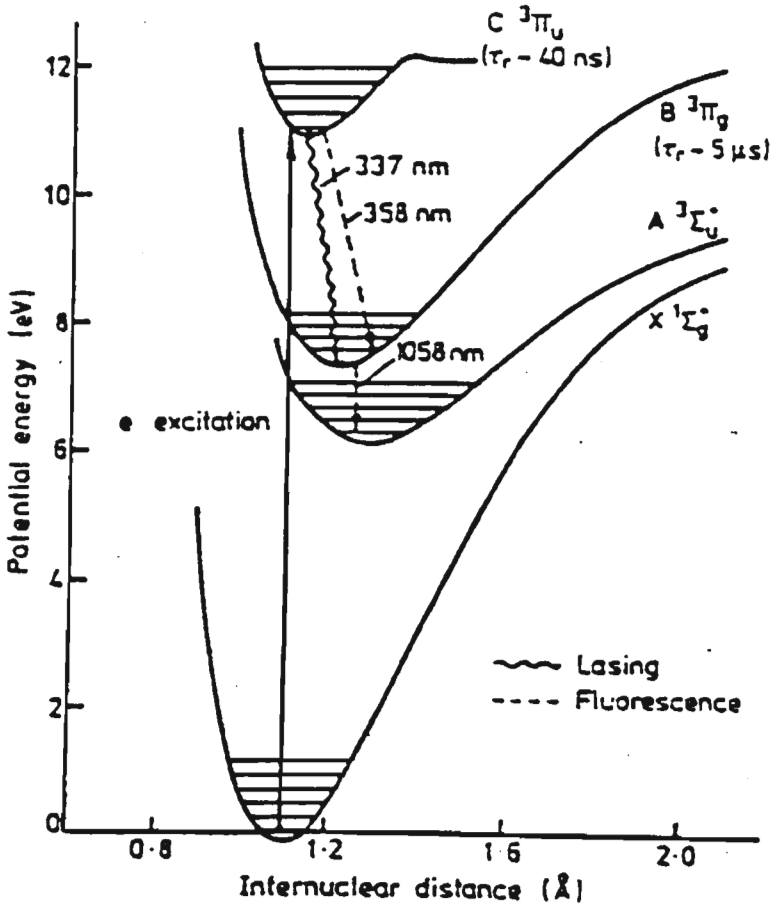

Figure (2.1.1): Energy levels of Nitrogen molecule (Bergmann, Thesis 1980).

[**Note**: The orbital angular momentum quantum number is given by the symbol Λ and the various electronic states are identified by the Greek letters as follows:

Λ : 0 1 2 3
electronic state: Σ Π Δ Φ

The orbital angular momentum quantum number for a diatomic molecule involves the sum of the projections of the orbital angular momentum of each atom onto the axis connecting the two atoms. For any specific value of Λ, the rotational quantum number J can take on values of Λ, $\Lambda + 1$, $\Lambda + 2$, ... The spin determines the multiplicity of the electronic state, and is given by $2S + 1$ as in the case of atoms; it describes the number of sublevels for a given J value. Thus, there are singlet states ($S = 0$) $^1\Sigma$, $^1\Pi$, $^1\Delta$, ..., doublet states ($S = 1/2$) $^2\Sigma$, $^2\Pi$, $^2\Delta$, ..., and so forth. As in the case of atoms, the multiplicity or number of degenerate sublevels is always odd if the total number of electrons is even, and vice versa. Historically, the lowest electronic "manifold" or ground state is usually labelled X followed by the notation just outlined for the specific angular designation for that configuration. Excited states that have been identified are labelled A, B, C,....., usually in the order of their identification. For example, a ground state designation might be $X^2\Sigma$, and an excited state might be labelled $A^2\Pi$ for molecular transitions, the subscript notation is either g (gerade), which refers to an even-parity state, or u (ungerade), which denotes an odd-parity state. Thus, the two levels listed previously might be expressed as $X^2\Sigma_u$ and $A^2\Pi_g$ states.].

The mechanism for the production of rapid current pulses is the very fast switching action of the Blumlein generator. A simple design for the laser system which can be readily assembled with inexpensive components is illustrated in Figure (2.1.2). The nitrogen gas pressure is in the range 4-13 kPa. So a high electric field of approximately 10 kV/cm is required for breakdown and this is achieved in the TE laser configuration. Two adjacent metal plates are separated from a third plate of equal total area by a thin sheet of plastic insulation, e.g epoxy fibre glass. The assembly behaves as an adjacent pair of connected capacitors, the space between them serving as the gap across which the pulse of current ($> 10^4$ A within a few nanoseconds) is discharged through the gas. A coil (10 turns) of Cu wire acts as the inductor connecting the upper plates. A potential difference of approximately 20 kilovolts is applied between the connected plates and the shared plate. Thereafter, one of the capacitors is rapidly discharged by means of a spark gap switch. A current pulse surges across the one upper plate and on encountering the gas in the laser tube, excites the N_2 molecules causing laser action within 5-10 ns. The coil connects the two H.T. plates during charging but isolates them for the few nanoseconds of the laser discharge. The inductance of the laser was calculated to be approximately 10 μH while that of the spark gap was approximately 30 nH.

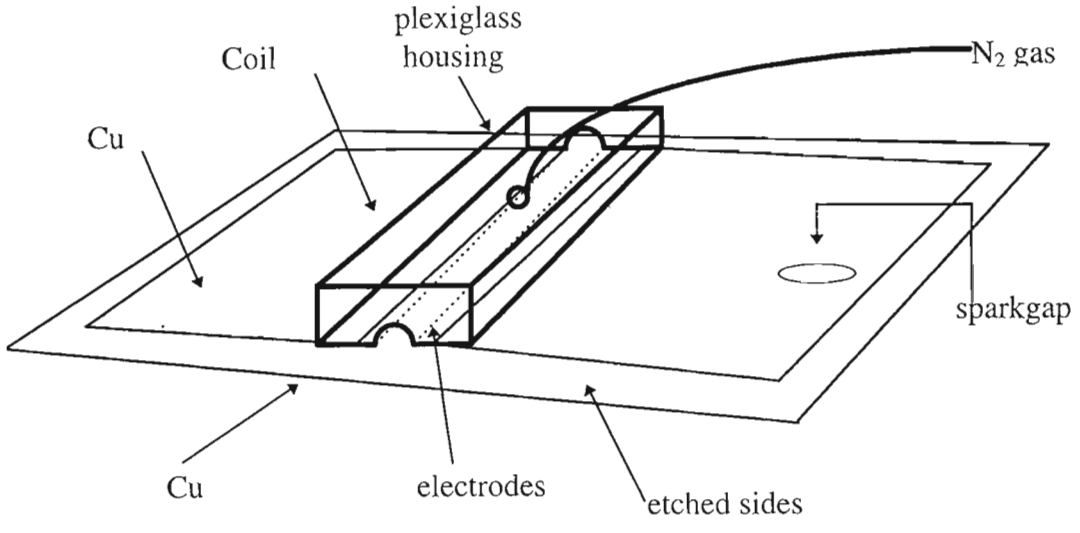

Figure (2.1.2): The N_2 laser.

Repetition rates of a few Hertz (5-10) can be achieved with peak pulse of powers of up to 100kW and pulse widths of about 10ns. The coherence length is of the order of 10 cm. With this type of laser, amplification by a mirror sytem is not required because of the extremely high gain. Very intense and quasi coherent beams are emitted at each end of the laser medium simply due to the very high gain amplification of their own internal spontaneous emission travelling along the length of the laser gain medium.

2.2 Review of some Experimental Nitrogen Lasers

Coherent U.V light generated at room temperature in a pulsed N_2 laser was first developed by Heard in 1963. The first transversely excited N_2 lasers were developed by Leonard in 1965. Since this discovery extensive experimental and theoretical work on this type of laser has been reported. In most cases, a flate plate, low inductance Blumlein circuit has been used to store the energy and then to energize the laser plasma through a spark gap. A simple theory that explains the excitation mechanism of the pulsed N_2 laser was devised by Gerry (1965). This is the mechanism whereby to achieve population inversion between the $C^3\,\Pi_g$ and $B^3\,\Pi_g$ levels of the second positive system of N_2 and hence a high proportion of stimulated emission the $C^3\,\Pi_g$ level must be populated in a time short compared to its natural radiative lifetime($\approx$ 40 ns). The excitation of the $C^3\,\Pi_g$ level occurs by direct electron collisions with ground state molecules (Gerry,1965). The $B^3\,\Pi_g$ level is essentially metastable and has a lifetime of 5-8 μs.

Bergmann *et al.*, (1975) deals with the adaptation of this principle for the excitation of molecular N_2 lasers at pressures ranging from 0 to 3 bar. Megawatt pulses of nanosecond duration may be obtained from a simple 25 cm atmospheric pressure device. The electrical excitation is effected by a flat-plate Blumlein circuit.

The nitrogen laser used by these authors was constructed from a copper-clad circuit board and a discharge channel consisting of two parallell strip razor blades. The circuit board formed the storage plates of the dc charged low impedance Blumlein impulse circuit shown in Figure (2.2.1). The circuit dimensions were chosen in such a way so as to provide a total capacitance of ~ 3.6 nF and a line-limited excitation pulse of ~ 2.5 ns; the period is matched to the lifetime of the $C^3 \Pi_g$ state at 1 bar. The blades serve as corona electrodes and were clamped at a height of 2mm above the circuit board
(Figure 2.2.2).

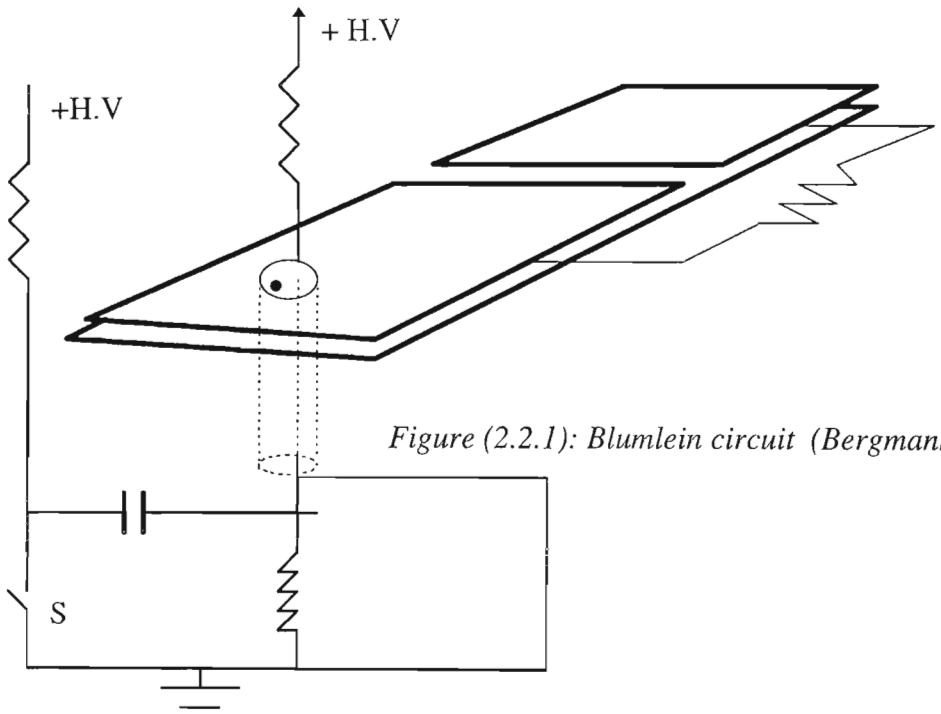

Figure (2.2.1): Blumlein circuit (Bergmann et al, 1975).

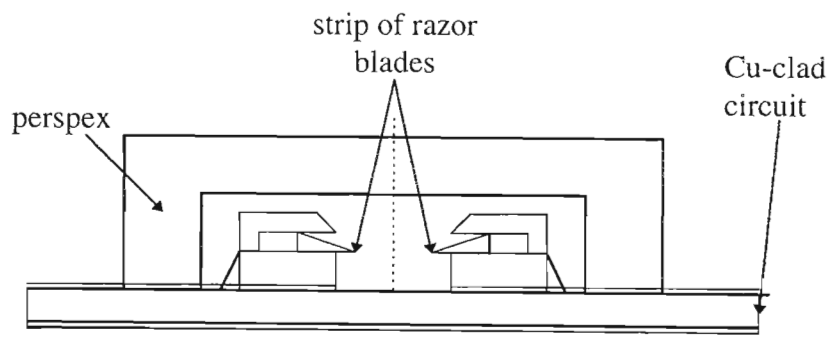

Figure (2.2.2): The Laser channel with corona electrodes.

Bergmann E.E, (1975) describes a method where the laser's pulse width is about 1ns and the best electrical efficiency is approximately 0.04% at 8.8 kV. At 21 kV, 335 μJ/pulse is obtained. Above 16.7 kV, the unfocussed output will pump a dye solution to superradiance at a distance of 1.5 m. For supply voltages less than 10 kV, a novel configuration for pre-ionization is shown (Figure 2.2.3).

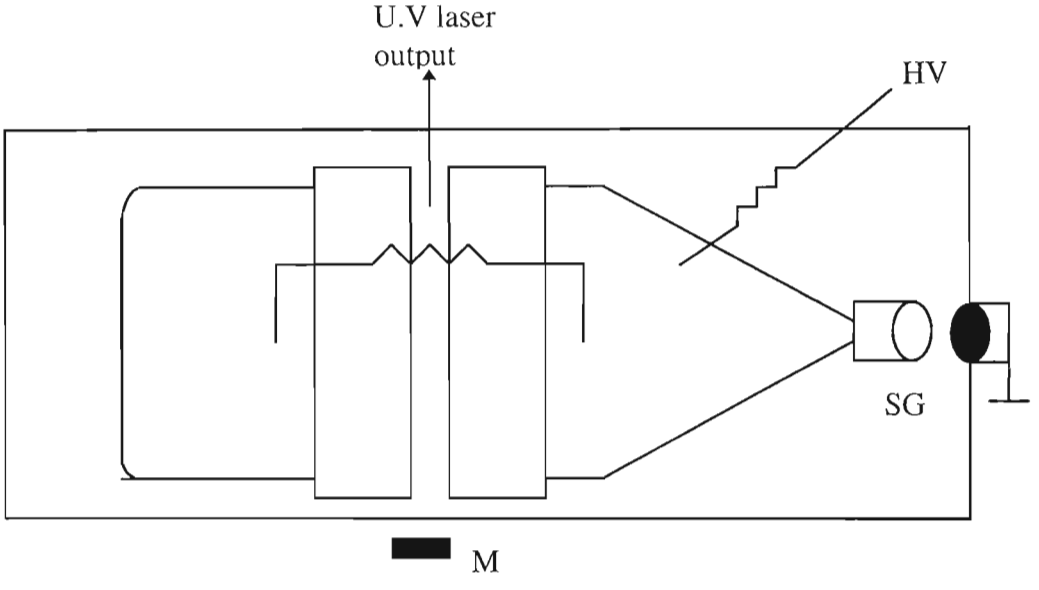

Figure (2.2.3): The laser system.

The laser is again excited by a Blumlein circuit. The dielectric insulation (with a low dielectric constant) between the upper and lower plates is 1mm thick. The total capacitance of the laser was measured to be 4.85 nF. A spark gap spacing was chosen for the operating voltage and the power supply was adjusted to produce the desired repetition rate, 5-25 pps. The output is directed towards a fluorescent screen and the mirror M is adjusted for best collimation. A 1-inch diameter disk calorimeter is interposed to monitor the average output power. The spacing and the angle between the two electrodes are varied until maximum output is achieved. Usually the angle is a critical adjustment compared to the adjustment of the spacing. The electrodes were closer at the mirror end than at the output end because this resulted in the electrical excitation occurring first at the mirror and progressing towards the output end of the laser channel. This laser could be used as a dye laser pump.

Bergmann E.E, (1977) describes a method to couple and synchronize two transversely excited atmospheric (TEA) N_2 laser in an oscillator-amplifier configuration to obtain spatially coherent 1 ns pulses at 337 nm with an energy/pulse of several 100 μJ. This technique is adaptable to other very high gain laser systems whose operation terminates so quickly as to render optical resonators impractical. Figure (2.2.4) below shows the optical and electrical arrangement.

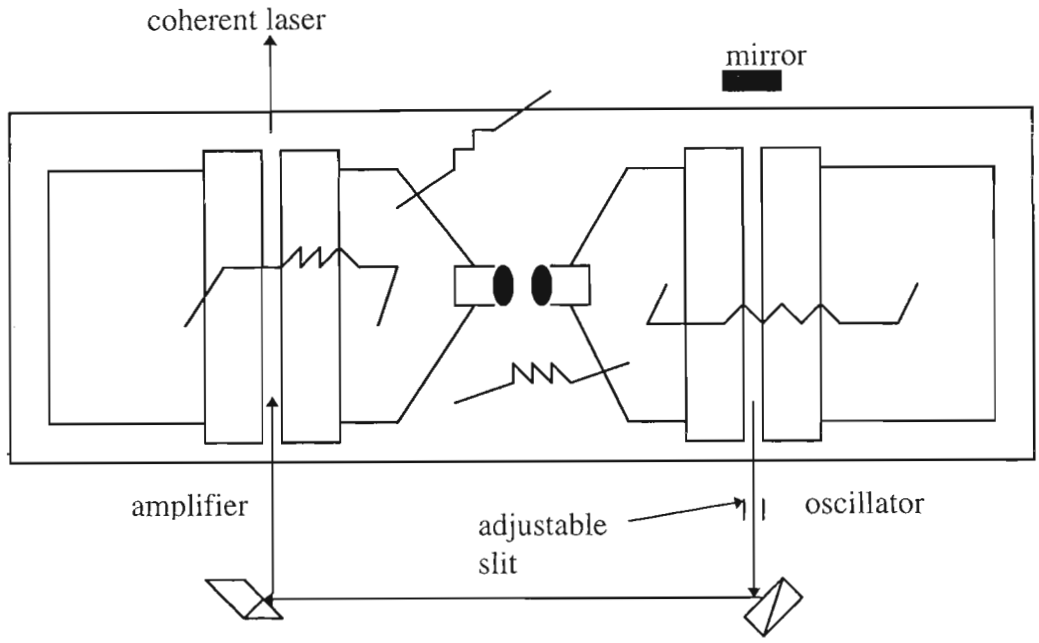

Figure (2.2.4): Top view of the optical and electrical configuration of the laser.

The oscillator produces a powerful but quasi-coherent output and the radiation produced passes through a vertical adjustable slit which increases the lateral coherence in the horizontal direction. This obviously causes the power of the beam to reduce significantly. The beam is then directed by a pair of mirror into the second laser channel which we call the amplifier. The operation of the latter must be in synchronization with the incoming signal and also to saturate the beam. Therefore, greater power than is normally supplied by the amplifier is achieved.

A novel discharge configuration which employs a " capacitor transfer" circuit made up of discrete capacitors was described by Armandilo and Kearsley(1982). The laser produced pulses of 337 nm radiation with peak powers > 5 MW and durations of 4 ns (FWHM). The output beam is reproducible, uniform and of large cross-section. The peak value of the radiance is greater than 3×10^{11} Wsr^{-1}. Figure (2.2.5) shows the schematic of the excitation circuit consisting of the spark gap (SG), the storage capacitor (C_S), the internal peaking capacitor (C_P).

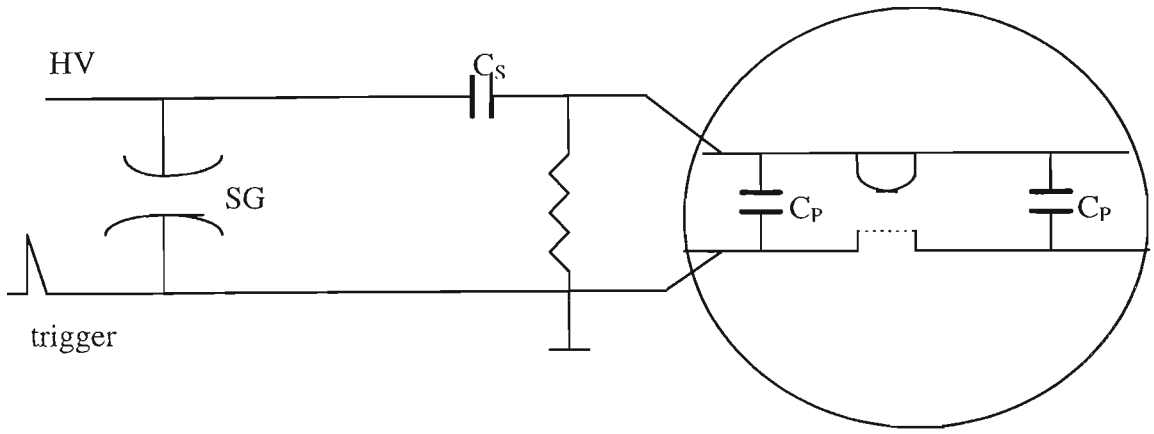

Figure (2.2.5): Schematic diagram of excitation circuit.

The gas envelope of the laser was a PVC tube closed at each end with a PVC flange. 30 capacitors (925 pF) were arranged in two rows of 15, one row on either side of and parallel to the length of the discharge electrodes. The anode used was made of brass bar of 40 mm width. Its convex surface had a cylindrical profile of large radius of curvature facing the main discharge gap of 25 mm spacing. The cathode surface is a planar grille of brass wires (100 μm diameter) which form a grid of 10 wires/cm from side to side. Electrical connection to the external storage capacitor (60 nF) is made through two rows of 8 parallel current feeds which penetrate through the tube at regular intervals of 70 mm along its length. The circuit is completed by a coaxially mounted triggered spark gap.

When an optimized gas mixture (60 Torr of N_2 in He to a total pressure of 800 Torr) was used energies of 20 mJ were recorded in pulses of 4 ns (FWHM) duration. Increasing the helium buffer gas pressure beyond 800 Torr caused the output pulse energy to decrease. Due to the absence of streamers or bright arcs at any gas pressure up to the working pressure limit (2.6 atm) of the laser tube, this behavior is attributed to the progressively decreasing E/N value rather than the degradation of the discharge uniformity. The laser pulse energy was improved on adding the electron attaching gas NF_3 to the He/N_2 gas mixture. With a 2 Torr partial pressure of NF_3 added to the gas mixture, the laser pulse energy output at constant charging voltage (40 kV) increased to 25 mJ. This improvement of 25 % over the value obtained without NF_3 seemed mainly to be due to an increase in pulse duration.

2.3 Theory: The Rate Equations

The three energy levels involved in the excitation of the 337 nm lasing transition in N_2 are shown in a simplified diagram in Figure (2.3.1). Thus, the N_2 laser can be considered as a three-energy level laser:

$X^1\Sigma^+_g$ is the ground level

$B^3\Pi_g$ is the second level

$C^3\Pi_u$ is the third level

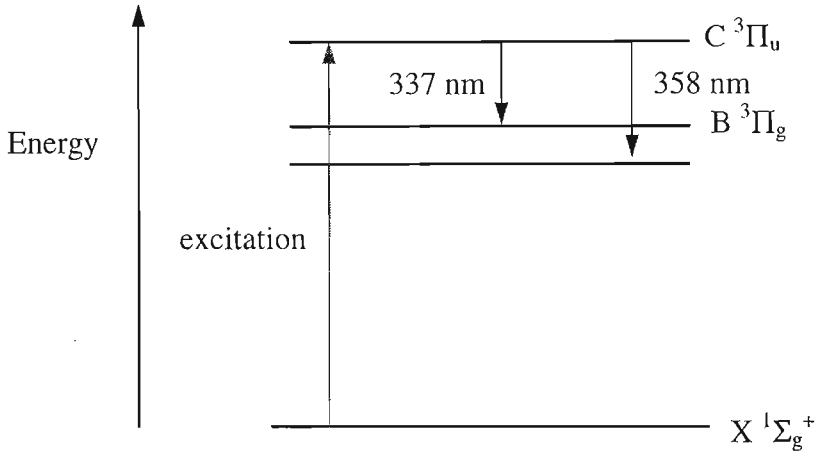

Figure (2.3.1) : Energy levels of the nitrogen molecule.

Let N_1, N_2 and N_3 represent the population densities of levels 1, 2, 3 respectively. In the theory the following symbol will be used:

X_{ij} : the collision excitation rate from level i to j, where $i < j$

Y_{ji} : the collision de-excitation rate from j to i

τ_{ji} : the radiative lifetime from j to i

$R_{ji}^{\ i}$: the induced emission rate which includes the line width, the Einstein coefficient B and the Energy density

Now ,

$$dN_3/dt = X_{13}N_1 + X_{23}N_2 - (Y_{31} + Y_{32} + \tau_{31}^{-1} + \tau_{32}^{-1})N_3 - R_{32}^{i}[N_3 - (g_3/g_2)N_2] \qquad (2.3.1)$$

$$dN_2/dt = X_{12}N_1 + (\tau_{32}^{-1} + Y_{32})N_3 - (\tau_{21}^{-1} + Y_{21} + X_{23})N_2 + \qquad (2.3.2)$$

$$R_{32}^{i}[N_3 - (g_3/g_2)N_2]$$

$$dN_1/dt = -(X_{12} + X_{13})N_1 + (\tau_{21}^{-1} + Y_{21})N_2 + (\tau_{31}^{-1} + Y_{31})N_3 \quad (2.3.3)$$

where g_3 and g_2 are the statistical weights of the high and low laser levels respectively. The induced emission and absorption rates as well as the de-excitation rate through collisions from the laser levels to the ground state can be neglected. It can be assumed (Ali *et al.*, 1967) that

$$\tau_{31} >> \tau_{32}$$

since the $C^3\Pi_u$ energy level is metastable and

$$X_{13} > X_{12}$$

in accordance with the Frank-Cordon Principle (see section 3.3, Chapter 3).

Further,

$$\tau_{21} > \tau_{32} \quad (\tau_{32} \sim 40 \text{ ns and } \tau_{21} \sim 10\mu s)$$

Ali *et al* (1967) showed that the population densities N_3 and N_2 are given by

$$N_3 = N_1X_{13}t - 1/2(N_1)(X_{13})(Y_{32} + \tau_{32}^{-1})t^2$$

and

$$N_2 = 1/2\ (N_1)(X_{13})(Y_{32} + \tau_{32}^{-1})t^2$$

and to obtain the condition for population inversion, i.e $N_3 > N_2$

$$t < 1/(Y_{32} + \tau_{32}^{-1}) \quad (2.3.4)$$

The equation (2.3.4)shows that population inversion can only take place during a time shorter than the radiative lifetime of the $C^3\Pi_u$ level if the Y_{32} is neglected with respect to τ_{32}^{-1}. This necessitates the fast excitation of nitrogen (less than 40 ns).

2.4 Review of the construction of a Pulsed Molecular N_2 Laser

A pulsed molecular nitrogen laser similar in design to that described by H.M.von Bergmann (1980) was constructed by Niresh Bhagwandin (1983) at the Department of Physics, Laser Group, University of Natal. The laser is excited by a simple flat Blumlein pulsers as shown in Figure (2.4.1). The device is switched by a pressurized spark gap as shown in Figure (2.4.2) and the atmospheric discharges are produced with the electrode system shown in Figure (2.4.3).

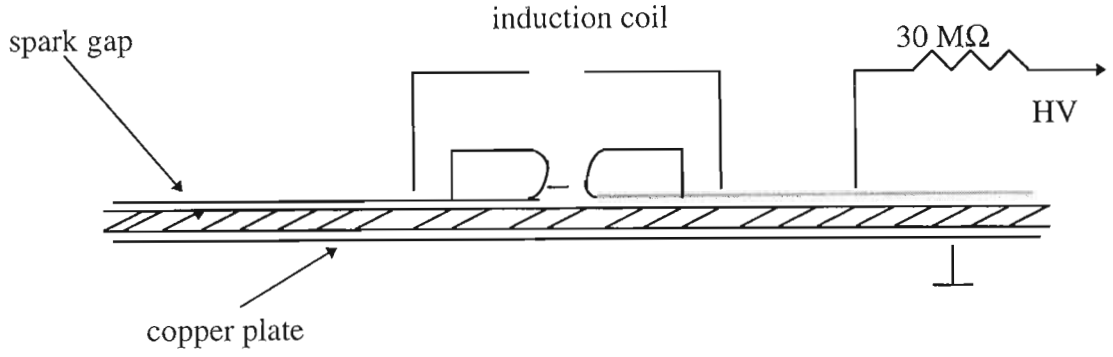

Figure (2.4.1) : The Flat Blumlein pulser.

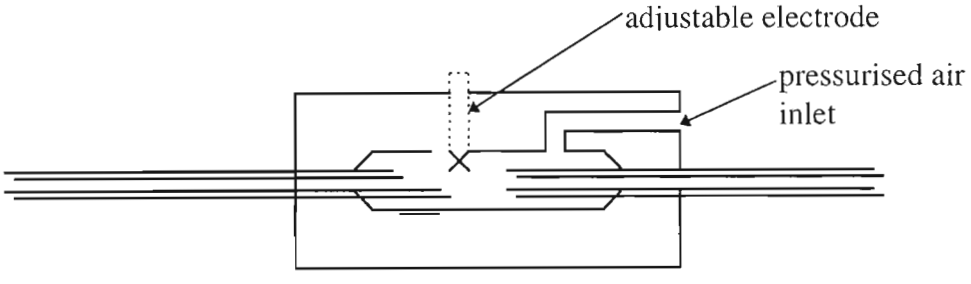

Figure (2.4.2): The Pressurized spark gap.

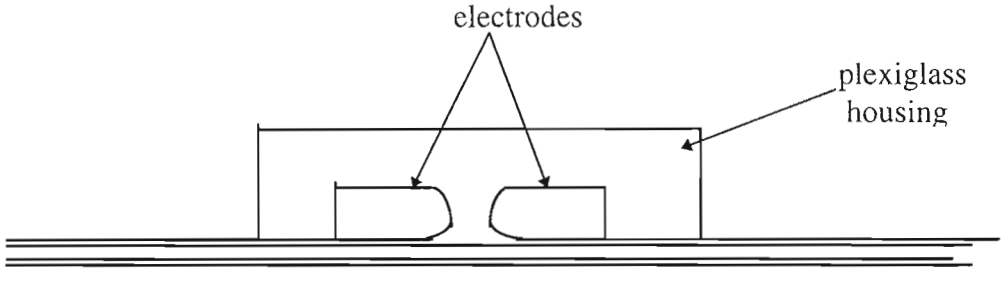

Figure (2.4.3): The electrode system.

The capacitors were made from commercial fibre-glass copper-clad circuit board of dimensions 58 x 43 x 0.1 cm. The copper was etched by Ferric chloride on both the top and bottom sides of the board to prevent arcing between the charged upper and lower plates. A strip was etched across the top side to form two adjacent capacitor plates of dimension 24 x 35 x 0.15 cm each. The electrodes were made of 2 aluminium strips with dimension 35 x 1.9 x 0.625 cm and are mounted to the perspex housing. The electrodes were profiled to prevent arcing between them and their separation can be varied to approximately 6 mm. The spark gap consisted of two copper cylinders of thickness 1.4 cm and diameter 3 cm. It was held fixed on the board by a perspex clamp. The electrodes of the spark gap were two rounded brass screws and the spacing between them were adjustable to about 5 mm. Since the spark

gap was a pressurized two electrode non-triggered sytem, this resulted in its erratic performance and hence fluctuations in the laser light output. Figure (2.4.4) shows an exploded view of the pulsed N_2 laser.

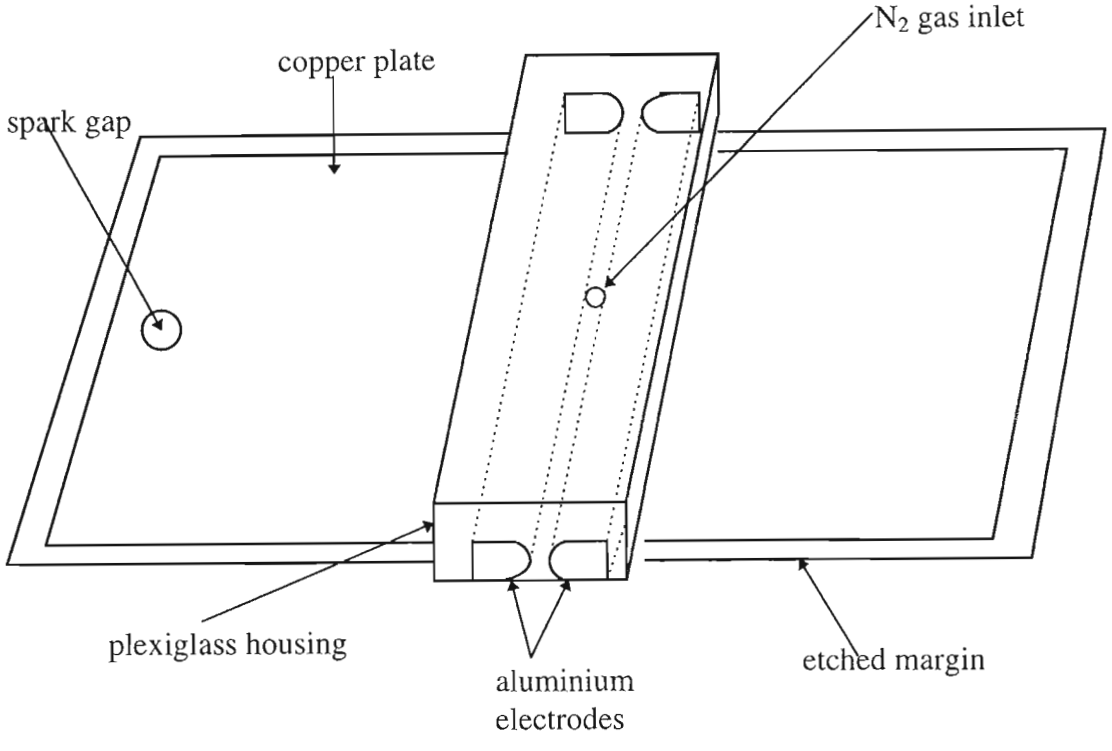

Figure (2.4.4): An exploded view of the pulsed N_2 laser (Bhagwandin N. 1983).

As discussed earlier in the previous articles, the Blumlein circuit behaves like an adjacent pair of capacitors and the space between them provides a gap across which current can be discharged. The capacitors are charged by applying a potential difference across the lower and upper plates. At predetermined voltages of the order of several kilovolts, the spark gap breaks down. The voltage depends on the spacing of the electrodes in the spark gap. This results in a large potential difference across the electrodes and the discharge excites the N_2 molecules.

This switching phenomenon is illustrated in Figure (2.4.5) (Bhagwandin N., 1983). When there is a break down at the spark gap, a circular voltage recedes from there along the charged copper plate at almost the speed of light. As it reaches the laser discharge channel the wavefront spreads across the edges of the channel, thus creating a potential difference across its center. This potential appears across the full length of the gap in less than 0.2 ns rising to a maximum value in about 1 ns. The adjacent plates are connected with an air coil inductance to allow simultaneous slow charging but also preventing coupling when the Blumlein circuit is switched.

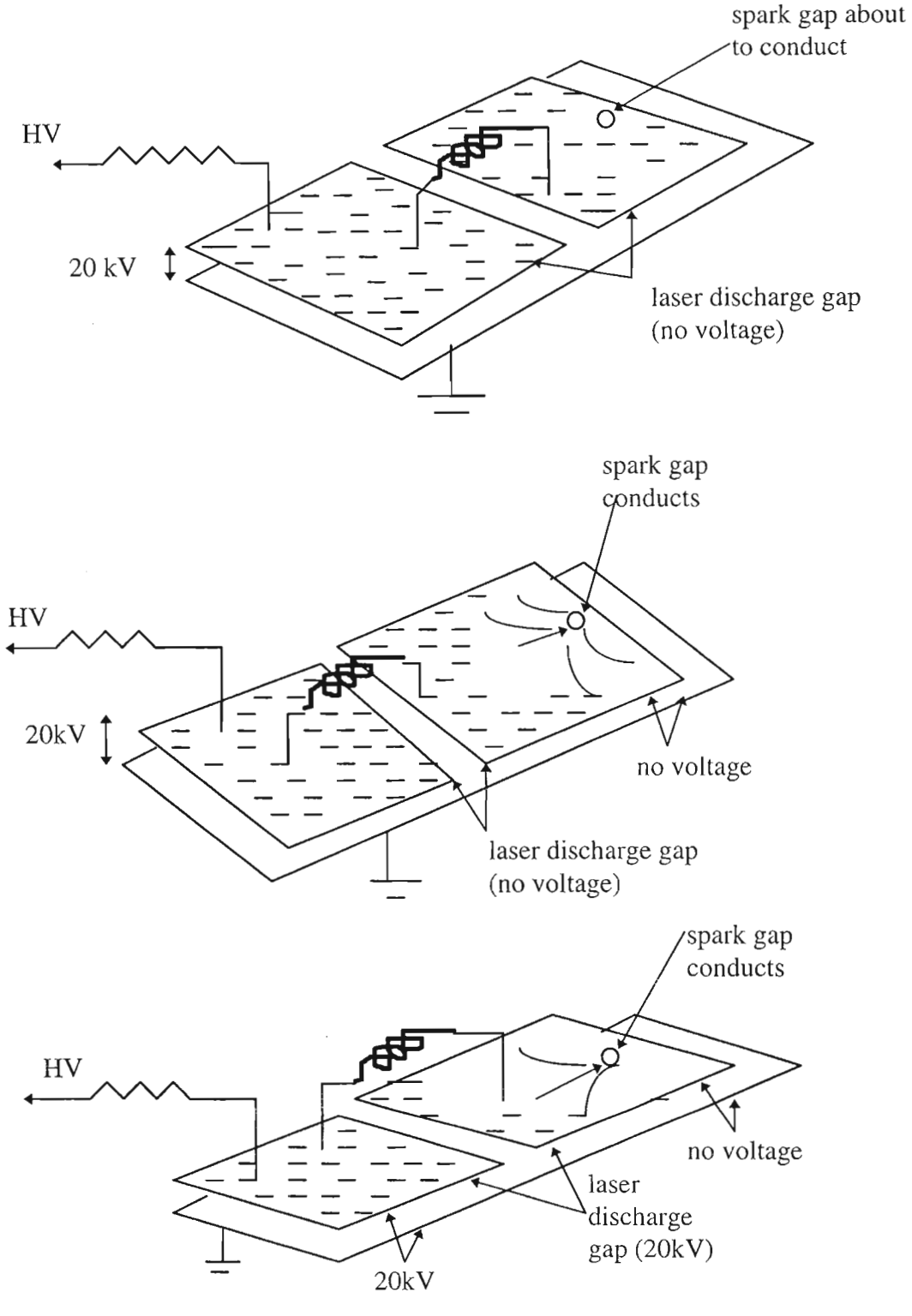

Figure (2.4.5): The switching phenomena (Bhagwandin N., 1983).

2.5 Summary

The theory of nitrogen lasers and the rate equations are given where the N_2 laser is considered as a three-energy level system. All the N_2 lasers mentioned in the review used a flat plate Blumlein circuit to discharge the lasers and the same discharge technique was used in all the lasers constructed by this author. From the review, it is found that several pre-ionization methods were used where corona discharges initiated the laser discharge in the laser channel. An oscillator-amplifier configuration is also described where pulse duration of 1 ns gave an output energy of 100μJ/pulse. The rectangular-plate N_2 laser constructed by N. Bhagwandin together with the discharge mechanisms are also reviewed. The literature also shows that an optimized mixture of gases such as He, NF_3 improved the energy performance of the laser. However, in our case, as we shall see, using N_2 vapour as the discharge medium improves the laser energy significantly.

CHAPTER THREE

3.0 THEORY OF GAS DISCHARGES

3.1 Excitation and ionization of gas discharges

In this thesis, mostly gas lasers such as N_2 and CO_2 lasers are going to be investigated as a result of which it is important to understand the processes and mechanisms which are involved in such lasers.

In gas-discharge lasers, collisions are responsible for the ionisation of gas molecules and which are also required for a self-sustained discharge and for the excitation processes which selectively populate the upper laser level and lead to population inversion.

There are three main types of collisions according to the energy transfer between the colliding particles.

(a) Elastic collisions

A collision is termed elastic if there are no changes in the internal energy of the colliding particles, but only a redistributiion of their respective kinetic energies. For electron-molecule collisions the large discrepancy between electronic and molecular mass leads to a negligibly small fractional energy transfer($\sim m_e/M$).

(b) Inelastic collision of the first kind

A collision is termed inelastic, if kinetic energy is converted to internal energy of the colliding particles. The energy can be transferred into rotational, vibrational or electronic excitation of the molecule or can lead to ionization or dissociation.

(c) Inelastic collision of the second kind

If excitation energy of the molecule is released as kinetic energy of the colliding particles, thus increasing their total kinetic energy, the collisions are said to be of the second kind or superelastic. Examples of this type of interaction are the Penning and Auger effect. In the Penning process, the metastable atoms have a long lifetime and therefore, on hitting other atoms, there is a high probability of ionising them. This phenomenon is known as the Penning effect. The origin of the Auger process can be understood from a diagram of the electron energy levels shown in Figure (3.1.1). If an atom is ionised by the removal of an electron from an atomic core level, a second electron can be ejected with an energy characteristic of the atom. The second electron which is the Auger electron has its energy independent of the energy of the ionising source. Referring to Figure (3.1.1), the ionisation radiation ejects an electron from an atom, leaving an empty space in the atomic core levels. This core level is quickly filled by an electron from a higher level shell and energy is released. There can be a competing process where another electron gains the energy and is ejected from the

atom. This second ejected electron is the Auger electron and its energy depends on the energy of the atomic level involved in its production, not on the energy of the initial ionising radiation.

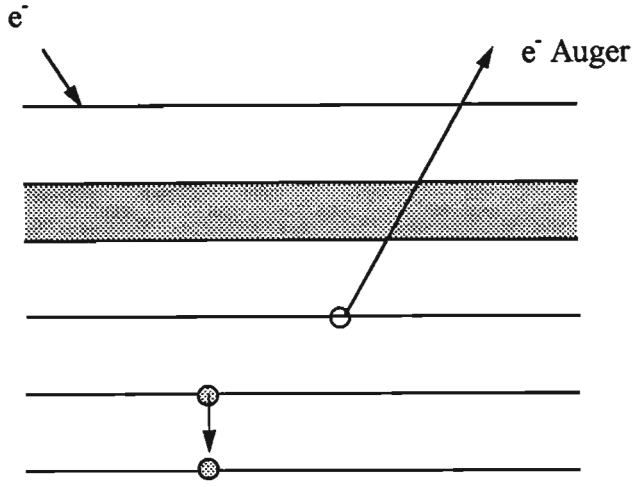

Figure (3.1.1): Schematic energy level diagram illustrating the origin of the Auger effect.

In gas discharges, the primary source of excitation and ionization is from collision of the first kind involving electrons and molecules.

3.2 Electron energy distributions

The energy distribution of the electrons is of fundamental importance for the excitation and ionization processes in an electric discharge. The average electron energy depends on the amount of energy that is acquired by the electrons from the applied electric field between inelastic collisions, while the form of distribution function is determined by the interactions of the electrons with the gas molecules and among themselves. If the collisions between electrons and the neutral gas molecules are assumed to be elastic and in the case of strong interaction between the electrons themselves, the distribution function will be Maxwellian and can be written as (Bergmann, 1980)

$$f(\varepsilon)d\varepsilon = dn_e/n_e = c_1 \sqrt{x}\, e^{-x}\, dx \qquad (3.2.1)$$

where n_e = electron density

$x = \varepsilon / \bar{\varepsilon}$

ε = kinetic energy of electrons

$\bar{\varepsilon} = kT_e$ mean electron energy

T_e = electron temperature

$c_1 = \sqrt{(4/\pi)}$.

which normalizes the distribution to unity.

Equation (3.2.1) is derived under the assumption that the mean free path λ_e of the electrons is proportional to the electron velocity v_e. In weakly ionized plasmas the electron-electron collision frequencies are low and energy exchange is mainly due to elastic collisions with molecules. In this case there is only slight dependence of λ_e on v_e and the energy distribution which is established is that of Druyvesteyn (Bergmann, 1980)

$$f(\varepsilon)d\varepsilon = dn_e/n_e = c_2\sqrt{x}\, e^{-(x)}\, dx \qquad (3.2.2)$$

where $x = \varepsilon / \bar{\varepsilon} = \varepsilon/(c_3\lambda_e E/N)$

c_2, c_3 = constants

E/N = ratio of electric field strength and number of molecules in gap

Both the distribution functions depend on the value of E/N only and not separately on E or N. The main difference between the distributions is that for the same mean electron energy, the Maxwellian distribution contains more electrons of high energies than that of Druyvesteyn. Both the above disribution functions apply strictly to elastic collisions. In gas discharges inelastic collisions have to be considered, which under certain conditions can lead to distribution functions which deviate considerably from those of equations (3.2.1) and (3.2.2). The electron energy distribution can be obtained from particular gases and excitation conditions by numerically solving the Boltzmann transport equation, if the various collision cross-sections are known.

Nighan (1970) found that in N_2 discharges at low E/N values of ~ 3×10^{-16} Vcm^2 the electron energy distribution assumed is strongly non-Maxwellian. Calculations of Judd (1976) show however, that at E/N values of 1 to10 x 10^{-15} Vcm^2 the distribution is close to a Maxwellian (Bergmann, 1980).

The E/N ratio of the parabolic laser is calculated as shown below:

The dimensions of the discharge gap of the parabolic nitrogen laser are (33.5 x 0.3 x 0.4) cm where 33.5 cm is the length of the electrodes, 0.3 cm is the electrode separation and 0.4 cm is the thickness of electrode. Thus the approximate volume of gas occupying this region is 4.02 cm^3. The volume of one mole of molecules at standard temperature and pressure is 22400 cm^3 and the number of molecules is given by the Avogadro's number, 6.023×10^{23}. After a simple calculation, the number of molecules occupied in the laser discharge gap is about 1.081×10^{20} ($(6.023 \times 10^{23} \times 4.02)/22400$)).

The electric field strength is given by

$$E = V/d_2$$

where V is the voltage across the gap
d_2 is the electrode separation

Hence,

$$E = (17 \times 10^3 \text{ V})/ (0.3)$$

$$= 56.67 \text{ kVcm}^{-1}$$

Calculating the E/N value, $((56.67 \times 10^3)/ (1.081 \times 10^{20}))$, gives approximately 5.2×10^{-16} Vcm^2. Thus, the electron energy distribution is non-Maxwellian considering the fact that the E/N ratio for the parabolic nitrogen laser is low and corresponds to the E/N values obtained by Nighan (1970).

3.3 Electron impact excitation

The process of electron impact excitation of a molecule A can be represented by

$$A + e(\varepsilon_1) \rightarrow A^* + e(\varepsilon_2) \qquad (3.3.1)$$

where the difference in kinetic energy of the electron $\varepsilon_1 - \varepsilon_2$ appears as excitation energy of the molecule.

The production rate for the energy state j of a molecule by electron impact from the ground state is given by

$$R_{oj} = Nn_e \int_e v_e \sigma_{oj}(\varepsilon) f(\varepsilon) d\varepsilon \qquad (3.3.2)$$

where $v_e = \sqrt{2\varepsilon/m_e}$ electron velocity

σ_{oj} = cross-section for electron impact excitation

ε_j = threshold energy

The production rate of molecules in the excited state is directly proportional to the pressure and the electron density, which tends to show the importance of operating gas-discharge lasers at elevated pressures and high current densities. If the electron energy distribution is known, equation (3.3.2) can be written in terms of the velocity-averaged cross-section $\bar{\sigma}_{oj}$ and the average electron velocity $\bar{v}_e$

$$R_{oj} = Nn_e \ \bar{\sigma}_{oj} \ \bar{v}_e \qquad (3.3.3)$$

Electron impact excitation of high-lying electronic levels in diatomic molecules is usually dominated by the high-energy electrons in the tail of the distribution function. If $f(\varepsilon)$ is Maxwellian, the excitation rate can be approximated by carrying out the

integration in equation (3.3.2) (Webb, 1976). The energy dependence of the excitation rate can then be written as

$$R_{oj}(\bar{\varepsilon}) = c_4\, \sigma_{oj}(max)\, \sqrt{\varepsilon_j}\, \phi(\varepsilon_j/\bar{\varepsilon})\, e^{-\varepsilon/\varepsilon} \qquad (3.3.4)$$

where c_4 = constant

$\sigma_{oj}(max)$ = peak value of the excitation cross-section

The function ϕ reflects the energy-dependence of the excitation cross-section and is usually a very slow varying function of the electron energy.

The electron impact cross-sections can be derived theoretically from quantum-mechanical calculations. By using Born approximation, it can be demonstrated that for high electron energies, where electron exchange collisions can be neglected, the cross-section is proportional to the Einstein transition probablity defined by equation(Bergmann, 1980).

$$A^u_L = (64\pi^4\nu^3_{uL})/3hc^3\, [1/g_J\, \Sigma_{M,M} |R^u_L|^2 \qquad (3.3.5)$$

where A^u_L = transition probability

ν_{uL} = transition frequency

$R^u_L = \int \Psi^*_u\, M\, \Psi_L\, d\tau$, Ψ_u , Ψ_L are the eigenfunctions of upper and lower state respectively , M is the electric dipole moment of molecules with components, M_x ,M_y, M_z

$g_J = 2J' + 1$ is the degeneracy of the initial states

Therefore,

$$\sigma_{oj} = A_{jo} \qquad (3.3.6)$$

Equation (3.3.6) indicates that optically allowed transitions have large cross-sections for electron impact excitation. The cross-section rises approximately linearly with energy above the threshold ε_j, peaks at energies ~ $2\varepsilon_j$ and is broadly resonant for electron energies of up to ~ 100 eV. It can be shown that for electron impact excitation of diatomic molecules, the relative probability of excitation for the various upper vibrational levels is proportional to the overlap integral of the vibrational eigenfunctions of the upper and lower states and is approximately independent of electron energy (Bergmann, 1980). One can therefore apply the Frank-Condon principle to the electron impact of diatomic molecules. The Frank-Condon principle is a very important concept in analysing radiative transitions in molecules. It states that all electronic transitions, either downward (via radiation or collisions) or upward (via excitation or absorption), must take place in a vertical direction on a diagram of molecular energy versus atomic separation (see Figure 3.3.1). The justification for

this principle is the assumption that electronic transitions take place so rapidly that internuclear separations do not have time to change during the transition. This rule places certain restrictions on which energy levels and sublevels can be involved in specific electronic transitions. Since vibrating molecules spend most of their time at the endpoints of their vibrational excursions, the Frank-Condon principle suggests that the vibrational levels of excited electronic states produced via excitation from lower electronic levels must have a portion of their allowed excursions in a direct vertical pathway above those endpoints.

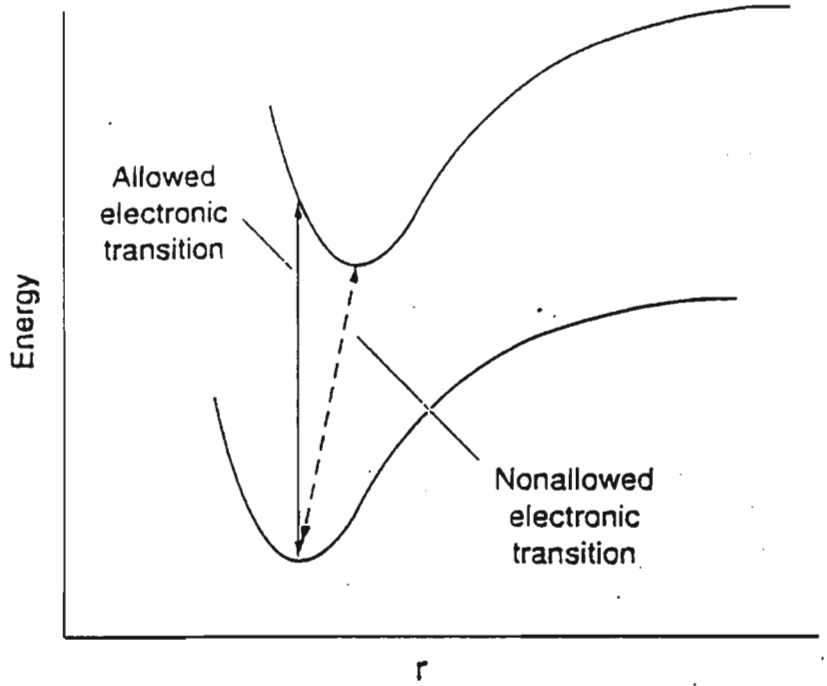

Figure (3.3.1): Illustration of the Frank-Condon principle.

3.4 Electron impact ionization

The process of electron impact ionization can be written as

$$A + e(\varepsilon_1) \rightarrow A^+ e(\varepsilon_2) + e(\varepsilon_3) \qquad (3.4.1)$$

where $\varepsilon_1-(\varepsilon_2 + \varepsilon_3)$ is equal to the ionization energy ε_i. The ionization rate R_{oi} can be expressed by equations (3.3.2) and (3.3.3) if ε_j and σ_{oj} are replaced by ε_i and the ionization cross-section σ_{oi} respectively.

Ionization processes in gases under the influence of an applied electric field are usually described by Townsend's first ionization coefficient α, which is defined as the average number of ionizing collisions caused by one electron drifting a distance of 1 cm in the direction of the applied field. The ionization coefficient is related to the ionization rate by

$$\alpha = N/ v_e n_e R_{oi} \qquad (3.4.2)$$

where v_e = electron drift velocity.

The ionization cross-section can be calculated quantum-mechanically in a similar way as the excitation cross-section. The energy dependence of the ionization cross-section is the same as that of an optically allowed transition.

3.5 Avalanche multiplication and Townsend breakdown

Electrons drifting with an average velocity v. under the influence of a uniform electric field can undergo ionizing collisions. The total number of electrons (n) formed in an electron avalanche after a time period t is given by

$$n = N_o \, e^{\alpha v \, t} \tag{3.5.1}$$

where N_o = number of initiating electrons

α = number of ionizing collisions per cm

α is known as Townsend's first ionization coefficient and is related to the velocity-averaged ionization cross-section by equation (3.4.2). Additional secondary electrons can be produced at the cathode by the action of positive ions, photons and metastables. Townsend's second ionization coefficient γ gives the number of secondary electrons produced at the cathode per ionizing collision in the gap.

A self-sustained discharge which is independent of the number of initiating electrons will develop if for every primary avalanche crossing the gap at least one sucessor avalanche is triggered at the cathode by γ processes. This condition is described by Townsend's breakdown criterion (Wadhwa C.L., 1994).

$$\gamma \, (e^{\alpha d} - 1) \geq 1 \tag{3.5.2}$$

where d_2 = electrode separation in cm.

The ionization parameter α/p, where p is the gas pressure, and γ are functions only of the ratio of electric field strength to pressure E/p. By substituting the functions for α and γ in equation (3.5.2) one can derive an expression for the static breakdown voltage:

$$V_{br} = f(pd_2) \tag{3.5.3}$$

This is Paschen's law stating that the breakdown voltage for any given gas is the function of the product 'pd_2' only. The Paschen curve (Figure 3.5.1) given by equation (3.5.3) attains a minimum for the breakdown voltage at low 'pd' values (typically 1 mbar cm) and increases towards higher and lower pressures. Paschen's law is no longer satisfied at very high pressures and small electrode separations, when the electric field strength reaches values of $\geq$100 kV cm^{-1}. Under these conditions breakdown is dominated by electrode processes such as field emission.

(Bergmann,1980). In the case of the parabolic laser, the charging voltage is about 17 kV and the electrode separation is 0.3 cm. This gives an electric field of ~ 50 kV/cm^{-1}. Therefore, in this case also, the Paschen's law is satisfied.

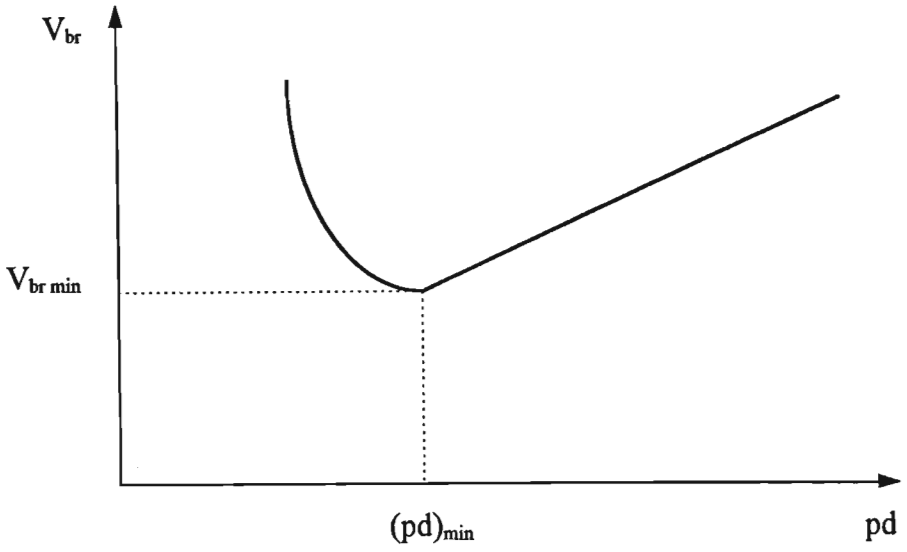

Figure (3.5.1): Paschen's Curve (Wadhwa, 1994).

The typical values for $(pd_2)_{min}$ and V_{br} (minimum) are 0.65 and 240 volts respectively for N_2 gas.

At static breakdown and small overvoltages the Townsend breakdown mechanism is operative. When initiated by a small number of electrons at the cathode, the Townsend breakdown is characterised by a sequence of avalanches, where the succeeding generations are triggered at the cathode after a time delay depending on the dominant γ process. The discharge formation is a slow process taking several generations of secondary avalanches to breakdown. The formation time is typically in the μs range. Breakdown occurs in two steps: due to the spreading action of the γ process and positive space charge build-up in front of the anode, a transient glow discharge is formed initially, lasting several μs, which then contracts radially leading to the arc stage (Bergmann, 1980).

3.6 Space charges effects and streamer formation

The Townsend mechanism describes the discharge formation satisfactorily as long as space charge effects within the avalanches can be neglected. The space charge distribution around an avalanche is shown schematically in Figure (3.6.1). Due to the big difference in mobilities between electrons and positive ions, the latter can be assumed stationary, while the electrons move towards the anode. This results in a net displacement of the electrons and ion clouds by one ionization length (α^{-1}). Their respective space charges will enhance the field in front and behind the avalanche but will reduce it within the avalanche head. Calculations show that for avalanches with

10^6 carriers the space charge contribution amounts to ≈ 1 % of the applied field. This can have a significant effect on the avalanche development as α is a sensitive function of the electric field. Space charges have the following two main effects on the avalanche growth (Bergmann, 1980).

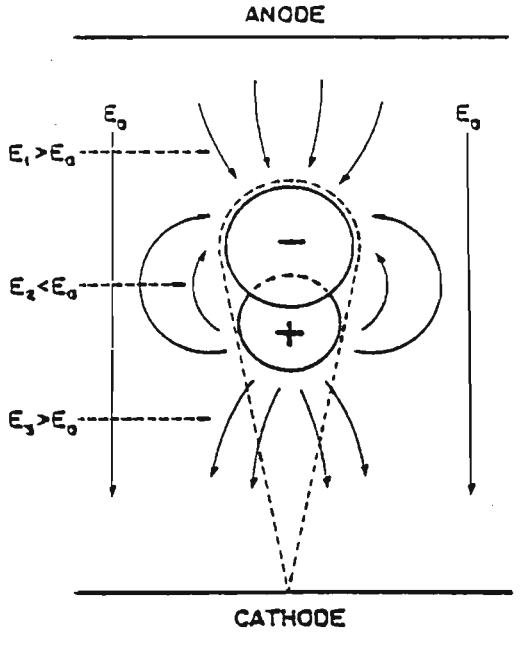

Figure (3.6.1) : Influence of space charge on the field of a single avalanche.

(a) For carrier numbers of $n \geq 10^6$, the reduced field within the avalanche head leads to space charge retardation of the electrons and a reduced effective α. In nitrogen discharges,

$$\alpha_{eff}(n) = \alpha_0 (1\text{-}B \ln n/N) \qquad (3.6.1)$$

where

n = number of electrons in avalanche
B = 0,666
$N = 1{,}4 \times 10^6$

(b) The space charge field of the avalanche becomes comparable to the external field when $n \geq 10^8$. The increased front field of the avalanche then leads to enhanced ionization ahead of the avalanche and to an increased effective α. A further increase of n transforms the avalanche into a so-called streamer and touches off an an ultra-fast breakdown mechanism, the streamer or "kanal" breakdown.

The observation of single avalanches by cloud chamber methods and by image intensifier measurements (Bergmann, 1980) lead to a critical amplification value for streamer breakdown (see equation 3.5.1) of

$$\ln (n_{crit}) = (\alpha x_-)_{crit} \approx 20 \tag{3.6.2}$$

where $x_- = v_- t$ distance travelled by avalanche.

This corresponds to a critical carrier number of $n_{crit} \approx 5 \times 10^8$. An avalanche which grows to the critical value is transformed by its own space charge field into a streamer (or ionizing front) which travels with greatly increased speed towards the anode. At the same time a cathode directed streamer is formed. During their different stages of development the propagation speeds exceeds the drift velocity of the electrons by more than a factor of ten. Once these streamers reach the electrodes, ionizing waves with velocities of up to 100 times v_- bridge the gap and lead to spark breakdown (Bergmann, 1980). The enhanced speed of this development has been explained by acceleration of the electrons in the enhanced field (Chalmers et al, 1972) and by secondary avalanches started ahead of the streamer by ionizing ultra-violet radiation. A criterion for streamer breakdown has been derived, demanding that the avalanche attains critical amplification within the gap length. With the assumption that an avalanche-to-streamer transition occurs when the radial field at the avalanche head is equal to the applied field and assuming diffusion spreading of the avalanche to be dominant, we have (Wadhwa C.L, 1994)

$$\alpha d_2 = 17.7 + \ln d_2 \tag{3.6.3}$$

In nitrogen at pd values of 1 bar cm streamer breakdown is operative for voltages exceeding the static breakdown voltage by ~10 % (Bergmann, 1980).
In contrast to the Townsend breakdown the streamer mechanism leads to the arc stage without intermediate glow. If the initial preionization is sufficient to eliminate the statistical delays, the formation times are governed by the time the avalanche needs to attain its critical value. From equations (3.5.1) and (3.6.2) it follows that

$$\tau = 1/ \alpha v_- \ln (n_{crit}) \tag{3.6.4}$$

Formation times are generally of the order of a few ns. In short gaps at high overvoltages subnanosecond formation times have been observed (Fletcher, 1949).

3.7 Summary

The theory given in this chapter provides an understanding of the processes and mechanisms which are involved in gas lasers . In gas-discharge lasers, collisions are responsible for the ionisation and excitation of gas molecules which then initiate processes such as population inversion, stimulated and spontaneous emission. In most gas lasers, the collision type is collision of the first kind. A calculation of the E/N value for the parabolic N_2 laser is given which shows that the energy distribution is non-Maxwellian. Moreover, the breakdown conditions at the laser discharge satisfy the Paschen's law since the electric field strength of the laser was found to be about 50

kV/cm^{-1}. In addition, the mechanism of Townsend breakdown is given which helps to understand the processes taking place in the discharge laser channel.

CHAPTER FOUR

4.0 SPARK GAPS AND CORONA DISCHARGES

4.1 Introduction

Electrical energy can be effectively switched at high voltages, for high currents (kA) and in nanosecond time scales by low-inductance spark gaps. For the excitation of high-pressure gas-discharge lasers with short inversion lifetimes the pulser performance during the first few nanoseconds is of overriding importance. Spark gaps with nanosecond rise times are therefore required. The synchronised firing of spark gaps, which is employed for parallel switching and cross-barring[1] requires small time lags and low jitter times.

The uniform-field breakdown voltage (V_{br}) in air at 20 ^{0} C is given approximately by the following empirical expression.

$$V_{br} = 23.9\ pd_l + 6.04\ \sqrt{(pd_l)}\ kV \qquad (4.1.1)$$

where p = air pressure in bar
d_l = gap separation in cm

In the case of the parabolic nitrogen laser, the gap separation is approximately 0.5 cm and the air pressure is about 1 bar, giving approximately a breakdown voltage of 16 kV.

This optimised value for V_{br} is normally not reached in spark gaps. The operating voltage is reduced by field inhomogeneities, especially at the trigger electrodes and also due to microdischarges on the electrode surface and dust particles in the gas (Wadhwa., 1994). The hold-off voltage can however be improved considerably by using gas mixtures containing electronegative gases such as SF_6 (Bergmann, 1980).

The time lag for breakdown τ_l is that time period required from applying a voltage high enough to initiate breakdown to a measurable drop in gap voltage and can be written as

$$\tau_l = \tau_s + \tau_f \qquad (4.1.2)$$

The statistical time lag τ_s is the time that elapses before an electron that can initiate breakdown appears in the gap. τ_s is reduced to small values in triggered spark gaps by externally providing the initiating electrons. The nitrogen laser used for the Colliding Shock experiment has a triggered spark gap which minimises jitter times. The formative time lag τ_f is a function of the number of electrons and the ratio of the applied electric field and gas pressure E/p.

[1: Cross-barring usually occurs in high-frequency circuits where due to the high frequency, the total circuit impedance becomes small.]

The jitter in breakdown time, its statistical time spread, is caused by fluctuations in τ_s and by the statistical nature of the avalanche development. In order to minimise time lag and jitters, a large number of initiating electrons has to be provided.

The risetime of the gap current is given by (Bergmann, 1980)

$$t_{rise} = B_1(E/p\ Z^{1/3}\ p^{1/2})^{-1} + 2.2\ (L_1/Z_0)\ \text{ns} \qquad (4.1.3)$$

where E/p is measured in kV cm^{-1} bar^{-1}. In the case of the parabolic laser, E/p ratio is approximately 56 kV cm^{-1} bar^{-1}.

Here,
p = gap pressure in bar
L_1 = gap inductance in nH
Z_0 = driving impedance in Ω
B_1 = 437 for nitrogen

The first factor describing the resistive break down phase gives the time required for the spark impedance to collapse from its initial value at the end of the formation time to a fraction of the pulser impedance. The minimum gap resistance at the end of the resistive phase is proportional to the gap separation and inversely proportional to the transferred charge (Frungel, 1965). Typical values for switched energies of 0.1 - 1 J are 250 - 25 mΩ mm^{-1}.

The second factor gives the inductance-limited rise time which is the dominant contribution for large, inductive spark gaps and for a small driving impedance Z_0. The total spark gap inductance is determined by the gap geometry and by the spark channel. A typical value for the spark inductance is 1.5 nH mm^{-1} (Bergmann, 1980). In order to minimise the rise time, the gap should be operated at high pressures with small electrode separations and close to self-breakdown. Rise times at static breakdown voltage are limited to 2-5 ns by the geometrical spark gap inductance and the decay time of the gap resistance. Faster rise times can be achieved with laser-triggered spark gaps, solid-dielectric switches and overvolted low-inductance surface line switches (Bergmann and Hasson, 1976).

4.2 Free-running spark gaps

Free-running spark gaps are used in the repetitive mode and are triggered by overvolting. The repetition frequency can be set by varying the charging rate. The use of simple symmetrical electrodes minimises field distortions and enables the operation at very small electrode separations and with small overall dimensions. Thus, minimum gap inductance can be obtained. The main disadvantage is the high breakdown jitter due to the small number of initiating electrons. Stable operation with small jitter can be achieved at high repetition rates, where initiating electrons are provided by the remaining ionization in the gap and by profiling the electrodes, to provide a low energy corona discharge prior to breakdown. Some of the lasers which were

Figure (4.2.1) shows a laser with a free running spark gap which was constructed by a vacation student. Figure (4.2.2) shows some spark gaps which were constructed by H.M.von Bergmann (1980).

Figure (4.2.2 a) shows a simple two-electrode spark gap which is clamped directly onto the transmission line. The adjustable electrodes are machined from tungsten-copper alloy and employ a flat-topped profile which minimises the effect of electrode burn-off. Independent tests have shown that the profile is generated by electrode burn-off in long term operation of the switch if the electrode separation is readjusted from time to time (Bergmann, 1980). The electrode erosion is a function of the charge transfer and amounts to ~ 8×10^{-5} gC^{-1} for tungsten-copper electrodes. Referring to our case, the laser has a capacitance of the order of 10^{-9} F and uses a power supply of 17×10^{3} V which gives a charge transfer of the order of 10^{-6} C at the spark gap switch for every shot. The average frequency of the laser is 5 Hz and if it is run for 2 hours, the electrode erosion would be around 3×10^{-6} g during this period. Therefore, the spark gap should still be operative even after 50,000 shots.

Figure (4.2.2 b) shows a scheme used for simultaneous switching of double transmission lines. Figure (4.2.2d) was used for high repetition-rate applications. It is designed for fast symmetrical gas flow and was operated at repetition rates of up to 2 kHz. The electrodes were profiled to provide a stable arc position in the gap centre to reduce heating of the insulator. The spark gap in Figure (4.2.2 c) was designed for long-term sealed-off operation and employs high-vacuum metal-to-ceramic soldering technology. The switch is filled with nitrogen at 3 bar and can be operated at repetition rates of ~ 30 Hz.

Figure (4.2.1): Free running spark gap.

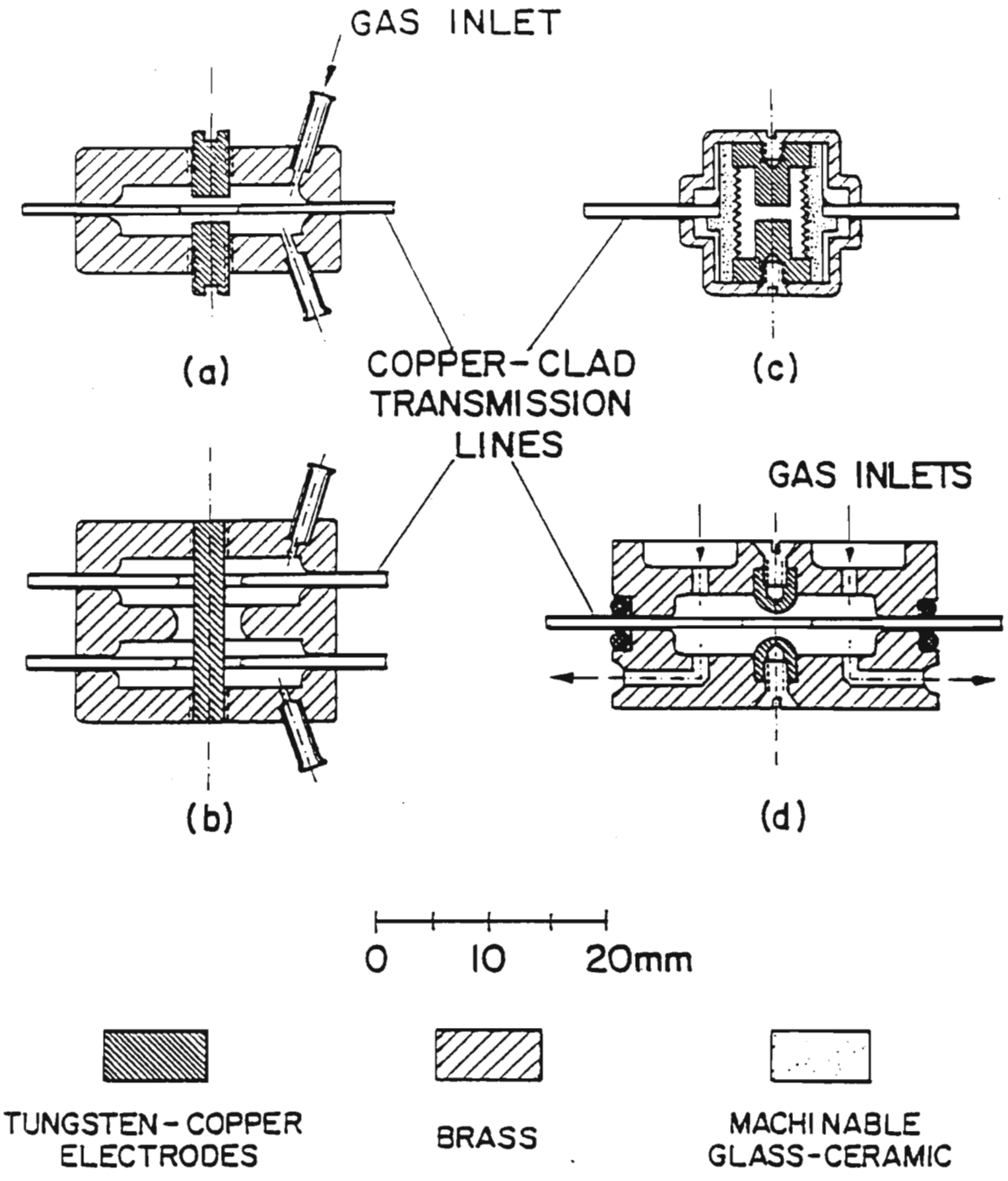

Figure (4.2.2): Various Types of Spark gaps (Bergmann, 1980).

4.3 Photo-ionization-triggered spark gap

Existing pressurized spark gaps rely on field distortion or low-intensity trigger sparks to provide initiating electrons. The discharge is effectively triggered by one or, at most, a few electrons. Formation times are typically $\geq$ 100 ns and jitter times $\geq$ 10 ns. Nanosecond formation times can be achieved if the breakdown is initiated by a large number of electrons. This has been experimentally verified by Kovalchuk *et al* in 1971 (Bergmann, 1980), who initiated the discharge with electrons derived from a pulsed electron beam. The required high values for n_0 (the number of electrons per unit volume) > 10^6 cm $^{-3}$ can be produced by volume photo-ionization and photoelectric emission when high-intensity trigger sparks are used. Surface sparks across ceramics are efficient sources of hard UV radiation and can therefore be utilised in spark gaps as photo-ionising trigger sources (Bergmann *et al.*, 1975).

Figure (4.3.1) shows the design of the triggered spark gap that was used for the excitation of high-pressure nitrogen lasers at voltages of up to 50 kV (Bergmann, 1980). The spark gap is mounted directly on the flat-plate transmission line made from double-sided copper-clad, fibreglass epoxy board. The insulator served to extend the tracking path. The cover plates were supported by two brass rings which were soldered to the copper foil. The adhesion between copper foils and the circuit board was sufficient to operate at pressures of up to 6 bar. The switch utilised a commercial surface-gap spark plug (Champion, LV20) as the triggered electrode. The spark plug was machined flush to the ceramic and rounded off in order to minimise field distortion and corona effects.

Switches with a gap separation of 2-3 mm provided hold-off voltages of 30 kV with nitrogen or air pressures of 5-6 bar and up to 50 kV when pressurised with SF_6 to ~3 bar. The overall switch inductance was ~ 2 nH resulting in rise times of 3-10 ns. Energies of up to 30 J with peak currents of 70 kA could be switched without damaging the electrodes (Bergmann, 1980).

Figure (4.3.2) shows the pressurised triggered spark gap used for the parabolic nitrogen laser. It works on the same principle as the one mentioned above. The gap separation used was 2 to 5 mm depending on the charging voltage required which was usually set to 17 kV. The air pressure was approximately 2 bar and in this case it was noticed that the spark gap does not work with nitrogen gas because it was the commercially available nitrogen gas which is likely to contain some impurities. A maximum energy of 65 J and maximum current of 60 kA could be switched efficiently. However, due to electrode burn-off, the electrodes had to be cleaned and polished from time to time after several shots.

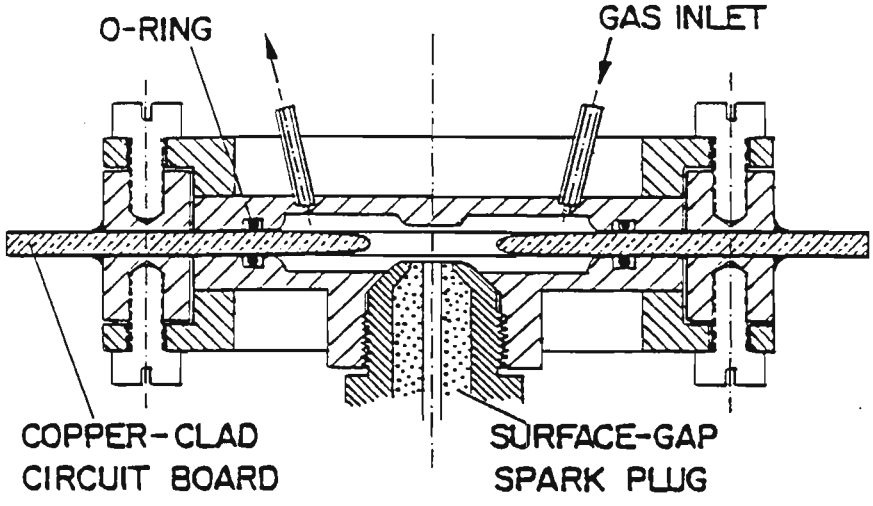

Figure (4.3.1): A triggered spark gap.

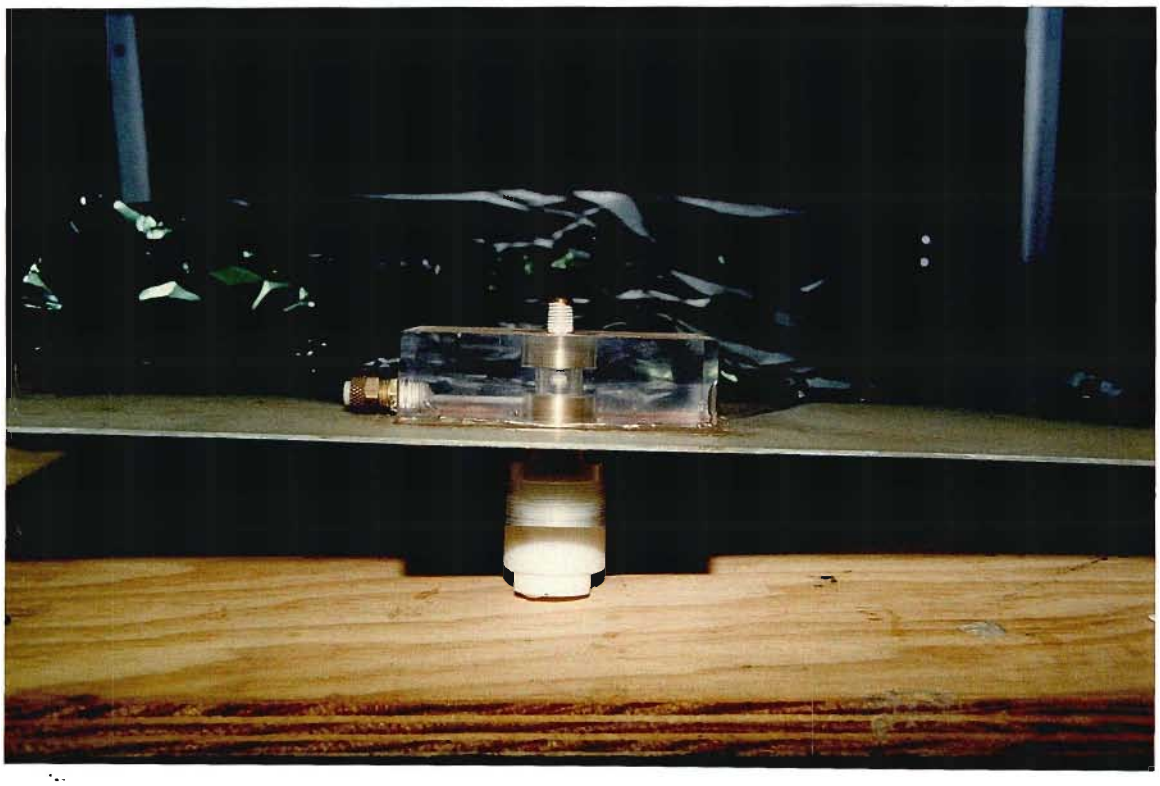

Figure (4.3.2): A pressurised spark gap.

4.4 Pulsed corona discharges

Corona is the generic term used for discharges which develop in highly non-uniform fields. The basic phenomena can be best explained by considering a point-to-point plane geometry with a highly stressed point and a relatively weak field at the plane. The discharge development will then be dominated by processes at the highly stressed electrode, while the plane will only influence the later development. For pulsed nanosecond corona discharges there is no time for drift and accumulation of ionic space charge, and consequently intermittent discharges caused by space charge inhibition (as can be observed in steady state coronas) cannot develop. The main formation processes in pulsed positive and negative point coronas are outlined below.

4.4.1 Positive point coronas

Electrons that are accelerated towards the point form avalanches which can reach critical amplification in the enhanced field and transform into positive streamers. These are essentially identical to the cathode directed streamers in homogeneous fields. Secondary avalanches created by photo-ionization will converge onto the streamer head, increasing the positive ion concentration.

As the streamer develops into the low field region, it has to rely more and more on the local field augmentation by the positive ion space charge in the streamer tip, while the external field has only guiding influence. This leads to strong branching and enables the streamer to propagate into low field regions as the streamer tip locally carries its own field necessary for its advance. Streamer propagation stops at an external field of ~ 500 Vcm^{-1}.

If a voltage above the corona onset voltage is applied to a gap, the streamer starts with subnanosecond delay and propagates towards the cathode with a speed that reaches values of up to 10^9 cms^{-1} and decreases with distance from the point. Breakdown is initiated if the streamer of sufficiently high tip potential reaches the cathode, leading to electron emission and triggering off a retrograde ionising wave, known as the return stroke (Bergmann, 1980).

4.4.2 Negative point coronas

Avalanches which start near the corona point propagate into a region of decreasing field. If they can reach critical amplification a negative streamer (similar to the anode-directed streamer) is formed. Secondary avalanches are started ahead by photo-ionization and develop in the space-charge-enhanced field of the propagating streamer. The avalanches follow the field lines and repel each other, leading to a feather-like, diffuse appearance. Negative streamers depend to a much greater extent on a strong external guiding field, their range is therefore generally smaller and they show less tendency to form branches than the corresponding positive streamers. Negative coronas have a slightly higher starting voltage. Their maximum propagation speeds are comparable to those of positive streamers with the difference of an accelerated development as they approach the plane anode. When the negative streamer approaches the anode, positive retrograde streamers start from the anode

leading to a rapid breakdown when they reach the oncoming negative streamer (Bergmann, Thesis,1980).

An example of this type of corona discharge occurred when the corners of the bottom plate of the laser caused considerable arcing to the ground plate as we should see in the later chapters. Due to the high electric field at the sharp corners, feather-like streamers could be seen and this phenomena resulted in great energy loss as a result of which, the laser was not lasing. The corners had to be rounded off.

4.4.3 Point-to-point coronas

In symmetrical point-to-point gaps essentially the same phenomena occur at the respective electrode as discussed above. Breakdown will be initiated at the positive point because of the lower onset voltage. Distributed ribbon-like corona discharges consisting of a large number of filamentary channels can be produced by fast rising voltage pulses applied across strip electrodes. These discharges have been used for the excitation of high-pressure gas-discharge lasers (Bergmann *et al.*, 1975).

4.5 Pulsed surface discharges

If a dielectric surface is placed across the discharge gap, the static breakdown voltage is reduced considerably because of field enhancement at the insulator-electrode junction. Breakdown across the dielectric surface proceeds in two stages. Initially a weak predischarge travels across the surface, which transforms into an arc once the gap is bridged. During the predischarge the dielectric has little influence on the discharge development and the phenomena are dominated by ionization processes in the gas.

In the second stage, the radiation from the spark heats the dielectric surface leading to rapid evaporation of the substrate and increased conductivity near the surface. The plasma is drawn to the substrate leading to increased surface evaporation and spreading of the discharge along the surface.

The cross-section of the surface spark is reduced by up to ten times as compared to that of the free spark which leads to an increased current density and subsequently higher temperature of the plasma. Surface sparks emit therefore light pulses of significantly higher intensity and due to electron-ion recombination at the dielectric surface, of shorter duration than free sparks. Such sparks have been used extensively for spark light photography (Frungel, 1965). The high plasma temperature leads to strong emission in the ultraviolet, which can be further enhanced by choosing dielectrics with constituents possesing strong emission lines in the UV. These facts make surface sparks, especially across ceramics, efficient light sources for the far UV.

The development of the initial predischarge can be enhanced significantly by using an electrode arrangement as shown in Figure (4.5.1).

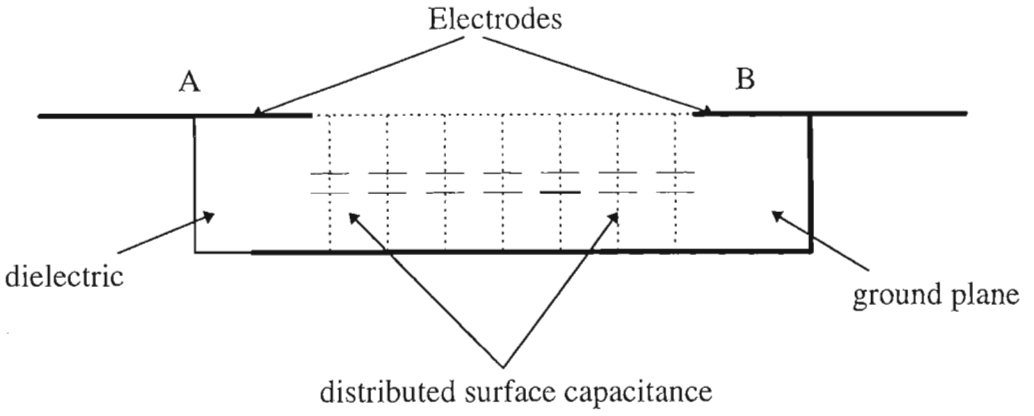

Figure (4.5.1): The development of an initial predischarge.

If a high-voltage pulse is applied to electrode A, a strong voltage gradient develops in the immediate vicinity of the edge due to capacitive coupling of the surface to the ground plane. Avalanche multiplification in the enhanced field leads to streamer formation as in the case of the point corona discharge. The streamers propagate in the strong field between the streamer tip, which assumes essentially electrode potential and the surface ahead which is held at ground potential, leading to strong ionization and propagation velocities of up to 3 x 10^8 cm s^{-1}. Because of their similarity to corona discharges these predischarges will be called surface coronas. The formation and distribution of these discharges depend strongly on the rate of rise of the applied voltage pulse and on the magnitude of the distributed surface capacitance.

The strong electric field and high ionization at the streamer tip lead to the emission of strong UV radiation, which together with the nanosecond formation of these discharges make them especially suited for use as preionization sources in high-pressure gas discharge lasers (Hasson and Bergmann, 1976).

4.6 Flat-plate Blumlein pulser

The Blumlein pulser, described by Shipman (1967) and Anderson (1971), is the transmission-line equivalent of the LC generator. However compared with the latter, the Blumlein pulser can provide significantly faster excitation pulses than those obtained from the LC generators (Bergmann, 1980).

The basic circuit is shown in Figure (4.6.1). Both transmission lines, the pulse-forming line Z_1 and the storage line Z_2 are charged in parallel through R_1 and L_1 to the voltage V_0. Initially the voltage across the load R_l is zero. When the spark gap S is switched, line Z_1 is shorted and a zero going voltage pulse travels down the line with a speed v given by equation

$$v = \sqrt{(1/L_0C_0)} = c/\sqrt{\varepsilon_r} \qquad (4.6.1)$$

where c is the speed of light

ε_r is the relative permitivity of the dielectric

In the case of the parabolic laser, the relative permitivity of the pc board is approximately 4.57 (a detailed calculation is given in Chapter 5). Therefore, speed v is 4×10^{8} ms^{-1} which is approximately half the speed of light.

If the load resistance is assumed to be infinite initially, the voltage pulse is doubled at the open end to $-V_0$ as Z_2 is still charged to $+V_0$ (the inductance L_1 effectively isolates both lines) a voltage of twice the charging voltage will appear across the load. The rise time of the voltage pulse can be expressed by equation (4.1.3), substituting Z_1 for Z_0. The matched condition is $R_l = Z_1 + Z_2$ as both transmission lines are connected in series with the load. Peak voltage at the load is given by

$$V_l = V_0 \tag{4.6.2}$$

$$i_l = V_l/(Z_1 + Z_2) \tag{4.6.3}$$

where i_1 is the current through the load resistance.

The duration of the current pulse is twice the propagation delay time of the shorter line (see equation 5.6.7 p. 72). For the ideal Blumlein system with $l_1 = l_2$, $Z_1 = Z_2$ and a matched load, a single voltage pulse will appear across the load. Subsequent line reflections are cancelled out because of the symmetric set-up where pulses on the pulse-forming side are reflected at the shorted spark gap end, while pulses on the storage line will reverse polarity due to reflection at the open end. For practical Blumlein systems the spark gap impedance may be significant compared with Z_0. This assymetry will result in successive reflections across the load (Bergmann, 1980).

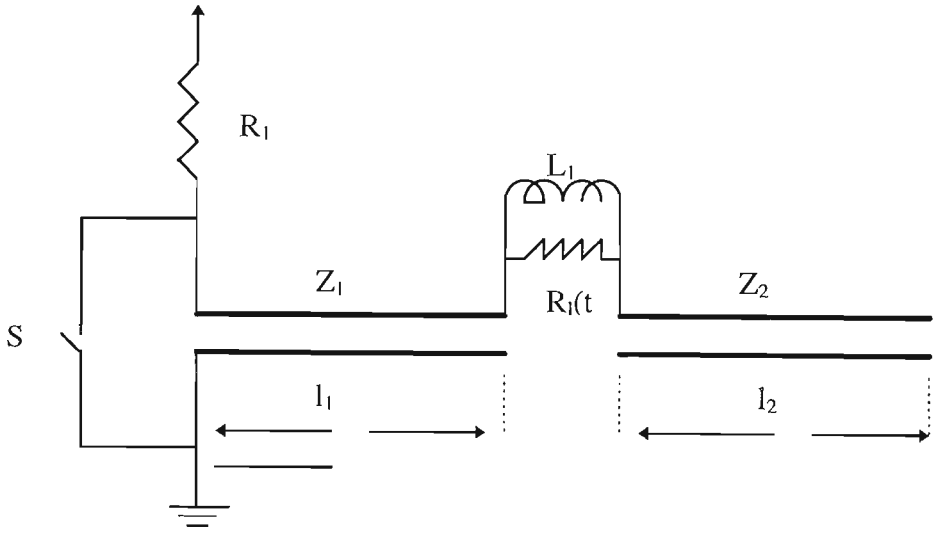

Figure (4.6.1): The circuit diagram of Blumlein pulser.

Higher energy storage can be obtained by operating two Blumlein pulsers in parallel as indicated in Figure (4.6.2). The double Blumlein sytem has half the impedance of a single line and has the safety feature that the outside plates can be grounded (Basting

et al., 1972). Several pulsers of this design with storage capacities ranging from 0.1 - 30 nF and charging voltages of up to 50 kV were being built by H.M. Von Bergmann.

A multi-layer laser is made to increase the energy storage in our case as we will see later. Several layers of aluminium foil are connected to the bottom plate of the laser and all of them discharge into a single laser channel. There, only one Blumlein pulser is being used.

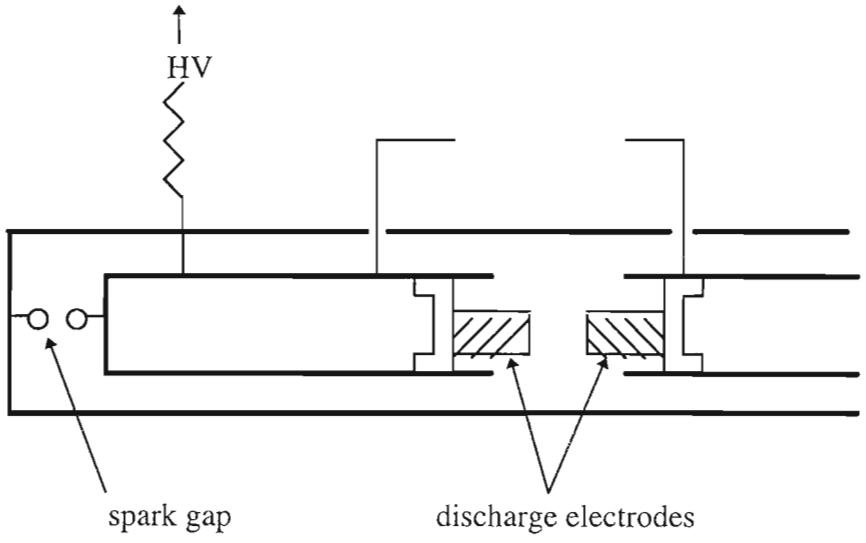

Figure (4.6.2): Two Blumlein pulsers in parallel.

The single line Blumlein pulser has the following characteristics:

(a) Capacitance = 4.97 nF.
(b) Separation between top and bottom plates = 0.5 mm.
(c) Charging voltage = 17 kV.
(d) Width of plates = 30 cm

Therefore, the approximate energy storage of a single line pulser is 0.65 J. Using the equations ((5.6.2) - (5.6.4) (p 70)), the series inductance, the distributed shunt capacitance and the characreristic impedance are calculated for the parabolic laser.

Since $L_0 = 12.5$ b/w nH cm^{-1}

$$L_0 = \{(12.5)(0.05)\}/(30) = 0.021 \text{ nH cm}^{-1},$$

$$C_0 = 0.0886\, \varepsilon_r \text{ w/b pF cm}^{-1}$$

$$= 242.94 \text{ pF cm}^{-1},$$

and, $Z_0 = 377/\sqrt{\varepsilon_r}$ b/w Ω

$$= 0.294\ \Omega$$

where b is the separation of plates
w is the width of plates

As can be seen above the impedance is much greater than that of a single line pulser compared to a value of 0.1 Ω for a double Blumlein pulser.

4.7 Summary

For efficient transfer of electrical energy at high voltages in nanoseconds time scales, low-inductance spark gaps are required. Due to the short inversion lifetimes in N_2 lasers, these spark gaps are more suitable and they are also easy and affordable to construct. In most of the experiments, described in the following chapters, the N_2 lasers constructed used self-triggered pressurized spark gaps. In addition, these spark gaps could be digitally triggered which lead to a constant electrical energy transfer to the lasers. The theory on spark gaps given in this chapter gave a thorough understanding of the mechanisms involved in these delicate nanoseconds switches which helped in optimizing the performance of the lasers. Very simple free-running spark gaps, triggered by overvolting were also constructed by the author. They are easier and more affordable to construct than the pressurized ones. However, they do not keep a contant voltage because of their erratic performance. These spark gaps are believed to have a higher inductance which can be of the order of μH. The understanding of corona discharges is also important since there are several corona mechanisms occurring in N_2 lasers especially in the discharge channel and in the pre-ionization techniques used to initiate a discharge. In the later sections, we will see that there were many instances when the lasers were not lasing because of corona discharges taking place at several points in the lasers. Finally, the flat Blumlein pulser is described together with some calculations on the characteristics of a single pulser.

CHAPTER FIVE

5.0 THE PARABOLIC NITROGEN LASER

5.1 Introduction

A parabolic nitrogen laser was first built by Bruno Godard (1974). The parabolic Nitrogen laser operates under the same principle as the N_2 laser previously discussed. In other words the same Blumlein circuit is used. However, this time one of the top plates is given a parabolic shape. The spark gap is fixed at the focus of the parabola. The Blumlein circuit is charged slowly to a given voltage. At a given time, the spark gap short-circuits the charged flat-line and thereby generating on each side of the line a circular wavefront centered on the focus of the parabola. After reflection from the edges of the parabola, these waves are converted into plane waves. As they arrive at the laser channel, they excite the gas molecules which are inside and laser light is produced at both ends of the channel. Since the latter is inclined at an angle α, the intensity of UV light from the lower end is higher. Details for the calculations of that angle are given later. A water wave simulation experiment was carried out by the author to confirm that the parabolic configuration does convert circular waves into plane waves. Several N_2 lasers were constructed by the author with the help of vacation students. All of them are similar in design but parameters like inclination angle of laser channel, area of plates, spacing between the plates and flow of N_2 gas were varied in order to observe their effects on the laser output. The first N_2 laser which was built had the laser channel inclined at an angle of 20^0 to the horizontal which was about 25 % off the correct angle. Figure (5.1.1a) shows a schematic diagram of the parabolic N_2 laser that was built and Figure (5.1.1b) shows a picture of the laser.

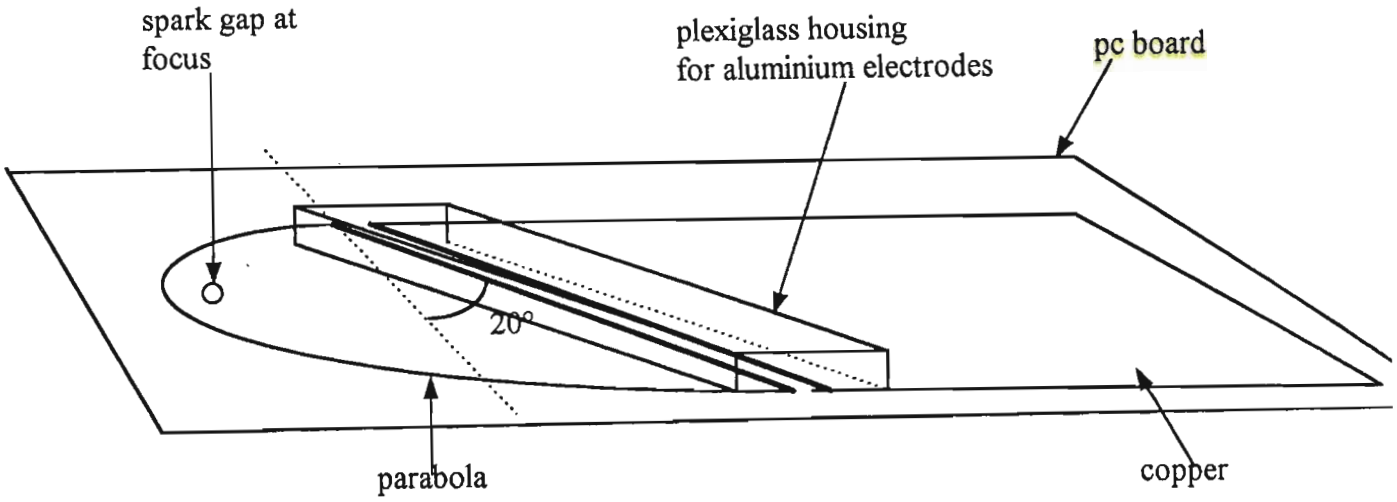

Figure (5.1.1a): The parabolic N_2 laser.

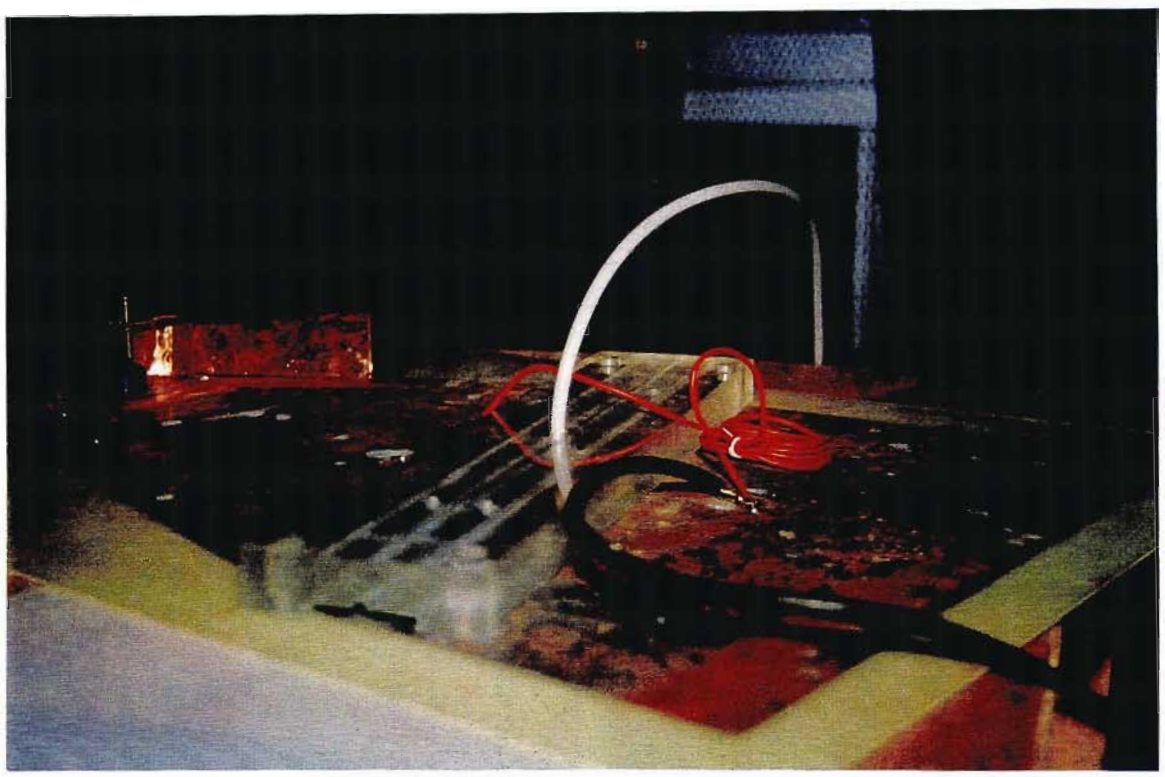

Figure (5.1.1b) : Picture of the parabolic laser.

5.2 Understanding the conversion of circular waves into plane waves

The use of a parabolic shape might be obvious but it is important to know how the circular waves get converted into plane waves on reflection at the parabolic edges. This leads us to the properties of a parabola.

Consider a parabola P (Figure 5.2.1b) with the focus F and directrix D. Also consider a point M on the parabola. The parabola is defined in the folowing way:

$$M \in P \Leftrightarrow MK = MF \qquad (a)$$

where K is the projection of M on D

By drawing an arc with center M and radius FM and taking another point M′ on P, M and M′ are joined (Figure 5.2.1a). Then we let M′ tends to M while M is kept fixed. By definition, M and M′ are the centres of circles passing through F and tangents at K and K′ at D. The common axis of these two circles passes through F, the middle of KK′ and is perpendicular to MM′. Thus we have KK′ < MM′, while M tends to M, the point K′ tends to K and I. The line FI has a limit which is FK and the line MM′ which is perpendicular also has a limit. Therefore, this proves that there exists a tangent at any point on a parabola.

The above analysis shows that the tangent at M is the perpendicular from M to FK (refer to Figure 5.2.1c). The triangle FMK is isoceles and the mediator MT is also the bisector of the angle FMK. This proves that a wavefront propagating in parallel to the axis of the parabola is reflected to the focus. Similarly, a wave originating at the focus is reflected in parallel to the axis. The other important point is that the reflected waves are converted to plane waves bearing in mind that the waves propagate at the same speed and the distance travelled by each wave is the same after being reflected.

Considering Figure (5.2.1b), D′ is the line perpendicular to the axis of the parabola. We have to show that

$$M'F + M'A = MF + MB$$

As mentioned earlier, M and M′ are two points on the parabola and K, K′ are their projections respectively on the directrix of the parabola. A and B are the intersection points of the parallel reflected waves with the line D′.
Using the property of the parabola,

$$MK = MF \text{ and } M'K' = M'F$$

Graphically we have (refer to Figure 5.2.1b),

$$MK + MB = M'K' + M'A$$

From the relation (a), we have

$$MF + MB = M'F + M'A$$

Therefore the circular waves originating at the focus are converted into planes waves on reflection at the edges.

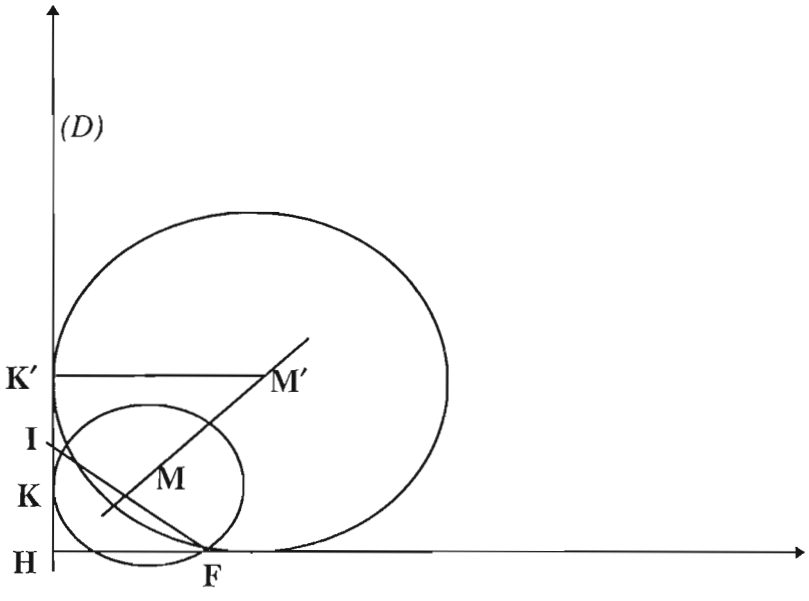

Figure (5.2.1a): The geometrical construction.

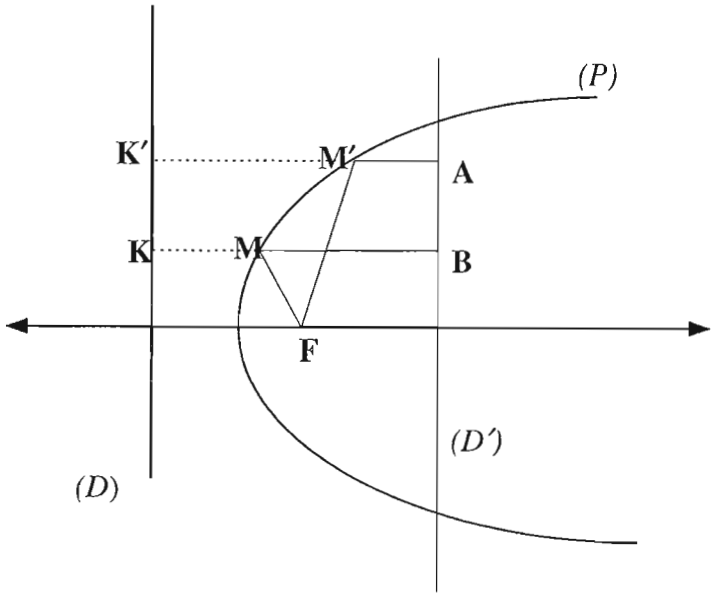

Figure (5.2.1b): The parabolic geometrical construction.

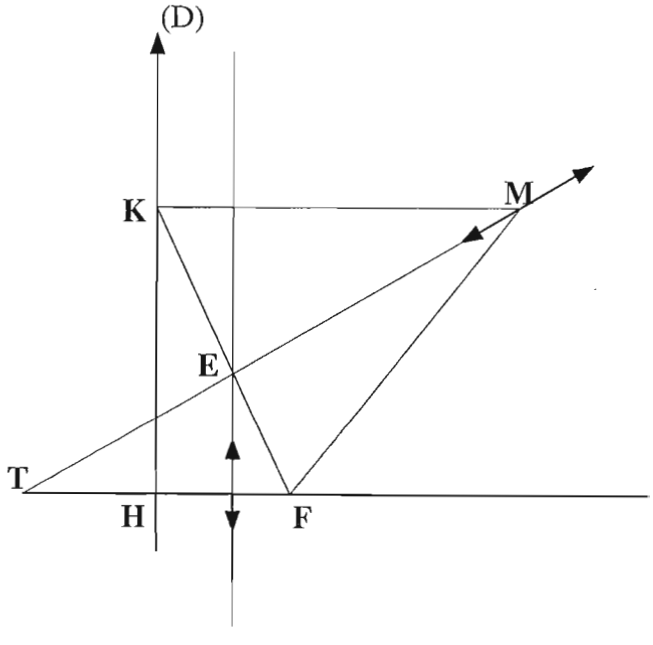

Figure (5.2.1c): Property of a tangent of a parabola.

5.3 Water Wave Simulation experiment

A water simulation experiment was carried out using a ripple tank arrangement (Figure 5.3.1) to understand how the waves propagate after reflection at the parabolic egde. The equipment used for this experiment was a ripple tank, a small d.c motor, a 12 V power supply, an electrical stroboscope, and a video camera.

A thin transparent plexiglass plate of dimensions (20 x 15 x 2 cm) smaller than the size of the ripple tank was taken. Using graph paper, a parabola was drawn on it. The location of the focus was precisely drawn. The plate was cut in such a way so as to simulate the propagation of the travelling waves that occur on the top plate of the actual parabolic laser. In order to simulate the reflection of circular waves at the edges of the parabola, a long strip of rubber was glued on the parabolic trace drawn on the plexiglass so that on hitting this barrier the circular waves created at the focus are being reflected and converted to plane waves. The simulation of the inclined laser (refer to Figure 5.3.1) channel was done by cutting the plexiglass at an angle as shown in the picture below. The conversion of circular waves launched from the focus into plane waves reflected off the parabola was observed for single waves. These could be launched by dipping a small object, e.g. a finger, into the water at the focal point. It was also observed that there were no reflections from the inclined edge; this is because the water is deeper beyond the edge and water wave reflection from such discontinuities is weak. This is analogous to the electrical discharge wave being absorbed at the electrodes. Having observed the behaviour of single waves, the experiment was repeated with a vibrating bead immersed in the water. The bead is attached to a small d.c motor with an eccentric wheel as seen in the picture in Figure (5.3.1).

As can be seen in Figure (5.3.1), the disturbance was generated by the d.c motor at the focus of the parabola. A circular wavefront was generated at the focus and after reflection at the edges of the parabola, the circular waves were converted into plane waves. In order to prevent the circular waves formed in the central region from interferring with the plane waves an obstacle (a strip of copper foil bent into a triangular shape) was placed near at the focus.

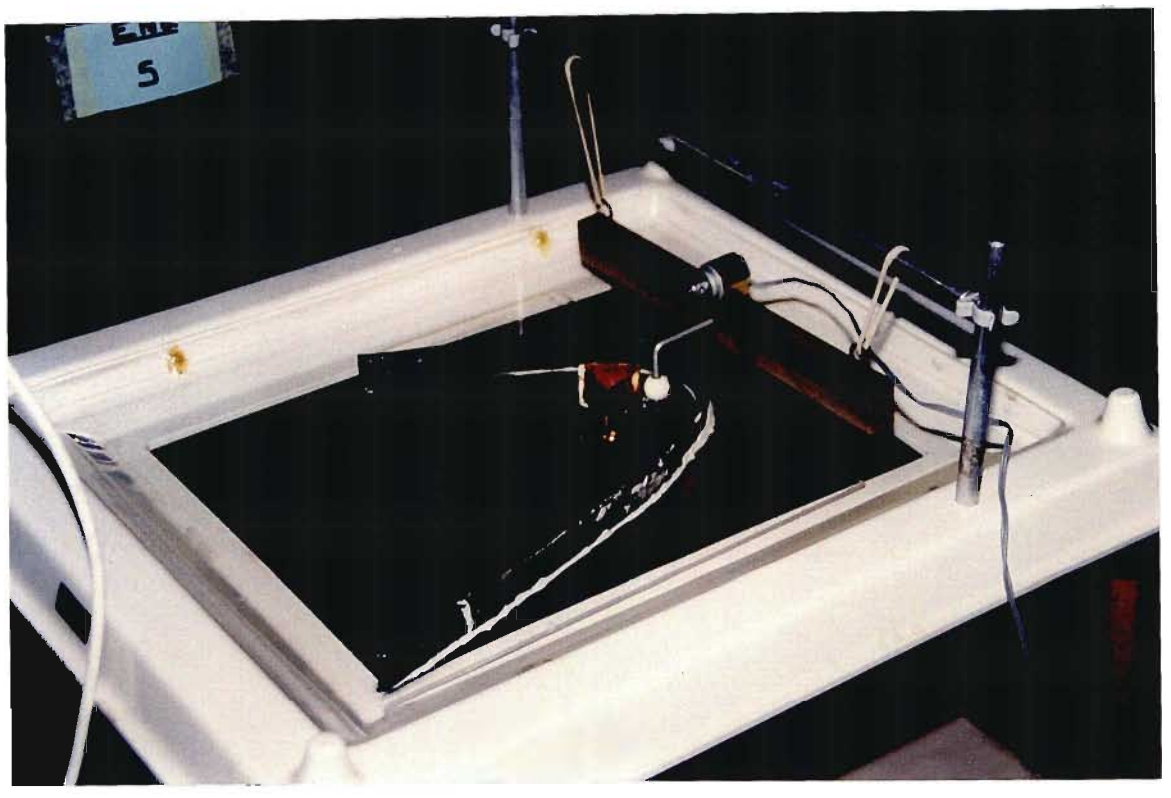

Figure (5.3.1): The ripple tank for water wave simulation.

Circular waves were generated at the focus and the speed of the motor was varied until the desired effect was observed which was the creation of circular waves at the focus, reflection at the edges then conversion to plane waves propagating towards the inclined edge. It was also observed that there were some circular waves in the central region near the focus which were propagating away from the focus and also plane waves on the other side of the focus which was due to the reflection at the top edge. When the source was slightly off the focus, plane waves could not be seen and only circular waves could be observed. A stroboscope was used whose frequency could be varied depending on the frequency of the propagating waves and this was used to 'freeze' the waves so that they could be filmed.

The film was played back on a video machine connected to a computer with a frame grabber sofware. The appropriate frames were selected and modified by changing certain parameters in the software program to improve the resolution. The following pictures (Figures 5.3.2-5.3.4) show the propagation of circular and plane waves with the source at the focus and others show the propagation when the disturbance was not at the focus. The reflector which reflected the circular waves created in the central region, was placed a few cm below the focus.

As can be seen in the picture below there are circular waves formed and some plane waves only at the focus because of the reflection of circular waves at the top edge.

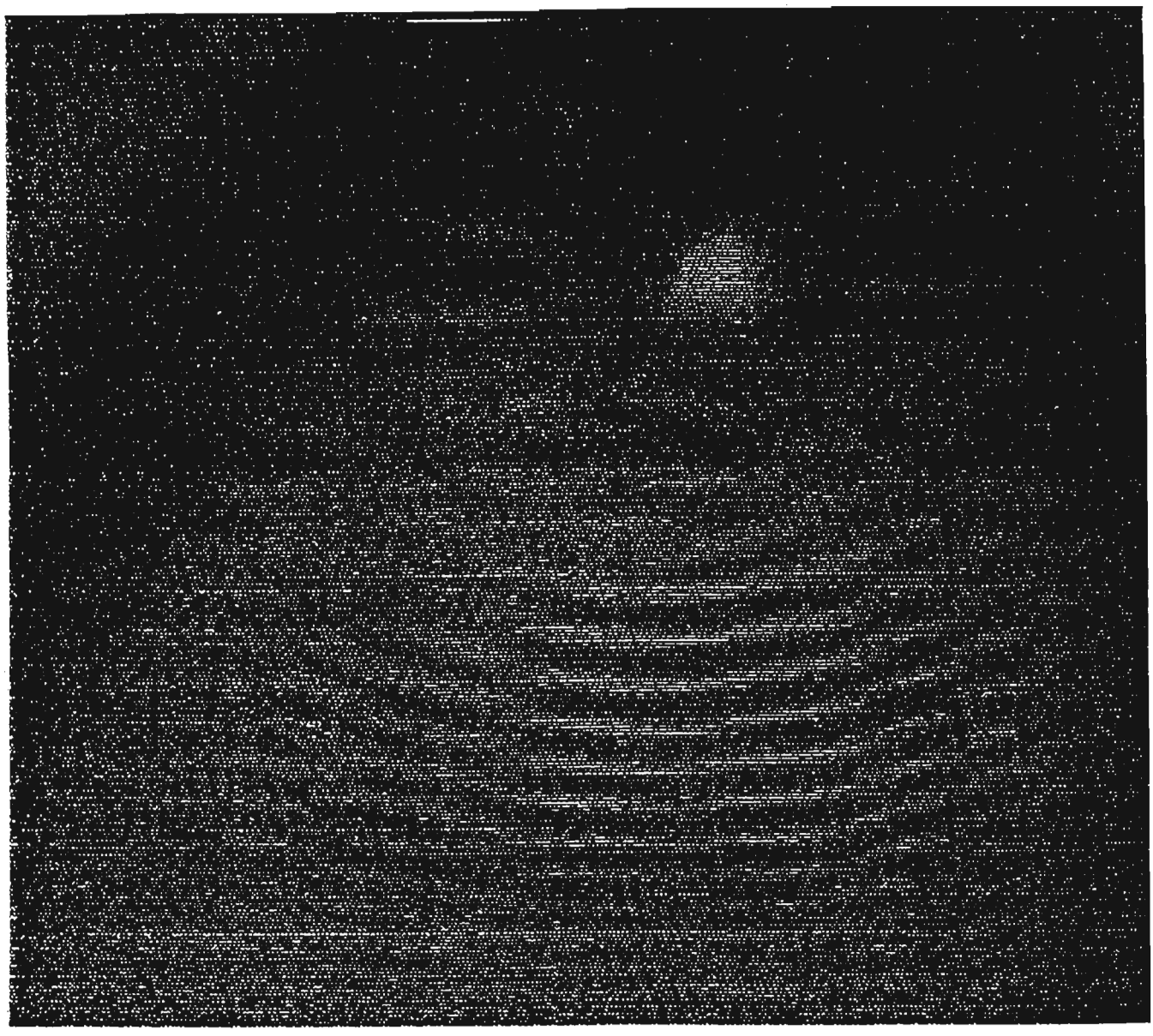

Figure (5.3.2): Source not exactly at focus and without the reflector.

As can be seen in the picture below there are only plane waves formed and almost no waves in the central region.

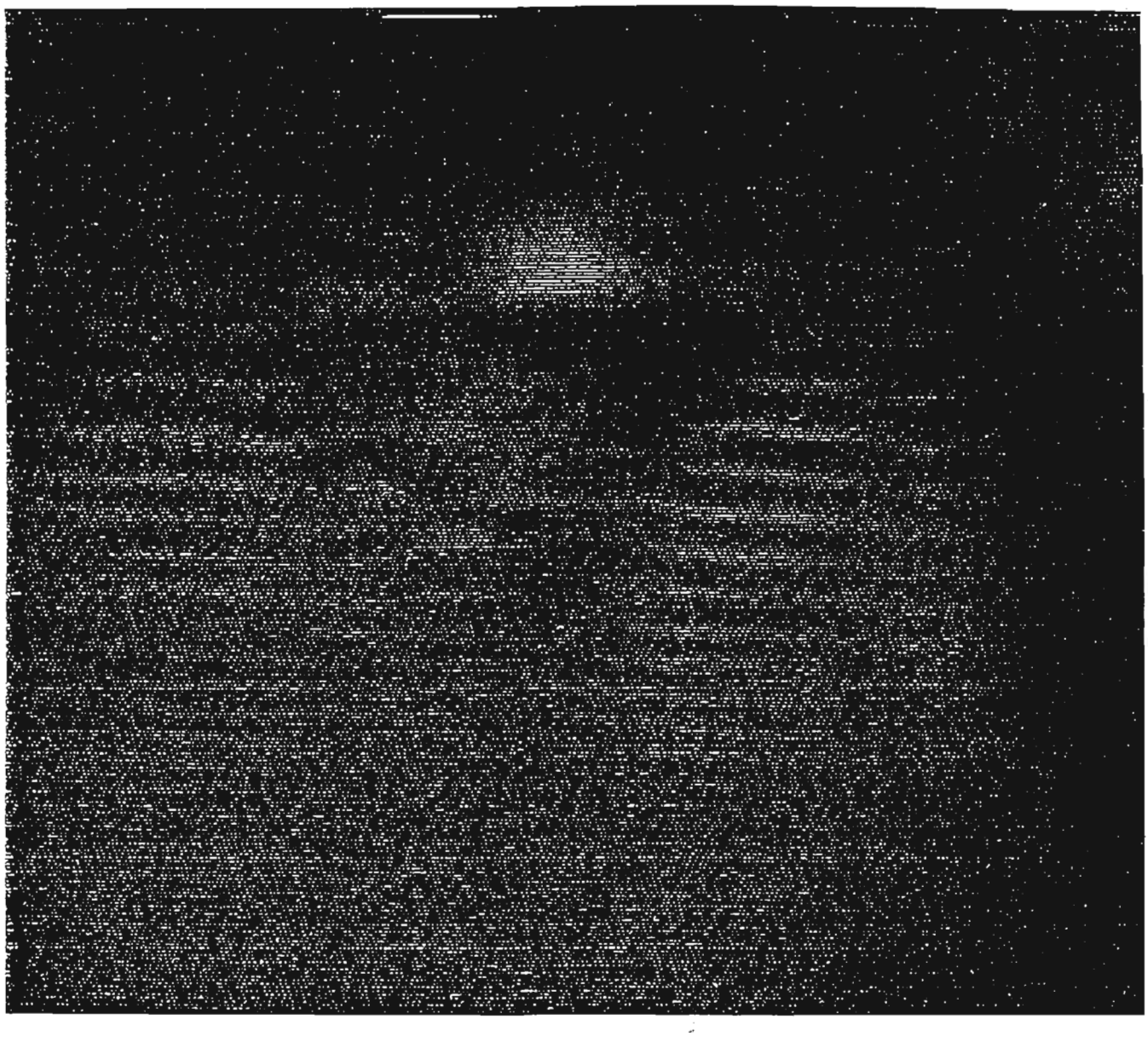

Figure (5.3.3): Source at the focus with a large reflector.

In the picture below one can again see clearly the plane waves but there was some formation of waves in the central region which is not visible here.

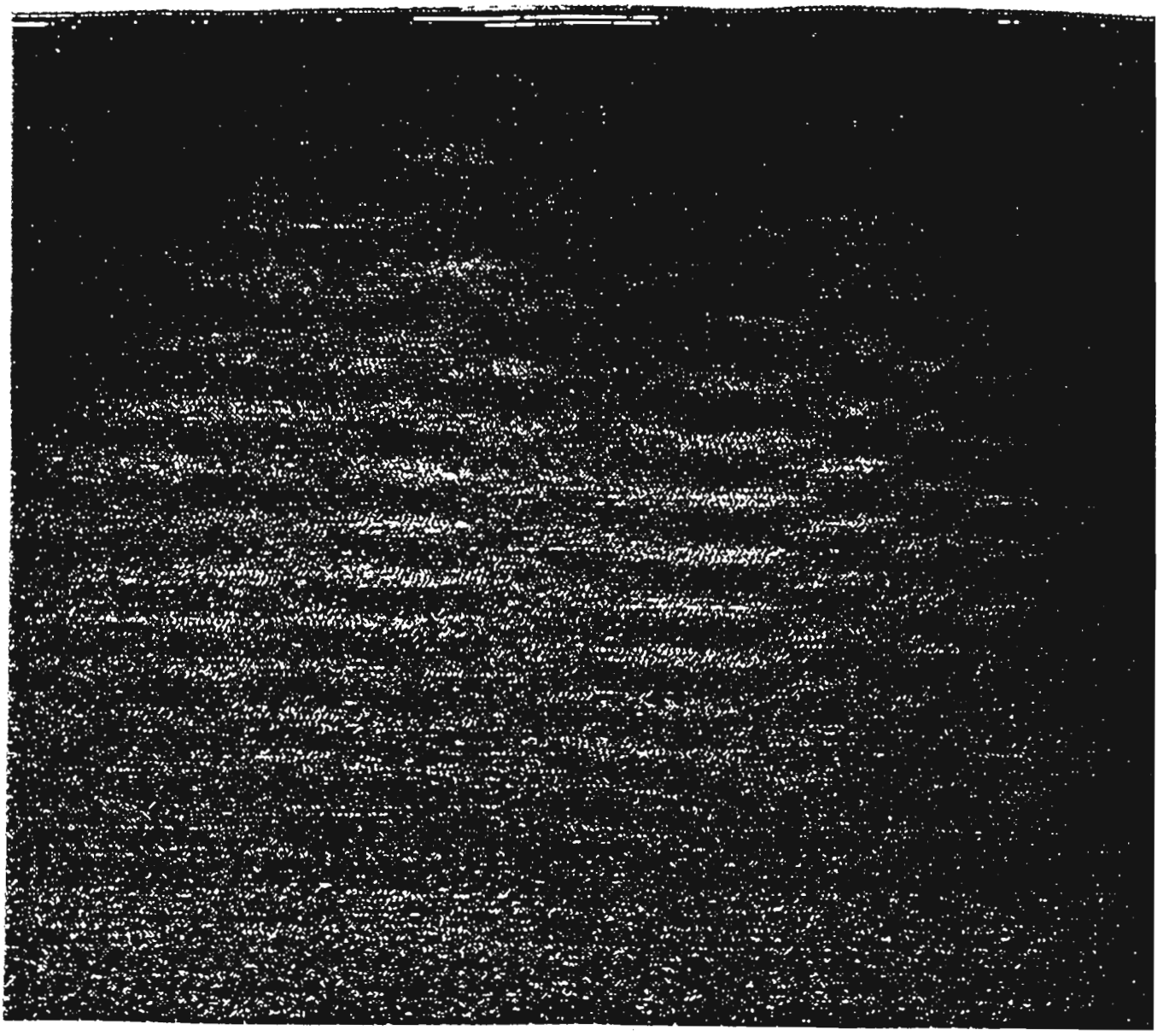

Figure (5.3.4): Source at the focus with small reflector.

The precise location of the disturbance source at the focus of the parabola is of critical importance otherwise the circular waves originating at the focus will not be converted to plane waves as can be seen in the pictures (Figure 5.3.2) above. In addition, a barrier or reflector should be placed infront of the focus in order to prevent the circular waves created at the central region from reaching the laser discharge channel. As shown above, in the ripple tank experiment, a barrier is placed close to the focus and on the other hand, a small section is etched out infront of the spark gap in the actual parabolic laser. The location of the spark gap at the focus and the barrier are very important for the parabolic shape to be efficient and thus, to achieve a higher energy output compared to that of the rectangular shaped nitrogen laser.

5.4 Construction of the Parabolic Nitrogen laser

The parabolic laser was constructed using double copper-clad board of thickness 1.5 mm. A large sheet of the pc board was cut and an appropriate parabola was chosen to fit (specifications of parabola given later). The parabola with the focus in the right position was first drawn accurately on a large sheet of graph paper. By placing this drawing on the pc board, the parabola was traced and the focus was located precisely in its position on the board. The laser channel which was approximately 2 cm wide was traced on the copper at an inclination angle of about 20^0 with the horizontal. The explanation for that particular angle will be given shortly. In order to prevent the lower and upper plates from arcing, the copper on the sides of the board were etched with hydrochloric acid. The laser channel where the discharge occurs was also etched. The parts which needed no etching were sprayed with a black paint so that the acid would not react with the copper in those regions. A wooden container to support the laser was made. A plastic sheet was placed inside the box to contain the acid. Finally, each side of the board was dipped in the acid. It took approximately 20 mins for all the copper on each side to be etched. After etching one side, the board had to be washed with water to remove the remaing acid on the surface. The acid had to be changed from time to time because the reaction of the acid with the copper was slowing down due to the formation of copper chloride. A small circle was also etched at the focus of the parabola. The electrodes were aluminium strips fixed on a plexiglass housing and the spacing between them could be adjusted. Figure (5.4.1) shows a schematic diagram with dimensions.

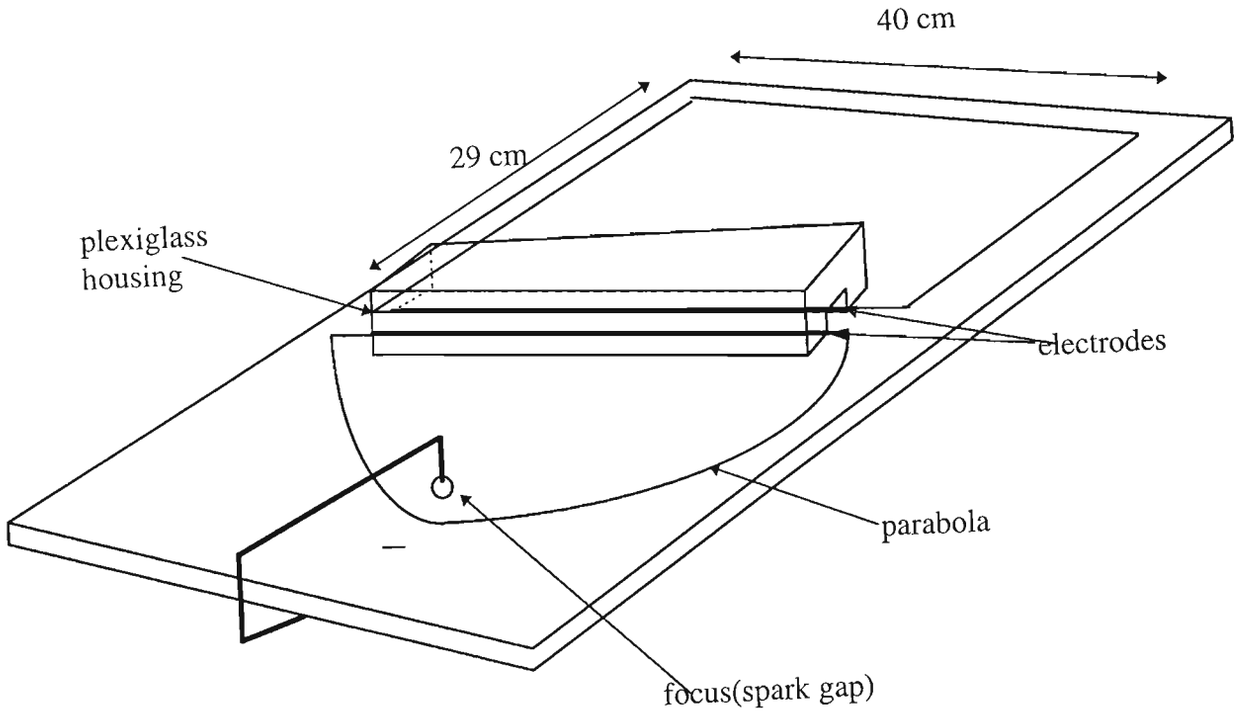

Figure (5.4.1): Construction of the parabolic laser.

The dimensions and specifications of the parabolic laser were as follows:

The equation of the parabola is:

$Y(X) = 1/10(X^2 - X)$

A computer program (refer to appendix B) was used to draw the parabola with gave the location of the focus and the X, Y coordinates. The program also allowed a graphical representation of the parabola. This software facilitated the drawings of the parabolas required for the contruction of all the parabolic N_2 lasers.

This curve was plotted as mentioned earlier on a graph paper with values of X ranging from -18 to 21.5. The constant in the above equation was taken to be zero due to which it was symmetrical about the y axis.

The surface area of the parabola was 963 cm^2.

Width of the laser channel: 2 cm

Angle of inclination of the electrode $\approx 20^0$

Total surface area of copper(top plate) ≈ 1842.52 cm^2

Total capacitance: 4.97 nF

This first parabolic N_2 laser was only constructed to test that the parabolic configuration lases. It was later discovered that the inclination angle of the laser channel was not optimised.

5.5 Inclination angle of the laser channel

In the design of the parabolic laser, the inclination angle of the laser channel with the horizontal is very critical since it affects the laser output. The angle of inclination must be calculated such that the time taken for a plane wave to travel from A along the channel to the lower end C must be equal to the time for a plane wave to travel from B to C (see Figure 5.5.1). This is important to achieve amplification of light along the laser channel and this is done by a mechanism called amplified spontaneous emission. The propagation velocity (v) of the electric wave is given by the relation

$$v = c/\sqrt{\varepsilon} \qquad (5.5.1)$$

where c is velocity of light in vacumm

ε: relative permitivitty of the dielectric

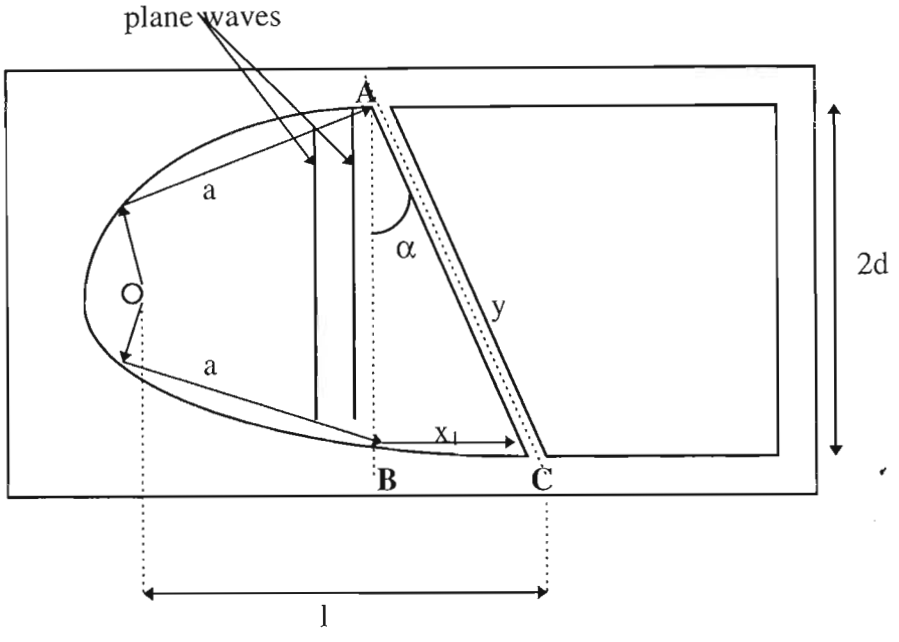

Figure (5.5.1): Slope of laser channel.

Let,
the width of the plate be **2d** ,
the distance from the spark gap to the upper end of the electrode be **a**
the length of the electrode be **y**
the distance travelled by the wave to reach the lower end **C** of channel be **l**
α be the angle of the laser channel with the horizontal

Also let $\mathbf{x_1}$, which is unknown, be the distance as shown in the figure above.

The time taken (t_{AC}) for the light to travel from **A** to **C** is

$$t_{AC} = y/c \tag{5.5.2}$$

Similarly, the time taken (t_{BC}) for the electric pulse to travel from B to C is

$$t_{BC} = x_1/(c/\sqrt{\varepsilon}) \tag{5.5.3}$$

In order to have light amplification along the laser channel the condition below must be satisfied,

$$t_{AC} = t_{BC} \tag{5.5.4}$$

which after simplifying, gives

$$y = x_1\sqrt{\varepsilon} \tag{5.5.5}$$

Considering firstly if the propagating waves were spherical.

By Pythagoras theorem,

$$l^2 = (a+x_1)^2 - d^2 \tag{5.5.6}$$

And,

$$l^2 = [\sqrt{(a^2 - d^2)} + \sqrt{(y^2 - 4d^2)}]^2 \tag{5.5.7}$$

By equating equation (5.5.5) and (5.5.6) and using (5.5.4), we obtain the following polynomial after some simplification,

$$(1 + \varepsilon^2 - 2\varepsilon)(x_1)^4 + 4a(1 - \varepsilon)(x_1)^3 + 4[a^2(1 - \varepsilon) + d^2(2 - \varepsilon)](x_1)^2 + 16ad^2 + 16a^2d^2 = 0 \tag{5.5.8}$$

After entering the parameters **a** and **d**, the above equation can be solved. By calculating the value of x_1, the angle can be found. The solution x_1 is chosen real and positive among the four roots of this fourth degree polynomial. The angle is given by

$$\alpha = \sin^{-1}(2d/y) = \sin^{-1}(2d/x_1\sqrt{\varepsilon}) \tag{5.5.9}$$

However, in the case of the parabolic laser where the reflected waves are plane, the calculation is much simpler and straightforward.

$$t_{AC} = t_{BC}$$

implies

$$x_1/y = 1/\sqrt{\varepsilon} = \sin\alpha$$

which gives

$$\alpha = \sin^{-1}(1/\sqrt{\varepsilon}) \tag{5.5.10}$$

As can be seen in equation (5.5.10), the angle of inclination of the laser channel depends only on the relative permittivity of the dielectric used.

The capacitance of the laser was measured using a capacitance meter. The meter read 4.97 nF. Care was taken to prevent the dielectric from touching any other material because any contact even with the human body can lead to a wrong reading of the capacitance.
Using the relationship,

$$C = (A\varepsilon_0\varepsilon_r)/(b) \tag{5.5.11}$$

where C: capacitance = 4.97 nF
A_1: area of the plate = 1842.52 cm^2
ε_0: permittivity of free space= 8.85 x 10^{-12} $C^2/N\ m^2$

ε_r: relative permittivity of the epoxy fibre glass
b: the distance between the top and bottom plates = 1.5 mm

Substituting the above values in equation (5.5.11) and the relative permittivity of epoxy fibre glass which is found to be, $\varepsilon_r = 4.57$.

Hence, the propagation velocity of the electric wave in the dielectric is

$$v = c/\sqrt{\varepsilon_r} = (3 \times 10^8)/\sqrt{4.57} = 1.40 \times 10^8 \text{ m/s} \approx c/2$$

and using equation (5.5.10)

$$\alpha = \sin^{-1}(1/\sqrt{\varepsilon r})$$

$$= \sin^{-1}(1/\sqrt{4.57})$$

$$= \sin^{-1}(0.4678)$$

$$= 27.89^0$$

Therefore the laser channel must be at an angle of 27.89^0 with the horizontal to achieve maximum laser output.

5.6 Transmission lines

In this section we are going to look at the propagation of electromagnetic waves in the dielectric into more details and the effect of the relative permittivity on the propagation velocity. Figure (5.6.1) shows the variation of laser channel inclination angle with relative permittivity. This relation was obtained in the previous section.

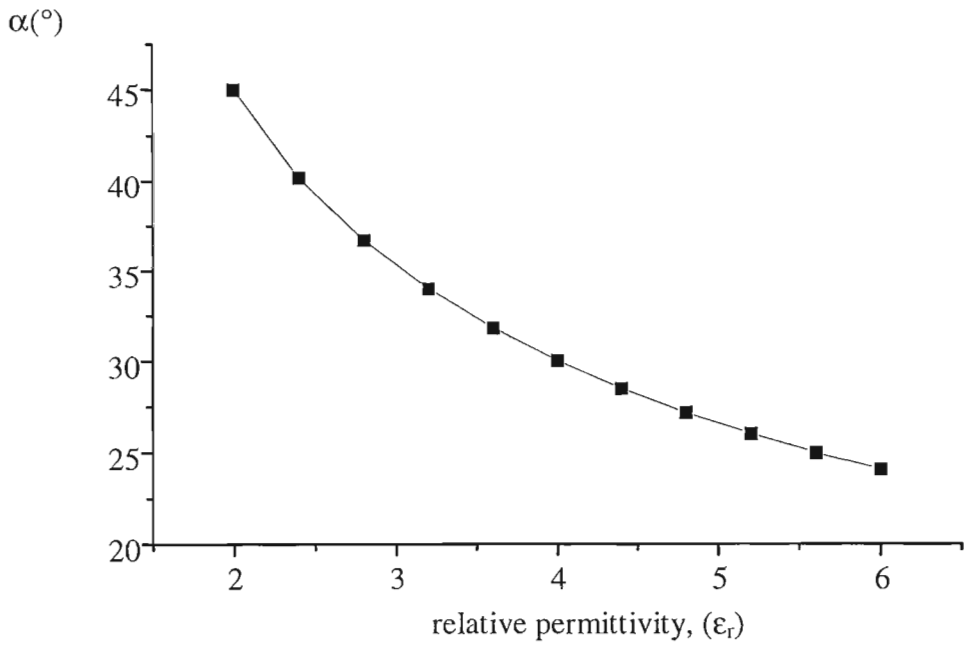

Figure (5.6.1): The dependence of laser channel inclination angle on the relative permittivity.

In general,the characteristic impedance Z_0 of a flat-plate transmission line with a distributed shunt capacitance C_0 and series inductance L_0 per unit length (refer to section 4.6, p 51) is given by

$$Z_0 = \sqrt{(L_0/C_0)} \tag{5.6.1}$$

Impedances of 0.1 - 1 Ω are required for the transverse excitation of high-pressure gas discharge lasers and in our case an impedance of 0.3 Ω is obtained. The relevant line parameters can be calculated from the following equations (Bergmann, 1980):

$$L_0 = 12.5\ b/w\ nH\ cm^{-1} \tag{5.6.2}$$

$$C_0 = 0.0886\ \varepsilon_r\ w/b\ pF\ cm^{-1} \tag{5.6.3}$$

$$Z_0 = 377/\sqrt{\varepsilon_r}\ \ b/w\ \Omega \tag{5.6.4}$$

where b = separation of plates
w = width of plates
ε_r = dielectric constant

The table (5.6.1) below shows a list of parameters of the various transmission lines (Bergmann, 1980)

Table (5.6.1) : Transmission-line parameters for lines of 1 cm width.

Material	b(mm)	ε_r	L_0 (nH)	C_0 (pF)	$Z_0(\Omega)$	v(x 10^9cm s^{-1})
	3.2		**4.00**	**1.6**	**50**	
Fibreglass epoxy	**1.6**	**5.8**	**2.00**	**3.2**	**25**	**12.5**
	0.8		**1.00**	**6.4**	**12.5**	
Polyester (Mylar)	**0.3**	**3.7**	**0.38**	**10.9**	**5.9**	**15.6**
	0.16		**0.20**	**20.2**	**3.2**	

The solution of Maxwell's equations for an ideal transmission line (Bergmann, 1980) shows that the electromagnetic waves propagate along the line without distortion and with a speed determined only by the dielectric constant ε_r of the medium given by and which was mentioned earlier:

$$v = \sqrt{(1/L_0C_0)} = c/\sqrt{\varepsilon_r}$$

where c is the vacuum speed of light.

The characteristic propagation delay time T_0 per unit length of line is

$$T_0 = v^{-1} = \sqrt{\varepsilon_r}/c_0 \qquad (5.6.5)$$

The propagation delay time T_0 for the parabolic laser is therefore,

$$v^{-1} = (1/1.4 \times 10^8)^{-1} = 7.14 \times 10^{-9} \text{ s m}^{-1}$$

While the behaviour of lumped parameter circuits can be described by oscillations, transmission lines are treated by the concept of successive reflections, which occur at points of abrupt changes in circuit constants (Bergmann, 1980).

If a rectangular voltage pulse of amplitude V is fed into a transmission line terminated by an ohmic load R_l (Figure 5.6.2a), the reflected voltage pulse V_r is given by

$$V_r = (R_l - Z_0)/(R_l + Z_0)(V) \qquad (5.6.6)$$

The incident and reflected pulses will add up to the total voltage at the transition point. The following three cases can be distinguished:

(a) For $R_l = 0$ (short-circuited line) the pulse will be reflected with the same amplitude but opposite polarity and then $V_r = V$ leading to no consumption of energy by the load.

In our case, the incident voltage pulse is about 17 kV and the reflected one is about 12 kV.

(b) For $R_l = Z_0$ (matched termination) there is no reflection and all the energy is consumed in the load.

(c) For $R_l = \infty$ (open-ended line) the pulse will be reflected with the same polarity, and voltage doubling will occur at the open end.

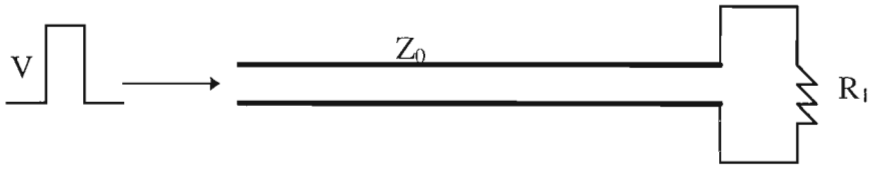

Figure (5.6.2a): Transmission line terminated by Ohmic load.

In the intermediate cases part of the energy is consumed in the load and the pulse is reflected with reduced amplitude.

The basic pulsed discharge circuit employing a transmission line is shown in Figure (5.6.2b). The line of length L_l and impedance Z_0, charged to a voltage V_0 is switched by an ideal switch S into the load R_l.

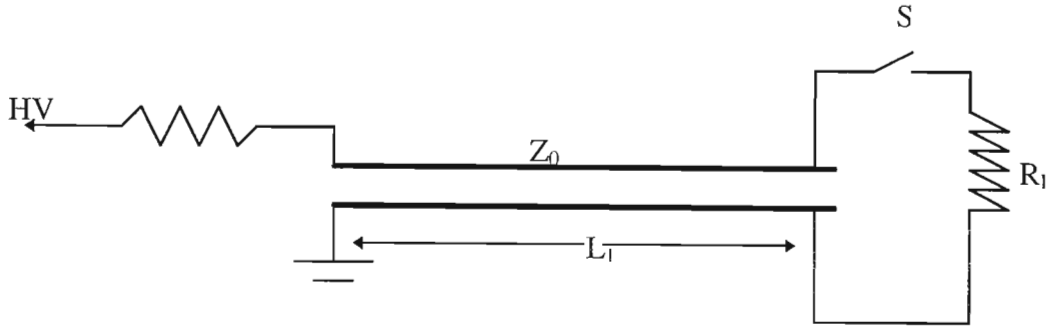

Figure (5.6.2b): Basic pulsed discharge circuit.

The magnitude of the voltage and current pulse at the load is determined by the series connection of Z_0 and R_l. The duration of the current pulse T_l is twice the propagation delay time per unit length of the line and is given by

$$T_l = 2\,T_0 \qquad (5.6.7)$$

$$= 2 \times 7.14 \times 10^{-9}\ sm^{-1}$$

$$= 14.28 \times 10^{-9}\ sm^{-1}$$

The power transfer into the load can be calculated from

$$P_l = R_l/(R_l + Z_0)^2\ V_0^2 \qquad (5.6.8)$$

In our case, R_l, the resistance of the spark gap is approximately $0.3 \pm 0.1\ \Omega$, $Z_0 = 0.29\ \Omega$ as calculated in section 4.6 and the input voltage V_0 is 17 kV. The calculated value of the power transfer is thus 2.4×10^8 W.

Maximum power transfer into the load occurs in the matched case, $R_l = Z_0$. The effect of load mismatch on the power transfer is shown in Figure (5.6.3). The power transfer is 75 % for loads within a factor of three of the matched condition. While in the matched case all the stored energy is transferred to the load in a single pulse of duration T_l, reflections will occur in the non-matched case leading to successive pulses over the load time intervals of $2T_L$

Since the characteristic impedance Z_0 of the parabolic laser is almost equal to the load resistance R_l, we have the matched case where there is the maximum power transfer. In most cases, the variation of the power transfer with the ratio is as shown in Figure (5.6.3c). As can be seen from the graph, a $R_l/Z_0 = 1$ ratio gives the highest power transfer.

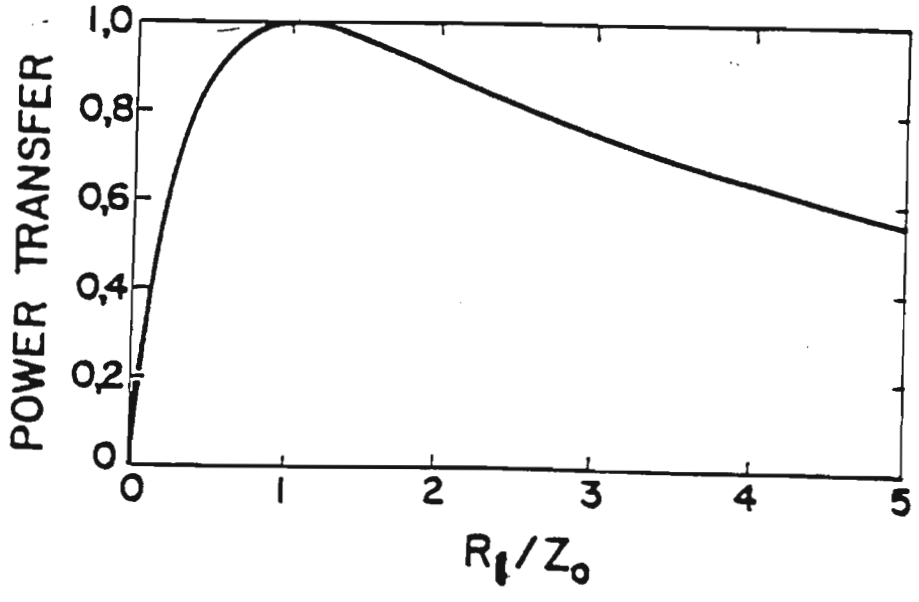

Figure (5.6.3c): Effect of Load mismatch on power transfer (Bergmann, 1980).

5.7 Summary

The theory of the parabolic laser is given and explained. A mathematical derivation is provided which shows that circular waves formed at the focus convert to plane waves after reflection at the parabolic edge. In order to support this fact further, a water wave simulation experiment was performed which showed the same phenomena. In this case, it was observed that the spark gap had to be precisely located at the focus of the parabola, otherwise the parabolic configuration would be inefficient. Moreover, a derivation of laser channel inclination angle for optimum laser energy output is given. It shows the dependence of laser inclination angle with the relative permittivity of the material used. For the ordinary pc board of thickness 1.5 mm, the relative permittivity was calculated to be about 4.57 leading to an inclination angle of about 27.89°, for the highest laser energy output. A few calculations on the transmission line were given which includes the effects of load mismatch on power transfer. In the case of the parabolic N_2 laser, it was found that there is a maximum energy transfer.

CHAPTER SIX

The test of all knowledge is experiment.
(Richard P. Feynmann)

6.0 EXPERIMENTAL

6.1 Experimental Set-up

The Nitrogen laser with the rectangular plates was first tested and the laser signal was detected using a fast vacuum biplanar photodiode with a risetime of 200 picoseconds. At that time, a joulemeter was not available for measuring the laser energy as a result of which in this experiment, the laser intensities were measured in millivolts at both ends of the laser channel. The output of the photodiode was connected to an HP Digitizing oscilloscope. Lenses were used to focus the beam because of its high divergence. Aligning was very important to ensure that the beam passes through the central axis of the lenses and is focused at the center of the photodiode.The set-up, Figure (6.1.1) was as shown below:

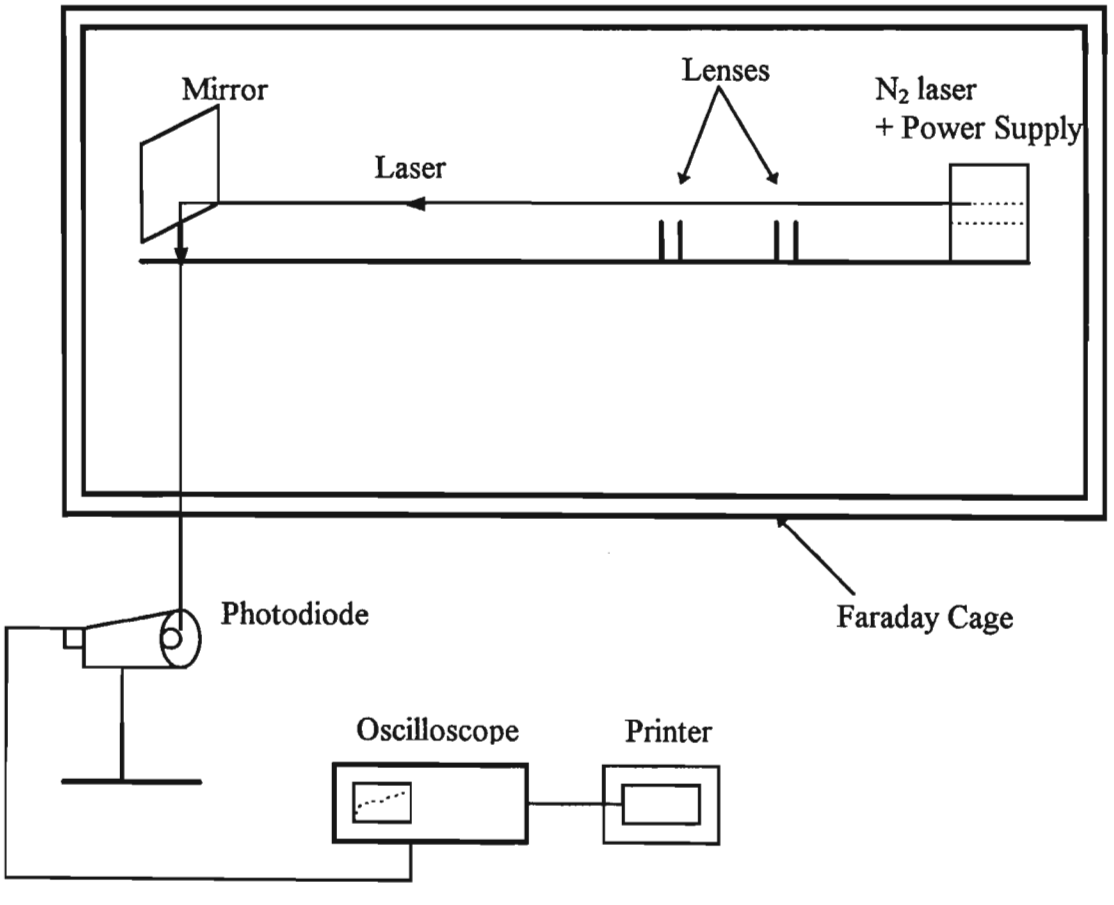

Figure (6.1.1): The set-up for detecting the laser signal.

The oscilloscope was set to a sensitivity of 2mV/divisions and the timebase was set at first to 2ms/div and then to 500 μs/div. Figures (6.1.2) and (6.1.3) below show the print out copies of the laser signals of a single pulse received at different times and timebase settings of 2ms/div and 500μs/div respectively. As one can see the curve is not a smooth one because the photodiode was picking up noises from other nearby electromagnetic sources, e.g the laser and its power supply. The signal received on the oscilloscope was a trace of the laser because when the window of the photodiode was covered with a thick opaque piece of plexiglass, the laser signal could not be seen and on removing it, the signal reappeared on the oscilloscope screen. This confirmed that the trace was not due to noise but due to laser light. Later, we will discuss the ways by which these electromagnetic interference were reduced.

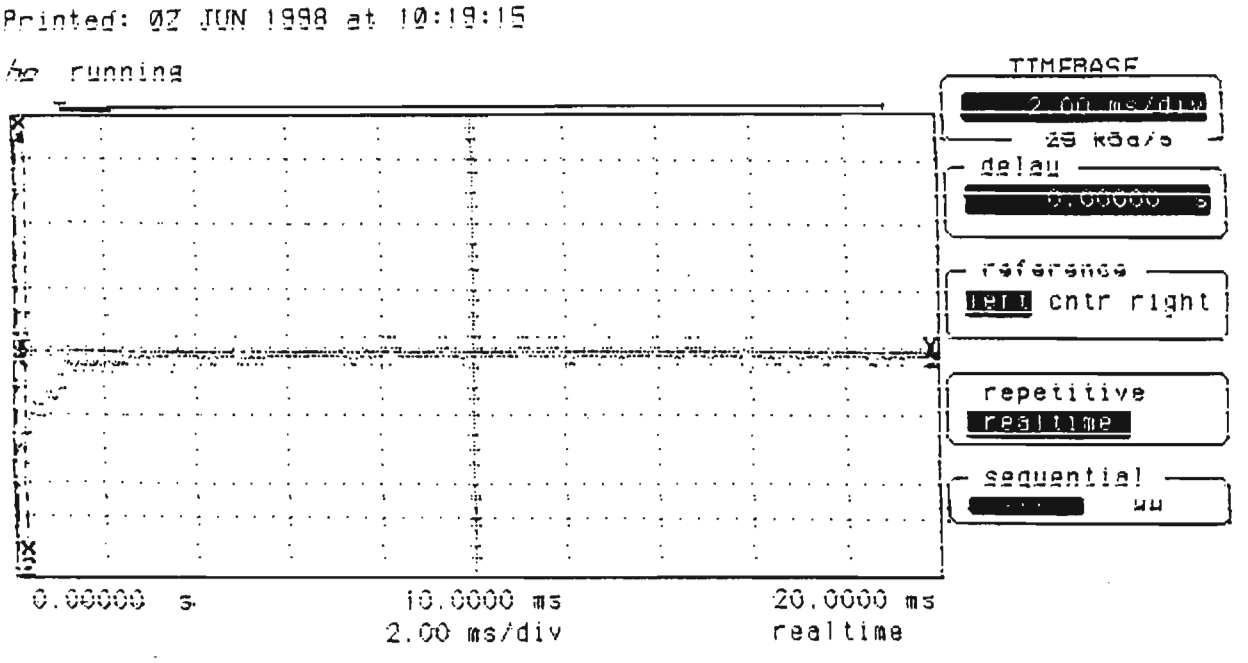

Figure (6.1.2): Trace of laser signal at 2ms/div.

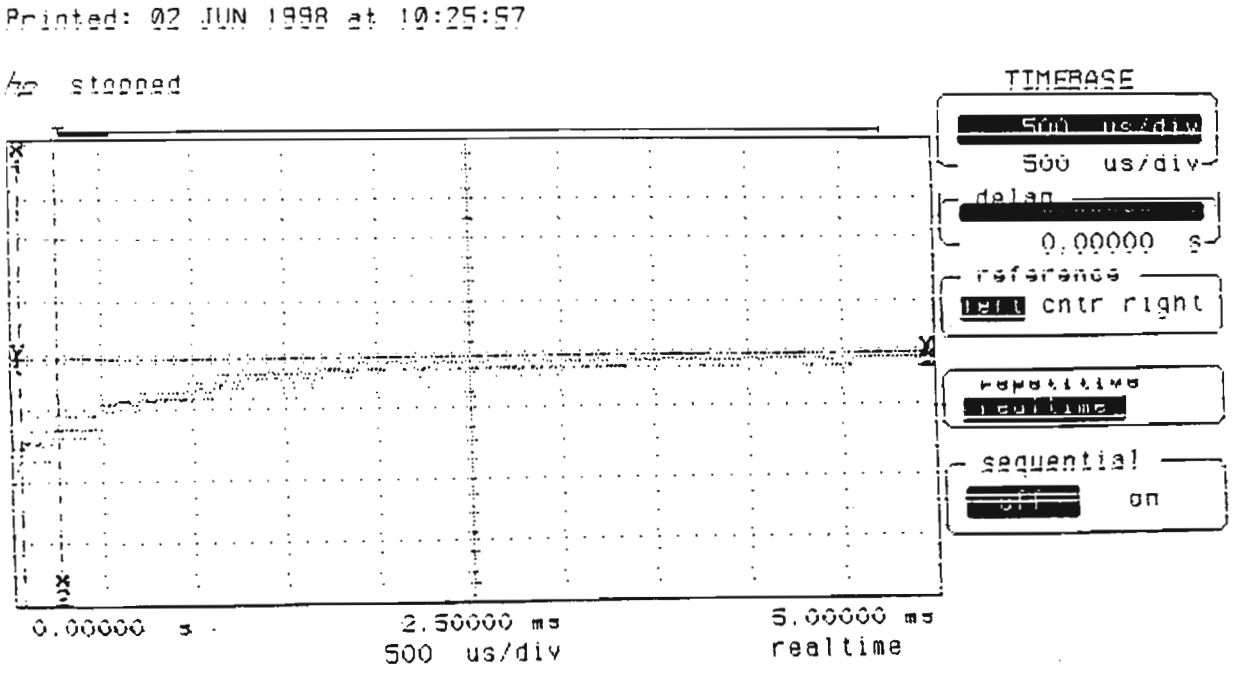

Figure (6.1.3): Trace of laser signal at 500 μs/div.

Figure (6.1.4) below shows a picture of the laser with rectangular plates used for the experiment. As can be seen, the spark gap consists of two electrodes enclosed in a plexiglass housing. The spark gap was self-trigerred and it was screwed with plexiglass screws on the plate. Having holes on the pc board is not actually a good practice since holes are potential regions for arcing between the top and bottom plates. This means that energy is being lost at those points leading to insufficient energy for the laser discharge. Later versions of the laser have the spark gap glued to the plate.

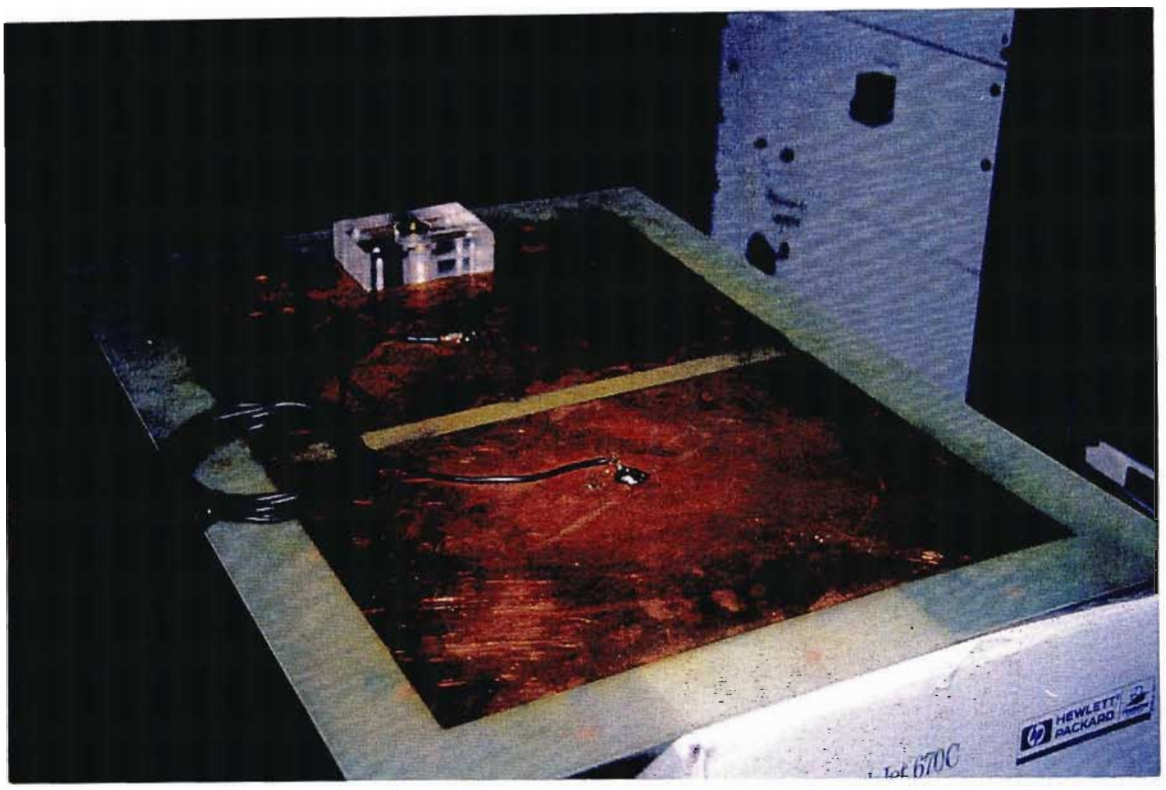

Figure (6.1.4): N_2 laser with rectangular plates (without the electrodes).

6.2 Experimental Investigation of the Parabolic N_2 laser

The same experimental arrangement was used to test the parabolic N_2 laser but it would be wrong to compare the laser signals received on the oscilloscope from the two lasers because parameters such as distance from the detector, the N_2 flow velocity, the level of humidity and input voltage might not be the same in both cases. Figure (6.2.1) below shows a picture of the parabolic N_2 laser connected to a 17.5 kV power supply. As shown, the spark gap was shielded with copper foil to improve the reflection of the waves at the top edge of the parabola and also to reduce magnetic energy losses. There is not enough evidence to say that the shield affects the output of the laser as this remains to be investigated. Throughout the thesis, the low end output is referred to the output from the end of the laser channel which is furthest from the spark gap and the high end output corresponds to the end which is closer to the spark gap (refer to Figure (6.2.2). It should be noted that in the following experiments, the laser was in the Faraday cage and the following steps taken before firing:

(a) Open the N_2 gas cylinder slowly to allow the gas to flow in the laser cavity.

(b) Ensure that there exists no short circuits by checking the connections and circuit and to make sure that the dump stick is connected to ground.

(c) Switch on the power supply and stand at a safe distance from the laser.

(d) Wear safety glasses because of the UV light and wear ear plugs due to the loud noise made by the spark gap.

(e) After each experiment, switch off power supply and discharge the plates (capacitor) of the laser by short circuiting with the dump stick.

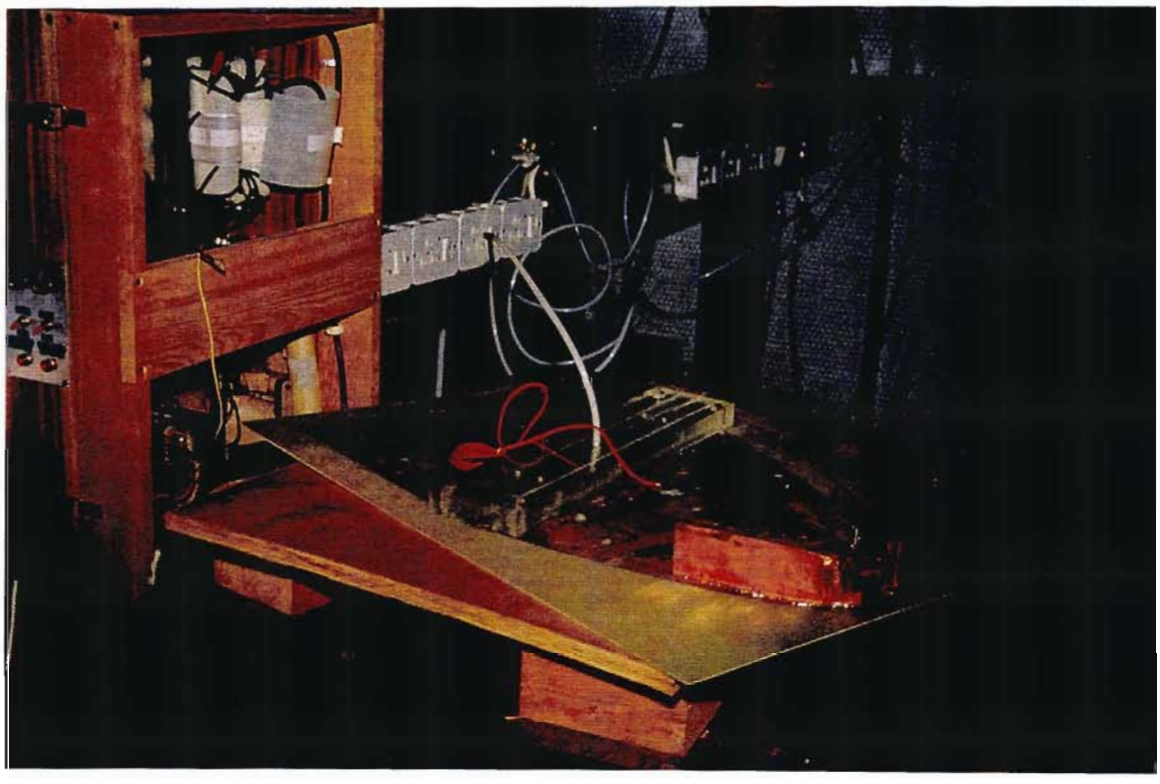

Figure (6.2.1): Parabolic N_2 laser with power supply.

When the laser was fired, it was observed that there was arcing between the screw tip of the spark gap and the copper housing and at times the top copper plate (Figure 6.2.2). Arcing at these places instead between the screw tip and the lower plate results in loss of energy and hence the energy at the laser channel was not high enough to excite the N_2 molecules to produce laser light. Arcing occurs between two points with the shortest gap between them and in this case the distance between the screw tip and the copper shield or the top plate was shorter. This caused the arcing. It has to be noted that the breakdown voltage for a 2 cm gap can be around 20 kV and in our case the gap was smaller (10 mm) than that and the breakdown voltage was around 17 kV. This problem was solved by redesigning the copper shield in such a way that the sides of the copper shield were at a greater distance from the tip of the screw compared to the spark gap. To solve the problem of arcing at the top plate, a piece of a hollow PVC tube 2 cm in diameter was glued at the focus as shown in the picture above. The diameter of the tube was smaller than the diameter of the circle etched at the focus. These changes solved the problem of arcing and the laser operated satisfactorily.

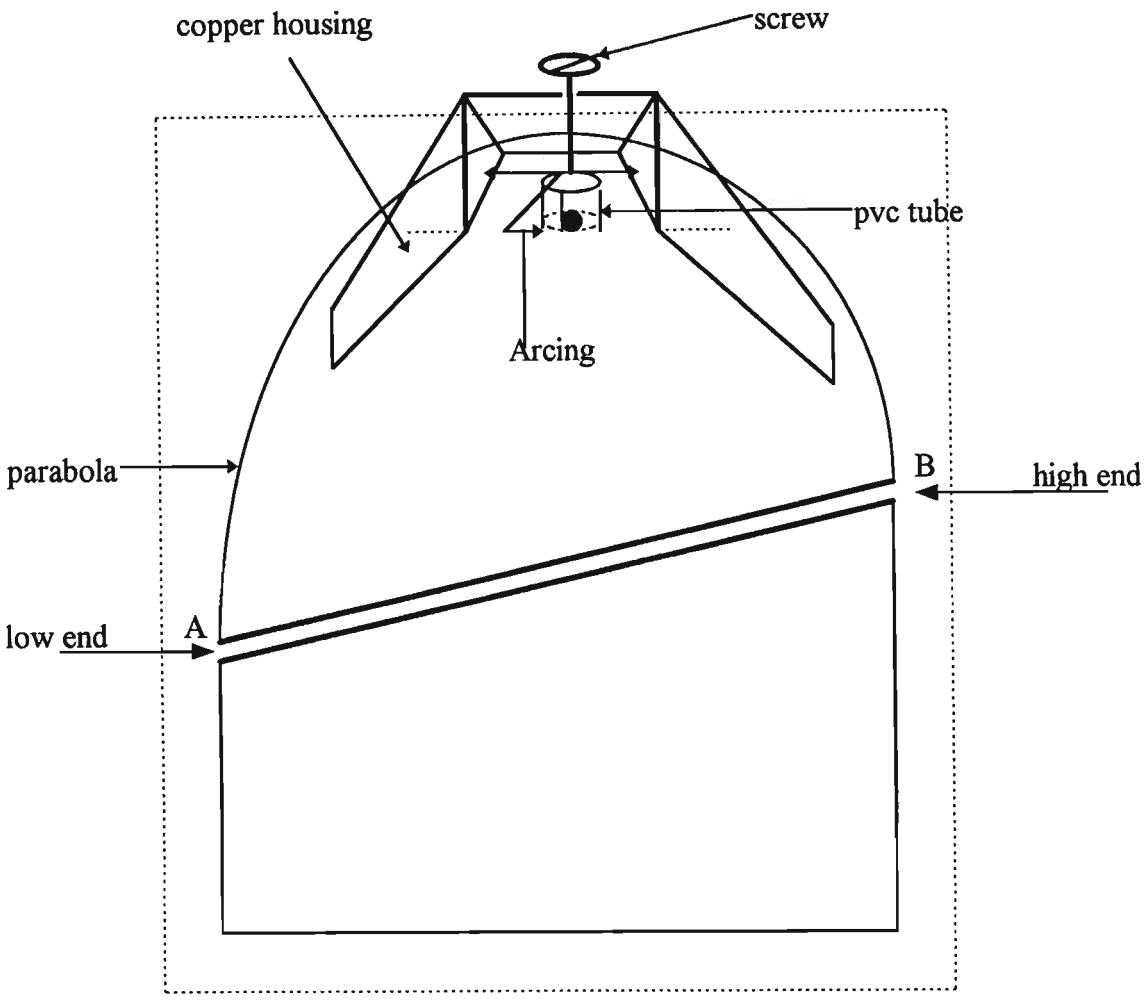

Figure (6.2.2): Arcing regions in the laser.

After the modification, intermittent lasing ceased. This was observed with a piece of fluorescent paper placed in the path of the UV laser beam. The same experimental set up using the photodiode (Figure 6.1.1) was used for detecting the laser signal. Again alignment was necessary and this was done using the laser signal itself and fluorescent paper. It was ensured that the beam passes through the centre of the lenses and finally the beam falling at the center of the photodiode window. The output of the detector was connected to an oscilloscope. The laser was in the Faraday cage because the electromagnetic waves and the noise from the laser interfered with the photodiode. Figure (6.2.3) shows one type of the self-trigerred spark gaps which were used as nanosecond switches to transfer electrical energy by overvolting. The spark gap in the plexiglass housing used for the rectangular plate laser (Figure 4.3.2) can be used both as a self-triggered and triggered switch. The same spark gap was used as a pressurized self-triggered switch for the other lasers as we should see in later chapters.

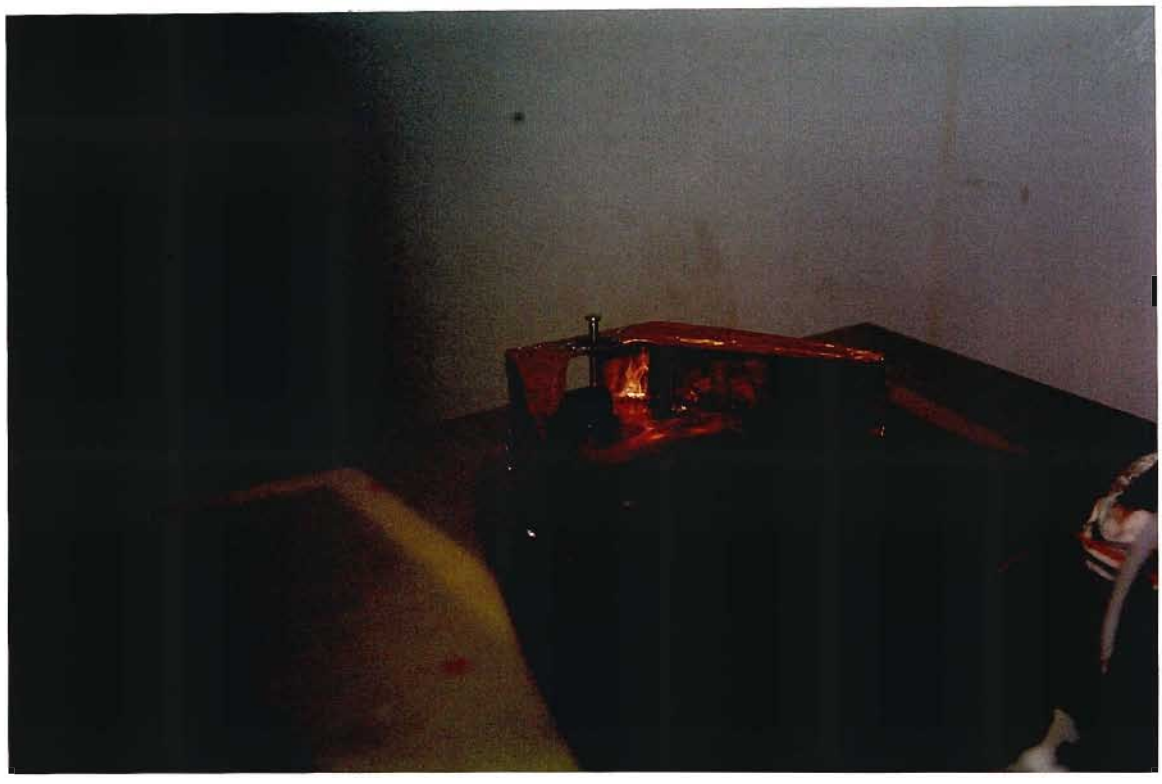

Figure (6.2.3): Self-triggered spark gap (triggered by overvolting).

6.3 Experiment 1: Results

The aim of this experimental section was to investigate the laser outputs from both the lower and higher ends of the laser channel. The output at the lower end of the channel should be higher than that at the opposite end because of the theoretical explanations given earlier. Therefore, the laser outputs at both ends were measured by trying to maintain the same experimental conditions in each case. Theoretically, the laser intensity at **A** should be greater at **B** (see Figure 6.2.2).

The N_2 laser which was self-trigerred at this stage was allowed to run for approximately 70 shots. After about 3-5 shots intervals, the reading of one laser pulse was noted down from the trace on the oscilloscope. This was done for 50 laser pulses and the sensitivity in millivolts were recorded. The sensitivity was set at 2mV/div and the timebase at 1ms/div. The table below shows the sensitivity in mV for about 50 laser pulses. In other words, these data show the intensity of the laser pulses from both ends of the laser channel and which were recorded within a period of 1 hour. As mentioned earlier, the same conditions such as N_2 flow velocity, distance of detector from the laser channel and voltage were maintained when measuring the intensity at each end. Figures (6.3.1) and (6.3.2) show the printouts of laser signal trace received from both the higher and lower ends respectively of the laser channel. As one can see the sensitivity (mV) is greater for the lower end than that of the higher end.

As shown in the table (6.3.1)(p.84), the sensitivity was not constant for most of the laser pulses which meant that the laser energy output was not constant. This behaviour is attributed to the erratic performance of the self-triggered spark gap which was triggered by overvolting. Therefore, these results are not very convincing because firstly due to the nature of the spark gap, it was not known exactly at what voltage the spark gap broke down. Therefore, the condition of the same breakdown voltage for each shot was not actually maintained. Secondly, the laser intensity of consecutive shots were not being measured and the level of humidity might have changed during the recording times. The ideal case would be to have a digitally triggered spark gap with a voltmeter connected across it in order to know and maintain the same breakdown voltage and also to measure the intensity of consecutive shots. In later experiments, a voltmeter with a high voltage probe was connected across the laser such that the breakdown voltage during firing was always known and kept almost constant. The voltage was varied by varying the distance of the spark gap and it was set to the maximum gap length to achieve a maximum voltage of 17 kV.

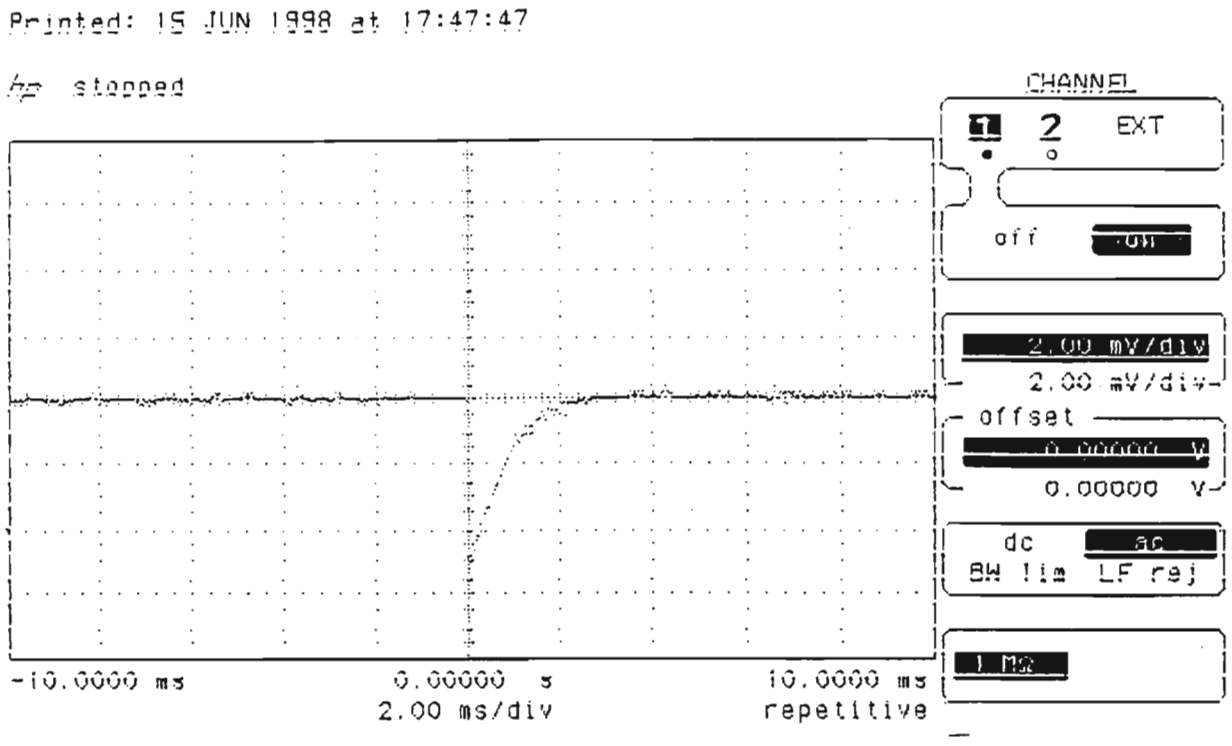

Figure (6.3.1): Trace of laser signal at 2ms/div (upper end).

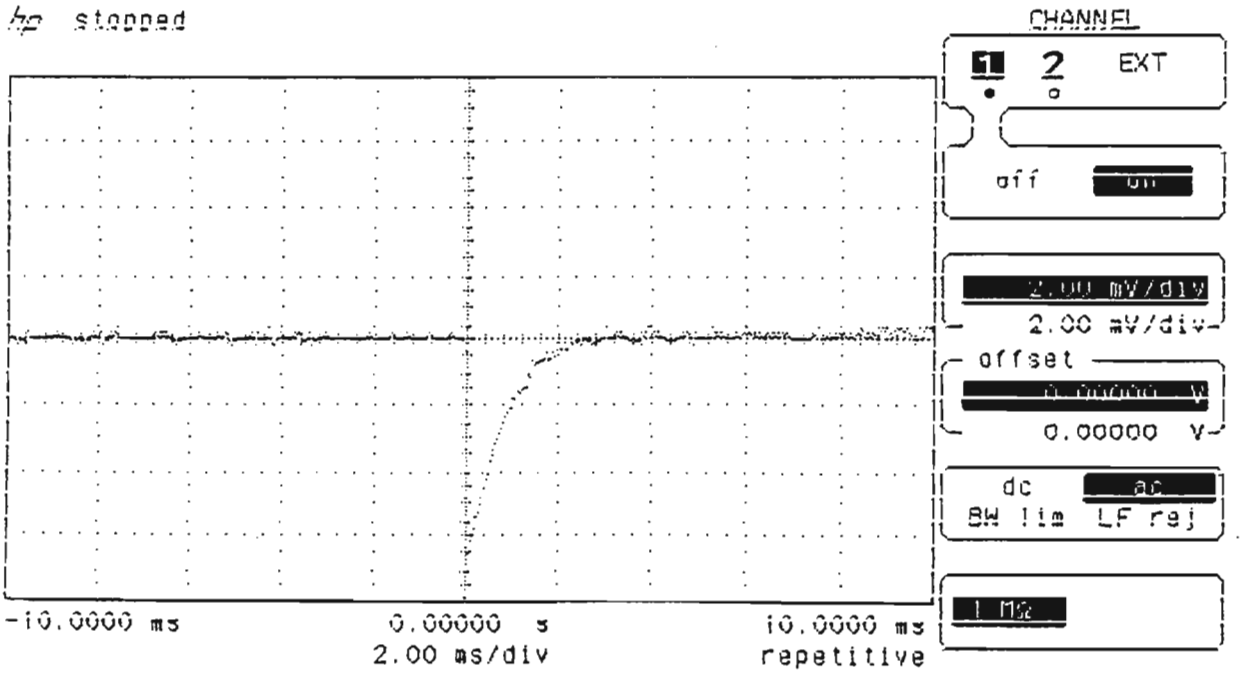

Figure (6.3.2): Trace of laser signal at 2 ms/div (lower end).

Table (6.3.1): Variation of voltage with the laser pulse number.

Pulse number	Sensitivity (mV) Lower end (L)	Sensitivity (mV) Higher end(H)
1	2.5	2.5
2	2	1.75
3	3	2.75
4	3	1.25
5	2.25	1.5
6	1.5	2
7	3	2.5
8	2.75	1.75
9	2.25	1.5
10	1.5	1.5
11	2.75	1.5
12	1.75	1.5
13	2.25	1.75
14	1.75	2.5
15	3.25	1.5
16	2.75	3.25
17	1.5	1.75
18	1.75	2.75
19	2	2
20	3	2.25
21	3	2
22	3	2.25
23	2.25	2.25
24	3	2.5
25	2	3
26	3.5	2
27	3.75	2.25
28	4	1.25
29	1.75	2.5
30	2.25	2
31	2	1.5
32	2.75	1.25
33	3	3
34	4	2
35	2	2.25
36	2	2.25
37	2.25	3
38	2.25	3.5
39	2.25	2

40	3	3
41	2.75	3
42	3	2.5
43	2.75	1.25
44	2.75	1.25
45	2.25	2
46	3	1.5
47	1.5	3.5
48	3	3.25
49	4	3.25
50	4	2.5

The graph Figure (6.3.3) is a plot of the data from the table. As one can see (refer to Figure (6.3.3)) the laser intensity from the lower end was higher than that from the higher end. The lower end output energy was approximately 20 % more than that at the higher end. The energy difference was not remarkable since as mentioned earlier, the inclination angle of the laser channel was 20^0 instead of the correct angle of 30^0. A significant energy difference between the lower and higher ends was obtained as we would see shortly. However, the above results show that the parabolic configuration does have an effect on the laser output and it confirms the theory of the parabolic laser discussed in the previous sections.

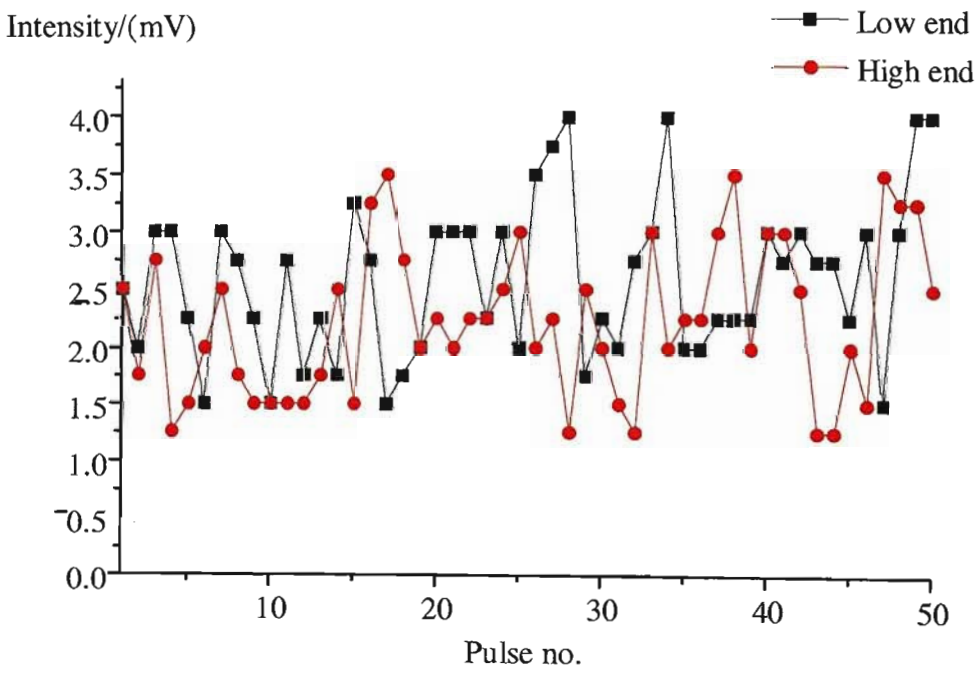

Figure (6.3.3):Variation of laser intensity with laser pulse number.

6.4 Experiment 2: Interference fringes from the parabolic N_2 laser

Since laser light is coherent and monochromatic it was necessary to do an interference experiment to investigate whether the light radiation coming out of the cavity was laser light. The set-up (Figure 6.4.1) shown below was used to obtain interference fringes and since photographic paper was used, the experiment had to be done in the dark.

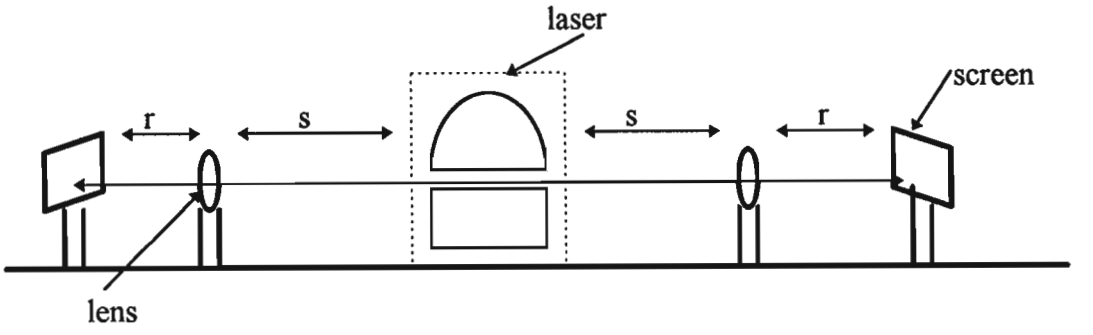

Figure (6.4.1): Experimental arrangement to observe fringes.

Due to the divergent nature of the laser beam, it had to be focused on the screen. The system of laser, screen and lenses were aligned and it was made sure that the light passes through the centre of each lens. Strips of photographic paper labelled L and H were placed on the screen at each side of the laser channel, with L at the lower channel side and H at the higher channel side. As can be seen in Figure (6.4.1) above, the distances (r) and (s) were kept the same. The photographic papers were at about 48 cm from the ends of the laser channel.

Since this laser was self-triggered, it was firing several times and several laser pulses would overexpose the photographic paper. As a result of this, the paper was exposed for only one laser pulse. Some practice was needed to switch the laser on and off to produce a single pulse. The spark gap was increased in order to have a longer time interval between laser pulses, that is a higher pulse length leading to an increase pulse duration. The picture (Figure 6.4.2) below shows the experimental arrangement.

Figure (6.4.2): Experimental Set-up.

The photographic papers were developed in the dark room of the Physics Department. The paper had to stay immersed in the acid (the developer) for approximately 20 secs and another 20 secs in the fixer and finally in water.

The photographic paper, labelled L showed a large black spot and the one labelled H showed a few black streaks (shown only on the original photographic paper) but much paler compared to the other one (Figure 6.4.3). This means that the intensity of light from the lower channel was greater than that at the higher channel. Even at this stage, this evidence was considered insufficient because interference fringes had yet to be investigated. Cross-wires were placed in the path of the beam to obtain interference fringes. Again, alignment was necessary to produce an image of the cross-wires on the screen. However, even after several attempts fringes could not be seen. This occured because the cross-wires were not thin enough to produce diffraction patterns.

Lower end *Higher end*

Figure (6.4.3): Photographic paper exposures with laser light from both ends of laser channel.

It was then decided to use a diffraction grating with 1200 lines/mm. This would allow not only to obtain fringes but also to find the wavelength of the laser light. The picture (Figure 6.4.4) shows the traces of the laser light on a photographic paper. The distance from the zero maximum to the first order maximum was measured. It was difficult to focus the broad laser spot to a point and due to this the distance measured between the zero and first order was taken approximately from the centres of the traces.

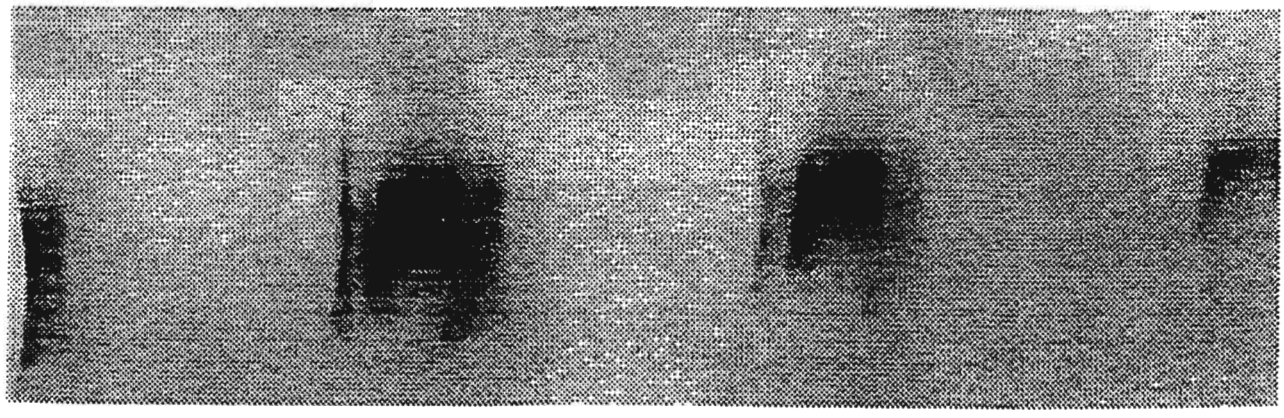

Figure (6.4.4): Diffraction patterns from laser light.

Using the equation

Using the equation

$$d_4 \sin\theta = n\lambda \qquad (6.4.1)$$

where d_4 = distance from grating to sreen (Figure 6.4.5)

θ = angle between the zero and n th order

n = 1, 2, 3, ...

λ = wavelength of laser light

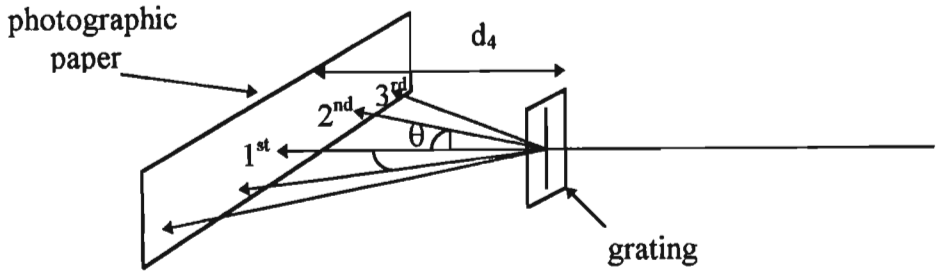

Figure (6.4.5): Orders of maximum.

The following were the measurements:

distance between the zero and first order = 8.0 cm

d_4 = 17.0 cm

angle $\theta = 25^0$

Therefore the wavelength λ is (using equation 6.4.1) = 350 nm. This wavelength is in the U.V region and it corresponds to the wavelength at which the Nitrogen laser lases that is, at 337 nm.

6.5 Experiment 3: Michelson Interferometry to measure coherence length

The principal components of the usual Michelson interferometer are shown schematically in Figure (6.5.1). A ray of light from the monochromatic source **A** strikes the beam splitter **C**, which is a glass plate with a thin coating of silver on its right side. Part if the light (ray 1) passes through the silvered surface and the compensator plate **D** and is reflected from mirror $\mathbf{M_1}$. It then returns through **D** and is reflected from the silvered surface of **C** to the observer. The remainder of the light (ray 2) is reflected from the silvered surface at point **P** to the mirror $\mathbf{M_2}$ and back through

C to the observer's eyes. The purpose of the compensator plate **D** is to ensure that rays 1 and 2 passes through the same thickness of glass; plate **D** is cut from the same piece of glass as plate **C**, so their thicknesses are identical to within a fraction of a wavelength. The compensator plate is not essential for producing fringes in monochromatic light but is indispensable when white light is used. The whole apparatus must be mounted on a very rigid frame where there is the least possible vibrations. The position of the mirror $\mathbf{M_2}$ can be adjusted with a fine, accurate micrometer screw.

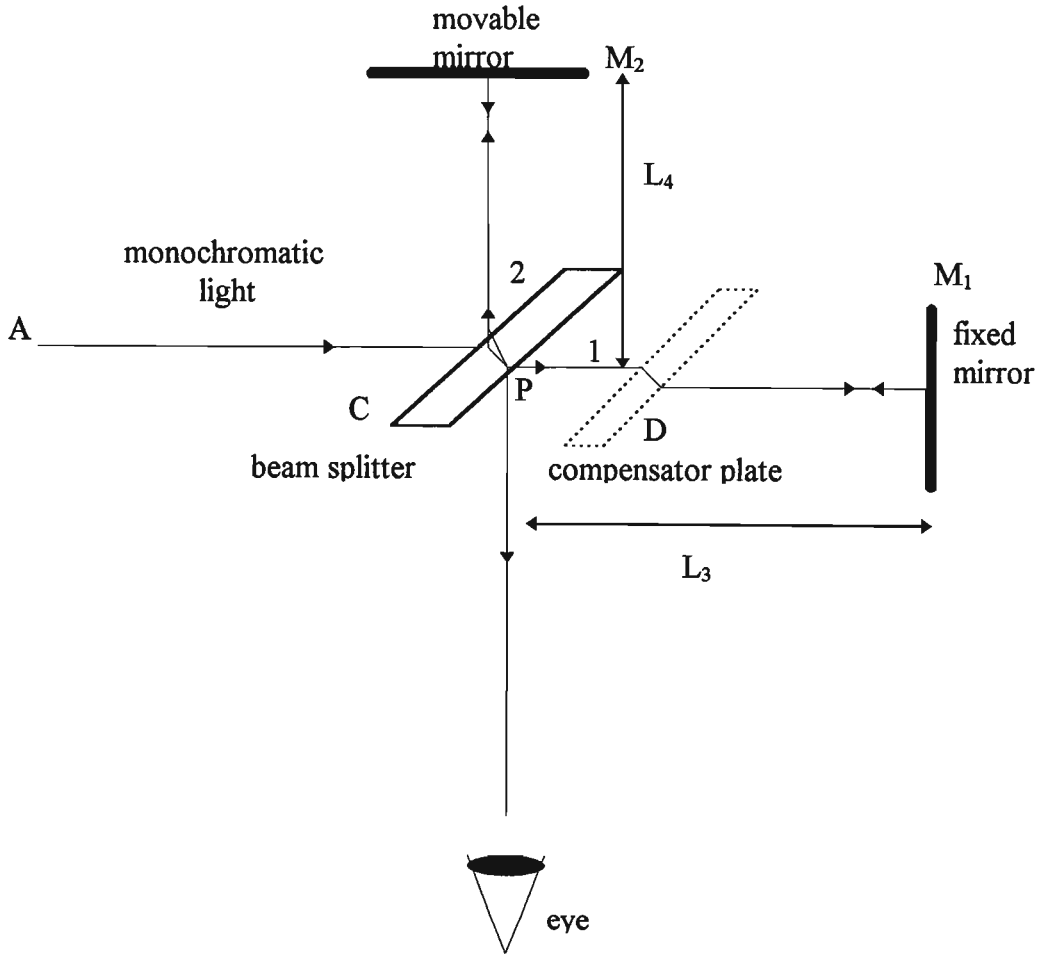

Figure (6.5.1): Principle of Michelson Interferometry.

The path difference is given by $L_4 - L_3$ and the coherence length is twice this distance since the ray 2 is reflected and returns to the beam splitter.

6.6 Experiment 3: Results

The set-up of the actual experiment to measure the coherence length of the parabolic Nitrogen laser was slightly different since a compensator was not used and the positioning of mirrors were not the same as shown in Figure (6.6.1).

It is worthwhile noting that interference apparatus may be divided into two main classes, those based on division of amplitude and those based on division of wavefront. Here, the interferometer used belongs to the former class. The laser pulse wavefront is divided into two parts by the beam splitter to provide two wavefronts of identical shape. The two mirrors serve to recombine the wavefronts at the screen. If the movement of either mirror perpendicular to its plane results in the disappearance of the fringes then the distance through which the mirror has moved is half the length of the wavetrain as mentioned earlier. Thus the coherence length is measured by twice the path difference.

The whole experiment was carried out in the dark room since at first photographic paper was used to observe the interference fringes. In this experiment, the N_2 laser was aligned using a 0.5 mW He-Ne laser and it was found that alignment was a very important and critical for the observation of fringes. As seen in Figure (6.6.1) the He-Ne laser was placed close to the end of the N_2 laser channel and its height adjusted until the infra-red laser coincided with the N_2 laser discharge gap. The latter was at a fixed height. The Michelson interferometer was placed on three stands with adjustable height and a smooth adjustment could be done without disturbing the system.

Firstly, interference fringes were obtained using the He-Ne laser with zero path difference. The spacing of the fringes were made wide enough by adjusting the micrometer screw of mirror M_1. Caution had to be exercised not to confuse the interference fringes with other fringes which were formed due to poor optical quality of the reflecting mirrors and beam splitter. Due to this problem, each time the interference fringes appeared, their orientation was changed using the micrometer screw in order to confirm that they were the real fringes. Another way of doing this was to block one arm of the light or the other and to observe whether the fringes disappear on the screen.

After having aligned the N_2 laser and interference patterns from the He-Ne laser were produced on the screen, the N_2 laser was fired. It was made sure that both lasers were in almost the same plane and showing light at the same point on the screen. The path difference was set to zero and this time with the infra-red laser blocked, the UV light from the N_2 laser was made to pass through the interferometer. Being a pulsed laser it was difficult to see fringes even on a fluorescent screen. A photographic paper was placed on the screen and only 2 to 3 laser shots were used to avoid overexposure. The exposed photographic paper were developed according to the procedure given earlier.

The path difference was changed by changing the distance of the movable mirror from the beam splitter. Care was taken not to disturb the system. Alignment was necessary and this was done again using the He-Ne laser by aligning the reflected light from the movable mirror on the N_2 laser channel. At times a mirror had to be used to ensure a parallel beam. This was repeated for each different path length and each time photographic papers were exposed to see the fringes. Figures (6.6.2a) to (6.6.2f) show the pictures with interference fringes at different path difference or different coherence lengths.

As the movable mirror was moved closer to the beam splitter, i.e the path difference was made larger, it was observed that the fringe spacing was getting smaller and smaller as a result it was difficult to see them. Therefore, a CCD camera connected to a monitor was set up to observe the fringes. The monitor was then connected to a video machine which recorded the fringes. In order to reduce the effects of electromagnetic interference, the electronic equipments and the laser were placed in separate rooms. Moreover, the UV light coming from the laser was too bright for the monitor screen and there was poor visibility of the fringes. A normal glass of 4 mm thickness was placed in the path of the laser at a distance from the laser channel to attenuate the fluorescent light.

The fringes were recorded and the video counter was set to zero each time the path difference is changed and this enabled to distinguish between fringes formed at different coherence lengths. The tape was played back and the pictures were processed using a frame-grabber software. The experiment was reproducible since the measurements were taken again on a different day and the results were almost the same.

The maximum coherence length measured was approximately 21 ± 0.2 cm, bearing in mind that the pulse length of the N_2 is about 30 cm. The fringes which were observed at a coherence length of 24.6 were very close to each other (Figure 6.6.2f).The coherence length measured is much larger than the coherence length (7 cm) measured for the N_2 laser with rectangular plates and those mentioned in the literature.

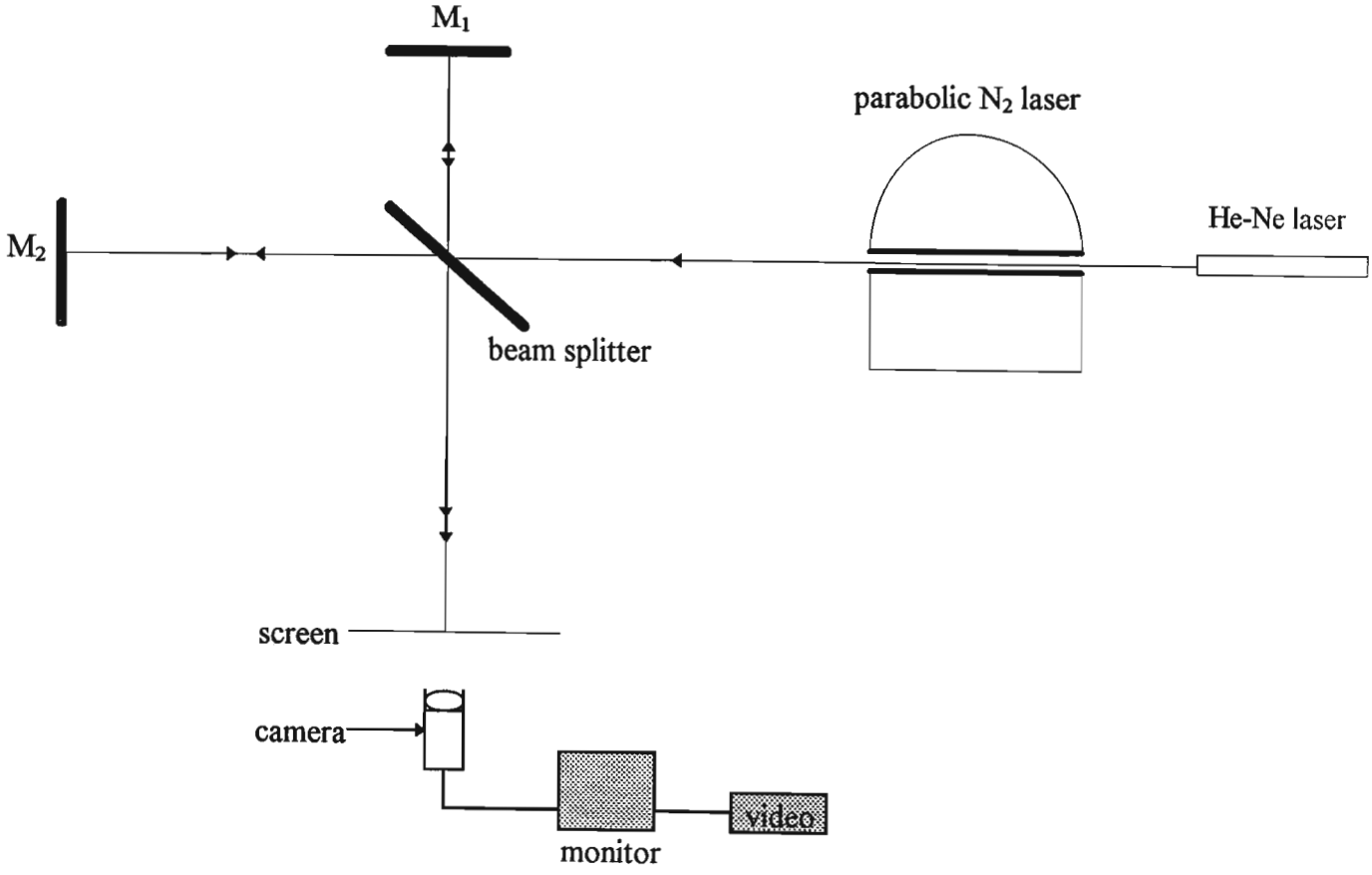

Figure (6.6.1): The set-up to measure coherence length of the parabolic N_2 laser.
[Note: The discharge laser channel is actually inclined at an angle (not shown here).]

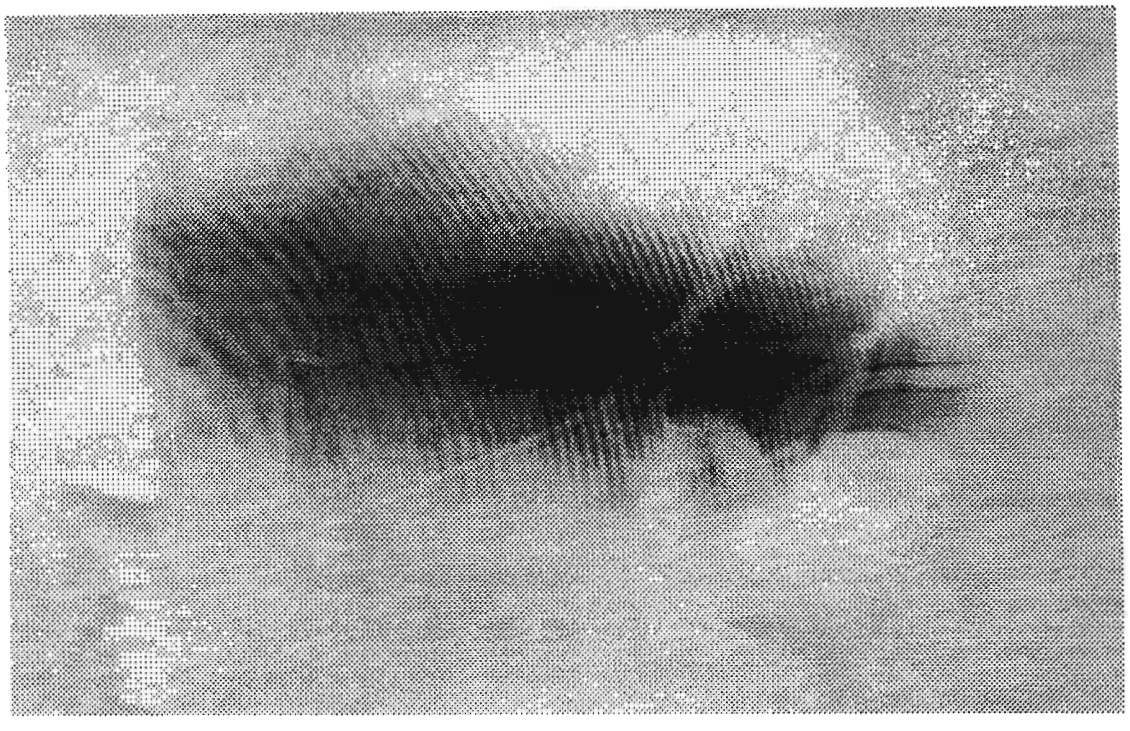

Figure (6.6.2a): Interference fringes at coherence length of 4.4 cm.

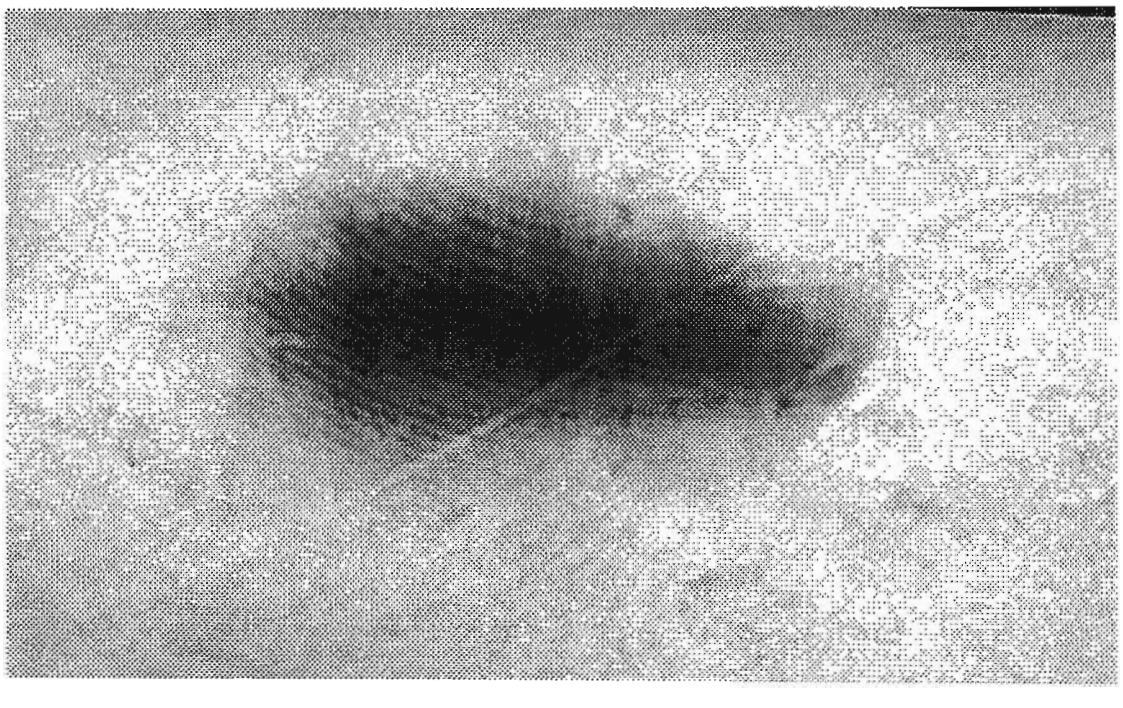

Figure (6.6.2b): Interference fringes coherence length of 8.7 cm.

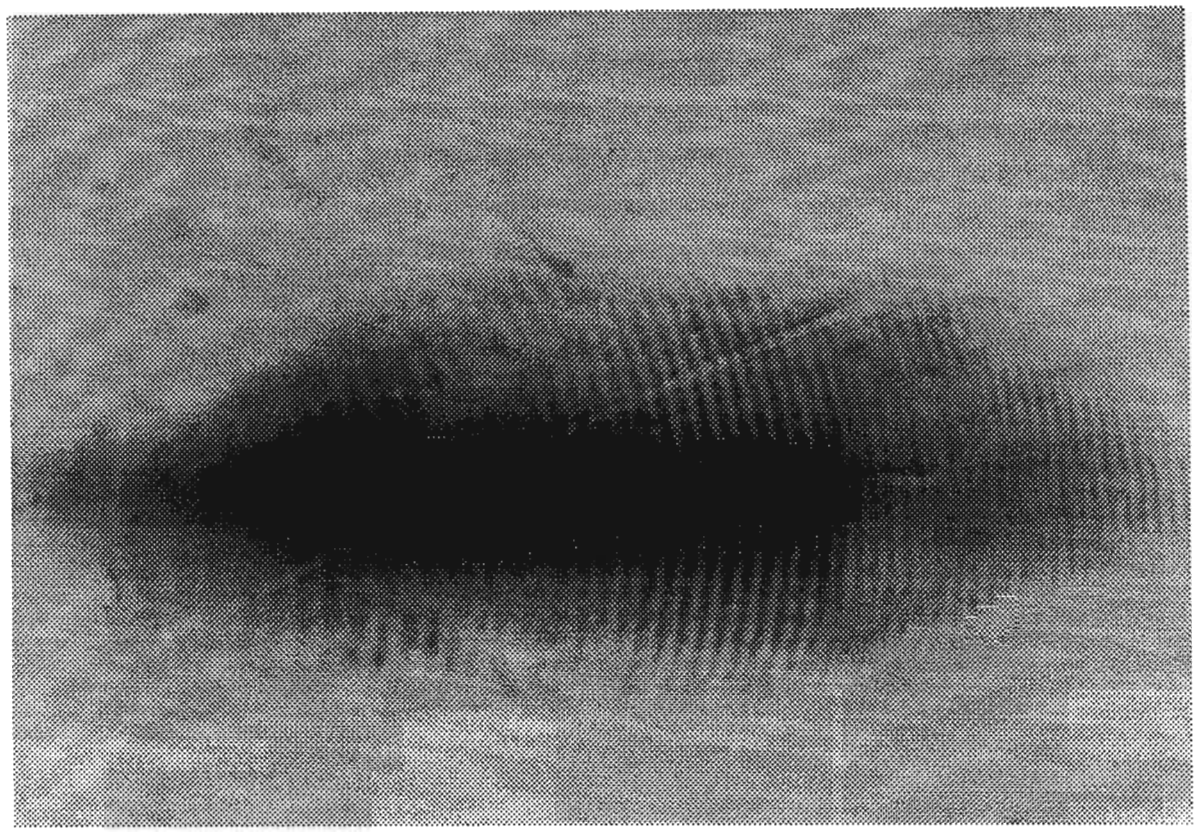

Figure (6.6.2c): Interference fringes at coherence length of 13.5 cm.

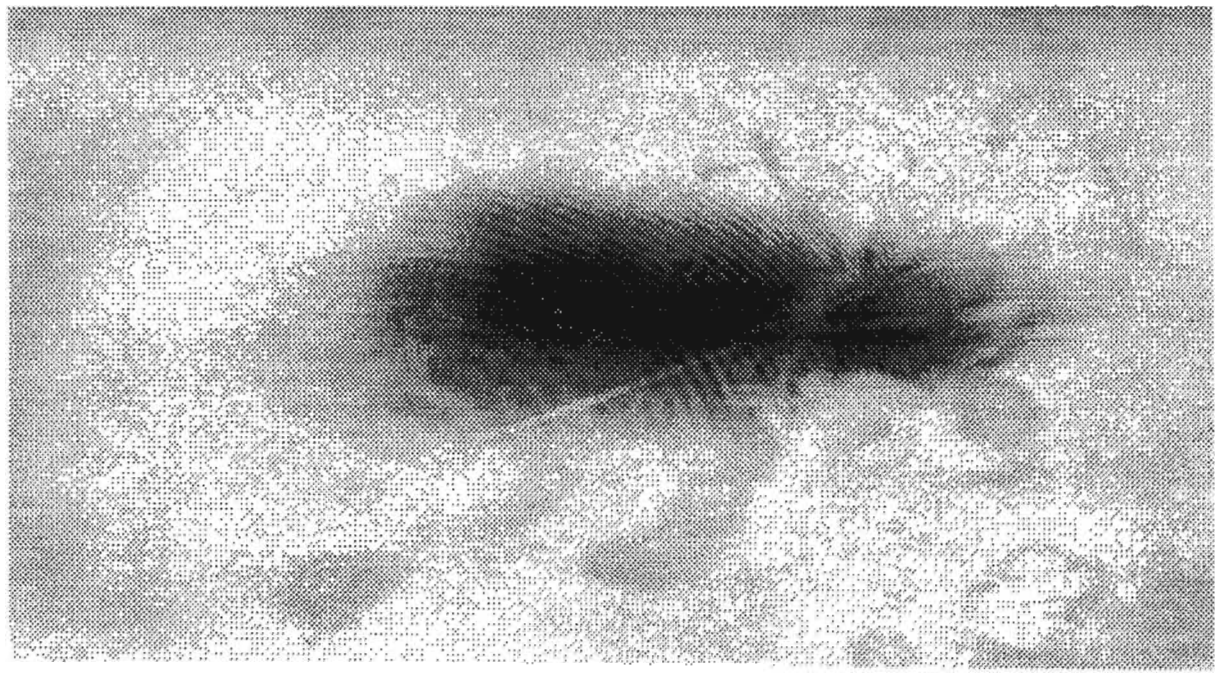

Figure (6.6.2d): Interference fringes at coherence length of 17.4 cm.

Figure (6.6.2e): Interference fringes at coherence length of 21.3 cm.

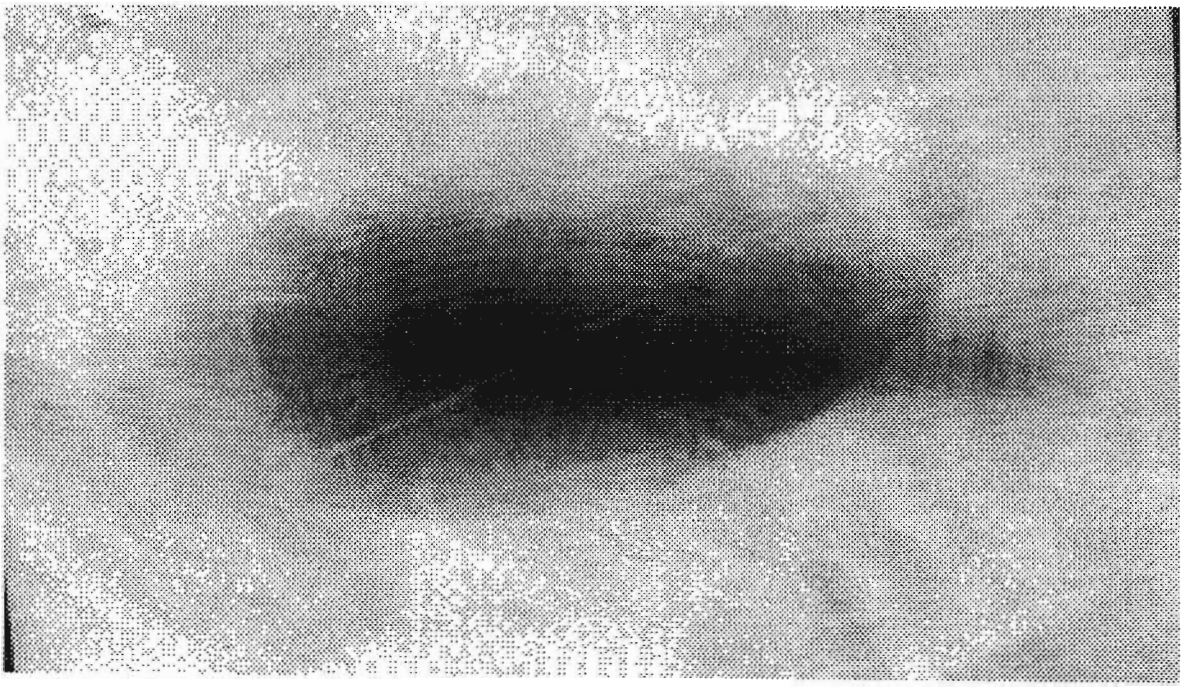

Figure (6.6.2f): Interference fringes at coherence length of 24.6 cm.

6.7 The Mach-Zehnder Interferometry

The Mach-Zehnder is another amplitude-splitting device. It consists of two beam splitters and two totally reflecting mirrors, as shown in Figure (6.7.1) below. Its principle is the same as that of Jamin's or Rayleigh refractometers. If a thickness t of a substance having an index of refraction n is introduced into the path of one of the interfering beams in the interferometer, the optical path in this beam is increased because of the fact that light travels more slowly in the substance and consequently has a shorter wavelength. The optical path is now nt through the medium, whereas it was practically t through the corresponding thickness of air ($n = 1$). This will introduce $(n - 1)t/\lambda$ extra waves in the path of one beam; so if we call Δm the number of fringes by which the system is displaced when the substance is placed in the beam, we have

$$(n - 1)t = (\Delta m)\lambda \qquad (6.7.1)$$

In principle a measurement of Δm, t, and λ will determine the value of n.

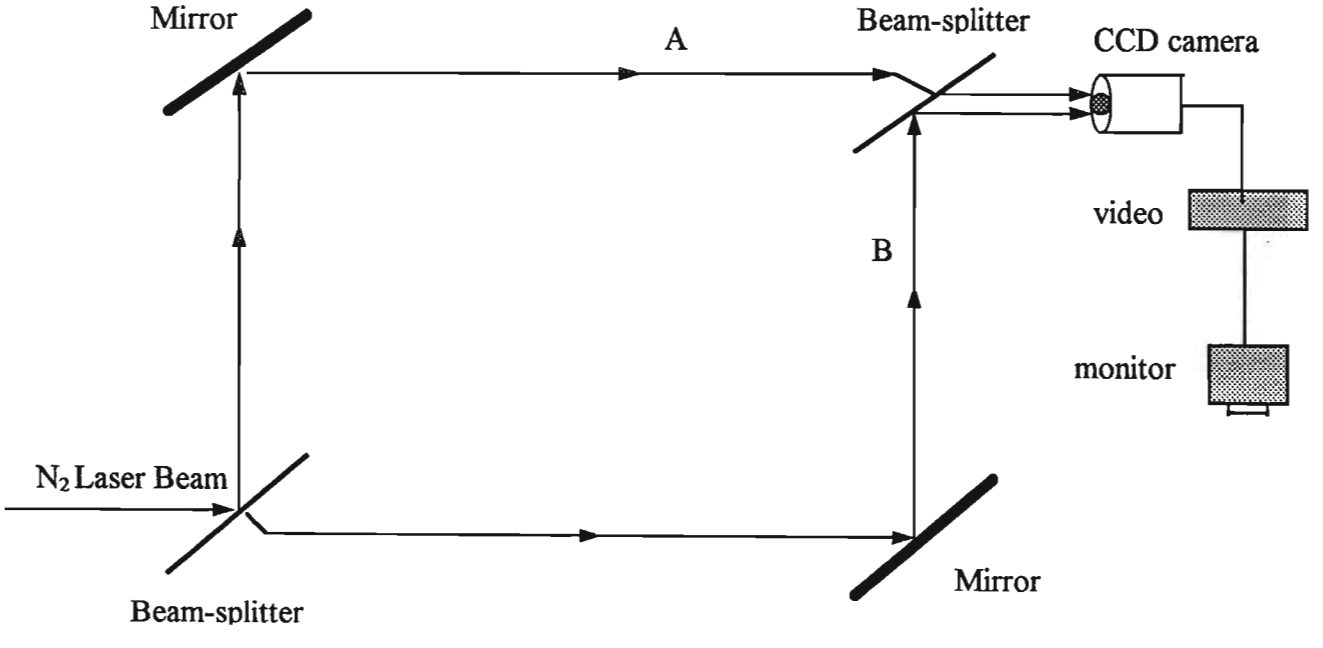

Figure (6.7.1): The Mach-Zehnder interferometer.

A common application of the device is to observe the density variations in gas-flow patterns within research chambers (wind tunnels, shock tubes). One beam passes through the optically flat windows of the test chamber, while the other beam traverses appropriate compensator plates. The beam within the chamber will propagate through regions having a spatially varying index of refraction. The resulting distortions in the wavefront generate the fringe contours.

In our case, this technique is used to measure the refractive index of gas lens formed during the Colliding Shock wires. In fact, at the time of writing, this experiment was being carried out by a PhD student and the part of experimental work which was done by the author was to use the Mach Zehnder interferometry to obtain fringes. The skill and experience acquired will then help in setting up the same experiment to measure the refractive index of the gas lens.

In this experiment, a long thin wire was threaded through a cylindrical device such that 8 sections of equal length are equidistant from each other and lie on a circumference of about 3 cm and a schematic diagram is shown in Figure (6.7.2). The wire was then charged to a voltage of 22 kV. A N_2 laser beam was aligned such that it passed the centre of the circle. When all the 8 parts of the wire explode with a big bang, a cylindrical shock wave was generated at each section. At the convergence of the waves which occurred at the centre, a region of high density and pressure was formed producing a gas lens which focused the laser beam. The firing of the laser and the convergence time of the waves were digitally synchronised. Photographic paper was used to observe the formation of the waves.

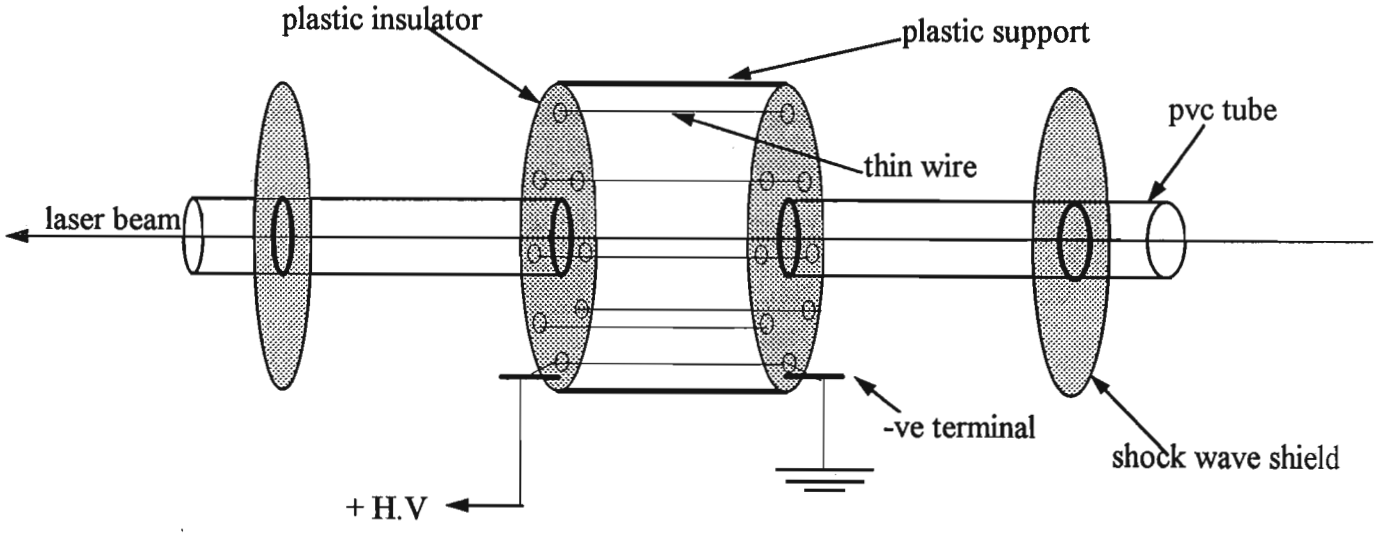

Figure (6.7.2): The Cylindrical device for supporting wire for Colliding Shock experiment.

In order to measure the refractive index of the gas formed during the convergence of the shock waves, the whole device shown above should be placed in one of the optical path of the beam. The laser beam must be aligned properly and made to pass along the optical axis of the mirrors and through the centre of the circle where the gas lens will be formed. Then, using photographic paper, changes or the effects on fringe patterns would be observed. If the number of fringes, Δm are counted, the value of n can be found by applying equation (6.7.1). Figure (6.7.3) shows a picture of the set-up for the Colliding Shock wire experiment.

Figure (6.7.3): Picture showing the set-up for the Colliding Shock Experiment.

Figure (6.7.4) shows the convergence of the shock waves using 8 wires where there was some air turbulence and Figure (6.7.5) shows the shock waves generated using only 4 wires. The focus spot of the laser beam can also be seen at the centre.

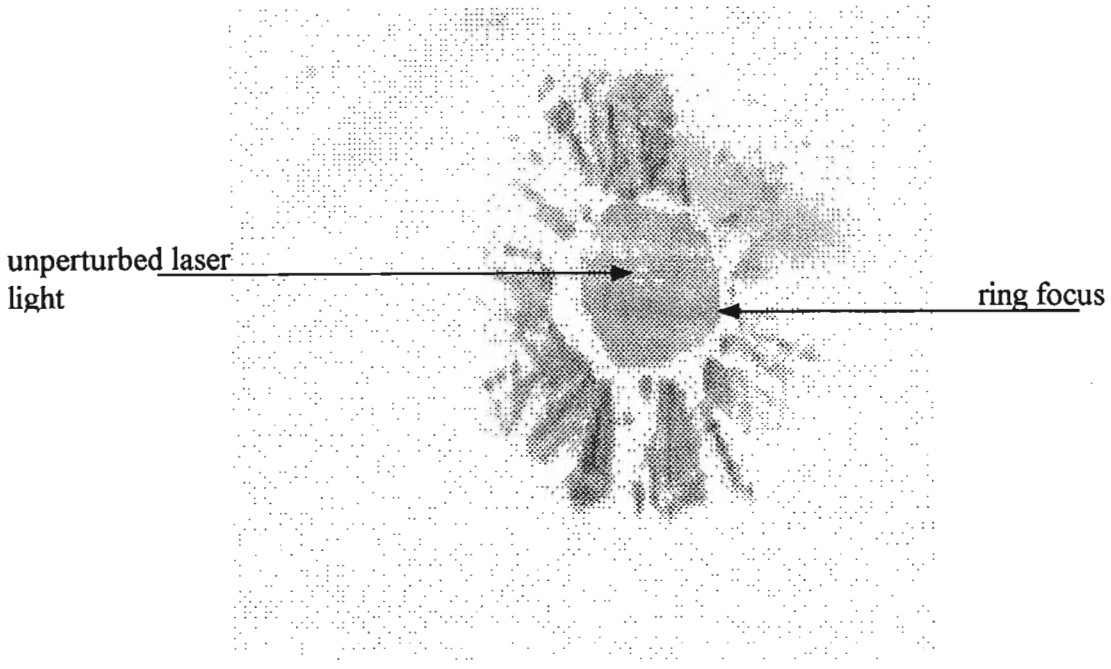

Figure (6.7.4): The shock waves generated with 8 wires.

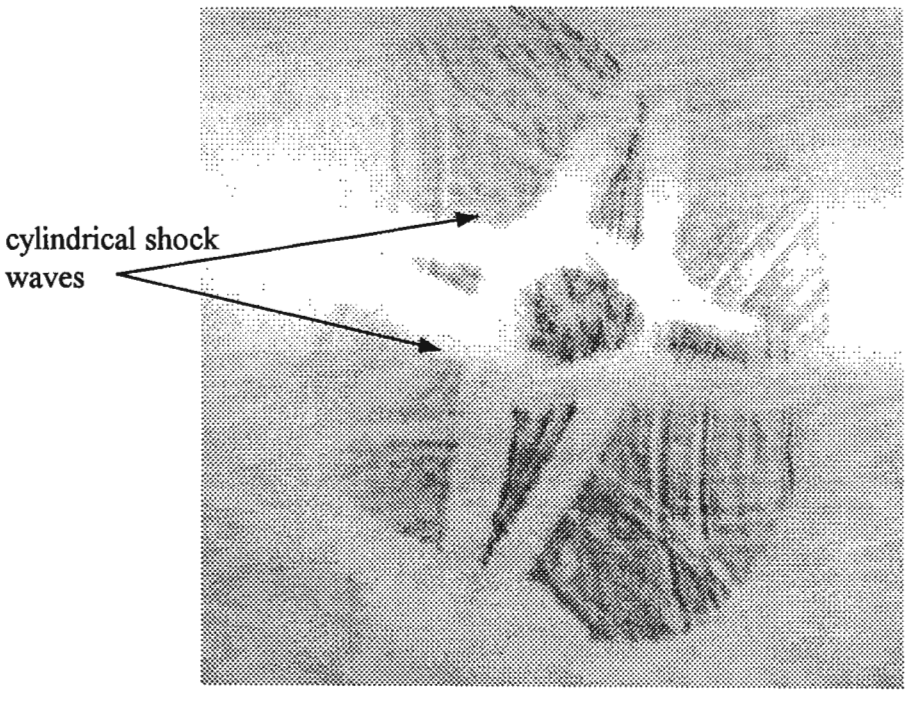

Figure (6.7.5): The shock waves generated with 4 wires showing also the focused spot of the laser beam.

6.7.1 Experiment 4: The Mach-Zehnder interferometry with the Parabolic N_2 Laser

Since the parabolic nitrogen laser was brighter and has a longer coherence length than the rectangular, it was practical to use it to observe the interference fringes. The same experimental set-up as shown in Figure (6.7.1) was used and the experiment was carried out in the dark room. A He-Ne laser was used for alignment and fringes with this laser were first obtained on the screen. Photographic paper was not used as a CCD camera was easier and more practical especially with a pulsed laser. Figure (6.7.1.1) shows a picture of the experimental set-up which includes the mirrors, beam-splitters and N_2 laser. As is the case of most interferometry experiments, the alignment was difficult and time consuming. However, a special technique was applied such that fringes could be observed in a relatively short time.

First, the He-Ne laser was used to obtain fringes on the screen. A match stick supported on a stand, was placed in the optical path A and its image was found and located on a paper screen placed on the CCD camera by fine adjusting the mirrors and beam splitters. The precise location of the stick's image was clearly marked on the paper.

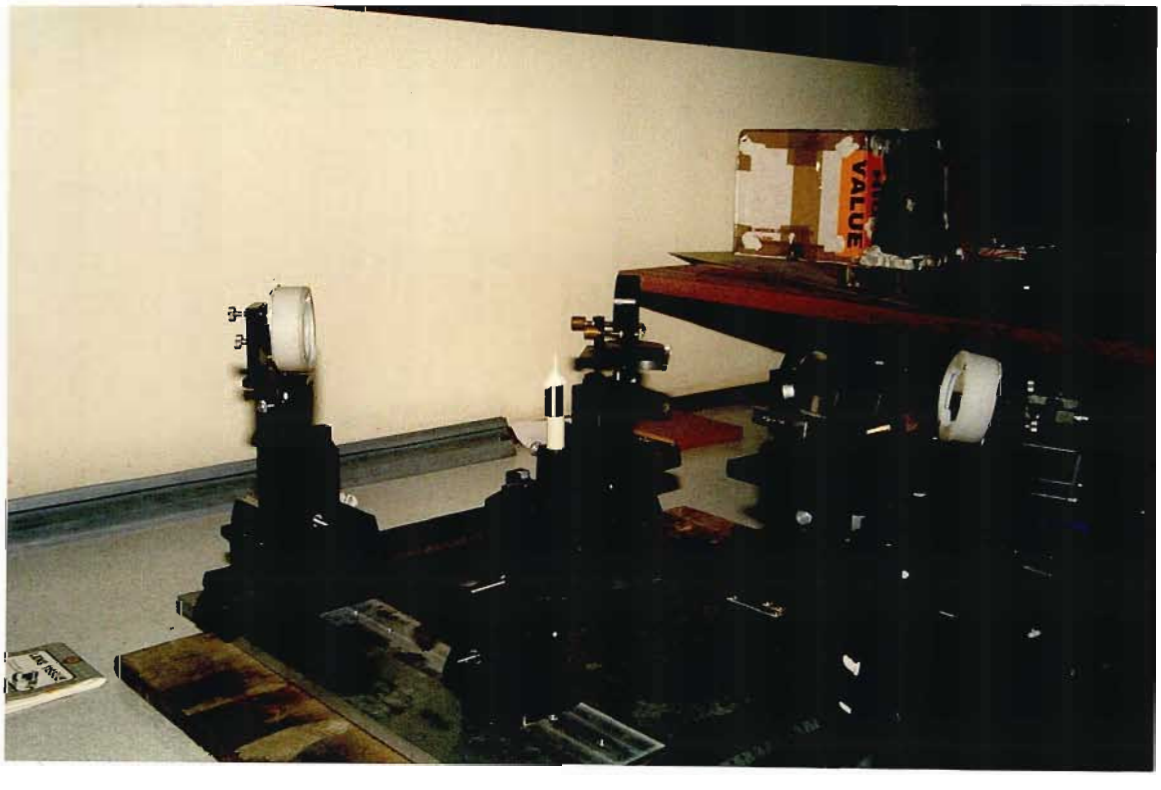

Figure (6.7.1.1): The experimental set-up in dark room for Mach-Zehnder interferometry.

Similarly, the match stick was placed in the optical path B and the image was located and made to coincide with the mark of the previous image. Again, here the screws for

the fine adjustments played a tremendous role in doing that. It is worth noting that the mirrors and beam splitters were placed on a rigid and solid optical base as shown in Figure (6.7.1.1) to prevent any vibration. In a similar way as the fine adjustment of the mirror screws can cause a change in the fringe patterns, any vibration can affect the visibility and clarity of the fringes.

After the two images of the stick coincided at the same spot on the camera, interference patterns could be observed on the monitor screen. By blocking one arm of the laser beam, the fringes disappeared and appeared again when it was unblocked. This confirmed that the fringes were not due to interference caused by other optical scattering but could only be from interference of the two beams A and B.

The parabolic laser which was aligned using the He-Ne was then fired. Since, the laser light coming out was too bright for the CCD camera, a UV filter had to use to attenuate its intensity. Interference fringes could then be observed on the screen. Again, in order to confirm that those fringes were real, two important steps were taken. Firstly, one arm of the light was blocked and it was observed on the screen that fringes disappeared. Secondly, the orientation of the fringes obtained with the He-Ne was observed and noted, since it should be the same as that of the fringes obtained from the N_2 laser. Figure (6.7.1.2) shows a picture of the experimental arrangement which includes the CCD camera, the N_2 laser, the He-Ne laser and the interferometer.

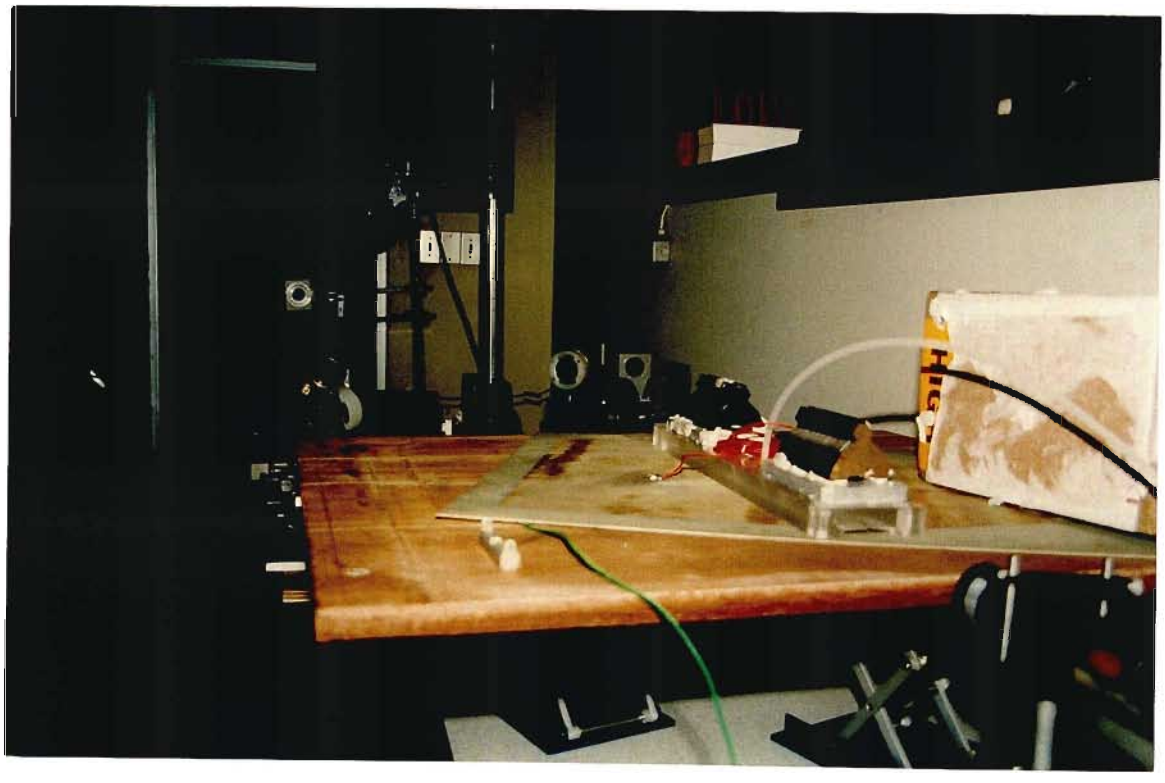

Figure (6.7.1.2): The experimental arrangement of the Mach Zehnder interferometry system showing the camera at the far end.

The interference fringes were recorded on a video tape and a frame grabber software was used to process the fringe patterns. Figure (6.7.1.3) shows interference fringes from the N_2 laser and Figure (6.7.1.4) shows the same fringes with a different orientation. This was done to ensure that the fringes observed were the real ones.

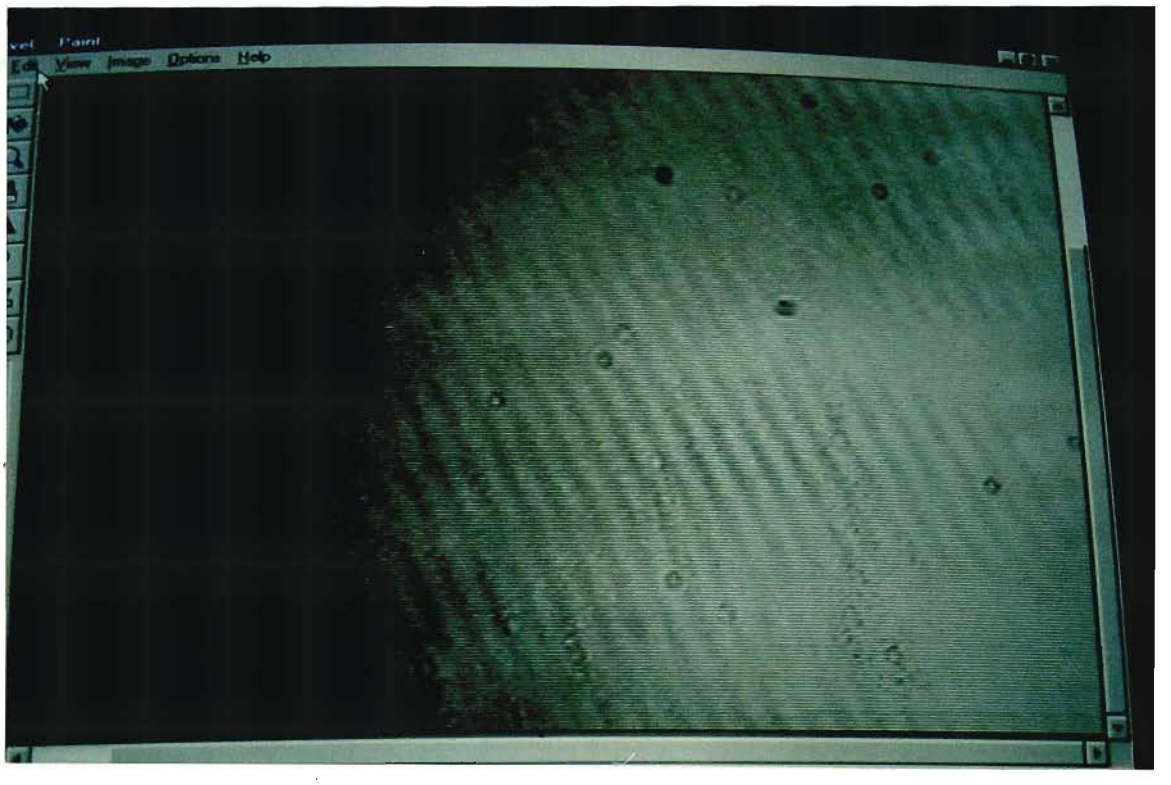

Figure (6.7.1.3): The interference fringes observed in a Mach Zehnder interferometry using the parabolic N_2 laser.

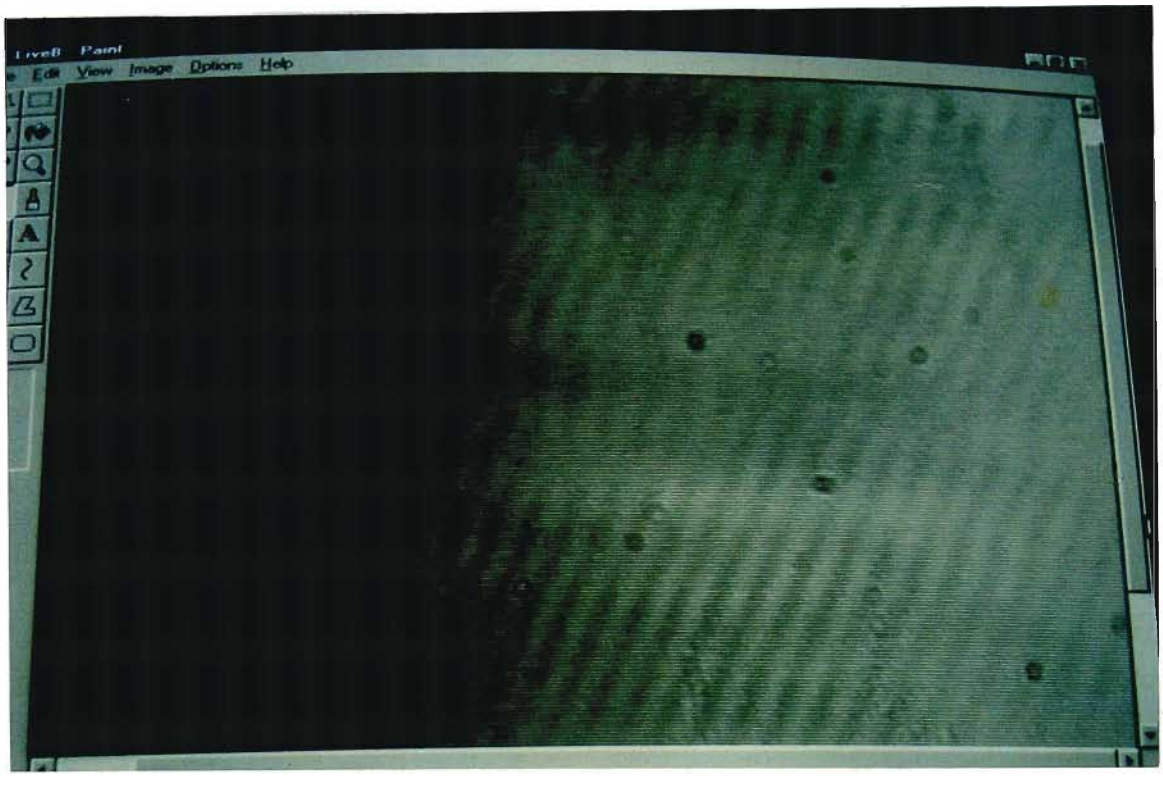

Figure (6.7.1.4): The same interference fringes observed at a different orientation angle.

Air was blown at a high speed over optical path A through a thin pipe which was connected to a cylinder of pressurised air. Slight changes in fringe patterns could be observed on the screen. The patterns became wavy and it seemed that the fringe width also changed slightly. However, these changes were too small to be recorded.

6.7.2 Experiment 5: The Colliding Shock experiment

Another side experiment was carried out by the author to observe the shock waves created from two oppositely charged pins. The experiment was similar in principle to the Colliding Shock wire experiment, except that in this case two pins instead of wires were used and the laser was not electronically triggered. The figure below shows the schematic drawing of the circuit.

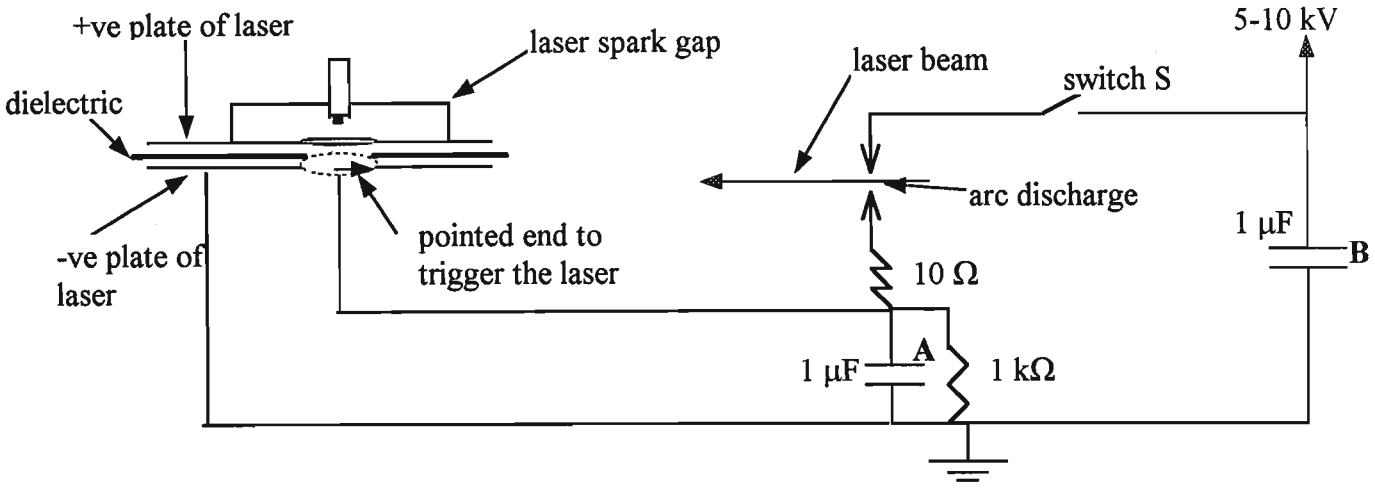

Figure (6.7.2.1): Schematic circuit of the Colliding Shock experiment.

As can be seen in the drawing above, the laser was triggered by the voltage which appeared across the capacitor **A**. It was believed that the delay would be appropriate to synchronise the triggering of the laser with the discharge of the shock waves at the two pins. The time constant (RC) of the capacitor which triggered the spark gap was calculated to be 10 μs and the laser discharge occurred in nanosecond timescale. The end of the wire leading to the spark gap was sharpened (a pre-ionisation technique) and placed very close to the negative plate of the laser inside the spark gap. This ensured that the latter would breakdown at a certain voltage which would then trigger the laser. The spark gap had to be air pressurised and the pressure inside the gap was varied until the hold-off voltage of the laser was reached. The above circuit was then charged to approximately 8 kV. The switch S was then closed. This resulted in the triggering of the laser and the discharge at the two pins. The switching was actually done by having the wire cut and two connectors soldered at their ends. One of the ends of the wire was made to hold over the other at a certain distance to avoid breakdown. Switching was then done manually using an insulated stick by pressing the two ends together at the right voltage. A multimeter was connected to the charging capacitor via a high-voltage probe to note the breakdown voltage of the system. This triggering technique worked as both the laser and the arc discharge triggered when the switch S was closed. The breakdown voltage of the spark gap was observed to vary for each shot. Figure (6.7.2.2) shows the experimental set-up. As can be seen in the picture, the arc discharge device was placed in one of the optical paths and pins were used to align the laser beams as was done in section (6.7.1). Traces of the laser signal and the arc discharge were fed into an oscilloscope in view to determine the time delay between the two signals. However, due to other electromagnetic sources several signals were observed on the oscilloscope as shown in Figure (6.7.2.3). These signals could be from the following: the spark gap, the pre-ionisation spark in the spark gap, the switching of switch S, the laser discharge at the electrodes, the arc discharge and other discharge at the resistors which could also be observed. As a result of this, it was difficult to

distinguish the laser and arc discharge signals from the above. An experiment which was thought to be a simple one turned out to be more challenging than expected as many other technical problems were faced. This experiment was not investigated further. However, it is believed that there could be a delay between the laser signal and the arc discharge which might be appropriate for their synchronisation.

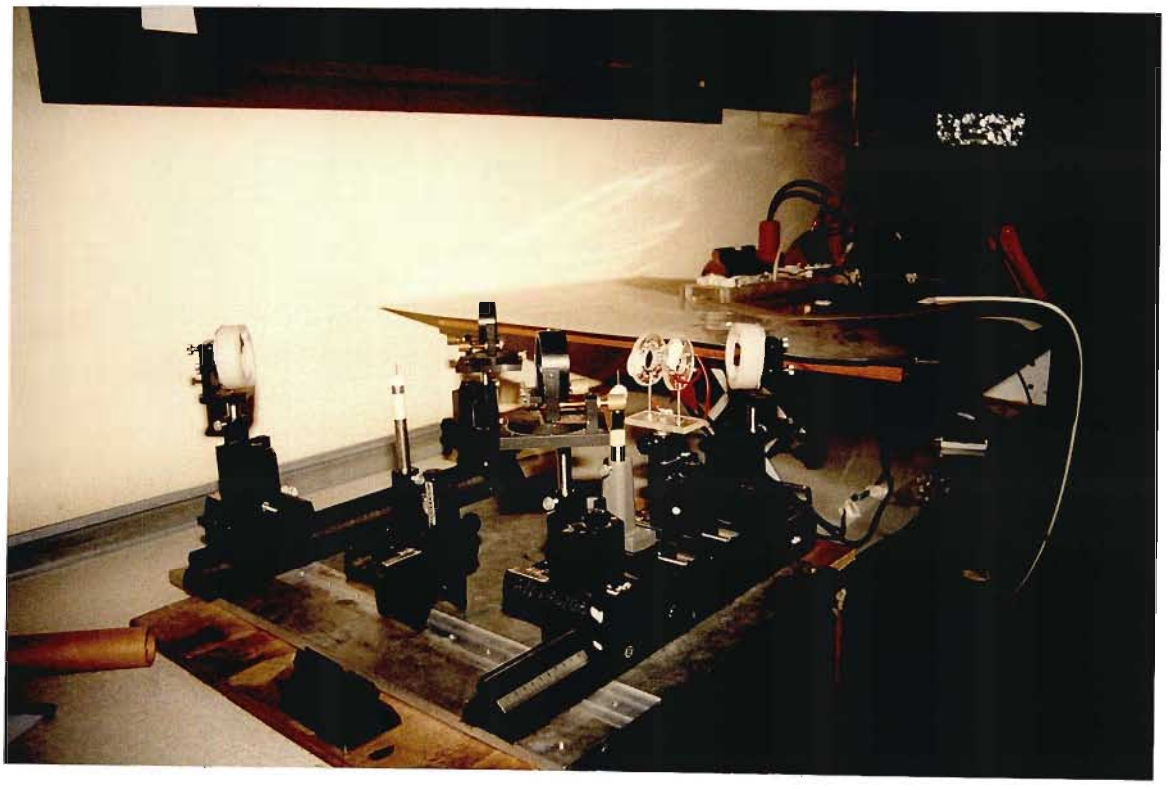

Figure (6.7.2.2): The experimental set-up for the Colliding Shock waves experiment.

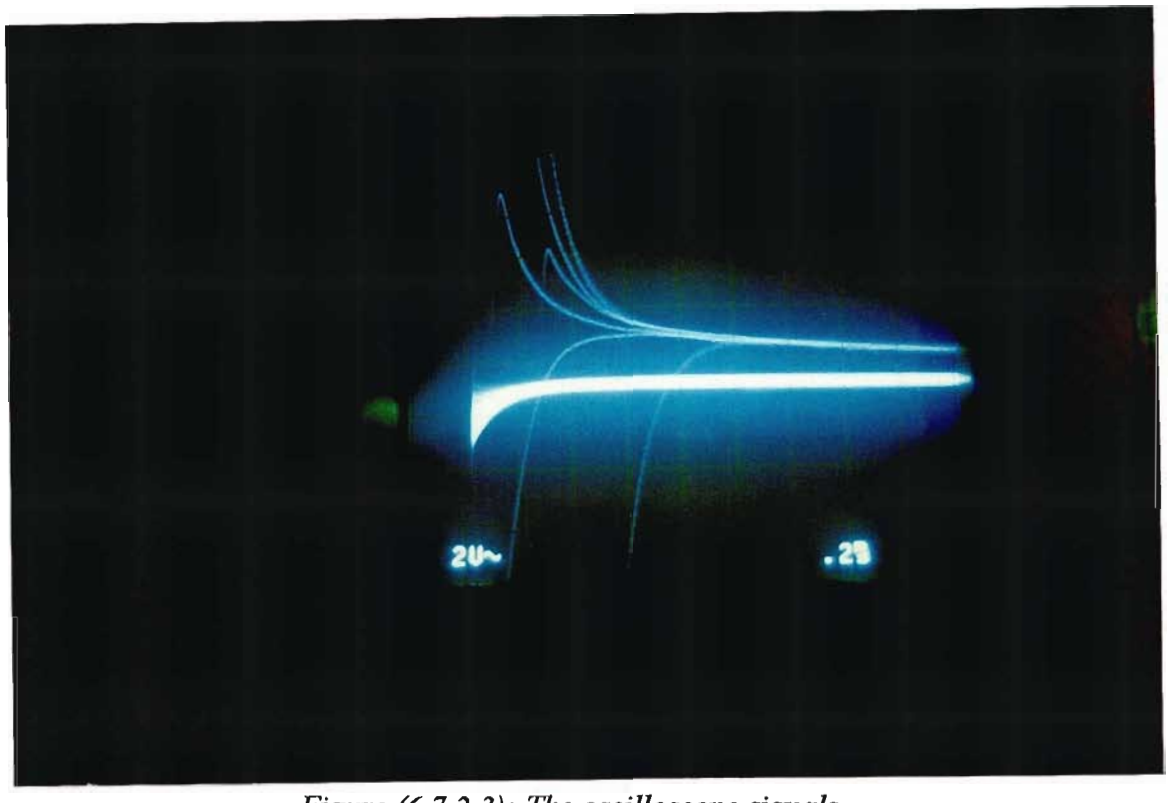

Figure (6.7.2.3): The oscilloscope signals.

6.8 Conclusion

This chapter deals with the experimental investigation of nitrogen lasers. The rectangular-plate N_2 laser was tested and measurements of intensity were recorded using the fast vacuum photodiode. The intensity at both ends of the parabolic N_2 laser were also measured. The intensity was found to be higher for the parabolic. In addition, the laser output from both ends of the laser channel differed considerably. This result confirmed that the parabola was effective in improving the energy performance of the laser. Moreover, photographic papers were used to show that light from the lower end output was more intense. A diffraction experiment was also carried out to determine the wavelength of the UV light and was found to be 340 ± 1 nm which is the wavelength at which nitrogen gas lases.

Michelson interferometry was carried out to determine the coherence lengths of the parabolic N_2 laser and a maximum coherence length of 24.6 cm was obtained, bearing in mind that the pulse length of the laser is approximately 30 cm. From the literature, it is known that the rectangular-plate N_2 laser has a coherence length of 7 cm. Being brighter and more powerful, the parabolic N_2 laser is more suitable for use in the Mach-Zehnder interferometry. Interference is more easily observed as the above results show. Having a higher coherence length than the rectangular-plate N_2 laser, the optical paths can be made longer which implies that the separation between the mirrors and beam splitters can be greater. As a result of this, the Colliding Shock wire device can be made to fit more easily in one of the optical paths. Moreover, parabolic laser light being brighter and less divergent makes the use of photographic paper more appropriate and practical. In the future, this laser will be used as a diagnostic tool in a Colliding Shock wire experiment to determine the refractive index of the gas wave guide.

CHAPTER SEVEN

7.0 LASER ENERGY MEASUREMENTS AND ANALYSIS

7.1 Energy Measurements of various lasers

Several parabolic nitrogen lasers of different dimensions were constructed by the author with the help of a vacation student. Different parameters such as the physical dimensions, the thickness of the plates, the area of the parabola, the area of the lower plate and flow velocity of N_2 gas were varied to observe their effects on the energy output of the laser. The energy per pulse for each laser was measured in Joules using a laser power/energy monitor. Since this instrument was sensitive to electromagnetic and mechanical noise, a wooden box had to be constructed to enclose the laser. Details of the shielding from electromagnetic and mechanical noise are given in section (7.10). The joulemeter was placed at approximately a distance of 15 cm from the ends of the laser which means that the energy values were higher than what are shown in the graphs to follow. Since most of the lasers were operated at high repetition rates of approximately 2 - 4 Hz, the energy of a single pulse represents the average energy of approximately 100 laser shots. The energy averaging of the laser shots was done by the joulemeter itself. The laser output energy was measured at both ends of the laser, i.e. the lower end and the higher end of the laser channel. This was done for each laser in order to investigate whether the parabolic configuration had an effect on the laser energy output. An investigation was also carried out to find out how the energy and divergence at the ends of the laser channel vary with different lasers . Figure (7.1.1) below shows the experimental arrangement for the energy measurements of each laser.

Figure (7.1.1): Picture of the experimental arrangement.

7.2 Experimental Results of Laser 1

The technical specifications of the laser were:

Capacitance (with plates connected) = 13.13 nF
Capacitance (with plates disconnected) = 8.59 nF
Distance between plates = 0.5 mm
Dimensions = 706 x 414 mm
Electrode separation = 2.0 mm

This was a laser made out of a 0.5 mm pc board and the laser channel was inclined at about 30 degrees to the horizontal. It was charged to17 kV and the experimental set-up was as shown below:

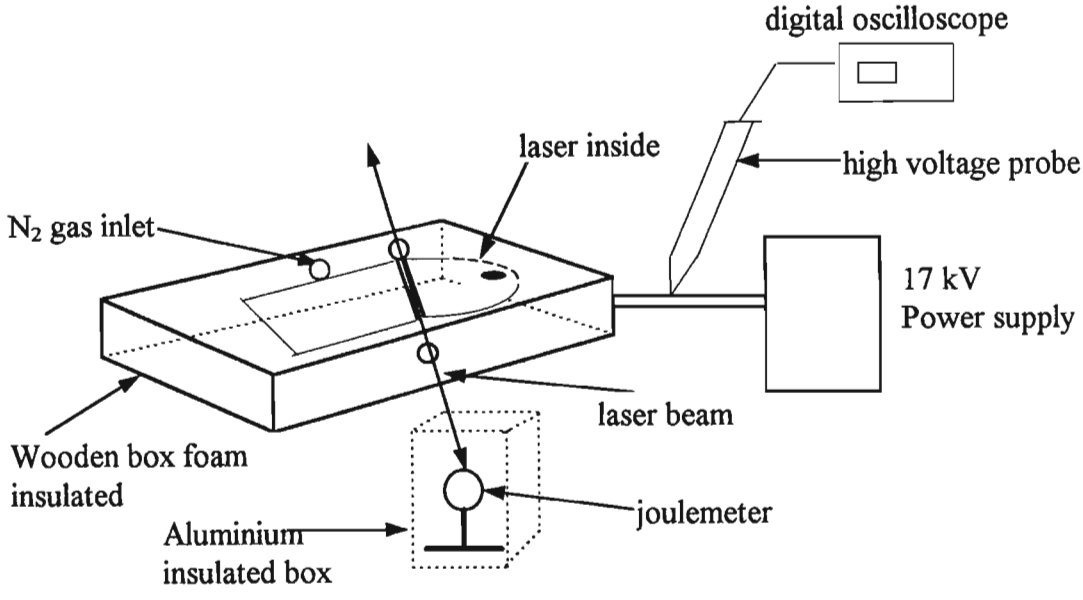

Figure (7.2.1): Schematic of the experimental set-up.

The laser output energy was measured and as mentioned above, the energy of about 100 laser shots was captured and the average energy of a single shot was then calculated. A set of energy measurements was taken at both ends of the laser channel and the conditions of constant voltage and same electrode-detector distance were maintained in each case. Measurements were taken at different nitrogen flow velocity and the following graphs show the energy variation with pulse number at the lower and higher ends of the channel. Figure (7.2.2) shows a picture of Laser 1. It would be worth recalling that the higher end output refers to the laser energy from the end of the laser channel which is closer to spark gap and the lower end output refers to the output energy from the end which is further from the spark gap.

The lower end of the channel was the one from which a higher energy output was expected and on the other hand at the higher end, a lower output energy was expected. Figures (7.2.3a – 7.2.3e) show the energy variation with pulse number at the lower and higher ends for different flow velocities of nitrogen gas. The minimum measurable energy with the Nova detector is approximately 10 μJ. Since a flowmeter was not

available to measure the flow velocity of the N_2 gas in the laser channel, the values shown in the table do not correspond to the actual flow velocities but the scale readings 2, 4, 6, 8, 12 represent a linearly increasing flow velocity or increasing amount of nitrogen flushed into the laser channel. One arbitrary unit approximately corresponds to 1 litre/minute. It should also be noted that the energy of one laser pulse in the graphs (pulse no.) represents the average energy of approximately 100 laser shots at 2 Hz recorded over a period of 1 min. A digital oscilloscope was at all times connected to the laser via a high voltage probe in order to measure the exact voltage at which the laser fired. Thus the same voltage of 17kV was maintained for each of the measurements.

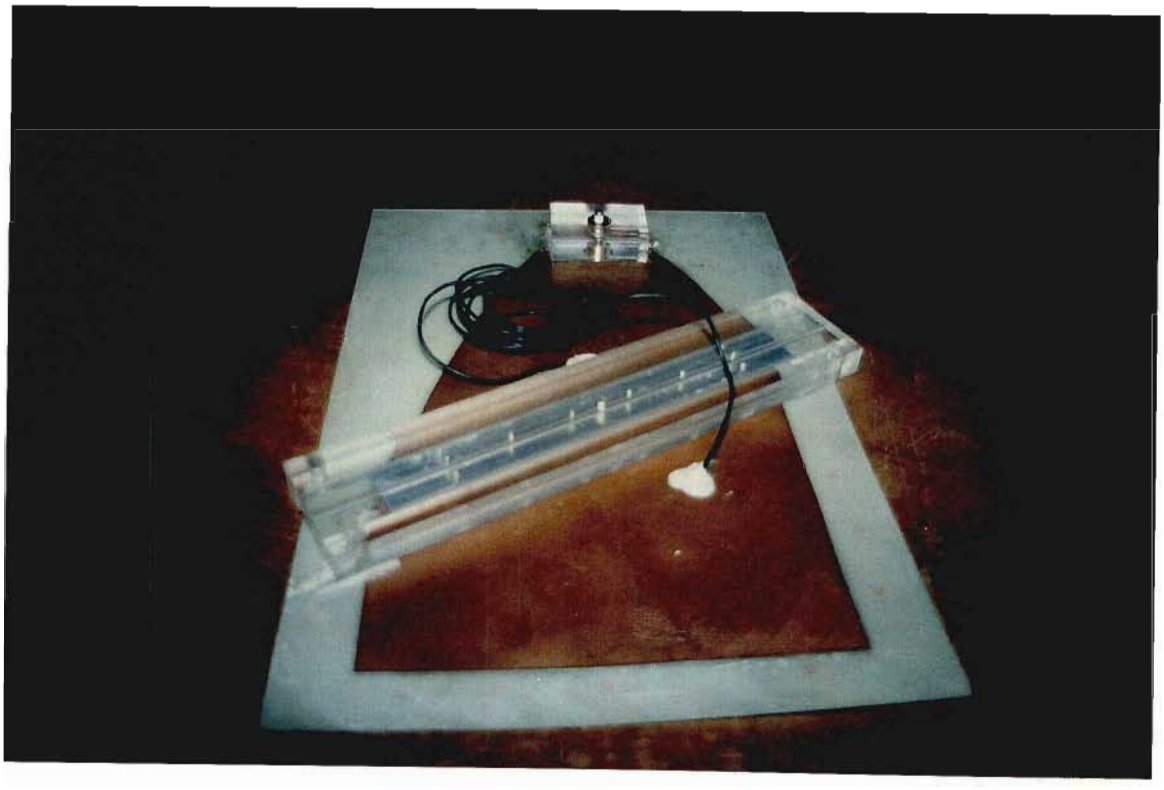

Figure (7.2.2): Picture of Laser 1.

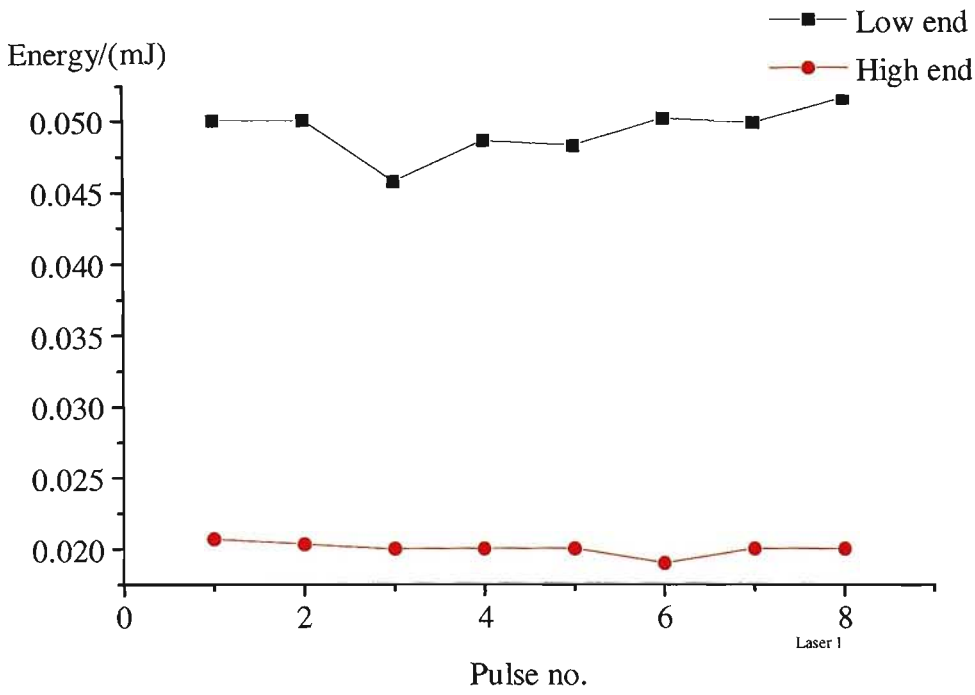

(Note: Each point is the average of 100 measurements).

Figure (7.2.3a): Variation of laser energy with pulse no. at N_2 flow 2.

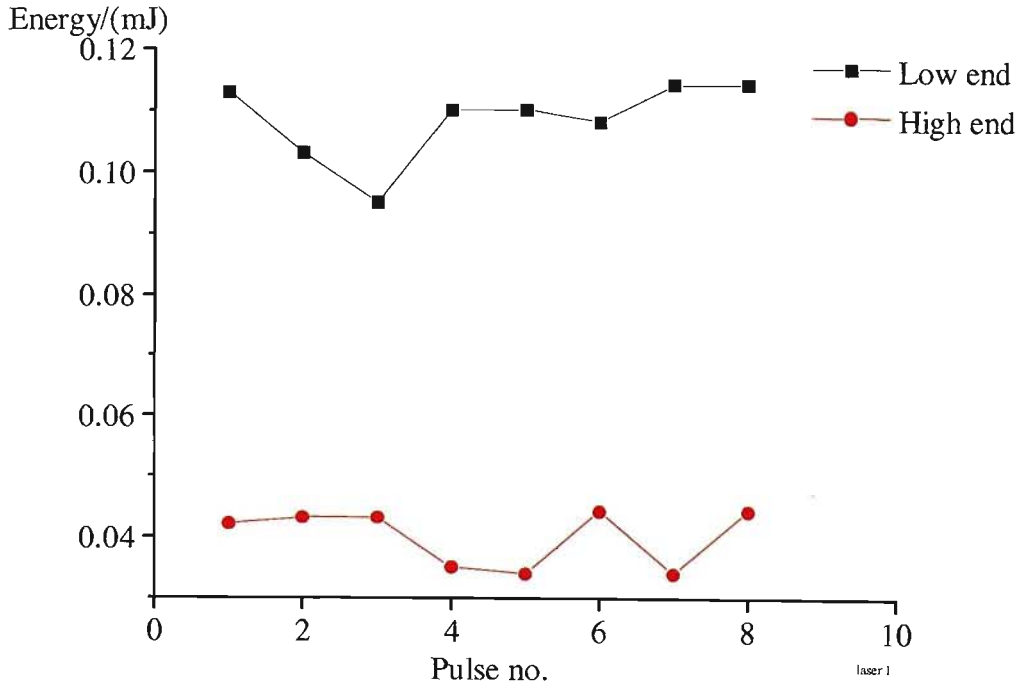

Figure (7.2.3b): Variation of laser energy with pulse no. at N_2 flow 6.

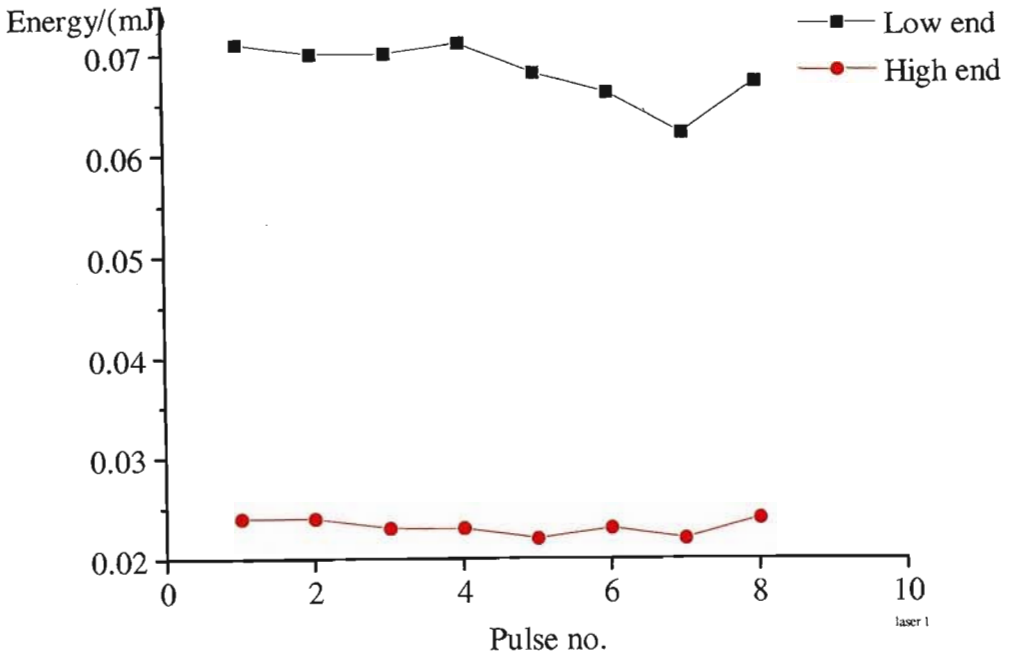

Figure (7.2.3c): Variation of laser energy with pulse no. at N_2 flow 12.

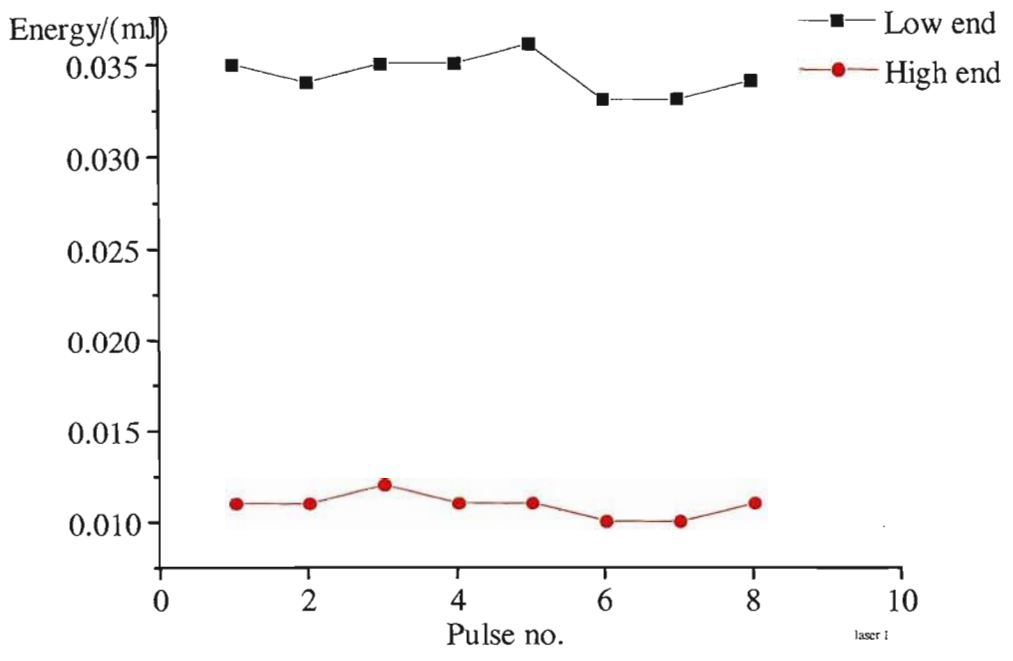

Figure (7.2.3d): Variation of laser energy with pulse no. at N_2 flow 18.

Figure (7.2.3e) below shows a graph of the variation of the laser output energy with the nitrogen flow velocity. In other words, it is a summary (the result of averaging) of all the measurements.

A polynomial regression fit was applied to the graphs to give a polynomial curve of second degree. This gave a better indication of the variation of the laser energy with the flow speed of N_2 gas.

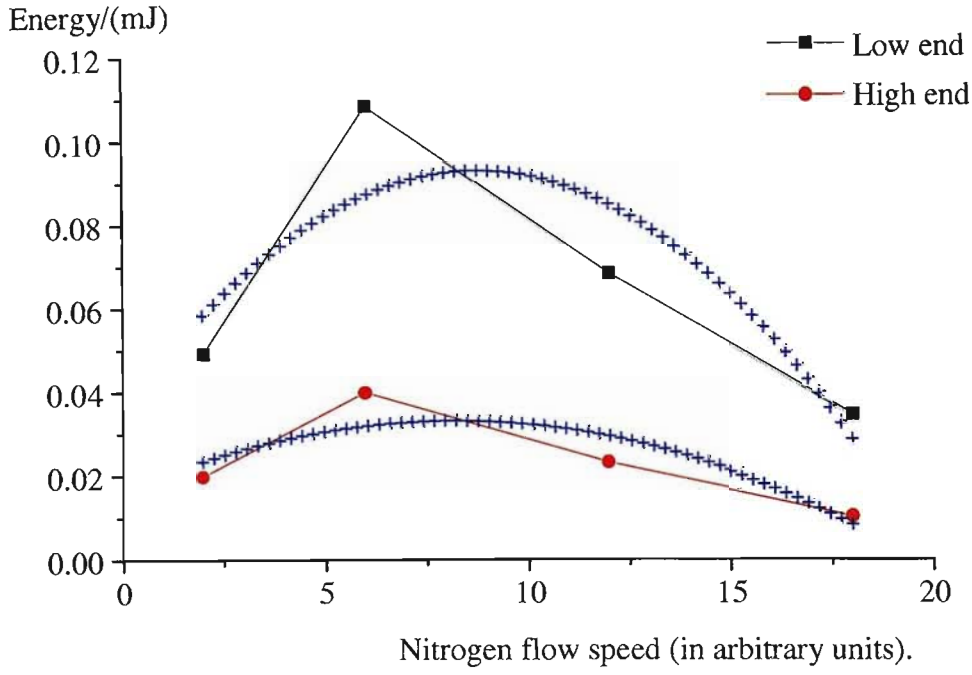

Figure (7.2.3e): Variation of the laser output energy with N_2 flow.

7.2.1 Discussion

The first point to note from Figures (7.2.3a –7.2.3d), is that the energy output at the lower end of the laser channel was greater, about 50-60 % more than that at the higher end. This means that the parabolic configuration is effective. It can also be seen that the energy output was not stable and varied from pulse to pulse. This could be attributed to the erratic performance of the pressurised self-triggered sparkgap which did not keep a constant electrical energy transfer to the plates. The highest energy output achieved was around 0.11 mJ at a N_2 level of 6. From Figure (7.2.3e), it can be seen that the trend of the energy variation with N_2 levels is similar for the lower and higher ends. Both reach their peak at almost the same nitrogen level (refer to figure 7.2.3e) and after the maxima both of them have a decreasing slope. It is also worth calculating the laser's efficiency ξ. The energy storage of the laser is given by

$$E = 0.5\, CV^2$$
$$= 0.5(13.13 \times 10^{-9})(17 \times 10^{3})^2$$
$$= 1.897 \text{ J}$$

The highest energy output obtained with Laser 1 was 0.11 mJ and hence the laser's efficiency $\xi = 0.006$ %.

7.3 Experimental Results of Laser 2

The technical specifications of the laser were:

Capacitance (with plates connected) = 4.42 nF
Capacitance (with plates disconnected) = 2.89 nF
Distance between plates = 1.0 mm
Dimensions = 706 x 414 mm
Electrode separation = 2.0 mm

The same experimental arrangement as shown in Figure (7.1.1) was used. This laser had exactly the same width and breadth as the previous one except it was thicker as the distance between the top and the bottom plates was 1.0 mm. Figure (7.3.1) shows a picture of Laser 2. A lower output energy than Laser 1 was expected due to its lower capacitance. Figures (7.3.2a) – (7.3.2e) illustrate the experimental results of laser energy variation with pulse no. and nitrogen gas level in graphical forms.

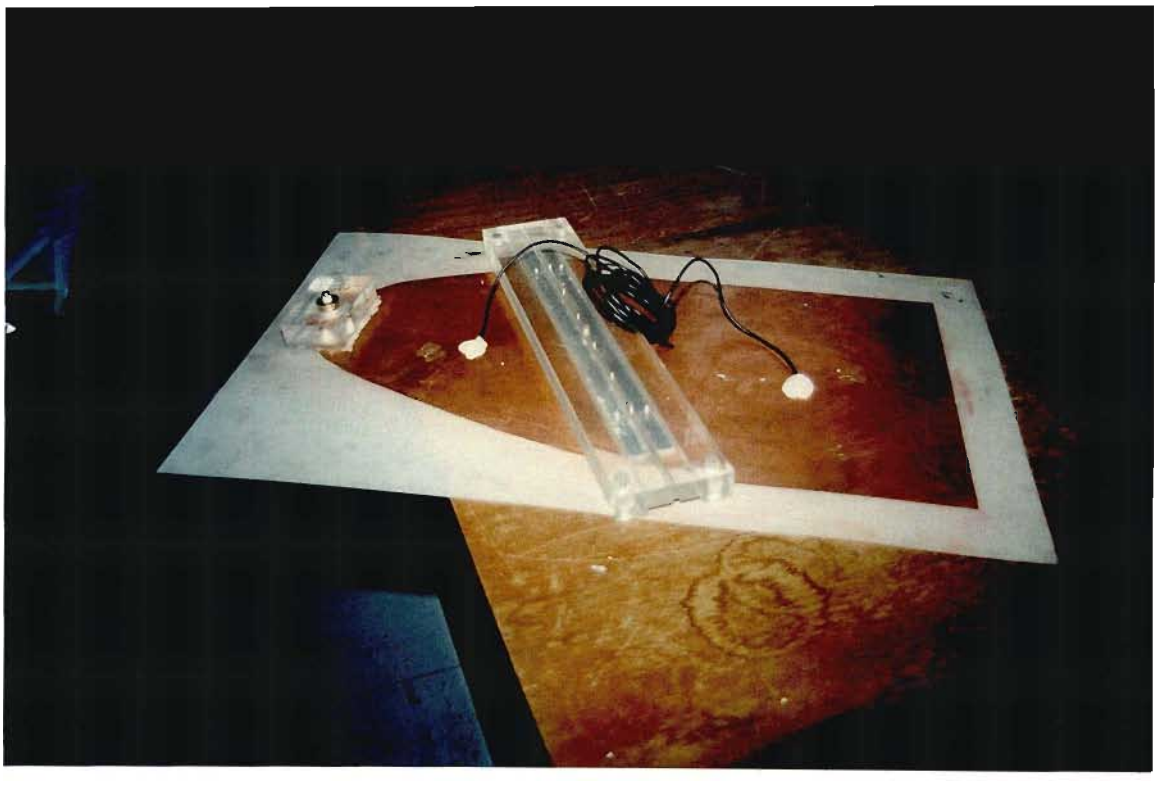

Figure (7.3.1): Picture of Laser 2.

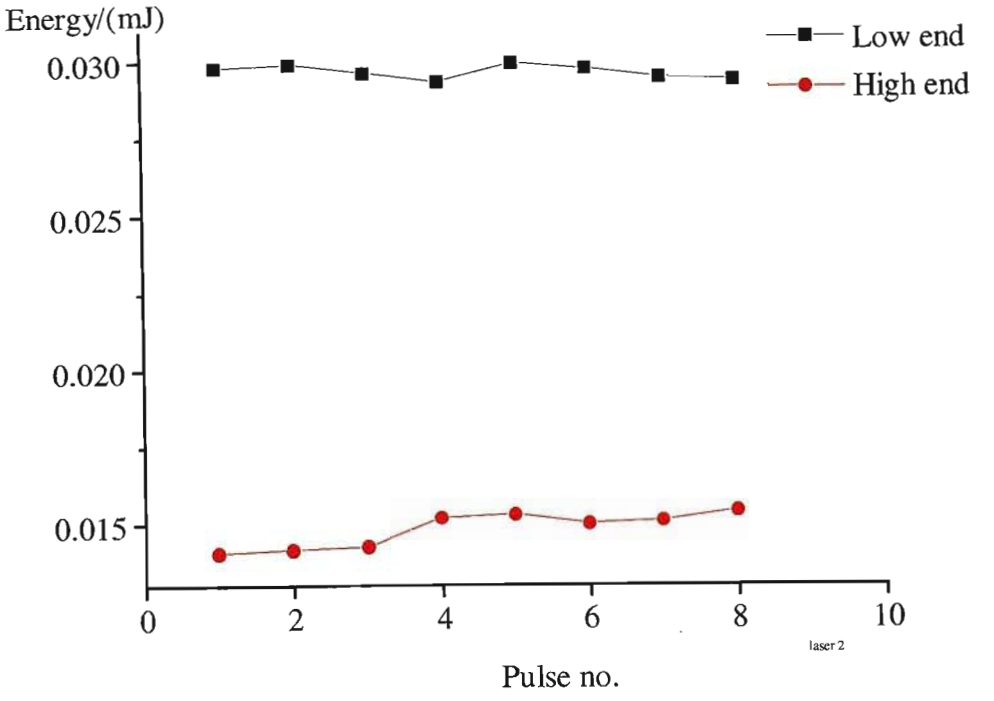

Figure (7.3.2a): Variation of energy with pulse no. at N_2 flow 2.

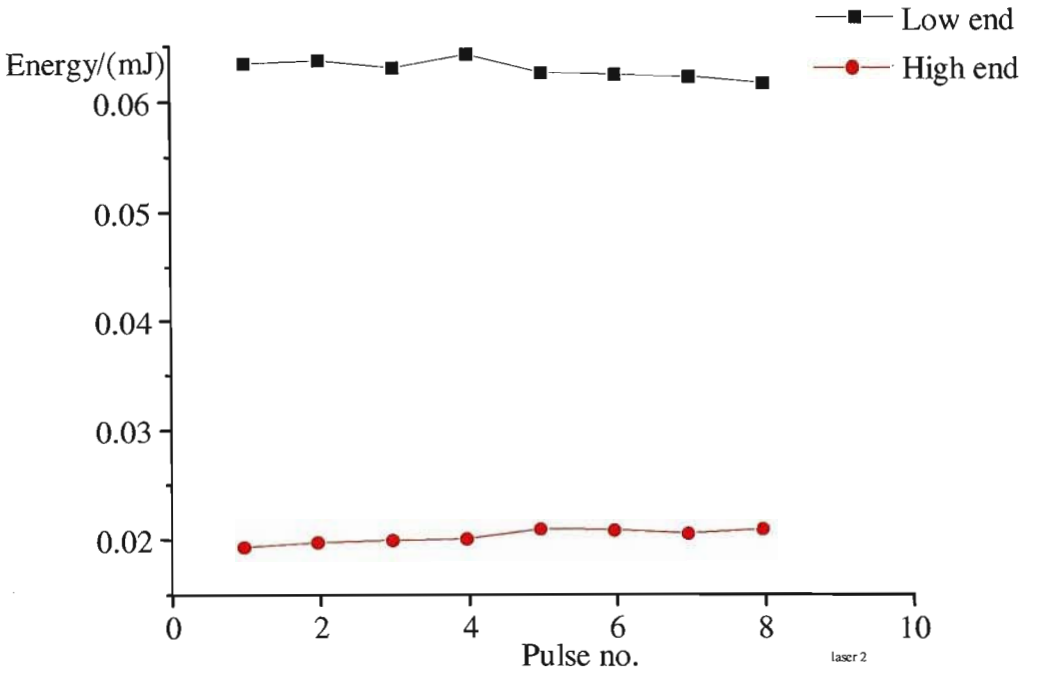

Figure (7.3.2b): Variation of energy with pulse no. at N_2 flow 6.

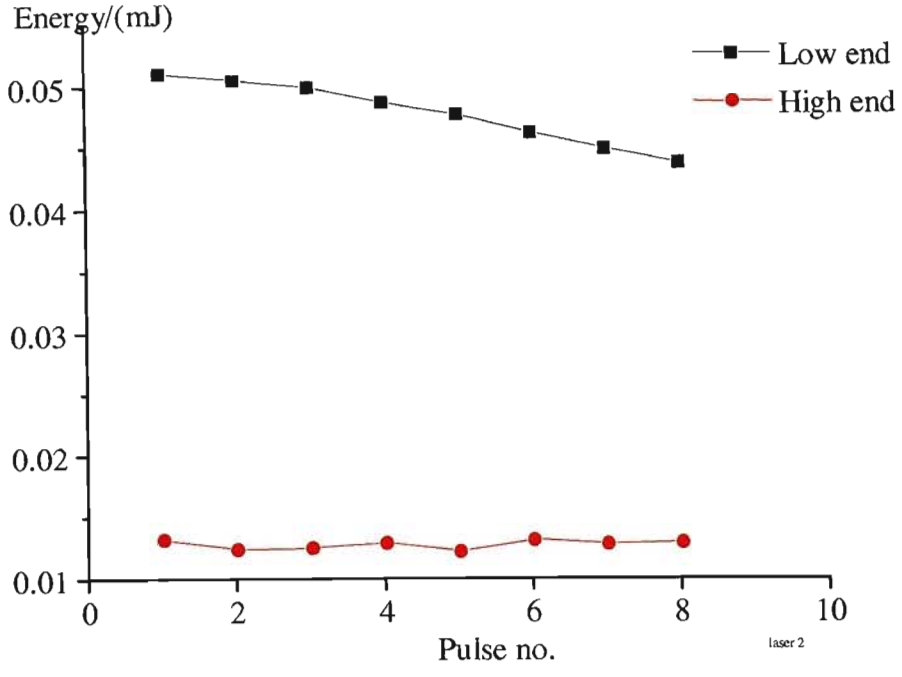

Figure (7.3.2c): Variation of energy with pulse no. at N_2 flow 12.

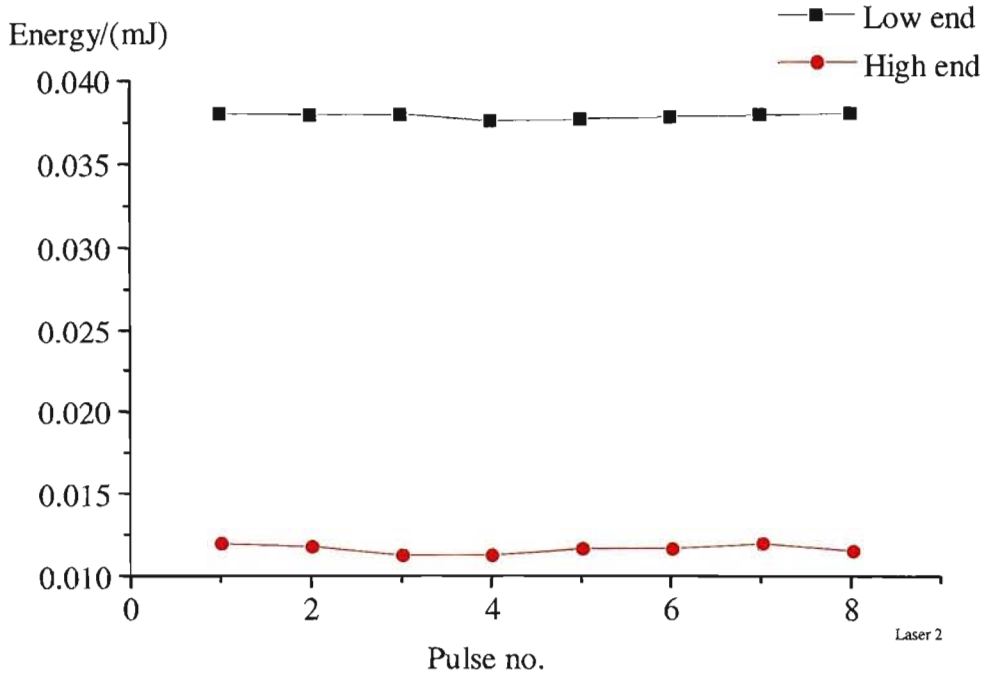

Figure (7.3.2d): Variation of energy with pulse no. at N_2 flow 18.

Figure (7.3.1e) sums all the experimental results by showing the variation of output energy with nitrogen flow velocities. Once again, a polynomial regression fit was applied to obtain a polynomial curve of second degree.

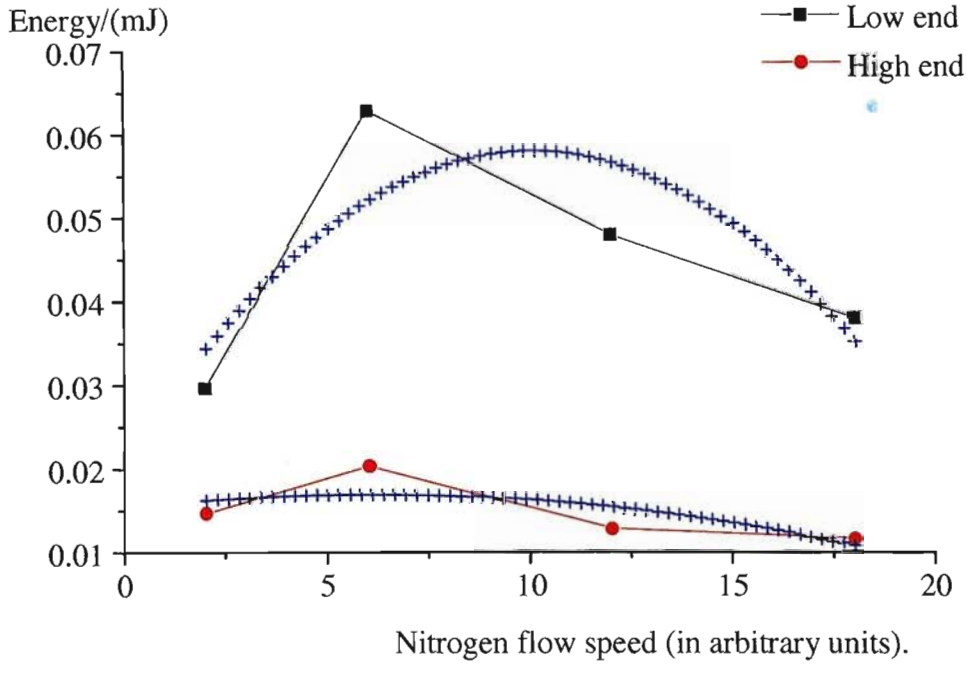

Figure (7.3.2e): Variation of energy with N_2 flow.

7.3.1 Discussion

As can be seen from Figures (7.3.2a) to (7.3.2d), the laser output energy was higher at the lower end that that at the higher end of the laser channel. Again, here it is seen that the energy output was not stable from pulse to pulse which was due to the spark gap. The average energy achieved was 0.063 mJ at a nitrogen level of 6 which corresponds to the results obtained with Laser 1. Here, again the highest peak output energy (average energy of 100 shots) for both the lower and higher ends occurred at approximately the same N_2 level and both graphs show the same tendency (refer to figure 7.3.2e). The energy storage of Laser 2 was calculated to be 0.639 J and therefore, its efficiency was approximately 0.01 %.

7.4 Experimental results of Laser 3

The technical specifications of the laser were:

Capacitance (with plates connected) = 2.04 nF.
Capacitance (with plates disconnected) = 1.95 nF.
Distance between plates = 1.0 mm.
Dimensions = 590 x 403 mm.
Electrode separation = 2.0 mm

(Laser 2) except that this one had smaller physical dimensions, meaning a smaller surface area of the plates, therefore a lower capacitance. Thus, a lower output energy was expected.

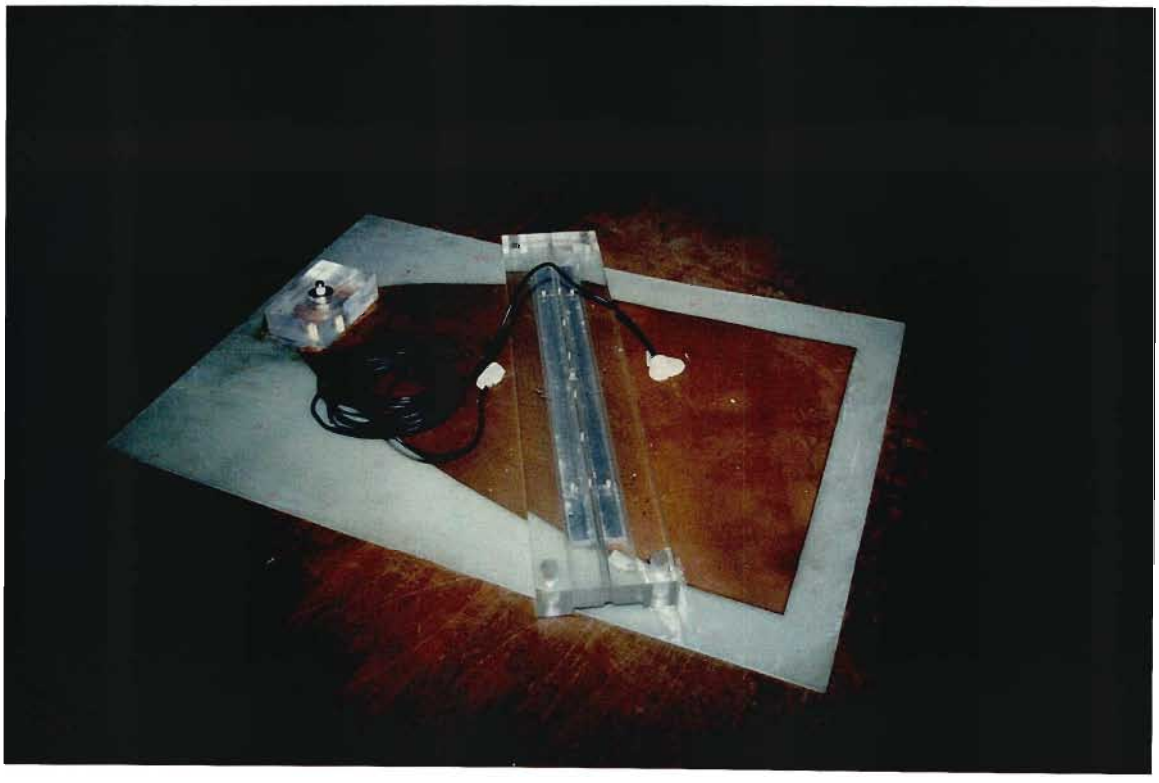

Figure (7.4.1): Picture of Laser 3.

Figures (7.4.2a) – (7.4.2e) show the variation of laser output energy with pulse number at different nitrogen levels.

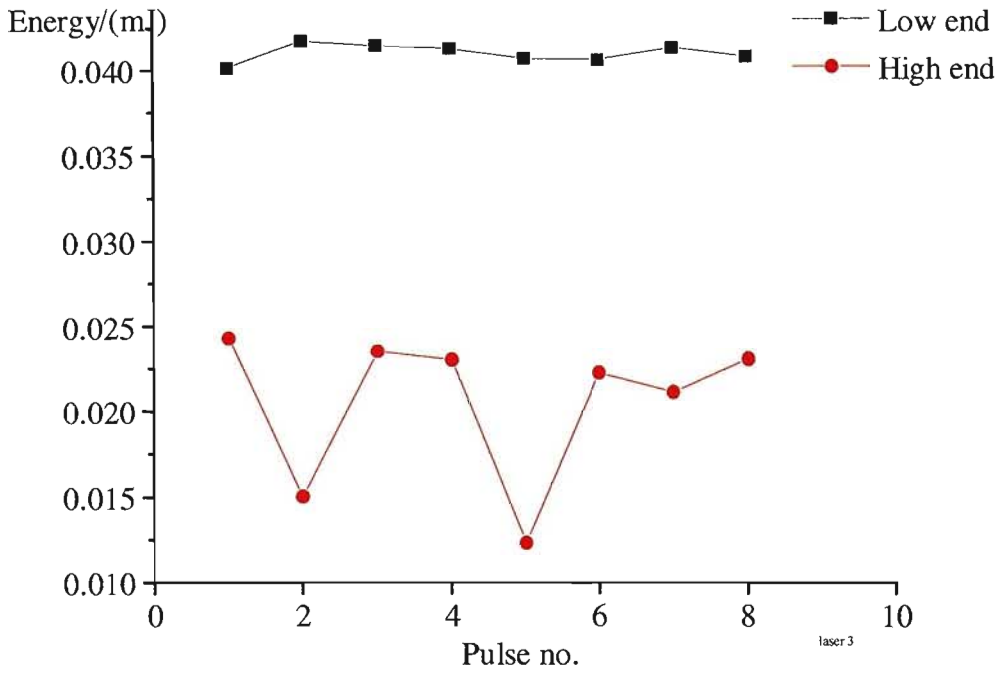

Figure (7.4.2a): Variation of energy with pulse no. at N_2 flow 2.

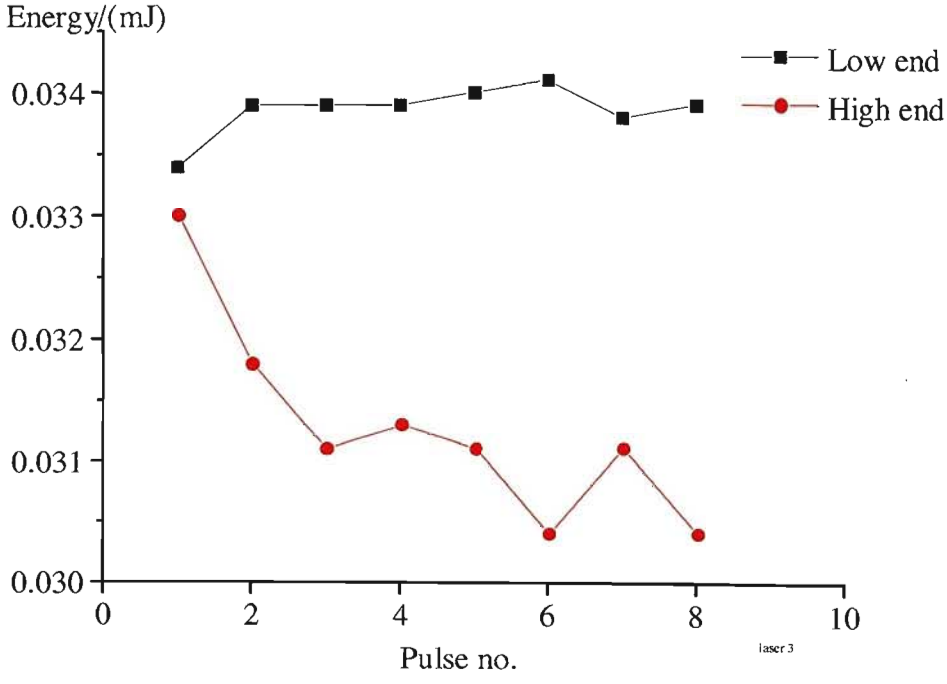

Figure (7.4.2b): Variation of energy with pulse no. at N_2 flow 6.

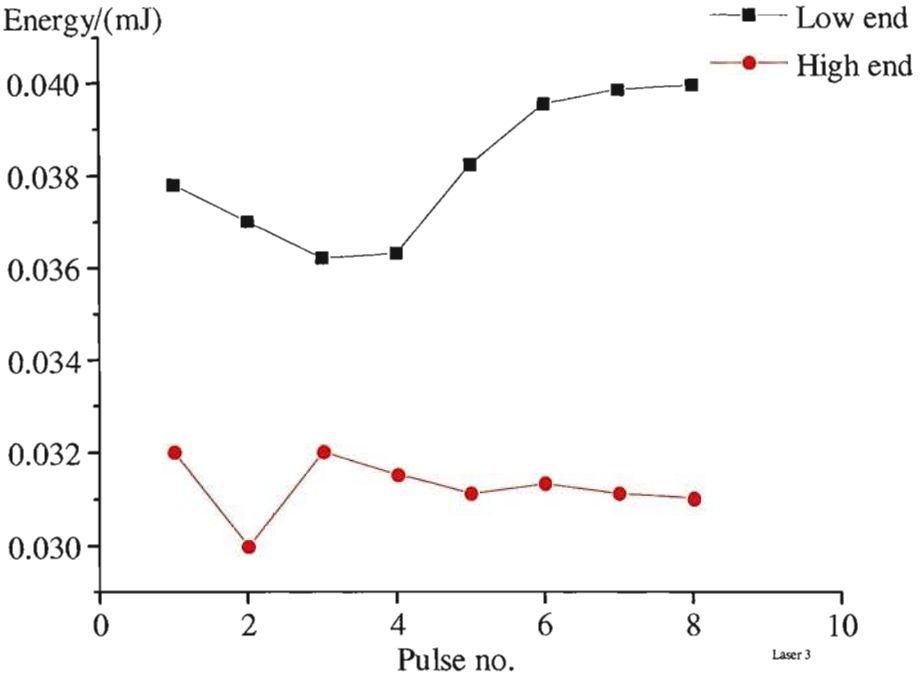

Figure (7.4.2c): Variation of energy with pulse no. at N_2 flow 12.

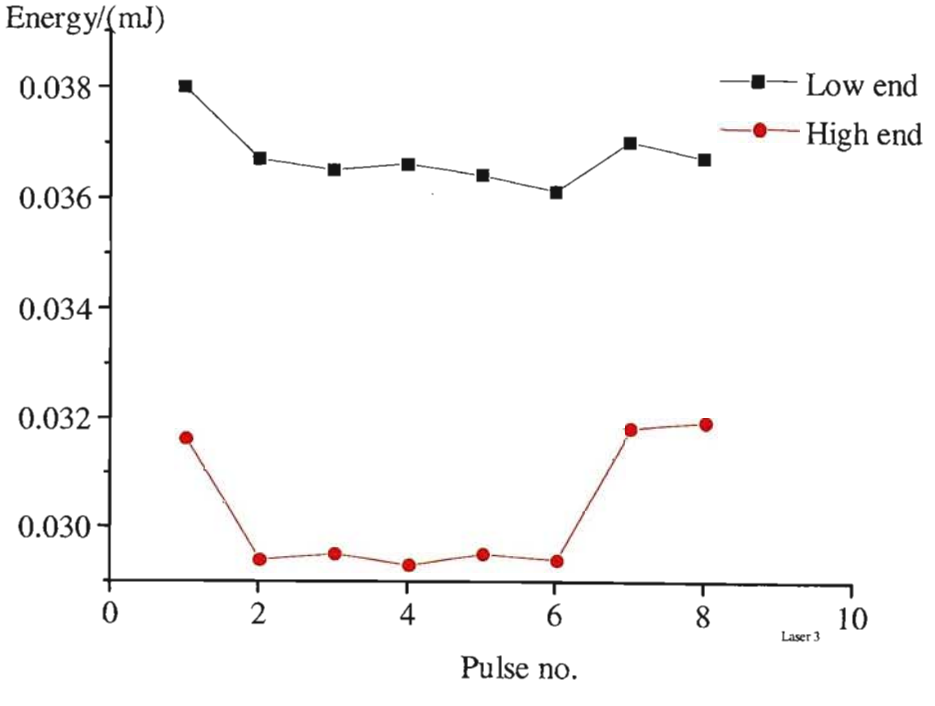

Figure (7.4.2d): Variation of energy with pulse no. at N_2 flow 14.

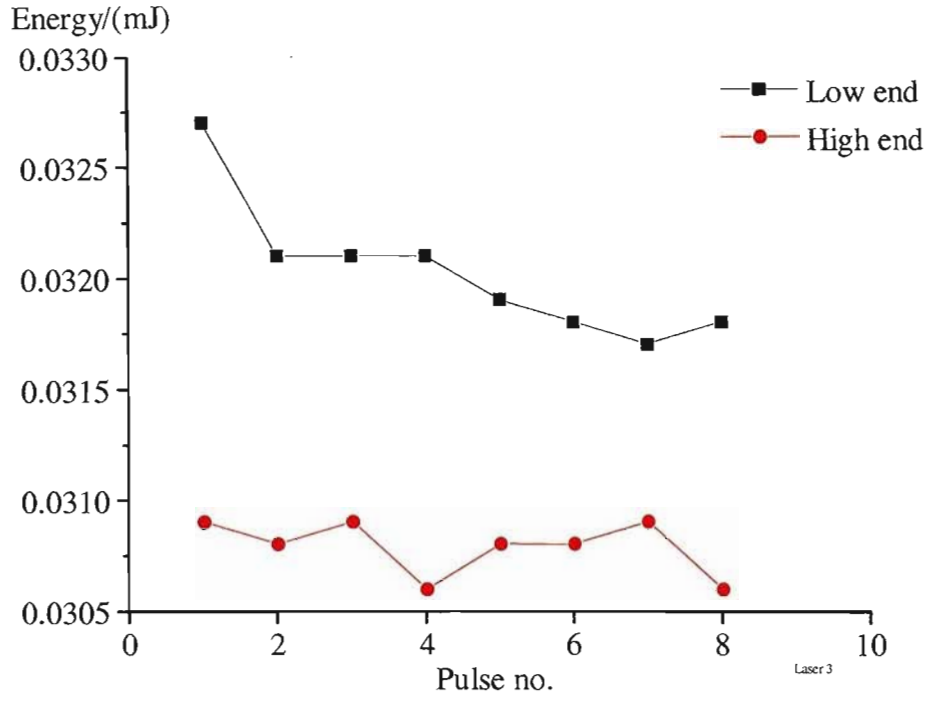

Figure (7.4.2e): Variation of energy with pulse no. at N_2 flow 18.

Similarly, as it was done in the other cases, Figure (7.4.2f) below shows the variation of the laser energy output with nitrogen level.

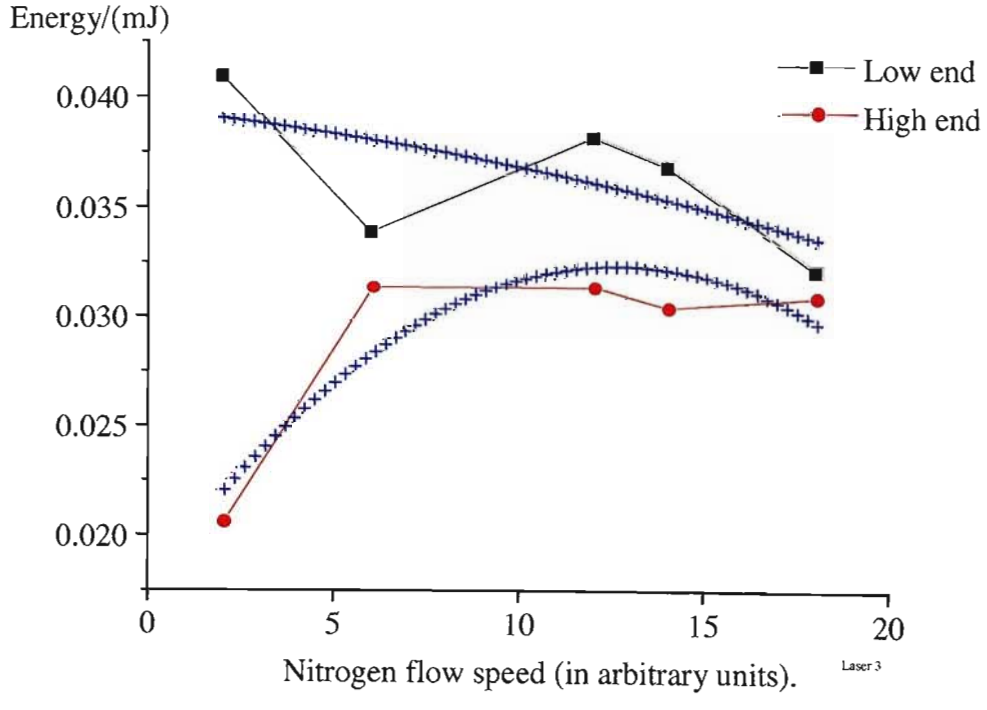

Figure (7.4.2f): Variation of energy output with N_2 flow.

7.4.1 Discussion

In this case the laser energy output values of the lower end and that of the higher end did not differ significantly compared to the energy values obtained from the Laser 1 and Laser 2. The energy values from both ends at N_2 level 6, 12,14 and 18 are within ± 0.05 mJ. However, there is a significant difference of 50% in the energy value at N_2 level 2. Again, in this case also, the energy output from one pulse to the next varied considerably which was due to the erratic performance of the spark gap. It has to be noted the energy output stability of this laser was the worst when compared to the other two lasers (Laser 1 and Laser 2). Considering the small size of the laser itself and the area of the parabola, it is highly probable that the parabolic configuration was not effective in this case. One other reason which could have contributed to the above was that the spark gap was not exactly at the focus of the parabola. After examining the location of the spark gap, it was found to be off-focus by a few mm. This would lead to circular electric waves reaching the laser discharge channel instead of plane waves. The water wave simulation experiment results (section 5.3, p 59) showed that if the spark gap is not precisely located at the focus, then the circular waves created there would not be converted to plane waves. It has to be noted also that the output energy from the lower end is the maximum (0.041mJ) at N_2 level 2 and then, as seen from the graph (Figure7.4.2f) the energy decreases with increasing N_2 level. In addition, the variation of the high and low ends output energy was different. The energy storage of Laser 3 was calculated to be 0.295 J which meant an efficiency of 1.39×10^{-4} %.

7.5 Discussion of the overall results and conclusion

The three lasers namely Laser 1, Laser 2 and Laser 3 work on exactly the same principle. However, Laser 1 and Laser 2 differ in the sense that the circuit board used in the latter is thicker. It is made up of a 1 mm pc board unlike laser 1 which is made up of 0.5 mm pc board. Laser 2 and Laser 3 differ in physical dimensions, the latter is smaller in size. Therefore, the aim of this experiment was to investigate the variation of the laser energy output (both the lower and higher end outputs) with distance between the plates and area of the plates. Moreover, the variation of energy with N_2 level was also investigated.

The common characteristic among the lasers except not entirely for the small Laser 3, was that the laser energy output from the lower end of the channel was about 60% more that the energy from the higher end. This implies that the parabolic configuration of the upper plate of the laser was efficient in increasing the energy output. As mentioned earlier, the parabolic geometry of Laser 3 did nothing to improve the laser. This is because of its small size and the fact that the spark gap was not precisely located at the focus. However, it was working as expected at the lowest N_2 level. The other common behaviour between Laser 1 and Laser 2, that is the lasers with same length and width but different thickness, was that both of them have their peaks at almost the same N_2 flow (6-8). The graphs of energy versus N_2 gas flow speed are similar. From these experimental data, it was evident that the speed of N_2 gas flow had an effect on the laser output energy. The other point to note is that both of these graphs (refer to Figures (7.2.3e) and (7.3.2e) have a decreasing slope after their maximum, meaning that the energy output increases with increasing nitrogen level until

a limit is reached where the laser energy decreases with increasing N_2 amount. In addition, these graphs also show that the lower and higher end trends of the energy variation with N_2 level almost coincide. In other words, as the lower end output energy increases or decreases, the higher end output energy follow the same tendency. However, this was not the case with the small Laser 3. The contrary to what is expected occurred since while the lower end energy output increases, the higher end output decreases and vice versa. This behaviour, as mentioned earlier, was due to the small size of the parabola and the spark gap not being exactly at the focus.

In the case of Laser 1 and Laser 2 which behaved as expected, a possible explanation about the variation of their energies with N_2 level is given below:

Initially, at a low flow velocity of N_2 there was a lower volume of nitrogen molecules or a low rate of N_2 molecules per second was being flushed through the laser discharge. Therefore, a lower number of nitrogen molecules was being excited by the discharge at the laser channel to cause laser light by stimulated emission. Due to a lower number of nitrogen molecules present in the laser channel, there were some O_2 molecules and other impurities present. This lead to a low laser intensity. Thus, initially at a low N_2 level, the output energy was low. As the nitrogen level flow velocity was increased, the output laser energy was observed to increase. This behaviour was attributed to the presence of more N_2 molecules and less O_2 molecules in the laser discharge. However, there was a limit, which could be called the 'saturation limit' or the maxima which did coincide in the case of Laser 1 and Laser 2. As can be seen from the graphs Laser 1 and Laser 2 reached their peak output at around the same nitrogen level (level 6-8). At this level of 6 to 8, which corresponded to the maxima of both lasers, there was pressure turbulence in the laser channel and at this stage, the distribution of N_2 gas was not symmetrical in the discharge region. It is worth noting that the same set of electrodes and electrode separation were used on each of those lasers.

In conclusion, the parabolic configuration of the upper plate does increase the laser output energy. The thinner laser of thickness 0.5 mm had a greater output energy due its greater capacitance. The effectiveness of the parabolic shape of the top plate depends significantly and remarkably on the precise location of the spark gap at the focus. A few mm away from the focus of the parabola, the laser would not produce the desired results. The small Laser 3 demonstrated this behaviour. The nitrogen flow velocity or the amount of N_2 flushed through the laser channel has an effect on the output energy of the laser and a possible explanation is given above. However, the lasers described and constructed are not stable with regard to the energy output of each pulse and the reason attributed to this behaviour is the unreliable performance of the spark gap. However, it must be mentioned that a more or less constant voltage has been maintained for all the measurements.

The highest output average energy achieved was 0.11 mJ per laser pulse which was the average energy output of Laser 1 with thickness 0.5 mm. The average output energy of Laser 2 with thickness 1.0 mm was 0.063 mJ/pulse and the lowest average output energy of 0.04 mJ/pulse was achieved by Laser 3. The highest laser efficiency of 0.01 % was given by Laser 2 which was constructed from a 1 mm pc board and the lowest laser's efficiency of 1.39×10^{-4} % was demonstrated by Laser 3 which was also made

from the 1.0 mm thickness of pc board. Laser 1 gave the highest average laser energy output with an intermediate laser efficiency of 0.006 %. The parabolic shape was effective since the energy at the lower end of the laser channel was approximately 60% more than that at the higher end.

7.6 Experimental results of Laser 4

The technical specifications of the laser were:

Capacitance (with plates connected) = 47.5 nF.
Capacitance (with plates disconnected) = 20.7nF.
Distance between plates = 0.5mm.
Dimensions = 105.8 mm x 72.3 cm.
Electrode separation = 2.5 mm
Area of parabola = 3200 cm^2

A laser with the above specifications was constructed by the author. It was set-up in the same way as was done for the other lasers and Figure (7.6.1) shows a picture of the laser. It was approximately twice the size of the other lasers. In this case, the bottom plate was larger in surface area than the top parabolic plate. However, having a higher total surface area, a greater energy output was expected.

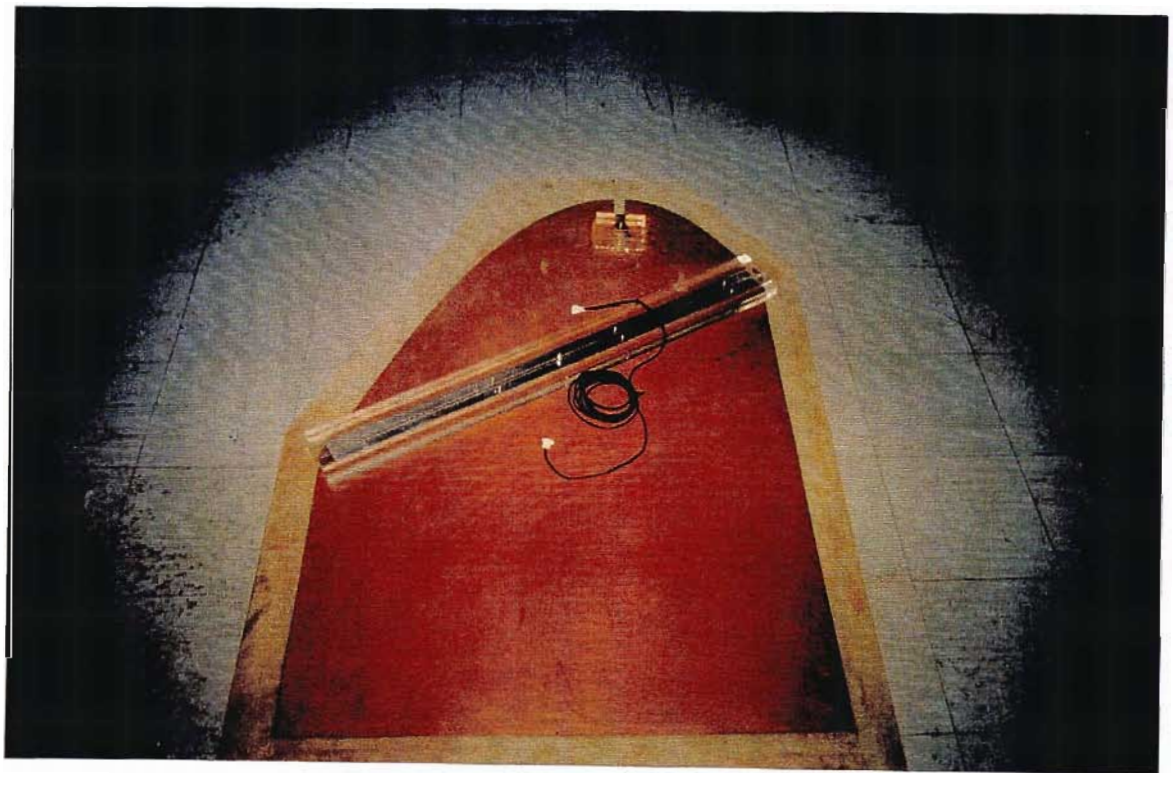

Figure (7.6.1): Picture of Laser 4.

Due to its larger dimensions, this laser could not be placed in the insulated box as was done for the other lasers. There were two options: the first one was to build another box with the corresponding size to contain the laser and the second option was to place the laser and detector in separate rooms to reduce the mechanical and electromagnetic noises. The latter seemed to be more viable. Therefore, a 1 cm diameter hole was drilled through wooden wall which separated the two rooms. The thick wall ensured that mechanical noise did not reach the detector located on the other side of the wall. The detector was shielded against electromagnetic noise by placing it in a box wrapped with a thick layer of aluminium foil. A thin glass usually used as microscope slides was glued on the hole. It was made sure that this glass did not absorb much UV light. Another hole had to be drilled for energy measurements at the higher end of the laser channel. Figures (7.6.2a) and (7.6.2b) show the set-up for energy measurements at the lower end and higher end respectively. The conditions of same electrode-detector distance and voltage were maintained in each case.

Figure (7.6.2a): Set-up for energy measurements at the lower end of laser channel.

Figure (7.6.2b): Set-up for energy measurements at the higher end of laser channel.

The flow velocity of N_2 gas was varied to observe the effect on the energy output of the laser. Figures (7.6.3a) to (7.6.3c) show the variation of laser energy output with pulse number at particular N_2 flow velocity and Figure (7.6.3d) shows the variation of energy output at different N_2 flow velocities.

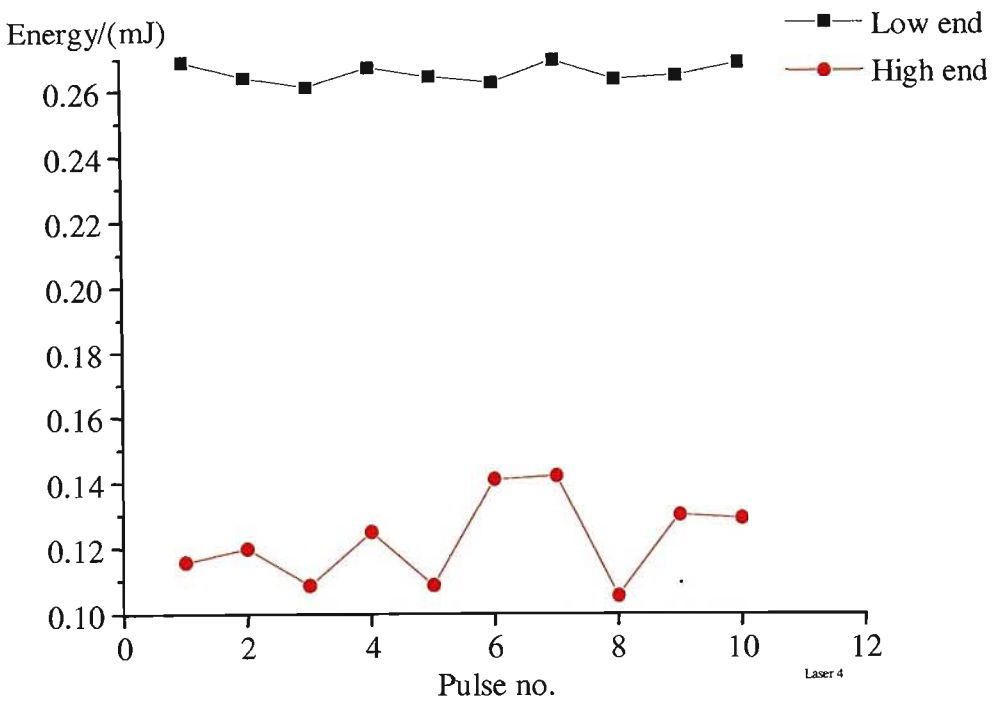

Figure (7.6.3a): Variation of energy with pulse no. at N_2 flow 2.

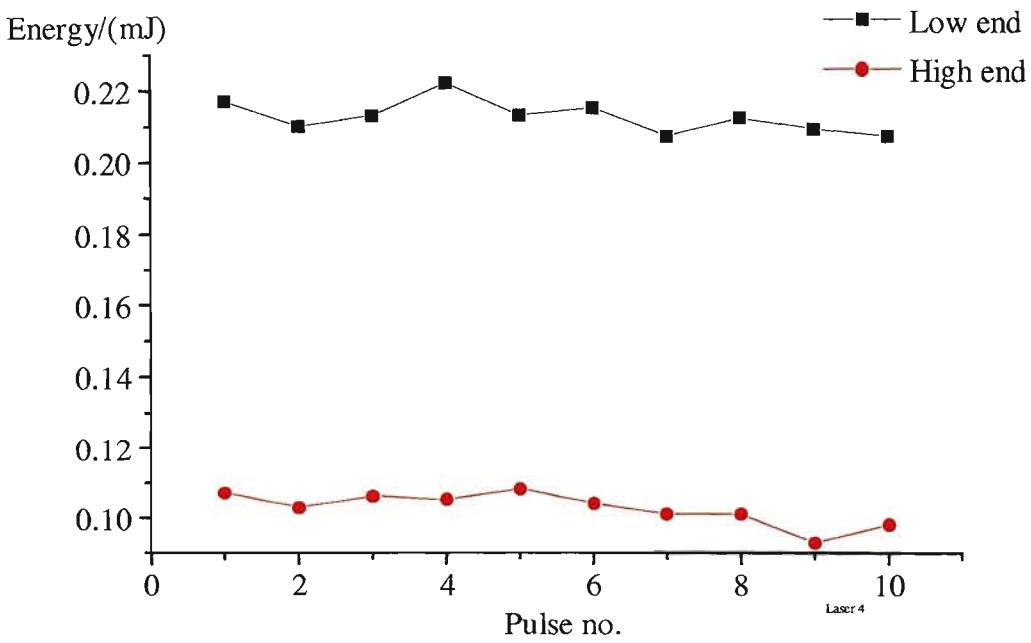

Figure (7.6.3b): Variation of energy with pulse no. at N_2 flow 6.

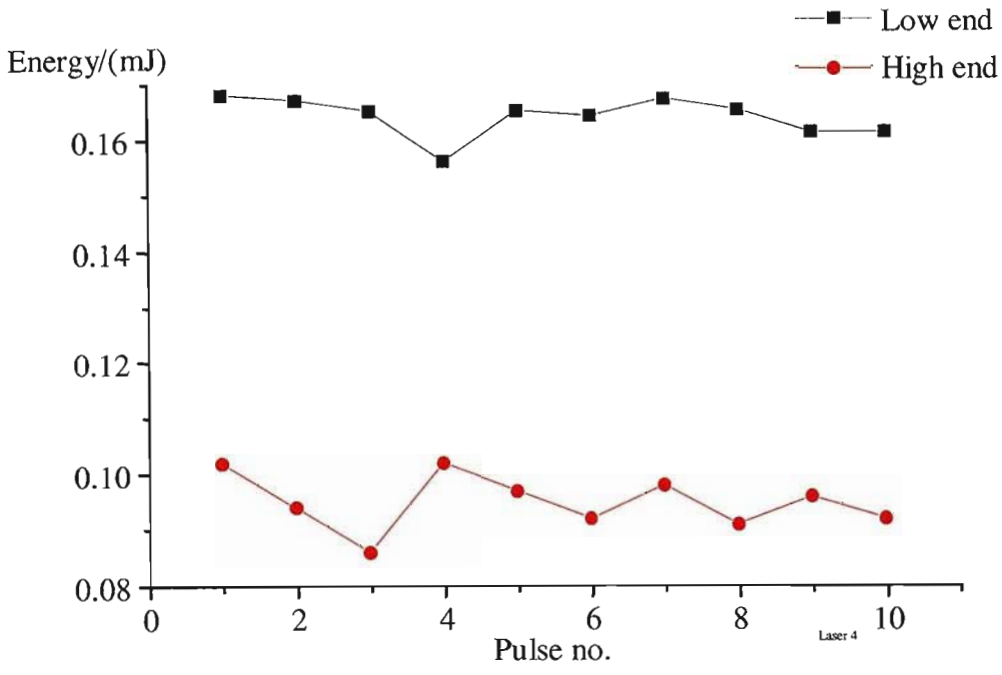

Figure (7.6.3c): Variation of energy with pulse no. at N_2 flow 9.

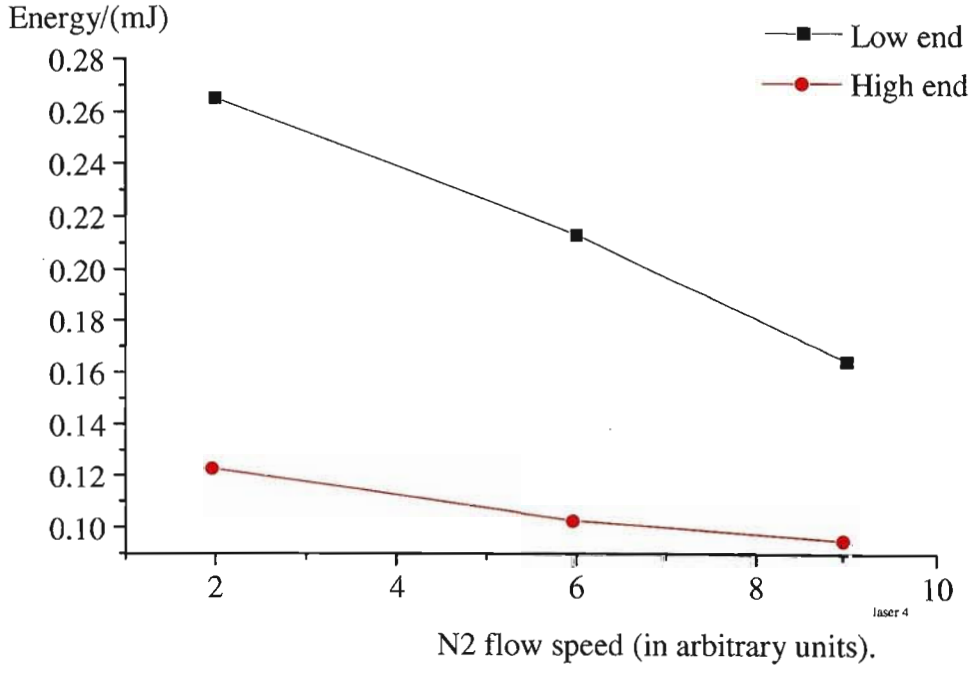

Figure (7.6.3d): Variation of energy with N_2 flow velocities.

7.6.1 Discussion

As can be seen from the graphs, the laser energy output from the lower end of the laser channel is approximately 50-55 % more than that at the higher end. Once again, this result proved that the parabolic shape was effective in increasing the energy. Moreover, the results show that the laser energy decreases with increasing N_2 flow velocity. A maximum average energy of 0.27 mJ was achieved at N_2 level of 2 and a minimum of 0.16 mJ at the highest flow velocity. This corresponds to a decrease of almost 40 %. Therefore, this laser also behaved in almost the same way as the other lasers. The most viable reason for this behaviour can be attributed to the occurrence of pressure turbulence at high N_2 gas velocities, as observed in previous cases. However, in this case, the energy is highest at the lowest measured N_2 velocity unlike other lasers. This behaviour was due to the use of a different set of electrodes which were greater in dimensions and where the flow of N_2 gas was more symmetrical at low N_2 level. The flow dynamics of the N_2 gas in the discharge channel was different in this case.

The energy output of Laser 4 was found to be 0.27 mJ and Laser 1 gave an energy if 0.11 mJ. This represents an energy increase of about 60 %. It has to be noted that Laser 1 and Laser 4 were made with the same thickness (0.5 mm) of pc board. The storage energy of Laser 4 was found to be 6.86 J which represents an efficiency of 0.004 % which is close to the laser efficiency of Laser 1. This result showed that the parabolic N_2 laser could be scaled up to larger surface areas to give higher laser energy output and the parabolic shape of the top plate was efficient in improving the laser's performance.

However, with our existing power supply voltage of 17 kV, there was limit on the size of lasers that could be used since a laser with larger dimensions would require a higher voltage input. An important problem which was encountered was that the laser stopped functioning after approximately 5000 shots. The reason was that there was direct arcing between the top and bottom plates because the pc board was too thin and weak to run at 17 kV for such a long time. In other words, there was dielectric failure after a few days operation. Thus, one disadvantage of using thin pc board is that they do not last long enough and a lower voltage should be used to extend their life span.

7.7 Experimental results of Laser 5

The technical specifications were:

Capacitance (with plates connected) = 48.4 nF
Distance between the plates = 0.5 mm
Dimensions = 105.8 x 72.3 cm
Area of parabola = 4949.2 cm^2
Electrode separation = 2.0 mm

Laser 5 was constructed with almost identical dimensions as those of Laser 4 except that it had a larger parabolic surface area. The aim of this experiment was to investigate the effect of the size of the parabola on the laser energy output and in

addition to observe the effect on the energy outputs and divergence at the lower and higher ends of the laser channel. Since Laser 5 had almost the same capacitance, the average energy output was expected to be the same as that of Laser 4. Figure (7.7.1) shows a picture of Laser 5.

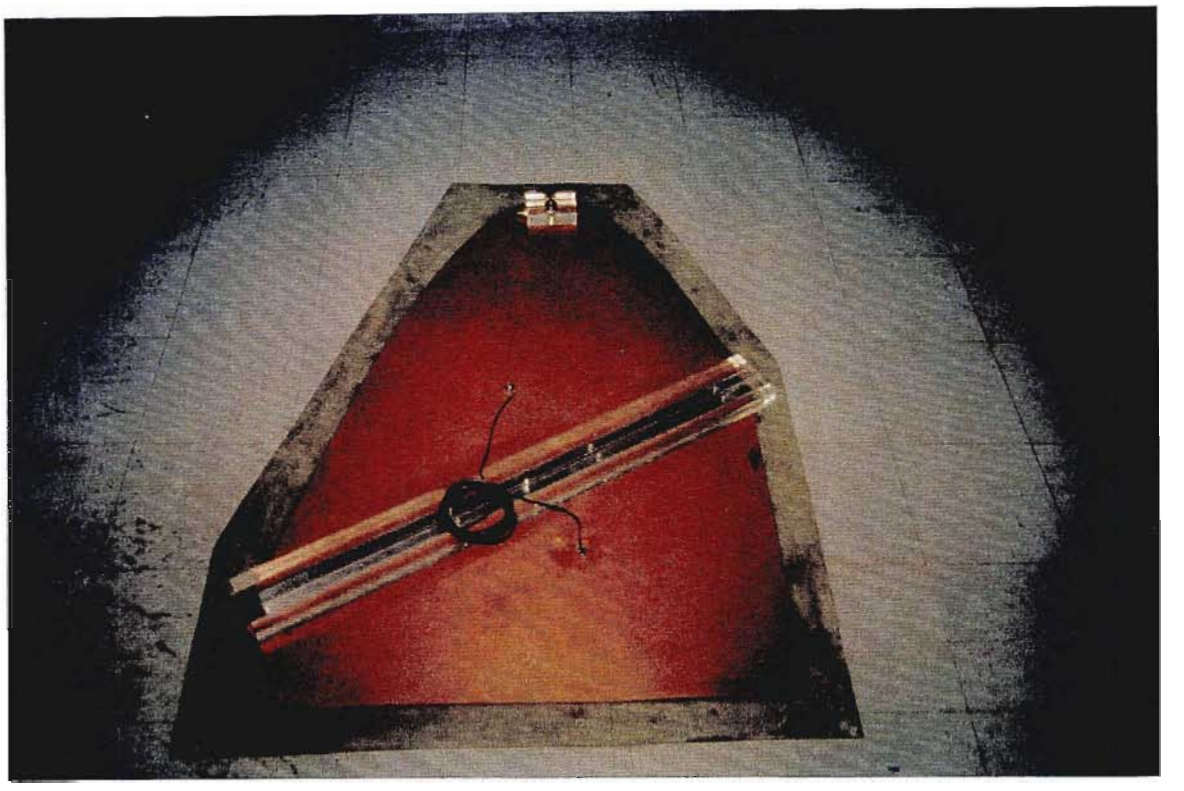

Figure (7.7.1): Picture of Laser 5 with larger parabola.

A similar experimental arrangement as shown in Figures (7.6.2a) and (7.6.2b) was used for the energy measurements at lower and higher ends of the laser channel for the varying flow speed of nitrogen. In this case, energy measurements were taken only at flow speed 2 and 8 since there was no further significant change in the energy output at other flow speeds. The same conditions of constant voltage and same electrode-detector distance were maintained. Figures (7.7.2a) and (7.7.2b) show the graphical illustration of the experimental results. A polynomial regression fit was applied to the graphs in order to have a clearer indication of the trends.

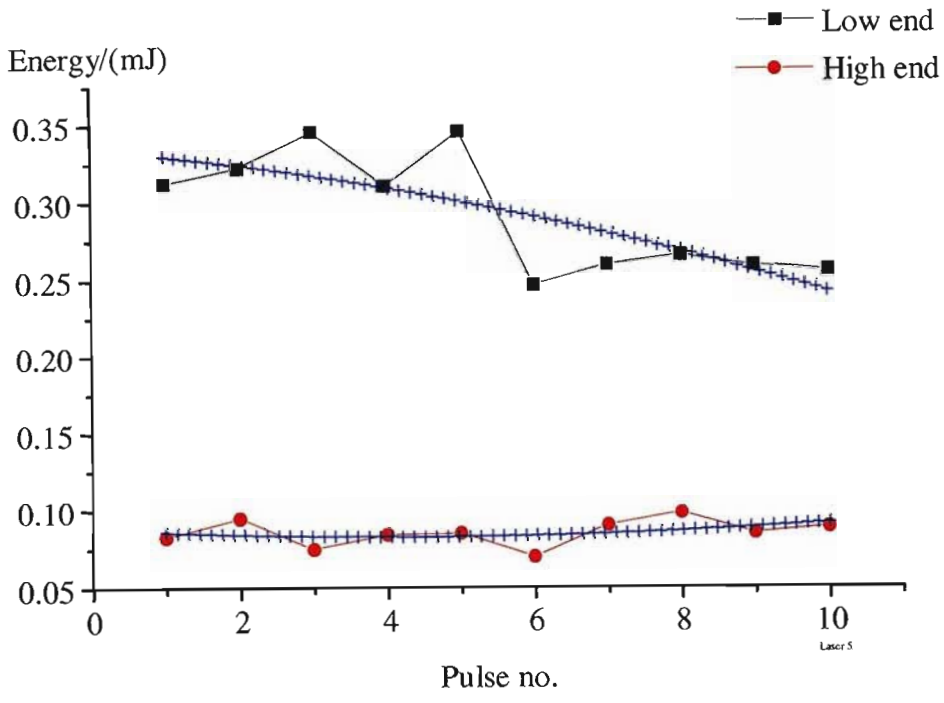

Figure (7.7.2a): Variation of energy output at N_2 flow speed 2.

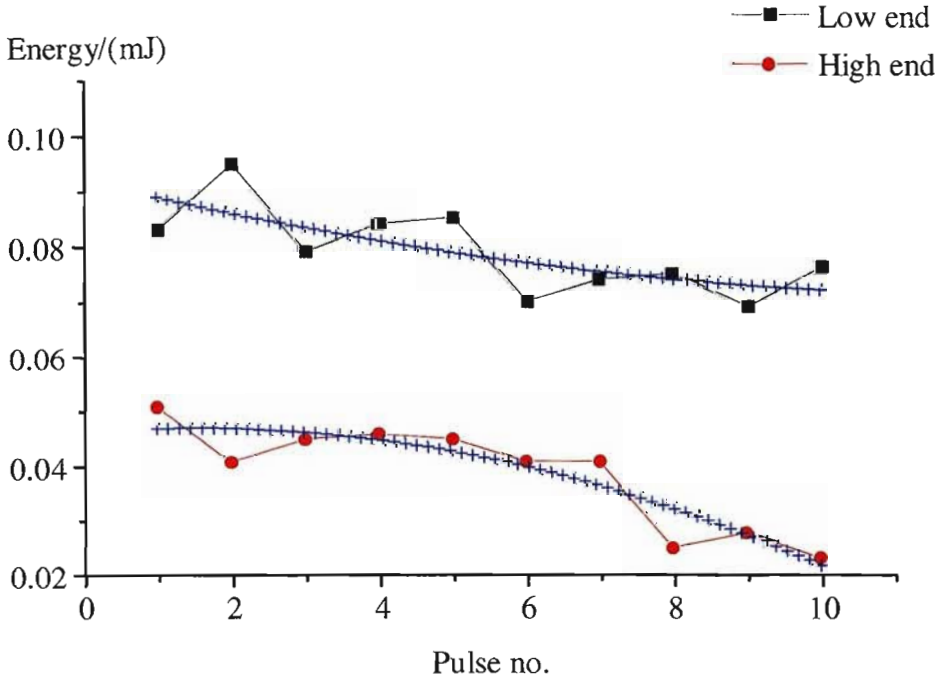

Figure (7.7.2b): Variation of energy output at N_2 flow speed 8.

7.7.1 Discussion and Conclusion

The above graphs show the same trends as those of Laser 4. The laser energy output decreases with increasing nitrogen flow speed. An average maximum energy of 0.29 mJ was calculated and this value was obtained at the lowest N_2 flow speed of 2. This value does correlate with that of Laser 4 where an average maximum energy of 0.27 mJ was obtained at the same N_2 flow speed. Referring to Figure (7.7.2a), the first point to note is that there is approximately 70 % energy difference between the lower and higher ends output whereas in the case of Laser 4, the percentage difference was about 55 %. An average energy output of 0.08 mJ was obtained at N_2 flow speed of 8.

Furthermore, this result was supported by the fact that the divergence at the higher end was much more than that at the lower end and visually, the laser light was more intense and concentrated at the lower end output. This behaviour is attributed to the larger size of the parabola. It is believed that a larger surface area of the parabola resulted in a more efficient propagation of the plane waves. As noted from the previous section, Laser 3 with a small parabola gave a low output energy and the energy difference at the low and high ends was not significant.

The above graphs also show one important characteristic which is that the energy variation shows a decreasing trend with the number of shots. This could mean two things: firstly, the spark gap was not transferring a constant electrical energy to the laser and its performance deteriorated with the number of shots. Secondly, the laser could be arcing at some points which could not be visually detected. Since the laser was made with a thin pc board of thickness 0.5 mm, the dielectric was not strong enough to withstand the high voltage. A similar problem was encountered before.

In conclusion, Laser 5 was considered to be more efficient than Laser 4 since the larger size of the parabola lead to more than 70 % energy difference (at the lowest N_2 flow) between the lower and higher ends of the laser channel. In other words, a larger surface area of the parabola proved to be more effective. The beam from the lower end was also observed to be much less diverging by approximately a factor of 2. A higher output energy was recorded at the lowest N_2 flow speed. The same reason of pressure turbulence as discussed before is attributed to a low energy output at high speed flow of N_2.

7.7.2 Variation of Electrode separation

The effect of electrode separation on the laser energy output was investigated on Laser 5. The same experimental set-up as before was used. The electrode distance was varied from 1.0 mm to 2.5 mm. Initially, the laser was run with a N_2 flow speed 8 and Figure (7.7.2.1) shows a graphical illustration of the experimental results. In this particular experiment, the laser energy output from the lower end of the laser channel only was measured.

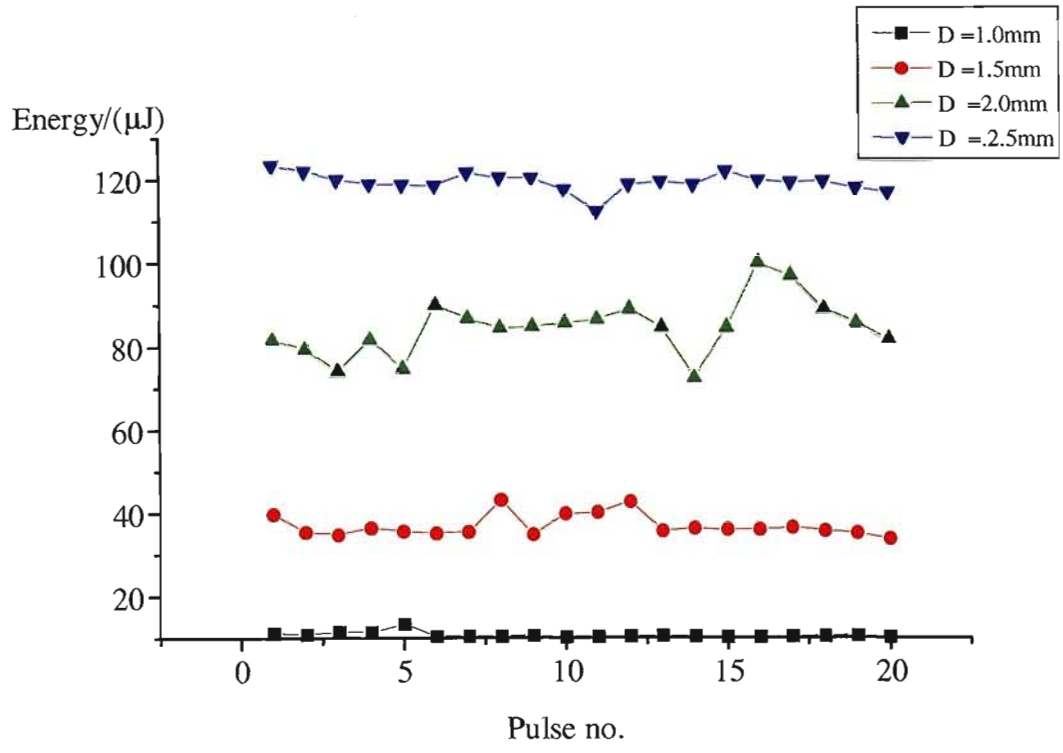

Figure (7.7.2.1): Variation of energy with pulse no. at different electrode spacing.

As can be seen from the graphs, the highest energy output (125 μJ) was obtained with an electrode separation of 2.5 mm. Greater electrode separation implies a greater volume for plasma formation to initiate a laser discharge.

The same experiment was carried out but this time the Nitrogen flow speed was changed to 2 while other parameters such as voltage, electrode-detector distance were kept constant. However, in this case, unlike the previous experimental results, the lower and higher end energy outputs were also recorded at the different electrode separation. In other words, an investigation on the effect of electrode separation on energy difference at the lower and higher output was carried out. Figures (7.7.2.2a) to (7.7.2.2d) show the variation the lower and higher ends output at different electrode separations.

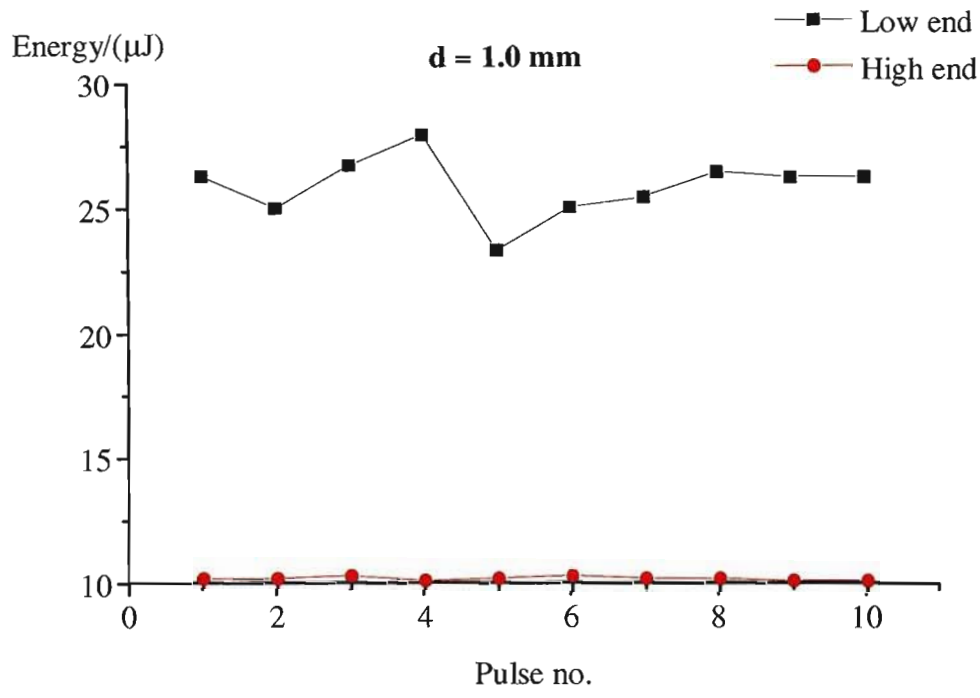

Figure (7.7.2.2a): Energy variation at lower and higher ends at d = 1.0 mm.

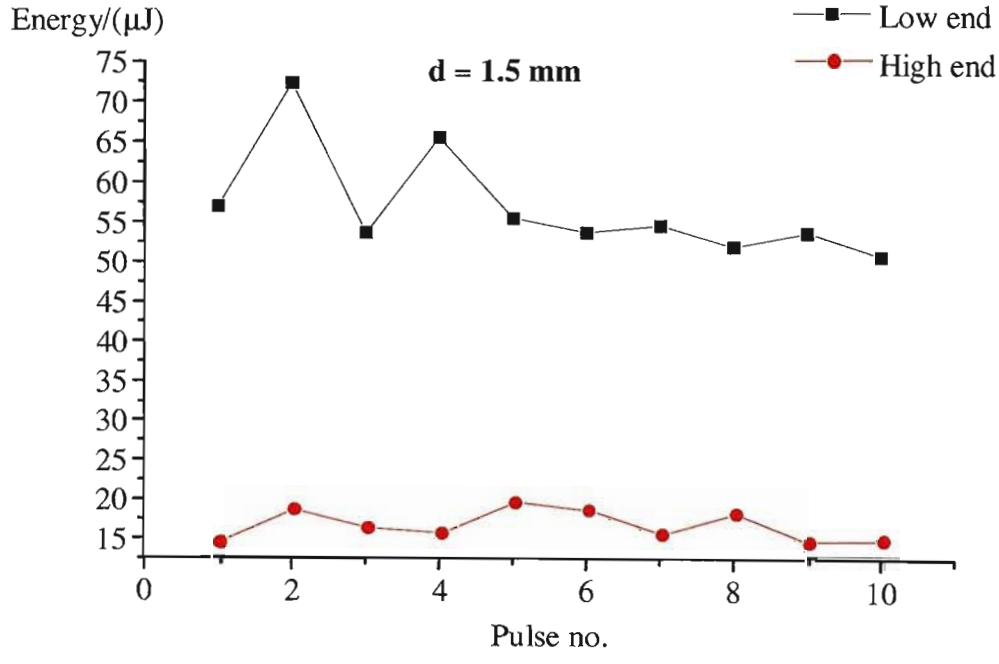

Figure (7.7.2.2b): Energy variation at lower and higher ends at d = 1.5 mm.

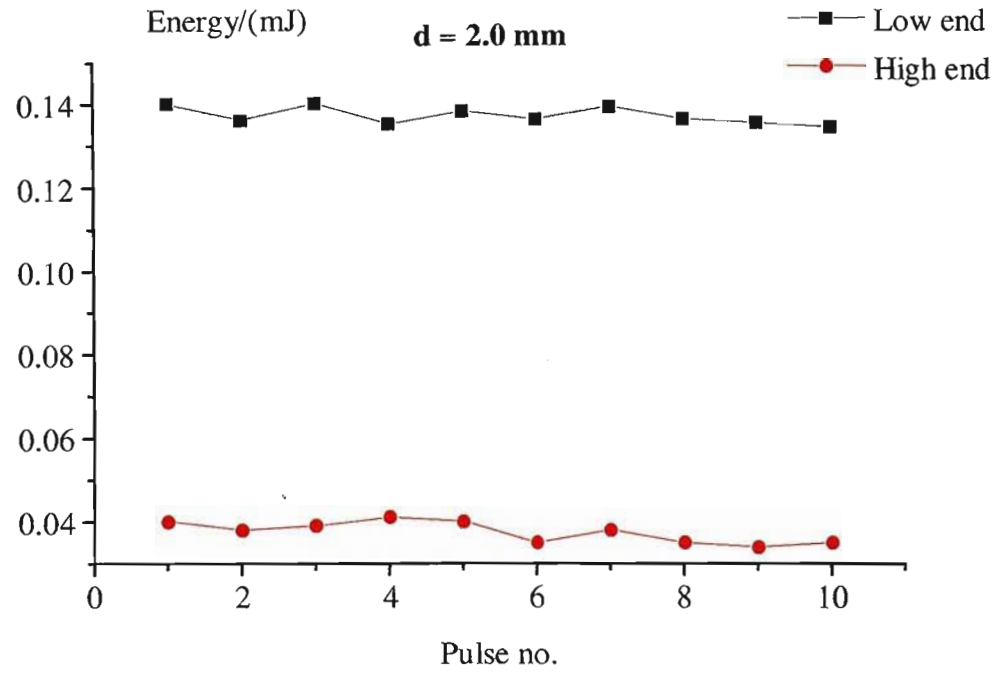

Figure (7.7.2.2c): Energy variation at lower and higher ends at d = 2.0 mm.

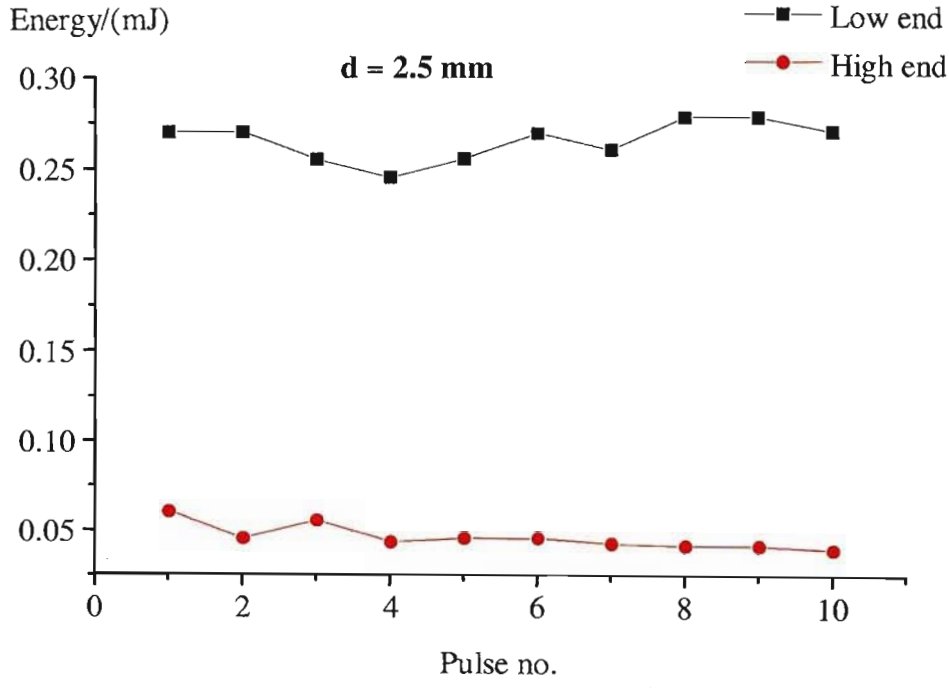

Figure (7.7.2.2d): Energy variation at lower and higher ends at d = 2.5 mm.

Figure (7.7.2.2e) below shows the variation of energy at the lower end of the laser channel with the different electrode separations.

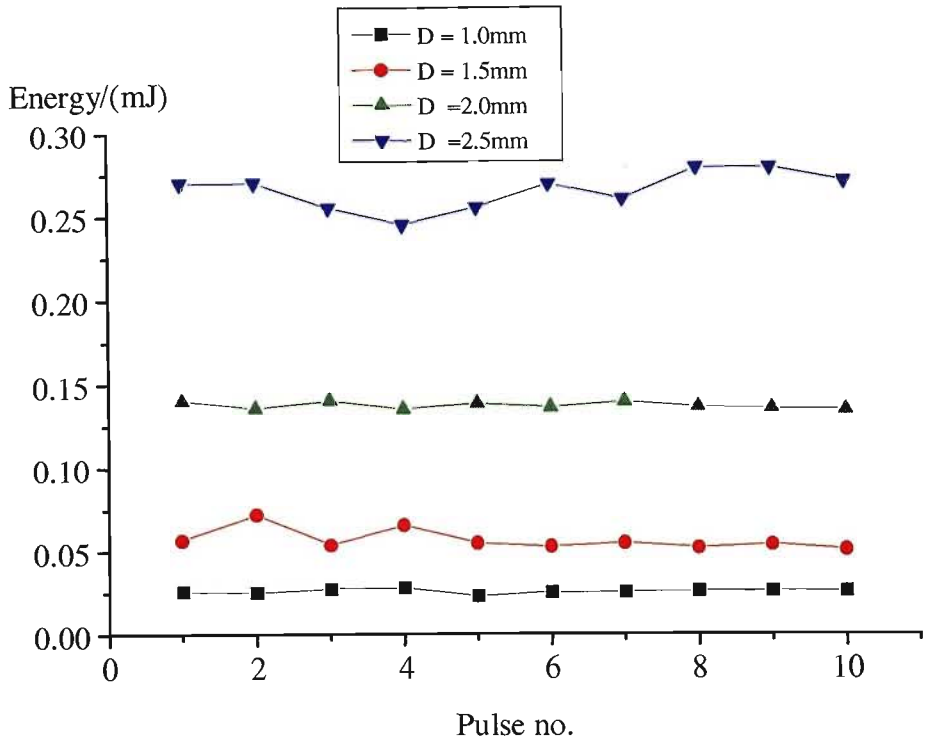

Figure (7.7.2.2e): Energy variation at the lower end output with different electrode separations.

7.7.2.1 Discussion and conclusion

The experimental results show that electrode separation has a significant effect on the laser output energy. A maximum output energy of 0.29 mJ was obtained at an electrode separation of 2.5 mm. Laser 4 gave a high output energy of 0.27 mJ at the same electrode separation. Both Laser 4 and Laser 5 reached their maximum output energy at that electrode separation. In both cases, increasing the electrode distance beyond 2.5 mm produced no laser light. The lowest output energy was obtained at the smallest electrode separation of 1.0 mm. Similarly, there was no laser light at a distance smaller than that. Considering Laser 5 which has the largest parabola, the percentage energy difference between the lower and higher ends was calculated to be more than 80 % at an electrode separation of 2.5 mm. On the other hand, that of Laser 4 was about 55 %. It has to be noted that the capacitance of the two lasers was the same and was measured to be approximately 50 nF.

The variation of laser energy with electrode separation is related to the volume of plasma formed in the laser channel which initiates a laser discharge. At a small electrode separation of 1.0 mm, the volume for plasma formation and the volume of N_2 gas in the channel is small. This results in laser light of low energy. The plasma volume is approximately proportional to the electrode separation. Similarly, at large electrode separation, the volume for plasma formation is greater and the amount of N_2

present in the channel is also higher. This leads to a higher laser output energy. However, no laser light was obtained at an electrode separation greater than 2.5 mm because the power input was not high enough to cause a laser discharge. The laser therefore did not lase. A similar experiment was carried out by V.Hasson, H.M.von Bergmann and D.Preussler (1975) to investigate the same effect. They found that the laser energy output increases with increasing electrode separation since there a voltage of 40 kV was used. However, they also found out that at high N_2 pressures of 1440 to 4220 mbar, the energy output reached a maximum at a particular electrode separation (5 mm) and then decreased with increasing electrode distance.

In our case, since we were running the laser with N_2 gas at atmospheric pressure, we should expect the laser energy to increase with increasing electrode separation (1 mm to 4 mm). Hence, in the future, a higher power input and greater electrode separation could lead to a significant increase in laser energy.

7.8 The Low Pressure electrodes

A pair of copper electrodes separated by 1 cm was enclosed in a round plexiglass housing. The latter was connected to a vacuum pump and the lowest pressure that could be reached was around 0.1 bar since a few leaks could be detected. This vacuum electrode was used on the large laser, i.e Laser 4. Initially, our aim in using the low pressure electrodes was to reduce the noise from the laser discharge which triggered the joulemeter. Figure (7.8.1) shows the variation of the laser energy with pulse number. The flow velocity of N_2 was set to the optimum level to produce the highest output energy. Figure (7.8.2) shows a picture of the low pressure electrode.

As the laser was fired, a very uniform laser discharge could be observed and the noise level was reduced significantly. The joulemeter did not trigger on the mechanical noise and it was shielded with aluminium foil to avoid interference from electromagnetic noise. The energy output was measured at both ends of the laser channel and the same experimental conditions were maintained each time. The low end was the one end furthest from the spark gap.

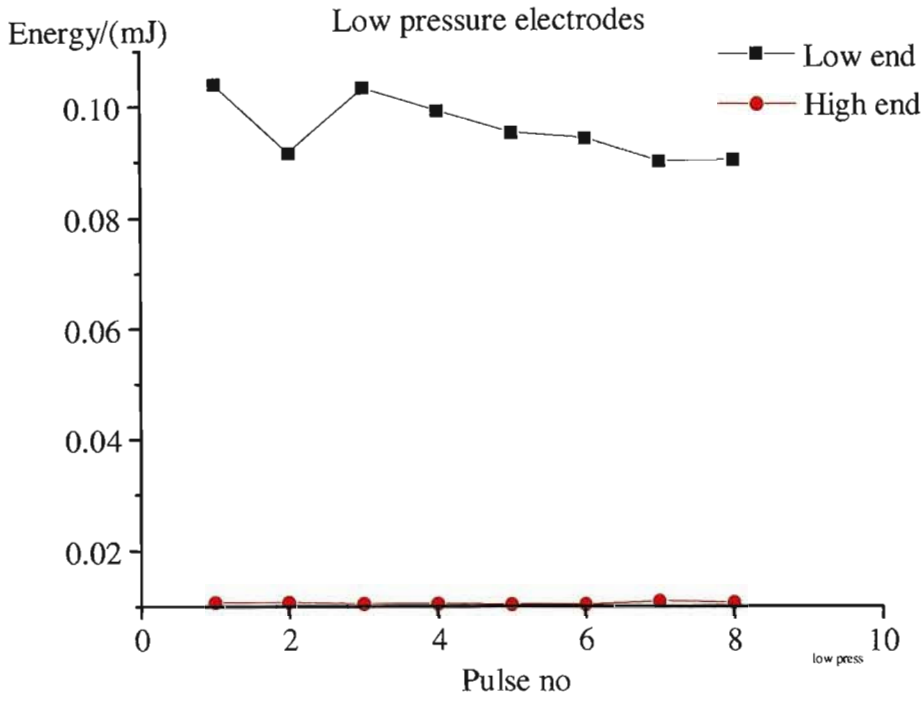

Figure (7.8.1): Variation of energy with pulse no. using low pressure electrodes.

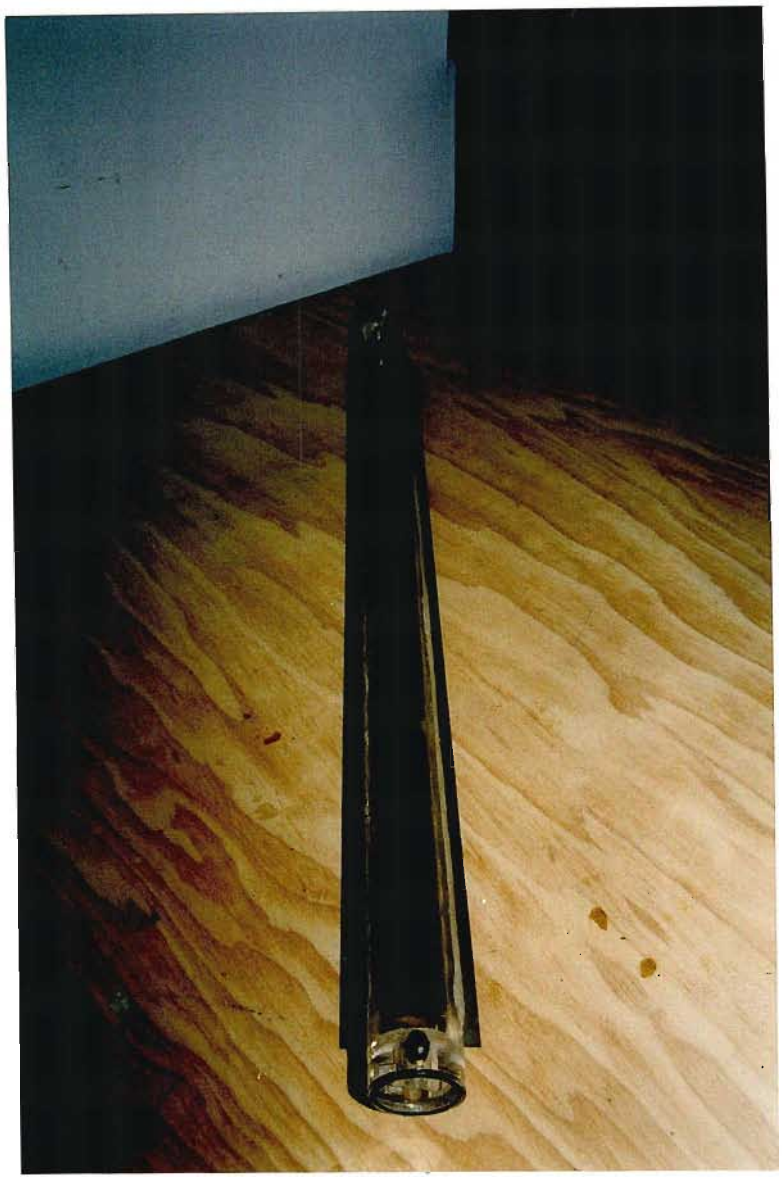

Figure (7.8.2): Picture of the low pressure electrodes.

7.8.1 Discussion

As shown in the graphs, the average energy achieved by the laser with the low pressure electrodes was 0.1 mJ from the lower end output. In this case, there is almost a 90 % energy difference between the lower and higher ends outputs. An average energy of 0.27 J was obtained from Laser 4 with the high pressure electrodes and an average of 0.1 mJ was obtained from the low pressure electrodes. This represents a 65% decrease in energy output.

The greater energy difference between the lower and higher ends outputs could be attributed to the electrodes being at a lower pressure which lead also to a uniform laser discharge. In addition, the flow of N_2 gas was more symmetrical along the discharge. It is worth noting that with the low pressure electrodes, the pulse length is longer as a result of which mirrors at the ends of the laser channel would be more efficient in producing a better beam quality.

7.9 The Multi-Layer N_2 laser

The multi-layer N_2 laser consists of several layers of aluminium foil connected together in parallel to give a laser of a higher capacitance. It is similar to connecting several capacitors in parallel. All of them are charged to 17 kV and the energy stored is used for the laser discharge in the laser channel. Layers of aluminium foil were added to the bottom plate of Laser 3. The reason for choosing the latter was because of its lowest energy output compared to the other lasers and therefore, by applying the multi-layer scheme on it, a more significant change in energy output might be observed. Figure
(7.9.1) shows the schematic diagram of the connection of the aluminium foil to the laser. Mylar which has a relative permitivitty of 3.7 was used as the dielectric insulator between the layers. A maximum of 3 layers was added to the bottom plate of the laser.

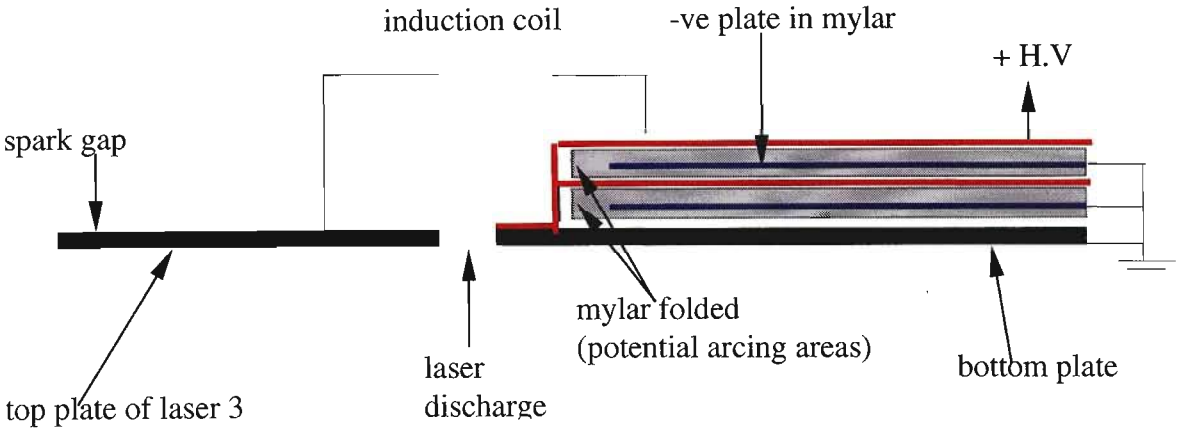

Figure (7.9.1): The connection circuit for multi-layer N_2 laser.

As can be seen in Figure (7.9.1), all the negative plates, i.e the aluminium foils were enclosed in sheets of mylar. The negative plates were connected together and all of them extended to make contact with the laser's ground plate. The positive plates were placed between the mylar and similarly all of them were extended to make contact with the positive plate of the pc board. As shown in the diagram above, the negative plate was ended a few cm from the folded end of the mylar. The folded end was the weak region where there could be arcing between the negative and the positive plate. In order to avoid this, the foil with negative polarity was placed 1.5 cm away from the folded end. Figures (7.9.2a) and (7.9.2b) show pictures of the multi-layer N_2 laser. Figure (7.9.2a) shows clearly the three layers of aluminium foil used. The spark gap was pressurised and self-triggered but a constant voltage of 17 kV was maintained for each measurement since a high voltage probe was connected to the laser and the output signal was fed to a digital oscilloscope. The foils had to be pressed tightly such that all the air found between the mylar and the foils would escape otherwise the relative permitivitty of the multi-layer system would change. This would then lead to

its initial capacitance was 2 nF. Hence, the addition of the 2 layers increased the laser's capacitance by a factor greater than 6.

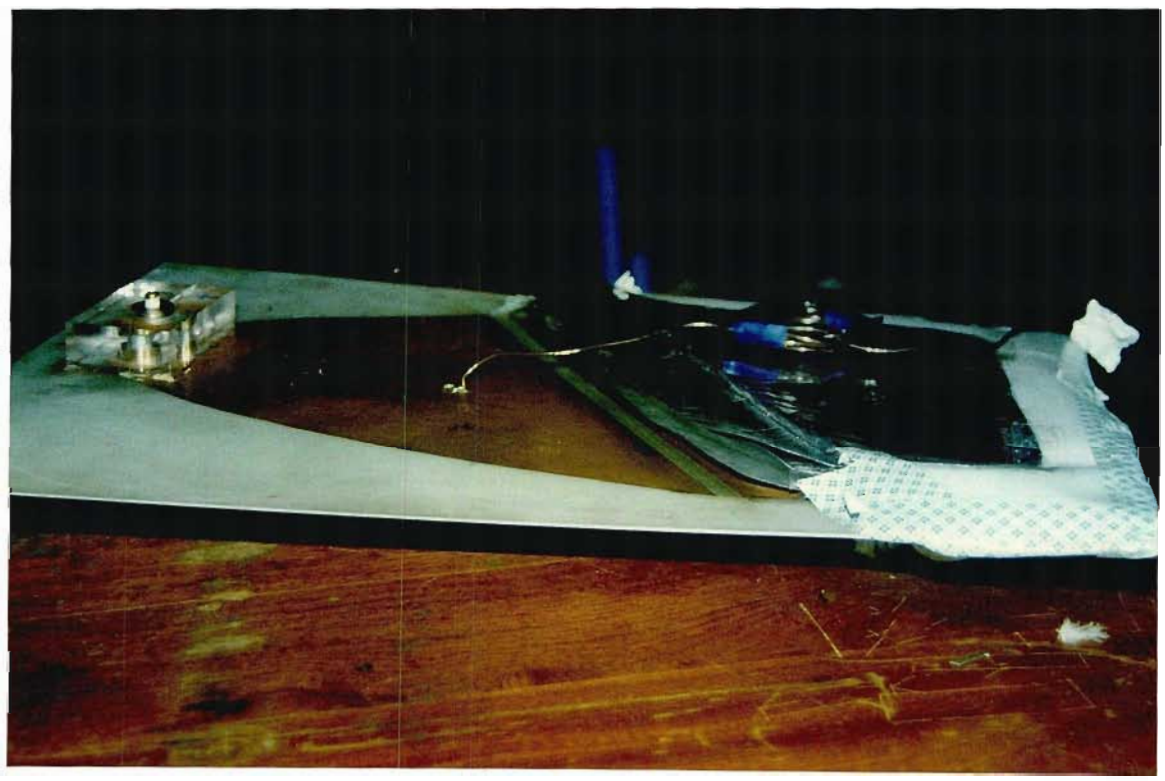

Figure (7.9.2b): Multi-layer N_2 laser using a pressurised spark gap.

7.9.1 Experimental Results

In this section, we investigate the effect of the multi-layer on the laser energy output. Energy measurements of the multi-layer N_2 laser was made using the joulemeter. The same experimental set-up as before was used, i.e the whole laser had to be placed in the insulated box. Energy measurements were taken at both ends of the laser channel. Initially, measurements were taken on a 2 layer N_2 laser. Figure (7.9.1.1) shows the graphical illustrations of the variation of energy output with pulse no. at the optimum level of N_2. The graph below firstly shows that there was not a significant difference (within experimental error) in energy output between the lower and higher ends and the energy output was not stable. Secondly, the 2 layers did not increase considerably the output energy at the lower end. An average energy of 0.05 mJ/pulse was obtained with the 2 layers of foil while the energy output without any layers was found to be 0.04 mJ/pulse. The 2 layers gave only a 25 % increase in energy output.

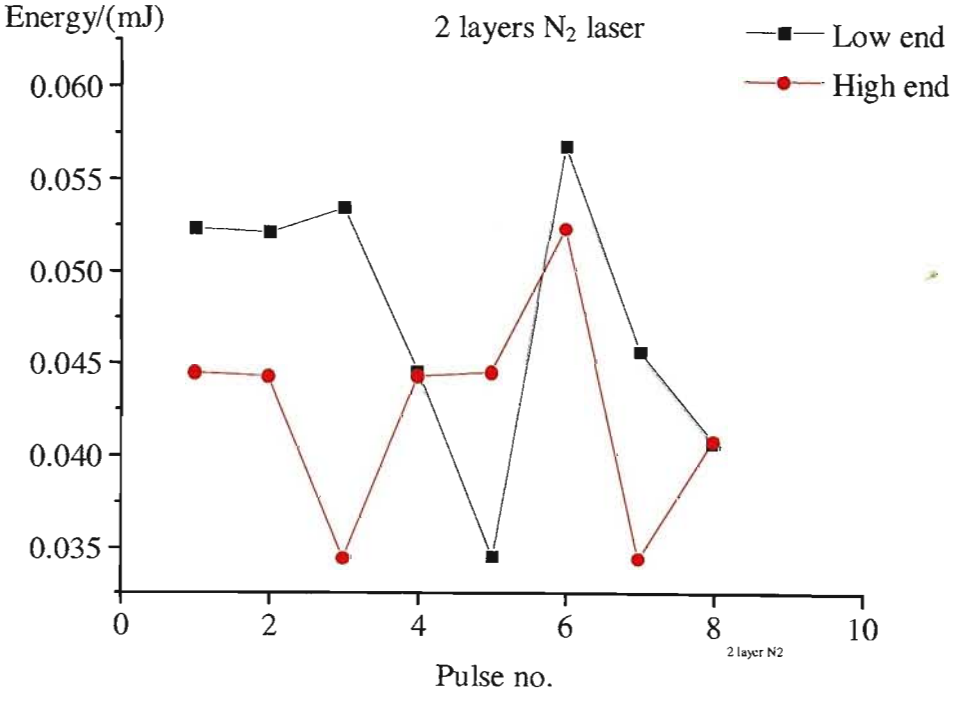

Figure (7.9.1.1): Variation of laser energy versus pulse no. at 2 layers.

The 3 layer N_2 laser produced more promising results. Figure (7.9.1.2) shows the variation of energy output with pulse number. It has to be noted that each time measurements were taken, a weight was placed on the layers of foil such that most of the air found underneath them would escape. This ensured a constant capacitance which was measured to be around 30 nF, high compared to other N_2 lasers.

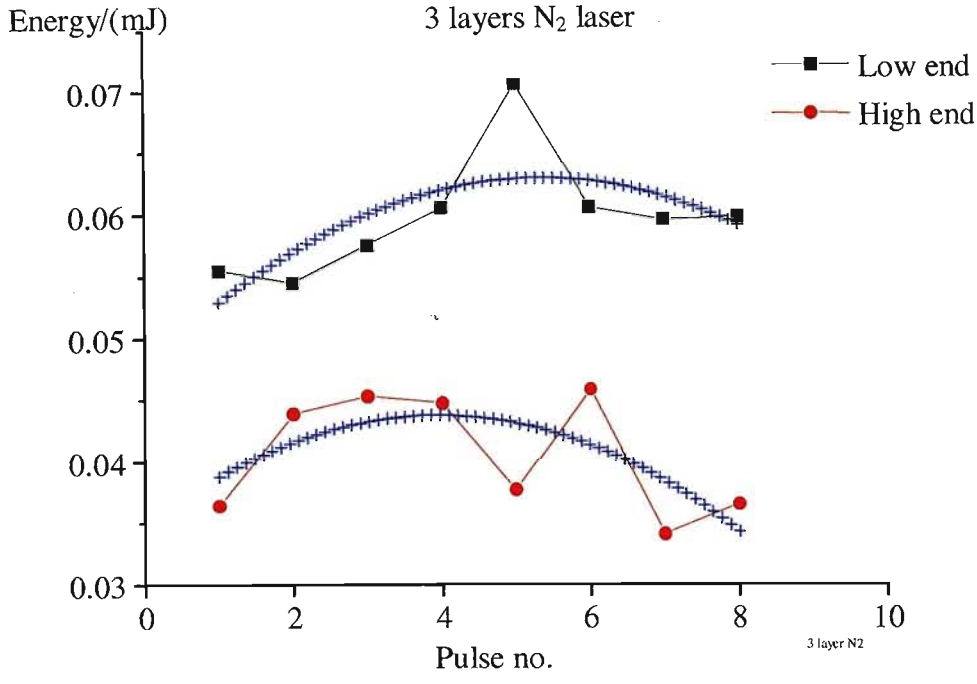

Figure (7.9.1.2): Variation of energy versus pulse no. at 3 layers.

The graph above shows that there was a significant increase in energy output. An average energy of 0.06 mJ/pulse was obtained with 3 layers of aluminium foil and this represents an increase of more than 30 % compared to the energy results of the 2- layer N_2 laser. The energy storage of the multi-layer laser was calculated to be around 4.34 J which corresponds to the laser's efficiency of 0.001 %. However, as observed previously, there was not a significant energy difference between the lower and higher ends outputs due to the reasons mentioned earlier. In the later sections, the multilayer idea was tried on lasers constructed using aluminium foil and mylar.

7.9.2 Discussion

From the above results, it is evident that the multi-layer N_2 laser produces more laser energy. A 3 layer laser produced an energy increase of more than 30 % (compared to the 2-layer N_2 laser). The multi-layer scheme was tried on the small laser 3 since the latter gave a low energy output and its spark gap was not precisely located at the focus of the parabola. As a result of this, the parabola was not effective in this case and this

gave a higher laser energy output and it can be scaled up to greater dimensions and more layers. However, having a bigger laser with several layers of foil would require a higher power input. In addition, by having several layers connected in parallel would lead to a high impedance of the laser. This would then affect the laser output energy. It is believed for electrical and optical reasons that there is a limit to the number of layers that could be added to the bottom plate of the laser as the laser might not lase if that limit is surpassed.

7.10 Cold N_2 vapour as a lasing medium

In this section, we investigated the effect of using cold N_2 vapour as a lasing medium instead of N_2 gas on the laser energy output. The pipe (1 cm in diameter) which transported the N_2 gas to the electrodes was wound into a coil (4 cm in diameter) of 20 turns. This coiled section of the pipe was then fully immersed in liquid nitrogen and after sometime, the N_2 gas coming out of the other end was cold N_2 in vapour state. When the vapour became visible, the end of the pipe was then connected to the electrodes. Figure (7.10.1) shows a picture of the set-up which shows the connection of the pipe to the electrodes. This particular experiment was also tried using the small laser, i.e Laser 3 which gave the lowest output energy. As can be seen in the picture below, there was formation of ice on the surface of the pipe leading to the electrode. This shows that the N_2 gas coming from the cylinder, passing through the coil in liquid nitrogen, got converted to nitrogen vapour at the electrodes. A weight was placed on the electrodes to press the latter firmly on the sides of the channel for a good electrical contact. It was more practical to take measurements with the detector and laser in separate rooms rather than to have the laser closed in the insulated box. The measurements were taken at the lower end of the laser channel since it was known from the previous work that for this particular laser, the energy difference between the two ends were almost the same. Moreover, we were only interested in observing the effect on energy output when using cold nitrogen vapour as a medium.

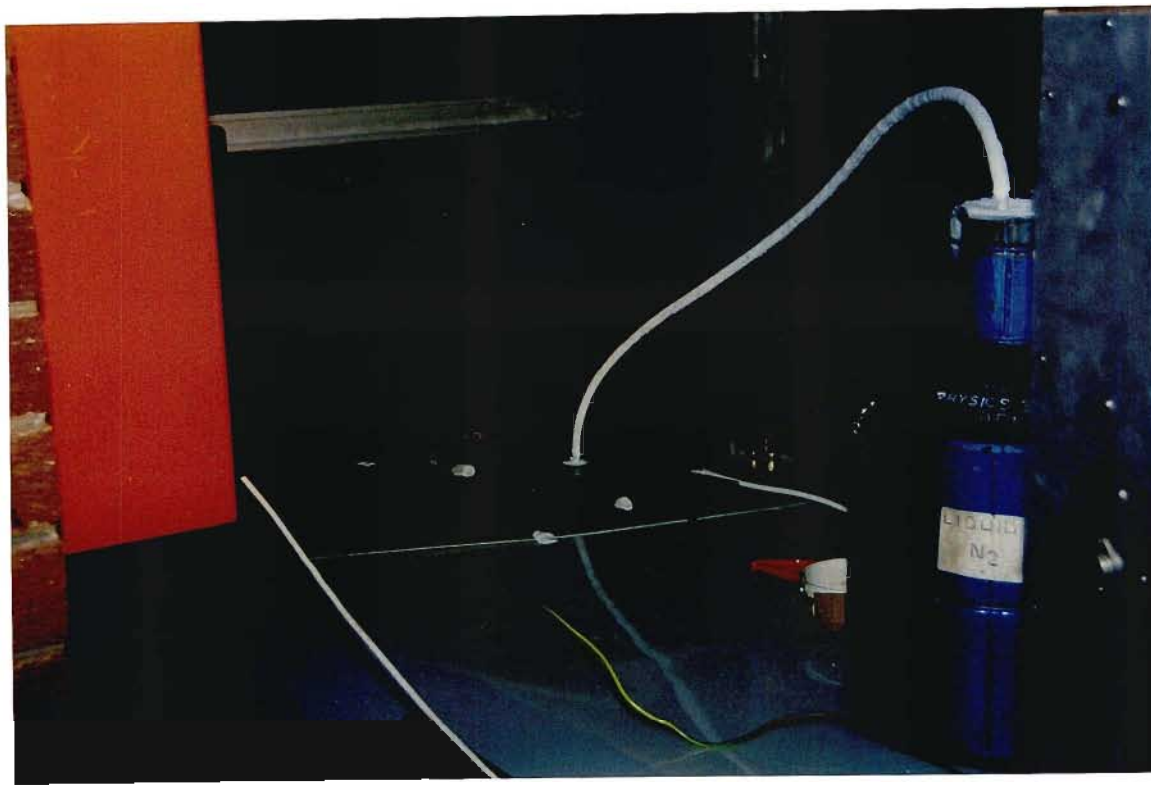

Figure (7.10.1): Picture of the N_2 laser using cold N_2 vapour.

It was observed that the intensity of the laser light was higher at both ends of the laser channel compared to the intensity when N_2 gas was used. Figure (7.10.2) shows the positioning of the laser, electrodes and the hole. The laser had to be aligned with the 1 cm diameter hole on the wall and alignment was done with the laser itself. The laser beam was exited through the hole and hit the detector on the other side of the wall. The approximate distance between the end of the electrodes and the detector was about 15 cm. As can be seen in the picture, the laser was placed on a large sheet of mylar as a precautionary measure to prevent arcing between the laser and the metal parts of the table.

Figure (7.10.2): The positioning of the laser near the beam exit.

For each set of energy measurements, the same conditions of constant voltage, electrode separation and same electrode- detector distance were maintained. Figure (7.10.3) shows a graphical illustration of the variation of the laser energy output with pulse number for cold nitrogen vapour and gas. As one can see in the graph, the laser energy output was higher when cold nitrogen vapour was used. It has to be noted, that the energy measurements with the N_2 gas and vapour were taken within the same hour. This ensured that the level of humidity in the atmosphere remained almost constant otherwise a change in the latter could affect the laser's output energy. It was also observed that after sometime the laser stopped functioning as it was not lasing at all. This was because there was formation of water droplets on the copper plates and on the epoxy board. The water droplets which have a high electrical conductivity acted as a short-circuit to ground. The water droplets on the laser were allowed to dry before it became operational.

as a short-circuit to ground. The water droplets on the laser were allowed to dry before it became operational.

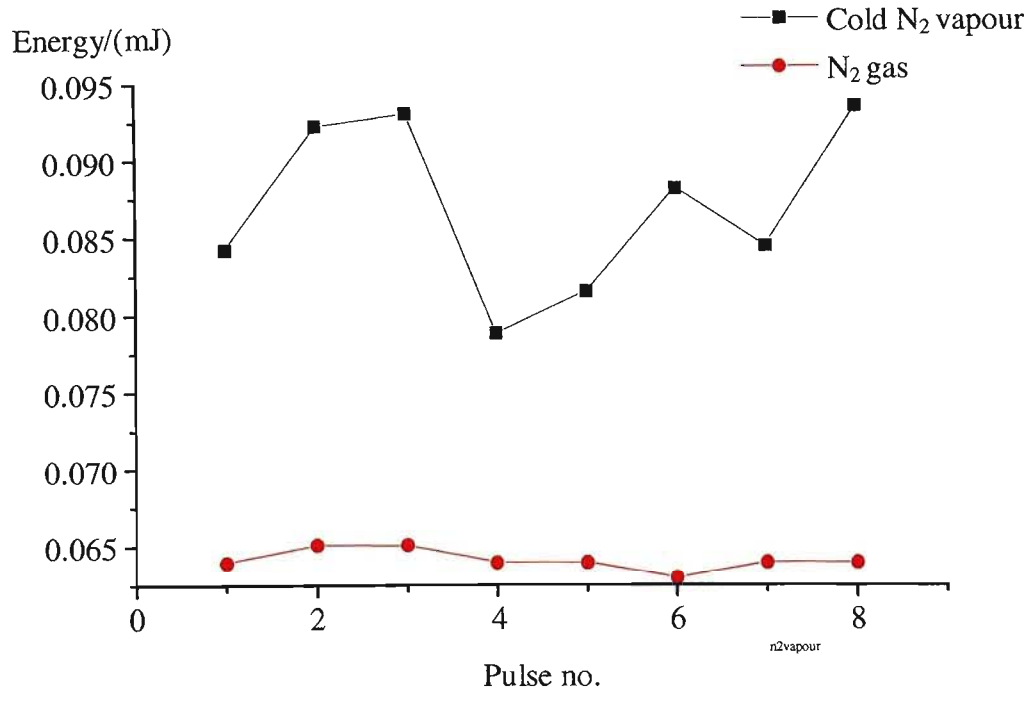

Figure (7.10.3): Laser Energy versus pulse no. using N_2 vapour and gas.

7.10.1 Discussion

The graph shows that cold N_2 vapour does increase significantly the energy output of the laser. The laser gave an output of 0.04 mJ with nitrogen gas and an average energy of 0.09 mJ was obtained with nitrogen vapour. This corresponds to an increase of laser energy by more than 50 %. The only problem encountered when using the vapour was that the laser got grounded quickly but there was enough time to take some energy measurements. This problem might be overcome if the whole laser is enclosed in a box with little air inside. By having almost no air in the box would cause a negligible formation of water droplets and the laser would then run for longer periods.

Therefore, the above results show that cold nitrogen vapour lases and compared to nitrogen gas, it produces a significant increase in laser energy. It is very likely to produce a relatively very high energy beam if cold N_2 vapour is used on a large multi-layer N_2 laser.

An attempt was also made to investigate if liquid Nitrogen would lase. Since the latter is volatile, a special set of electrodes had to be constructed to contain the fast evaporating liquid. The figure below shows a picture of the electrode. The casing was made of wood but the same aluminium electrodes was used. The wood had to be thick

Laser light with a very low intensity was observed. It is believed that the N_2 vapour was lasing instead of the liquid. This was because the power input was not high enough to cause a laser discharge. The dielectric strength of liquid N_2 is approximately 1.6-1.88 MV/cm. Therefore, a much higher voltage of the order of 10^6 volts should be applied to investigate this further. However, the laser might not resist such a high power input as the dielectric insulator of the laser could fail due to which a thicker dielectric should be used. Since such a power supply was not available, no further investigations were performed.

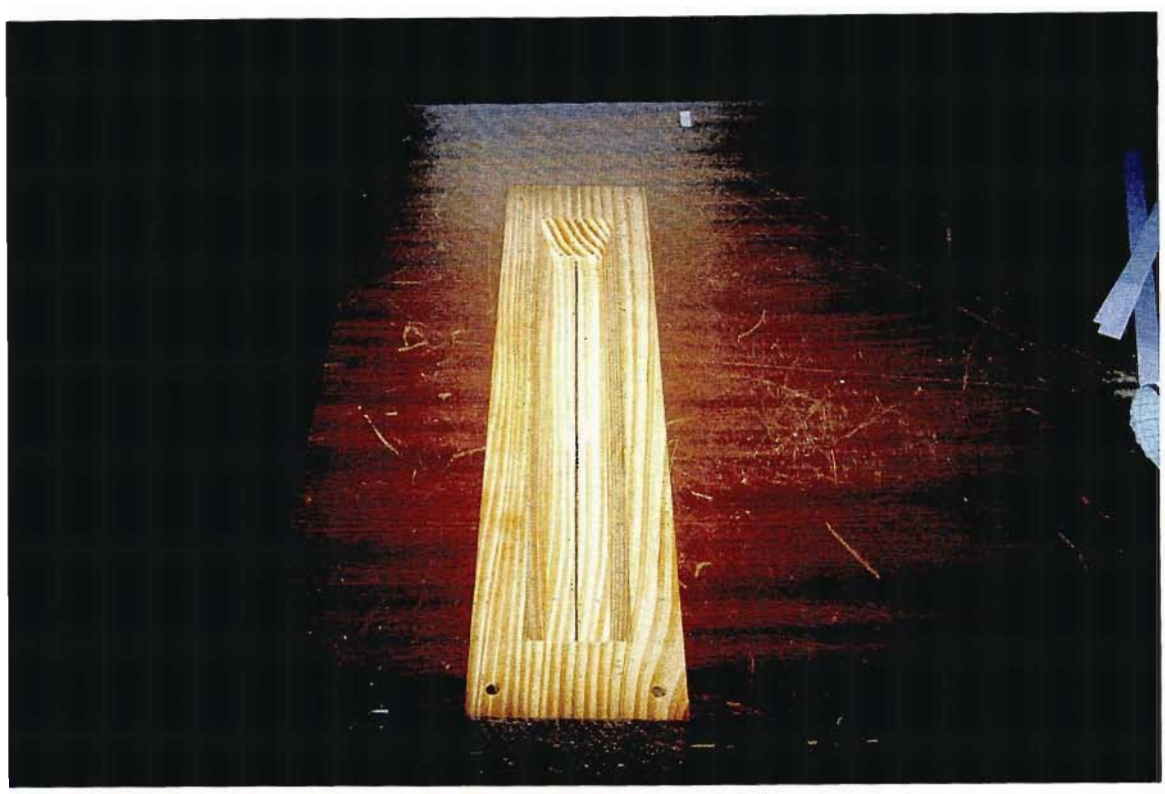

Figure (7.10.1.1): The set of electrodes for liquid N_2.

7.11 Nitrogen Lasers made of Aluminium foil

Several nitrogen lasers were constructed by the author and vacation students using the 'kitchen' aluminium foil paper with the view of producing good quality lasers at affordable prices, especially in the South African context where cost-effective but reliable technology could be the future of laser research.

A parabolic laser was therefore built and worked on the same principle as the others except that this time aluminium foil was used as the positive and negative plates and plastic materials were used as the dielectric insulator. The easy to build and cheap free running spark gap was used as the nanosecond switch. The same power supply was used to charge the laser but a simpler and more affordable power supply could be built which might include a car ignition coil. Figure (7.11.1) shows a schematic drawing of the laser.

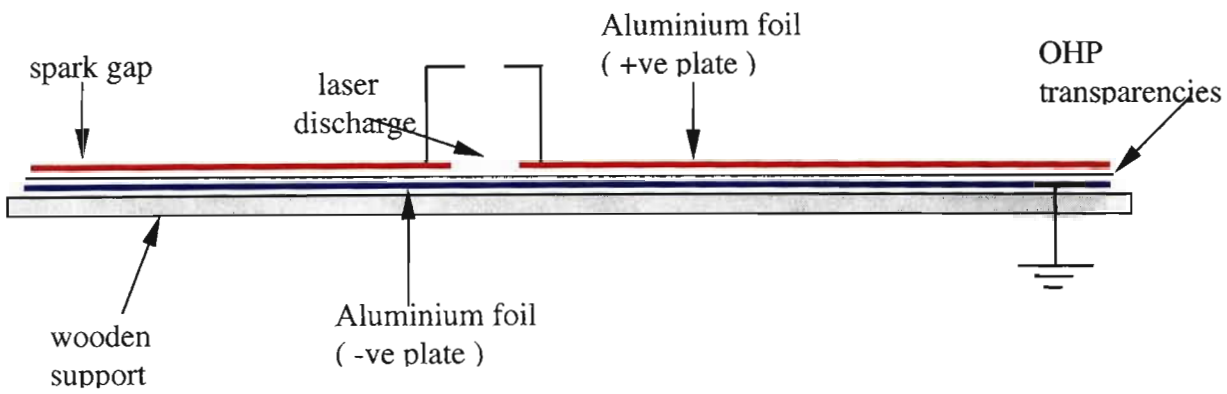

Figure (7.11.1): The Nitrogen laser made of Aluminium foil.

The same experimental set-up as before was used to charge the laser to 17kV. The capacitance of the laser was measured to be 50 nF and the electrode separation was 2.0 mm. The laser was observed to lase at all the times. It made loud noises since a free running spark gap was used. As a result of the electromagnetic and mechanical noise, the laser had to be enclosed in the insulated box. In addition, the laser and detector were placed in separate cabinets as it was done before. Figure (7.11.2) shows a picture of the set-up. One of the important things which could be observed was firstly that the light emitted was visually more intense. Secondly, the light from the higher end of the laser channel was highly divergent and that from the lower end was focused and intense. These observations imply that aluminium foil can be used to make a nitrogen laser and moreover, in this case also, the parabolic shape of the top aluminium plate seemed to be working efficiently.

Figure (7.11.2): Picture showing the set-up for energy measurements.

The pulse repetition frequency was adjusted to 2 Hz and the spark gap was adjusted for maximum voltage input before breakdown. However, the energy coming out from the ends of the laser channel was too low to be detected by the joulemeter. Since the joulemeter could only measure a minimum energy of 10 μJ, the laser energy output being given out by the laser should then be less than this value. Even though, the laser light appeared to be intense does not necessarily mean that the optical output is high. Some of that light could also be fluorescent light coming from the laser discharge. It was also observed that the dielectric insulator (transparencies) failed after several shots. There were holes at many places and the laser was arcing at those regions due to which it stopped lasing. It was obvious that transparencies are not strong enough to withstand the high voltage.

In order to investigate this further, several layers of aluminium foil were connected together to the lower plate. The same connection circuit as the multilayer laser was being applied here. In other words, a multilayer nitrogen laser was made using aluminium foil. It is worth recalling (refer to section 7.9, p 138) that in the previous multilayer laser, 3 layers of aluminium foil were connected to a laser made of pc board. Mylar was used as the dielectric insulator since it has a higher dielectric strength. In addition, there the mylar which contained the negative plate was folded. The same technique was employed here. The aluminium foil was ended a few cm from the folded end of the mylar. All the negative plates were connected to ground and the positive plates to the high voltage. Therefore, seven layers of aluminium foil were connected in

parallel. It has to be noted that each layer of aluminium foil consists of a positive plate and a negative plate. In other words, it acts as a capacitor and therefore in a way 7 capacitors were connected in parallel to the bottom plate. The same set-up was used for energy measurements. Figure (7.11.3) shows a picture of the multilayer N_2 laser with the folded ends. It was observed that the laser light was much brighter and also the noise the laser made was louder. It could also be observed that it took longer to charge due to a higher capacitance. The spark gap was adjusted for maximum voltage input. Energy measurements from the lower and higher ends of the laser channel were taken. It was found that the detector could not detect any signal coming from the higher end of the laser channel. The graph in Figure (7.11.4) shows a graphical representation of the energy output from the lower end only versus number of shots.

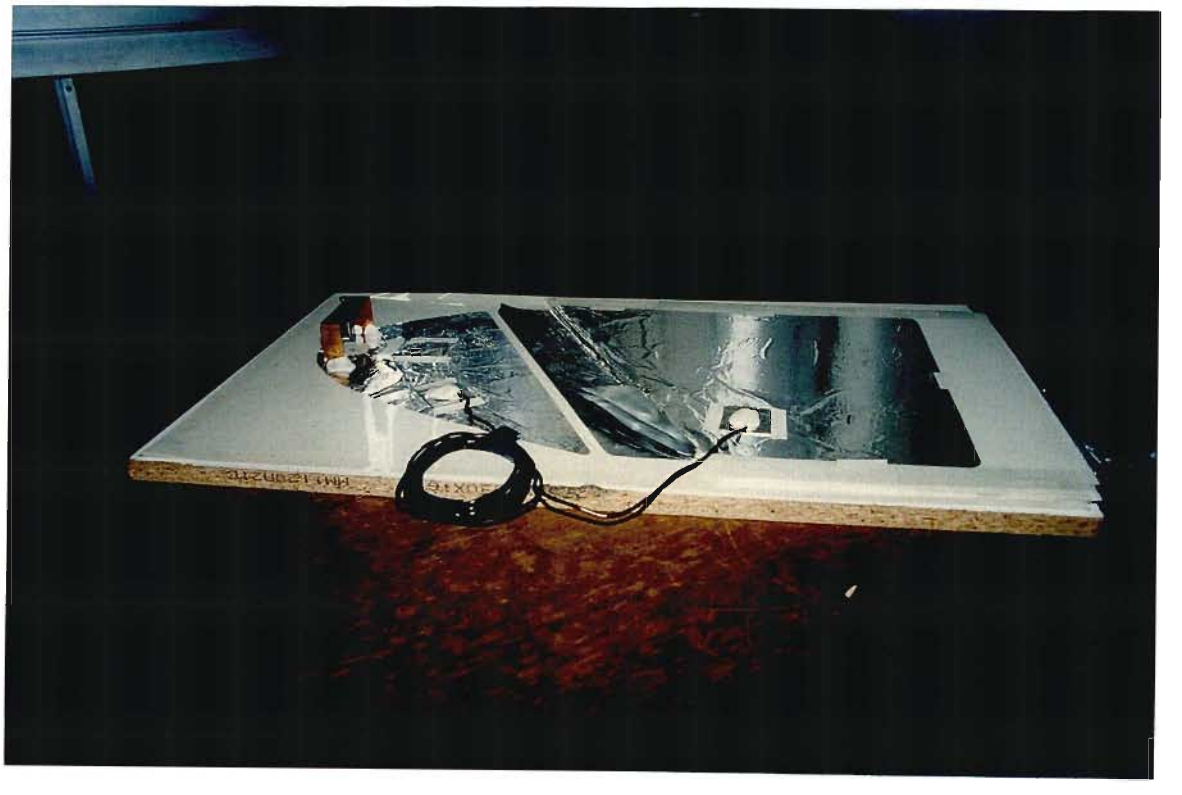

Figure (7.11.3): Picture of Multilayer N_2 laser made of Al foil (ends of mylar folded).

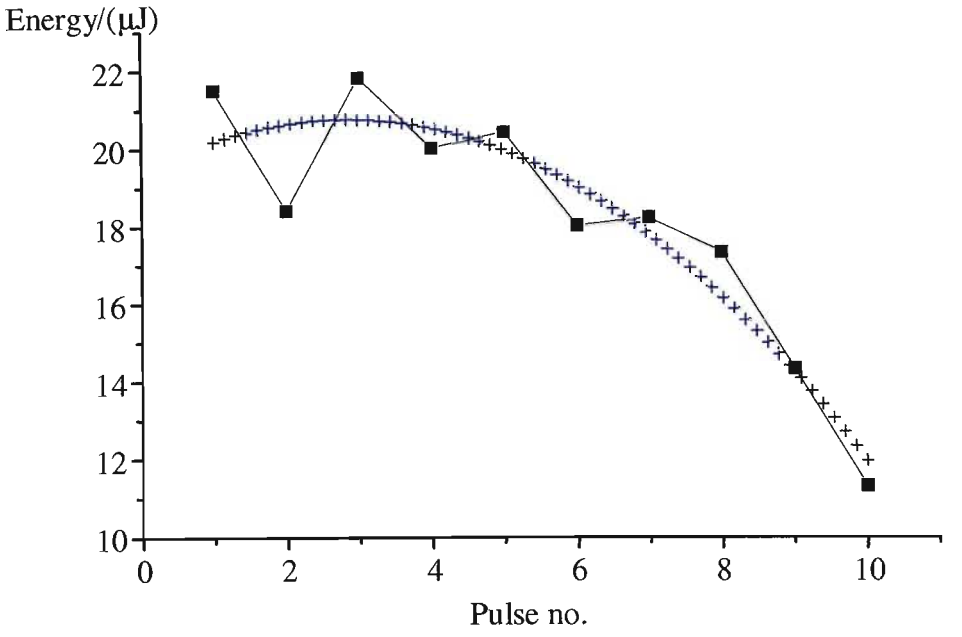

Figure (7.11.4): Variation of energy with pulse no. for 7 layers Al. N_2 laser.

An average energy output of 18.12 μJ/pulse and a peak value of 21.5 μJ were achieved with this laser. This may not represent a huge amount of energy but the idea demonstrated that a parabolic multilayer nitrogen laser can be made with aluminium foil. The low energy output could be attributed to the presence of air between the foil and the mylar. From the graph, it could be seen that the energy output decreases with the number of shots. This behaviour was common among the other lasers which also used a free running spark gap. The electrical energy transferred to the plates was not constant and the aluminium foil itself was not strong enough to resist high voltages. After some shots, tiny holes appeared through which arcing was observed.

The folding of the mylar lead to a considerable reduction in the laser's capacitance since air which also acted as a dielectric was present in between the layers. Since there were several layers of mylar which had to be folded to contain the negative plates, the laser could not be pressed firmly to avoid air from getting in. In addition, the separation between the plates became larger because of this problem. Therefore, the ends of the mylar were cut and glued instead of folding them. A strong epoxy glue had to be used which would prevent arcing between the negative and positive plate at the cut ends. In order to have a clearer picture of this new technique, it is worth referring to Figure (7.9.1) which shows the folded end of the mylar. Those ends were cut and glued together. In fact, all the sides of the mylar were glued to the foil to prevent air from entering inside. This technique resulted in a considerable reduction in thickness of the multilayer laser. This allowed the addition of more layers to the bottom plate and the electrodes could be placed on the laser channel without any difficulty. At that stage, only 5 layers of aluminium were connected to the bottom plate. Figure (7.11.5) shows a picture of the multilayer aluminium N_2 laser employing this new technique.

Figure (7.11.5): Picture of Multilayer N_2 laser with Al foil (ends of mylar cut).

The same set up was used and both the lower and higher ends energy outputs were measured. The capacitance of the laser was measured to be 50 nF. It was observed that the laser light was bright and the noise made when firing was much louder than that of the previous laser. Figure (7.11.6) shows the graphical illustration of the variation of the energy output with the number of shots. Here, once more, the energy output from the higher end of the laser channel was too low to be detectable by the laser energy monitor. Thus, the graph shows the energy values recorded at the lower end only.

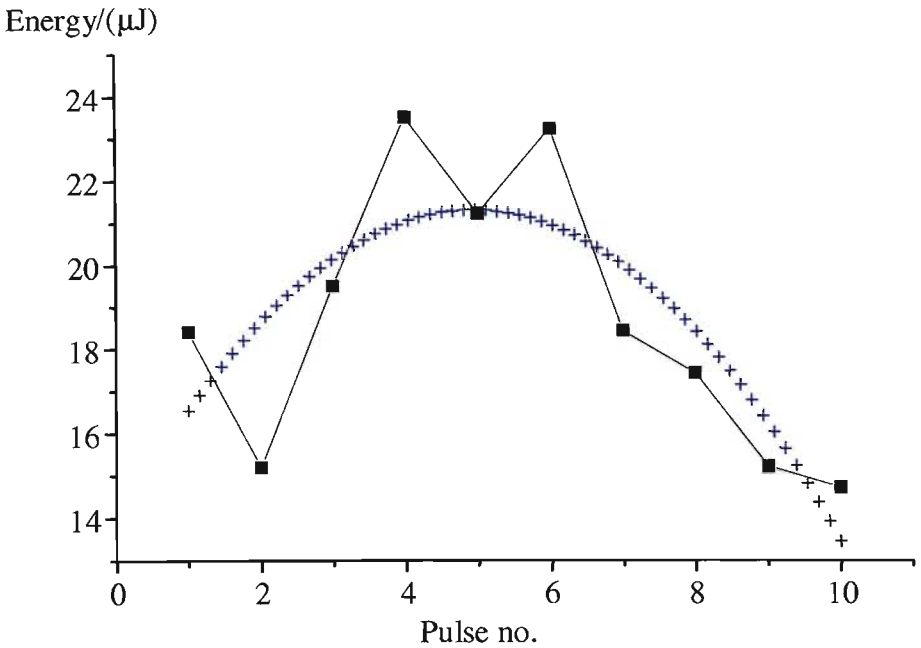

Figure (7.11.6): Variation of energy with pulse no. for 5 layers of Al foil.

A average energy of 18.67 μJ and a peak value of 23.5 μJ were achieved with this laser of 5 layers. The 7 layer parabolic nitrogen laser with folded ends gave approximately the same output energy. This could be attributed to the new technique employed. Referring to the graph, one can also see the same tendency as the previous laser, i.e, the optical output decreases with the number of shots which was due to the reasons given earlier (section 7.11). Moreover, the energy output stability was not good which may be attributed to the erratic performance of the free running spark gap.

Another layer of aluminium foil was added on the 5-layer nitrogen laser. The same experimental conditions were maintained for each energy measurement. An average energy output of 23 μJ was achieved. This represents approximately a 20% increase in laser energy output. In order to investigate this further, another layer of aluminium foil was added to the 6 layers. The graph below shows the energy output variation with pulse no. at 5, 6 and 7 layers of aluminium foil.

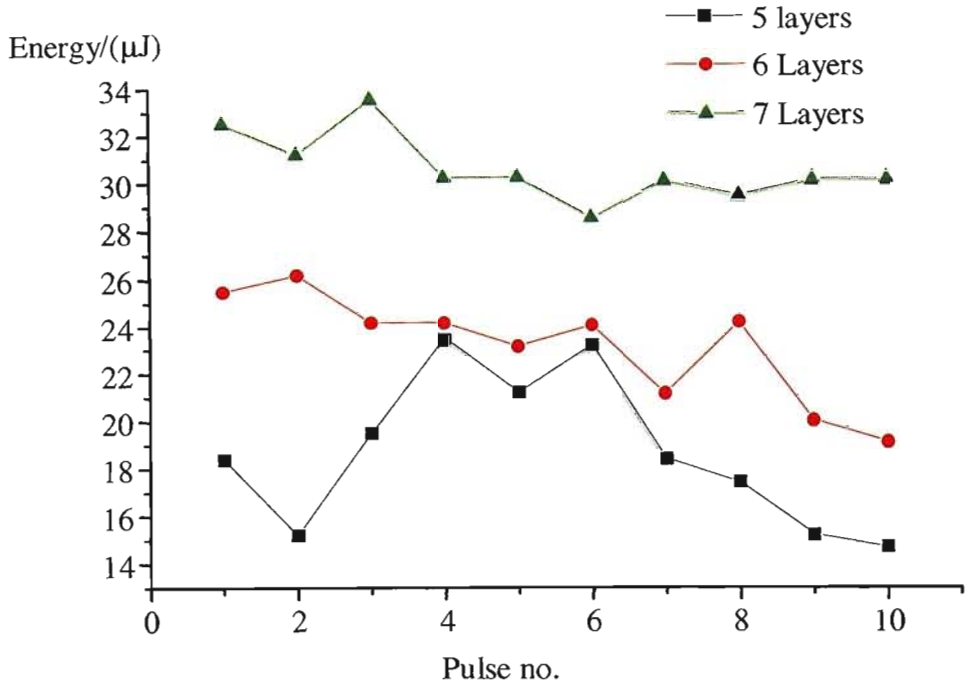

Figure (7.11.7): Variation of energy output with pulse no. at 5,6,7 layers Al. foil.

An average laser energy output of 30.58 μJ was achieved with the 7 layer nitrogen laser. This represents a 25% energy increase. Here, again, the same trend is observed, i.e, the energy output decreases with the number of shots. It would be worth recalling that the average energy achieved with the other 7 layer nitrogen laser (with folded mylar ends) was about 18 μJ. Therefore, by having the ends of mylar cut and glued resulted in an energy increase of about 40%. Another layer of foil (the 8th one) was added to the laser to observe its effect on the laser energy. However, at that stage, the laser could not be charged since the power input was not high enough to charge the 8-layer nitrogen laser.

7.11.1 Discussion and conclusion

Nitrogen lasers can be constructed with aluminium foil. However, several layers had to be connected in parallel to give an energy output high enough to be detectable by the joulemeter (threshold = 10 μJ). The laser light was observed to be much brighter than for the single layer device. It was also observed that the light coming out the higher end of the laser channel was highly divergent and the optical output was too low to be detected by the joulemeter. A 40 % increase in energy was obtained with the multilayer laser having the ends of mylar cut and glued. It was evident that air was entering the regions between the mylar and foil which could reduce the laser's capacitance. In addition, the graphs in Figures (7.11.6)
(7.11.7) show that the energy output decreases with the number of shots. This is attributed, as discussed before, to the formation of tiny holes in the aluminium foil after several shots as a result of which energy was lost at those potential arcing areas. The dielectric strength of the aluminium foil was not sufficiently high to resist the

calculated to be about 7.3 J and a maximum output energy of 31 μJ was achieved with the 7 layer nitrogen laser. Therefore, the efficiency of the laser was found to be 4.3 x 10^{-4} %. Compared with the other lasers which were constructed, this one had the lowest efficiency. It has to be noted that the capacitance of the multilayer N_2 lasers above and that of the large lasers, Laser 4 and 5 (section 7.6 and 7.7) were almost the same, i.e approximately 50 nF. However, their laser energies output differ considerably since the 7 layer N_2 laser gave an average energy of 31 μJ while the large lasers gave an energy output of 0.3 mJ. This could be attributed to the much higher impedance of the multilayer N_2 laser than that of the Laser 4 or Laser 5. It was also evident that the parabolic shape of the top plate of the multilayer N_2 laser was efficient in improving its laser energy output.

In the future, a stronger aluminium foil could be used to make a multilayer parabolic nitrogen laser. The same technique of gluing the mylar instead of folding could be employed in order to allow the addition of more layers. Then, a higher power input could be applied and in addition, a pressurised and triggered spark gap could be used.

7.12 Electromagnetic Interference (EMI) and Mechanical noise

The low impedance high voltage Blumlein pulsers used in the lasers described in this thesis, produce rapidly changing voltages and currents with rates greater than 10^3 V s^{-1} and 10^3 A s^{-1}. This leads to intense electromagnetic waves being radiated, unavoidable stray ground capacitance and ground currents of the order of kA. As a result, there is severe EMI caused that affects the operation of oscilloscopes and other sensitive electronic measuring equipment such as the laser energy monitor. In order, to obtain reliable and valid measurements, this interference has to be reduced to the lowest level possible.

There are three main sources of EMI:

(a) The radiated fields can penetrate thin shielding and induce noise directly in the amplifiers of the oscilloscope. This effect can be reduced by housing the equipment in a shielded room such as a Faraday cage. This was done when measuring the output energy of the rectangular and parabolic laser (refer to Chapter 6). Faraday cages are usually manufactured from 1.5 mm galvanised iron sheets, which are seam-welded in order to reduce electromagnetic leaks. Iron shows shielding properties comparable to copper at high frequencies and improved magnetic shielding at frequencies of less than 150 kHz. Improved shielding can be obtained from a honeycomb structure which is similar to our case. It is worthwhile to recall that the laser was placed in the Faraday cage and all the other electronic equipment were housed outside the cage.

(b) The electromagnetic interference can be conducted into the cage through the power lines of the oscilloscope. This conducted interference can be suppressed by power-line filters or by isolation transformers. The latter have the additional advantage that they permit floating of the Faraday cage to reduce unwanted ground currents. Isolation transformers with specially designed shields provide effective inter-winding capacities of 5 x 10^{-16} F and insulation resistances of greater than 10^{10} Ω. The noise rejection of these transformers is better than 140 dB. Conducted noise from power lines can be eliminated completely by operating the oscilloscope from a battery.

(c) Multiple grounding and ground loops caused by stray capacitance lead to ground currents flowing through the shield of the signal cable. This can cause a voltage drop across the cable which is superimposed as noise upon the actual signal (Bergmann, 1980)

This can be avoided by using a double-shielded signal cable, where the auxiliary shield acts as an extension to the Faraday cage. Ground currents are reduced by using a single common ground point as was done in our case. Coaxial cable connecting the detector to the oscilloscope was also used. A typical arrangement for the measurements of pulsed currents and voltages are shown in Figure (7.12.1) (Bergmann,Thesis, 1980).

Figure (7.12.1): A typical arrangement for voltage, current or energy measurements using double-shielded signal cable and floating Faraday cage (Bergmann, 1980).

The Colliding Shock experiments were carried out in the Faraday cage because of the intense electromagnetic energy being given out during the explosion. One of the major problems which the author faced during the energy measurements of the several lasers described earlier, was not only the electromagnetic noise due to the high frequency switch but also the mechanical noise from the free-running spark gap.The joulemeter was very sensitive to both of these interference as a result the readings recorded by the detector could not be considered valid unless these interference were reduced dramatically.

A wooden box was constructed to house the joulemeter. A 2 cm layer of polystyrene material was glued on both the inner and outer surfaces of the box. This was done to absorb the mechanical noise coming from the laser. In addition, the outer surfaces of the box were covered with a 0.2 mm thick aluminium foil which would reduce the electromagnetic interference. The joulemeter monitor and the detector were also wrapped in aluminium foil without forgetting to cover the lead connecting the monitor to the detector as well. Figure (7.12.2) shows the box and laser energy monitor shielded against EMI with aluminium foil. At first, 'kitchen' aluminium foil which is thinner was used and it was observed that it was not efficient in shielding the electromagnetic noise.

Figure (7.12.2): Picture showing the laser energy monitor and box shielded using Al foil.

In order to reduce, the mechanical noise due to the spark gap and laser discharge, a wooden box of appropriate size to fit the lasers was made. The inner and outer surfaces of the box was then insulated with 2 cm thickness foam. Holes had to be made on the sides of the box to cater for the passage of the laser beam.In addition, the line joining the two holes on opposite ends had to be inclined at an angle of 30° to the horizontal. Thin glass (microscope slides) which does not absorb much UV light were glued at the holes on the inner surface of the box. A cover for the box was also made and its top and bottom faces were also insulated using the thick foam. Figure (7.12.3) shows the foam-insulated box which contained the lasers. These shielding techniques provided a remarkable and significant reduction of the EMI and mechanical noise as a result the detector was not triggering due to these interference.

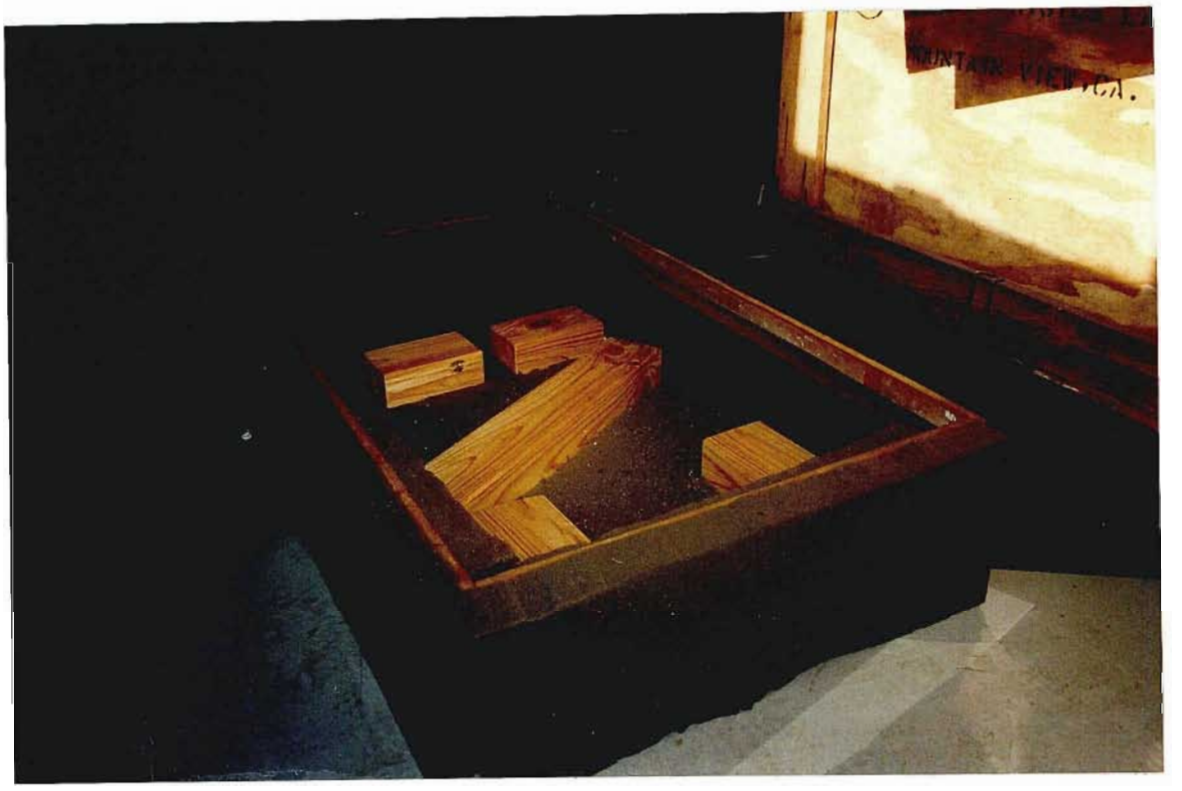

Figure (7.12.3): Picture showing the foam-insulated wooden box to provide shielding against mechanical noise.

In order to further reduce these interference, the detector was placed in a separate cabinet. The laser was placed in an open-spaced lab. and the detector in a closed room. They were separated by a thick wooden wall through which an appropriate hole had to be drilled to allow for the passage of laser beam. Figure (7.12.4) shows the insulated laser box next to the wall separating the laser and the detector.

Figure (7.12.4): Picture showing the foam-insulated laser box next to the wall which provided further shielding from noises.

CHAPTER EIGHT

8.0 BEAM PROPAGATION MEASUREMENTS AND ANALYSIS

8.1 Introduction: The Carbon Dioxide Laser

The author spent several weeks at the South African Atomic Energy Corporation, Pelindaba, Pretoria where he carried out an investigation of the beam propagation and beam quality of CO_2 laser beams. There are a number of medium, high energy repetition rate TEA carbon dioxide lasers which were developed for the isotope separation of Uranium. However, after the MLIS (Molecular Laser Isotope Separation) programme had to be closed down, efforts are being made to find alternative industrial applications of those lasers.

The Carbon dioxide laser is one of the most versatile types of lasers in the market today. It emits infrared radiation between 9 and 11 μm either at a single line selected by the user or on the strongest lines in untuned cavities. It can produce continuous output powers ranging from well under 1 watt for scientific applications to many kilowatts for material processing. It can generate pulses from the ns to ms regimes. Custom made CO_2 lasers can produce continuous beams of hundreds of kilowatts for military laser weapons research or nanosecond-long pulses of 40 kJ for research in laser-induced nuclear fusion. A general description of a CO_2 laser system is shown in Figure (8.1.1). CO_2, N_2 and He are the three gases which are mixed and fed into one end of a gas discharge tube at a pressure of a few torr. The gas flows down the end of the tube in about one second and is pumped out the far end with a mechanical forepump. An electric discharge is maintained between the metallic end flanges of the tube. The ballast resistance is required because of the negative dynamic resistance of the discharge. With a fully reflecting mirror on the left and a partially transmitting mirror on the right, the device lases in the far infrared at 10.6 μm.

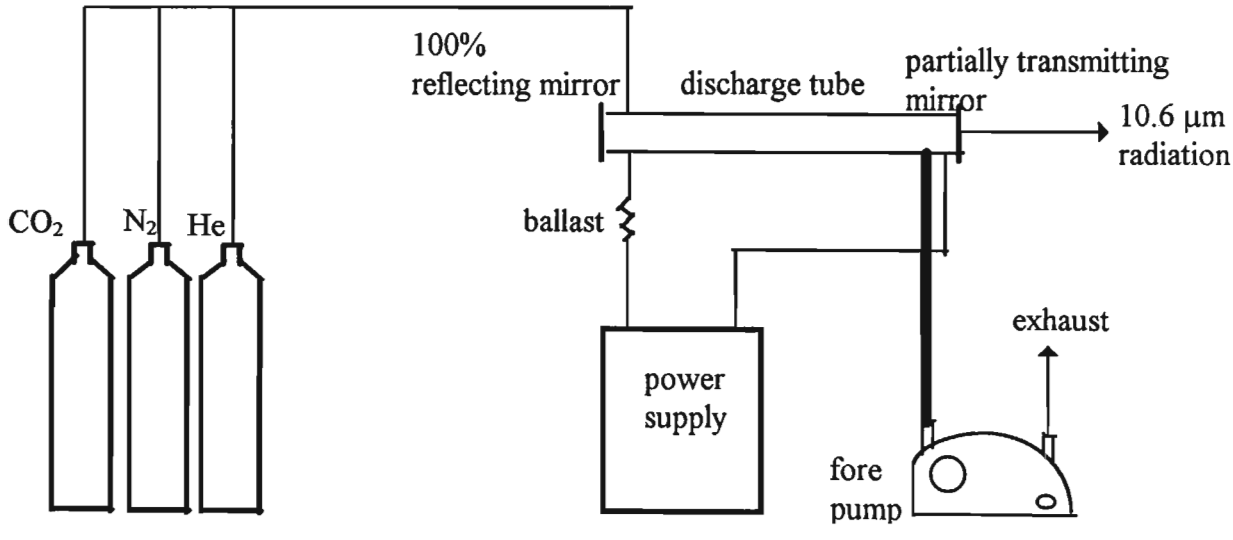

Figure (8.1.1): A simplified CO_2 laser system.

There are many parameters that affect the design and operation of the CO_2 laser. The gas discharge can be excited with dc, ac, RF, repetitive pulses, or any combination

thereof. The performance of these lasers can be optimised in several ways which may include maximising the multimode power, maximise single-mode power and maximise efficiency. The parameters that affect such optimisation for the following gas systems are:

(a) Tube length, diameter and wall temperature

(b) Gas mixture, pressure and flow speed

(c) Optical mode control, wavelength control and output coupling

(d) Electrical discharge control and current density.

In addition, for sealed-off CO_2 lasers, it appears that the gas purity and tube materials are also important. Optimisation is by no means simple because the various parameters are strongly interrelated. In the experimental sections to follow, a few of the optimisation techniques were carried out to observe their effects on the laser energy outputs.

8.1.1 The Carbon Dioxide Laser Theory

The possibility of using molecular vibrations for laser action was clearly pointed out by Polanyi in 1961. Soon after, Patel described in some detail the laser action on the vibrational-rotational (V-R) transitions of CO_2 in an electric discharge. Shortly afterwards, progress towards high power and efficiency was achieved by Patel with the addition of N_2 and by Moeller and Rigden with the addition of He. Molecular translation, vibration and rotation are the principal forms of energy storage and interchange. The important energy levels of the molecule are shown in Figure (8.1.1.1) (Patel, 1964).

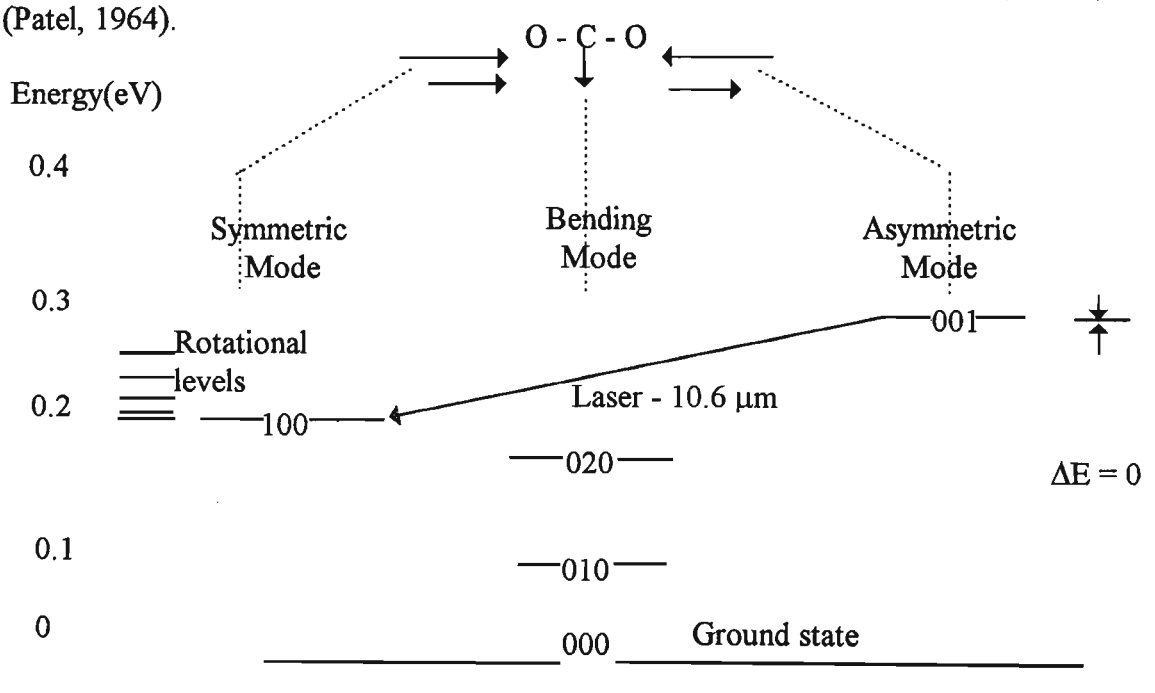

Figure (8.1.1.1): The important energy levels of the CO_2 molecule.

Carbon dioxide is a linear, symmetric molecule with the carbon atom balanced against the two oxygen atoms, O-C-O. Therefore, three characteristic vibrational modes exist:

the symmetric mode, where the two oxygen vibrate against each other; the bending mode, where the carbon atom moves out of the molecular axis, thus bending the molecule; and the asymmetric mode, where the two oxygen atoms oscillate against the carbon atom. Each of these vibrating modes is quantized and the particular vibrational state of the molecule is designated by three integral numbers: the first number is the quantum level or excitation number of the symmetric mode; the second number is the excitation number of the bending mode and the third number is the excitation number of the asymmetric mode. Only the energy levels of the pure modes are given but all the mixed vibrational modes exist as well.

Each and every vibrational state is degenerate or further subdivided into a whole series of levels brought about by gross rotation of the vibrating molecule. These levels are also quantized and designated by ***J***, the rotational quantum number. They are shown in Figure (8.1.1.2) on an expanded energy scale for the 001 and 100 vibrational levels.

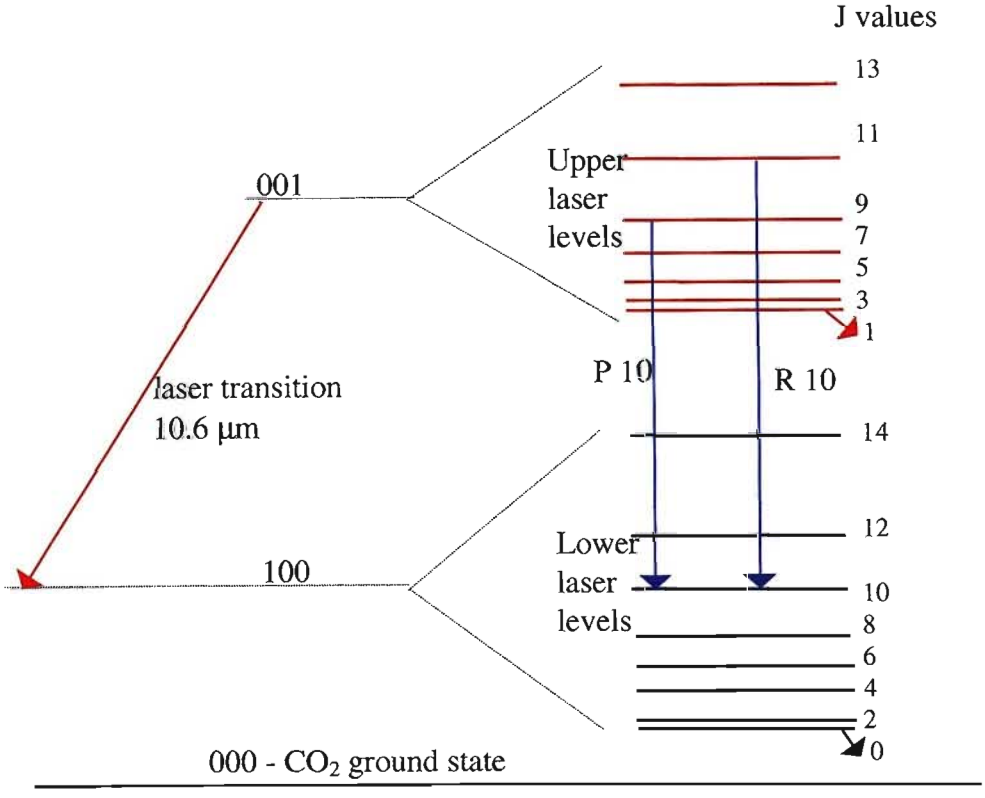

Figure (8.1.1.2): Expanded energy scale for 001 and 100 vibrational energy levels.

The lasing transition at 10.6 μm is a simultaneous change of these vibrational and rotational quantum states. However, this may occur on any one of the rotational transitions. The selection rules for the vibrational-rotational transition are that ***J*** must change by ± 1. Those transitions where ***J*** increases by 1 are called ***P***-branch transitions (for example P 10) and those that decrease are called ***R***-branch transitions (for example R 10). The wavelengths associated with the dominant transitions are ***P-18 - 10.57*** microns, ***P-20 -10.59*** microns, ***P22-10.61*** microns, etc. When the inversion in the total vibrational level occurs because of the discharge, the ***P*** branch transitions have more gain than their **R** counterparts. Since the **P** and ***R*** transitions compete with each other, the medium lases only on the ***P*** branches unless special precautions are taken. Those ***P*** branches which have the highest gain are most likely to show lasing

taken. Those ***P*** branches which have the highest gain are most likely to show lasing action. Experiments show that inversion is not a result of direct electronic excitation but is caused by vibrational energy interchange between N_2 and CO_2. The lowest vibrational level of N_2 is essentially metastable since the molecule is symmetric and cannot radiate. In a nitrogen discharge, about 20-30 % of the molecules are vibrationally excited, the energy level of n = 1 matches the level of the 001 state of CO_2 within 2 mV as shown in Figure (8.1.1.2). When the two gases are mixed, effective resonance collisional transfer occurs between the two states. Also, the second level of N_2 matches the 002 mode of CO_2 and so on up the ladder. The net result is that the asymmetric ladder, 00n, becomes highly excited.

The lower level and asymmetric ladder is not excited by N_2 because there are no energy resonances. However, when the laser is operative, the 100 mode and its chain become heavily populated. This chain cannot radiate to the ground state and can only radiate weakly to the lower bending modes. However, there is a close "Fermi" resonance of the 100 mode with the 020 mode and collisions can cause this transition. The addition of helium gas helps to increase the laser power. Its low mass makes it effective in trading its kinetic energy with the molecule internal energy modes for small energy changes. As a result the helium is effective in:

(a) Cooling the CO_2 rotational temperature (but not the vibrational temperature).

(b) Increasing the thermal conduction to the wall (thus keeping the translational temperature low, the Doppler width small and the gain high).

(c) Increasing the depopulation rate of the 010 level of CO_2 which in turn depopulates the 100 lower level. This is because the 010, 020 and 100 levels are all strongly coupled together through resonant collisions.

The important lifetimes in the CO_2 laser are practically all determined by collisional phenomena. The theory of gas discharge given in chapter 3 is applicable in this gas discharge laser as well. Here, the primary source of excitation and ionisation is from collision of the first kind involving electrons and molecules.The radiative lifetimes vary from a few ms to a few seconds whereas the mean free time between molecular collision is of the order 10 to 100 ns. These times must then be scaled up by the number of collisions needed to effect a certain energy transfer. The important transfer times are summarised in Figure (8.1.1.3).

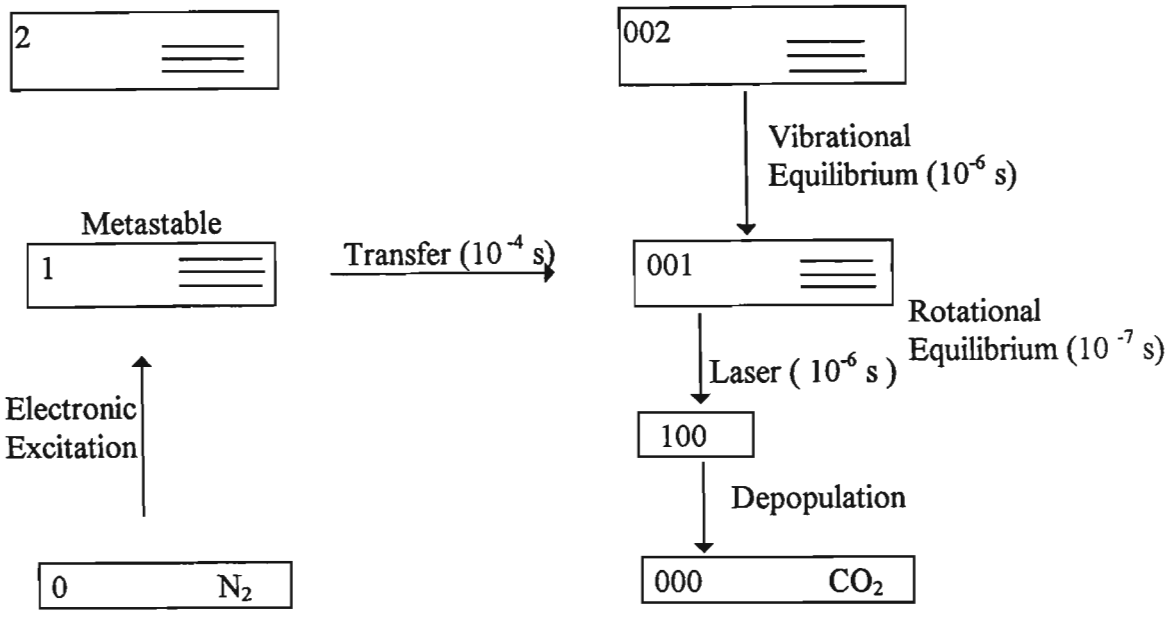

Figure (8.1.1.3): Important Collision Lifetimes in a He-N_2-CO_2 system.

8.2 The AEC Carbon Dioxide Laser System

The existing CO_2 laser system at the AEC (Atomic Energy Corporation), Pretoria consists basically of an oscillator and two amplifiers. The specifications and parameters of the laser are as follows:

(a) Wavelength: 10.6 μm
(b) Maximum repetition rate: 2 kHz
(c) Multimode pulse energy: 1 J at 2 kHz (2 kW average power)
(d) TEM_{oo} pulse energy: 250 mJ at 2 kHz (500 W average power)
(e) Pulse length: 80 ns
(f) Power Supply: 24 kV

Our main aim of experimenting with this system was to find viable ways to increase the energy output of the laser without sacrificing the beam quality. Since the laser group was looking into the possible industrial applications of the CO_2 laser, it was very important to have a beam which is close to the gaussian beam profile. The author investigated the beam propagation along the laser chain by varying the aperture sizes placed at the entry of the oscillator. The energy was measured using a Joulemeter with calibration factor of 2.50 volts/Joule at 1064 nm. The M^2 factor was calculated and a beam analysis software was used to find how the beam propagates along different sections of the laser chain. A burn pattern was also obtained at regions before and after the focus of the beam. The beam was then passed through two amplifiers in series and a double pass through one of them was also done. Finally, the laser was run at higher repetition rates and this time the beam diagnostics were obtained using a device called a Three Element detector. Figure (8.2.1) below shows a side view picture of the set-up which include the oscillator, amplifiers and their respective cooling systems.

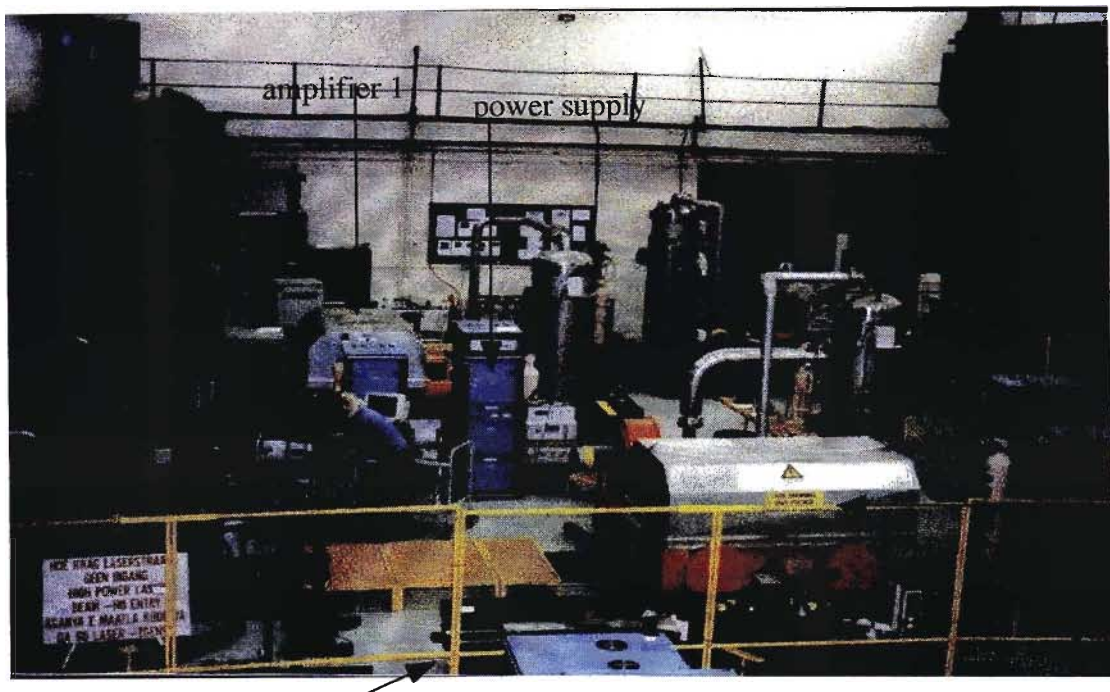

Figure (8.2.1): The AEC Carbon dioxide laser system.

[**Note:** The M^2 factor describes the relationship of the actual beam to that of an ideal Gaussian beam. It is also referred to as the propagation constant or a propagation factor. The theoretical beam divergence is given by:

$$\theta_{th} = (2 \times \lambda)/ \pi w_0 \qquad (8.2.1)$$

and the actual beam divergence is given by

$$\theta_{act} = (2 \times w)/ D \qquad (8.2.2)$$

where λ = laser wavelength in m.
w_0 = the minimum beam diameter in m (at the focus).
w = the beam diameter at a large Z value (far away from focus).
D = distance in m from the focus.

The M^2 factor is then the ratio of θ_{act} and θ_{th}, i.e $M^2 = \theta_{act} / \theta_{th}$.
For a perfect Gaussian beam, $M^2 = 1$. Values of M^2 greater than unity represent laser beams with higher-order modes than the TEM_{00} Gaussian mode.]

8.3 Experiment One: Method and Results

Firstly, the behaviour of the beam was investigated by measuring the energy of the laser before the oscillator or cavity aperture of the laser and at the exit of the oscillator. The laser was run at 10 Hz. Measurements were taken when both of the amplifiers were switched off and only the oscillator was running. The aperture was placed at the entry of the oscillator and for each aperture size the output energy was measured at the entry and exit of the oscillator. This was done in order to compare the energy coming out at either output of the oscillator and to determine the amount of energy that was lost through its optics. Table (8.3.1) shows variation of the energy before and after the oscillator at different aperture sizes.

Table (8.3.1): Variation of energy with aperture sizes.

Before Oscillator	Aperture size/(mm)	Energy/(mJ)
	10	278.7
	9	230.1
	8	183.5
After Oscillator	10	304.9
	9	249.4
	8	204.7
	7	154.2
	6	94.5

As can be seen from the above table, the energy output after the oscillator at different aperture sizes is greater by approximately 7 to 10 % and the energy decreases with decreasing aperture sizes. This means that there were some energy losses at the windows and there was a more significant loss at the reflecting plane mirror before the oscillator. The 98.8 % reflecting plane mirror or the back reflector is for reflecting back the beam into the oscillator. Figures (8.3.1a) and (8.3.1b) below show a picture of the oscillator and the position of the backreflector before the oscillator respectively.

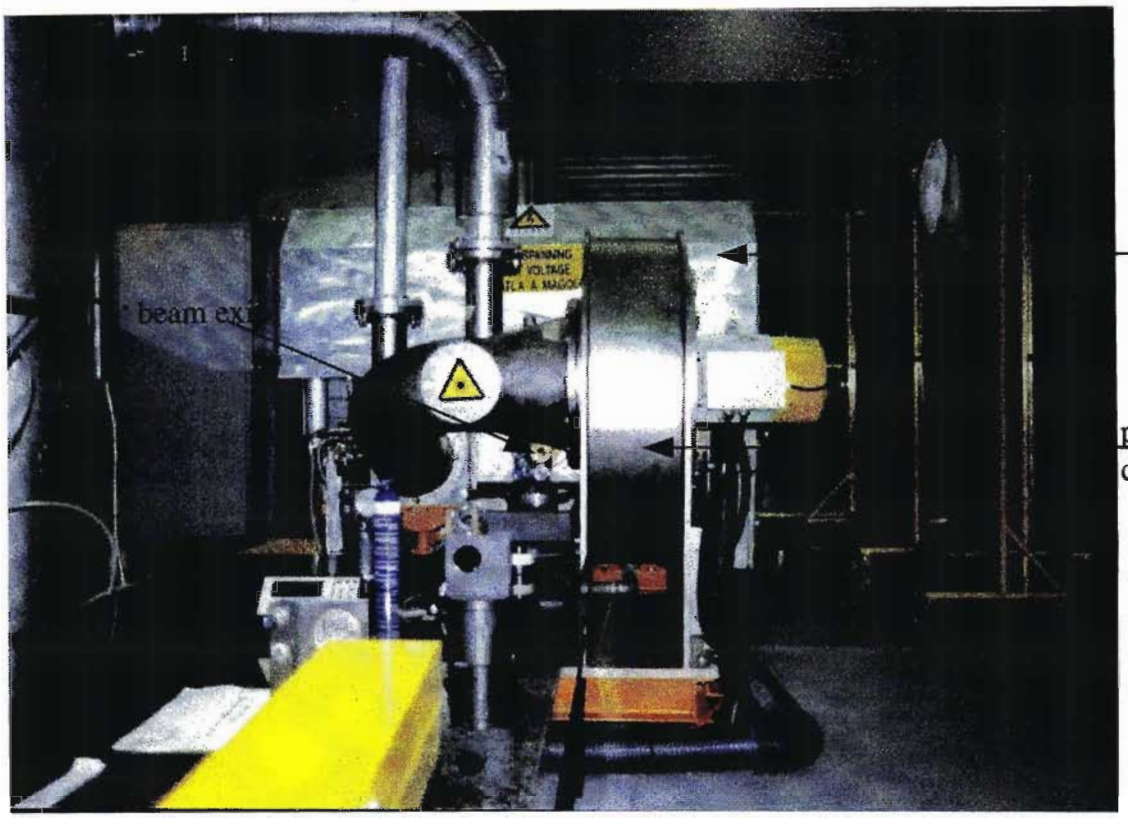

Figure (8.3.1a): The Laser Oscillator.

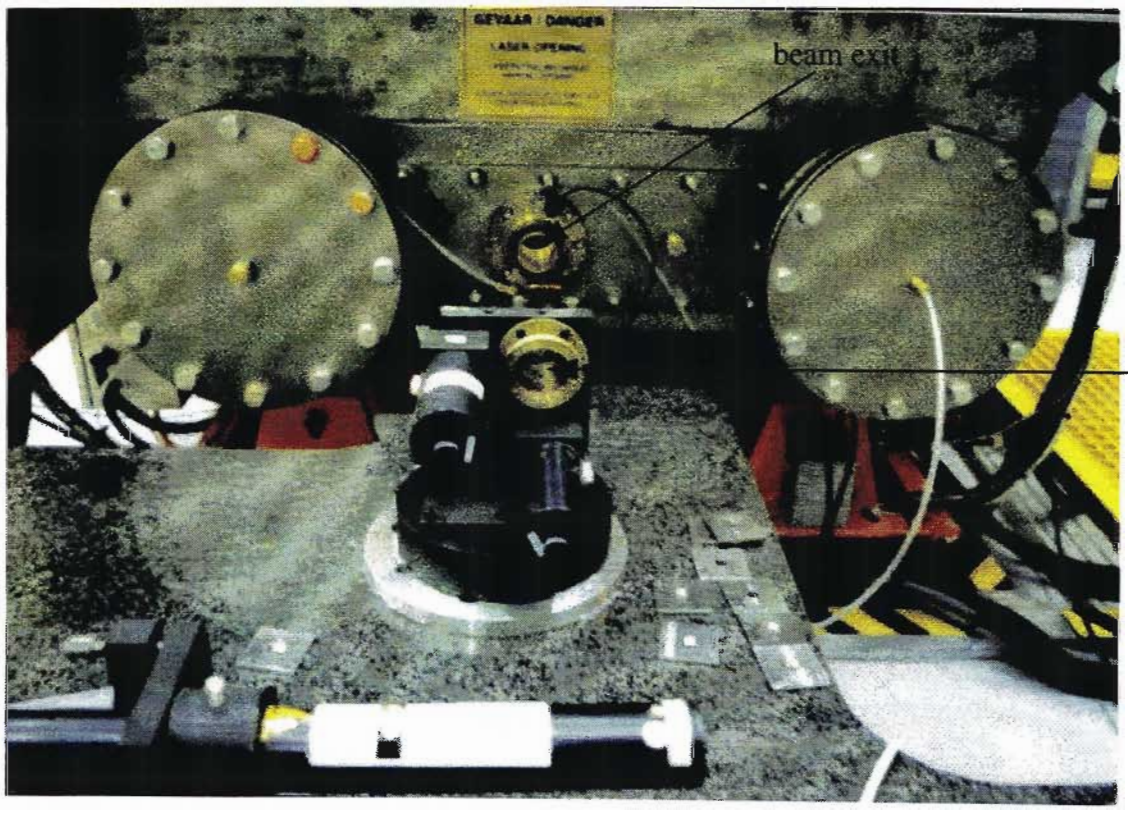

Figure (8.3.1b): The position of the backreflector before the oscillator.

With the same system set-up, an investigation was carried out by the author to observe how the beam propagates a few metres before and after the focus. The method used was almost the same as the previous one, that is the energy of laser beam was measured at distances before and after the beam's focal point at different aperture sizes. Using the recorded data, the M^2 value was calculated. At this stage, both the amplifiers were off and the beam was made to pass through only one of them. For that particular experiment, an aperture size of 10 mm was chosen and placed before the oscillator and the back reflector was aligned to give symmetrical patterns at a distance of 10 m from the focus. Thermal paper and beam stops were used to aid alignment. The laser output was high enough to cause a burn pattern on the thermal paper. The schematic set-up was as shown below in Figure (8.3.2) and at that stage only the oscillator, mirrors and one of the amplifiers (in the off mode) were involved.

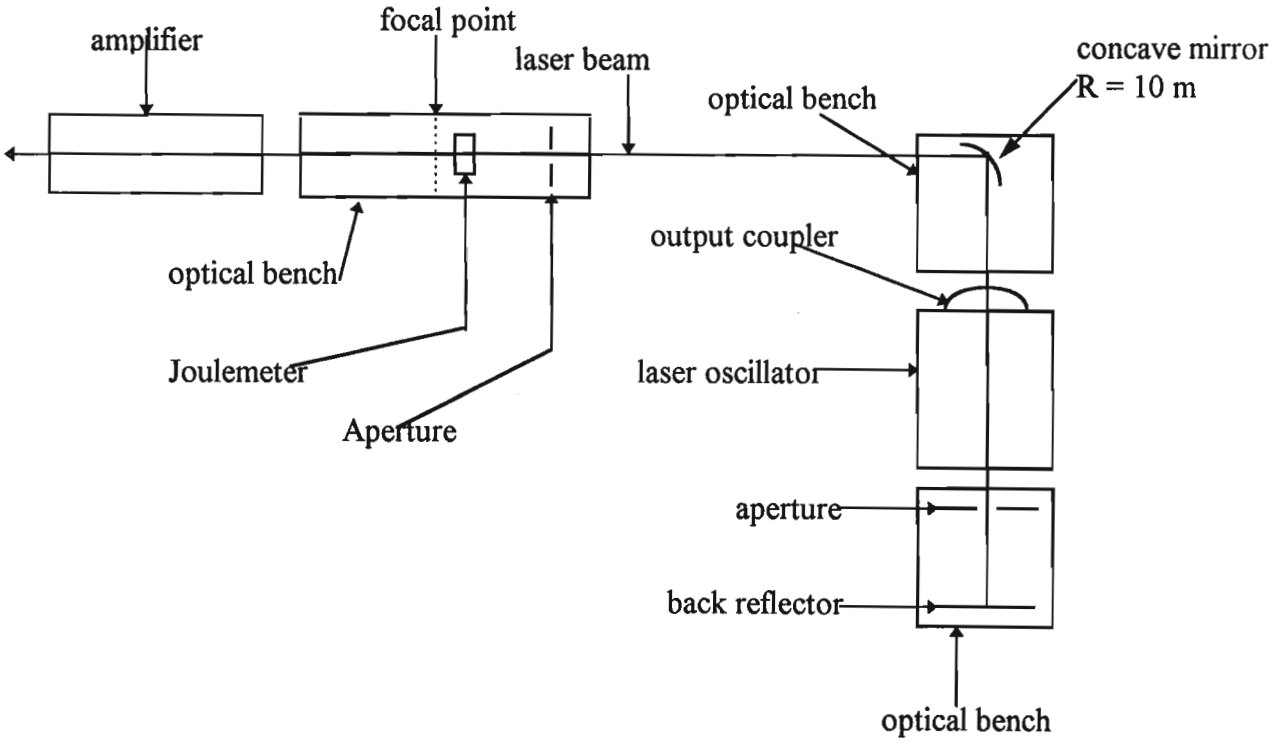

Figure (8.3.2): Schematic diagram of the initial laser system set-up.

The focal point of the laser beam was located and found to be approximately 3.5 m from the concave mirror (R = 10 m)(see Figure 8.3.2). The focus of the beam was located with the help of thermal paper. The way this was done was to place the paper along the path of the beam and determine the exact position at which the spot size became smaller. This method was not an accurate one but it did serve the purpose. The position of the focal point was clearly marked on the optical bench and it was used as the reference line for making distance measurements before and after the focus. The beam was transported through the amplifier since the latter was in optical axis with the beam.The output energy at a distance of 10.42 m after the focus was measured (after the amplifier). Note that at this stage the amplifier was switched off. The tables below show the variation of laser energy output with different aperture sizes for each distance Z measured before and after the focus. Note that - Z refers to the distance before the

focus and + Z refers to the distance after the focus. The aperture was placed a few centimetres from the Joule meter.

Table (8.3.2): Variation of energy with aperture size at Z = -1.20 m.

Aperture Size/(mm)	Energy/(mJ)
0	287.1
2	48.4
4	169.5
5	216.1
6	240.7
7	272.1

Table (8.3.3): Variation of energy with aperture size at Z = - 1.70 m.

Aperture Size/(mm)	Energy/(mJ)
0	291.3
2	48.6
4	174.8
5	221.0
6	249.4
7	273.5

Table (8.3.4): Variation of energy with aperture size at Z = -2.20 m.

Aperture Size/(mm)	Energy/(mJ)
0	295.7
2	46.3
4	168.9
5	214.9
6	248.8
7	273.9

Table (8.3.5): Variation of energy with aperture size at Z = + 0.70 m.

Aperture Size/(mm)	Energy/(mJ)
0	287.0
2	46.3
4	162.4
5	203.0
6	238.7
7	263.1

Table (8.3.6): Variation of energy with aperture size at Z = + 0.20 m.

Aperture Size/(mm)	Energy/(mJ)
0	294.2
2	36.3
4	138.4
5	182.6
6	218.5
7	249.7
8	266.1

Table (8.3.7): Variation of energy with aperture size at Z = + 10.0 m.

Aperture Size/(mm)	Energy/(mJ)
41.6	306.8
5	12.7
10	41.8
15	82.9
20	130.9
25	186.5
30	237.6
35	277.4

Note: The aperture sizes in the above table (8.3.7) are different from those of other tables since a variable aperture size had to be used because of the high beam divergence particularly at this distance (Z = 10 m) from the focus. A graphical illustration of the variation of energy with aperture size at the different Z values is shown in Figure (8.3.3).The graph does not include the readings of table (8.3.7).

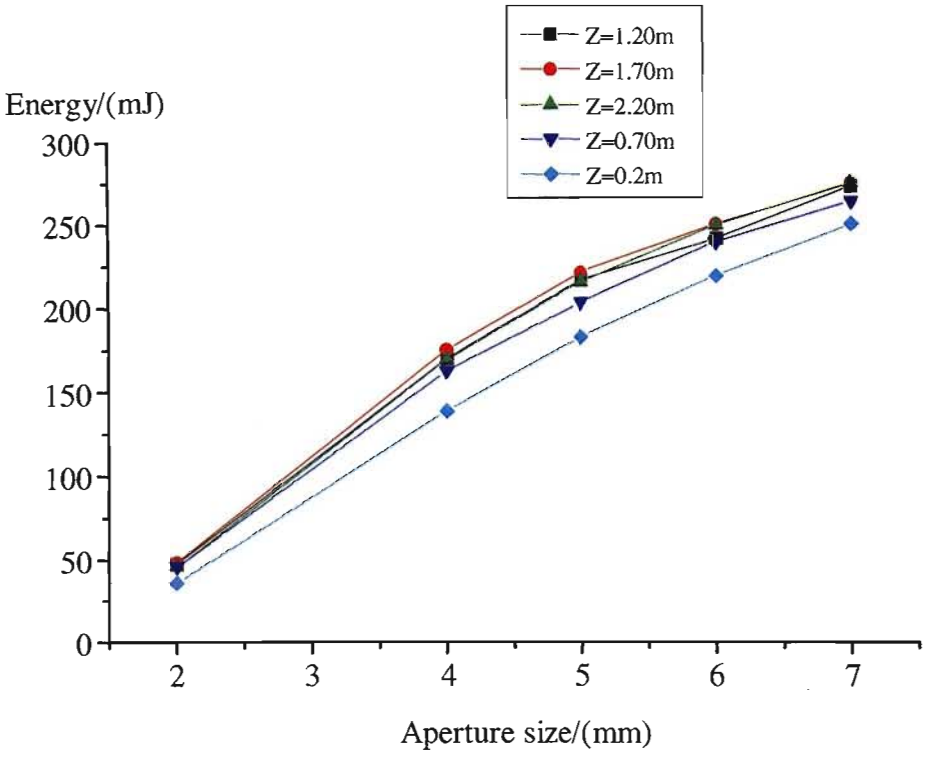

Figure (8.3.3): Variation of energy/(mJ) with aperture size at Z values.

Figure (8.3.4) shows a picture of the Joule meter with the variable aperture fixed on the photohead. The variable aperture was necessary since the beam was highly divergent at a Z value of 10 m.

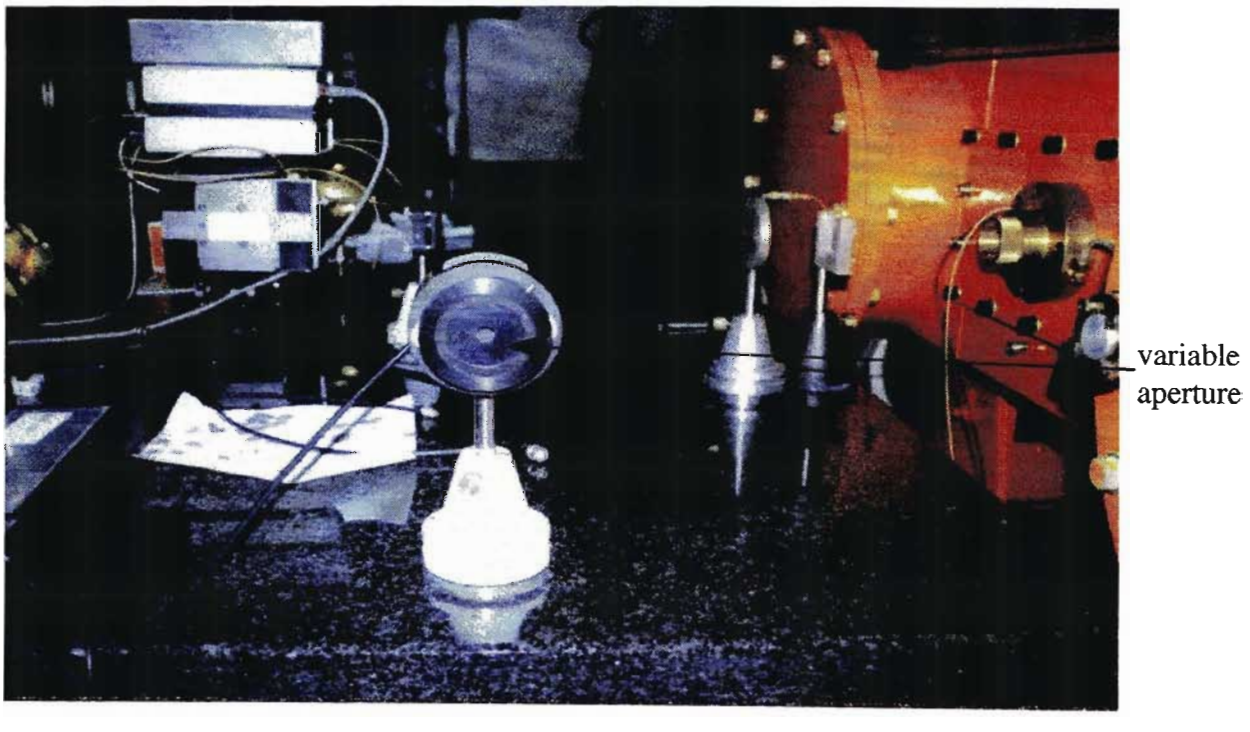

Figure (8.3.4): Picture showing the variable aperture fixed on the Joule meter.

The data in the above tables were fed into a computer software program which calculated the waist size at the above Z distances and the values at each Z distance from the focus is tabulated in table (8.3.8).

Table (8.3.8): The variation of the waistsize of laser beam with distance Z.

Z/(m)	Waistsize/(mm)
- 1.20	3.06 +/- 0.08
- 1.70	3.06 +/- 0.09
- 2.20	3.16 +/- 0.15
+ 0.70	3.20 +/- 0.11
+0.20	3.66 +/- 0.13
+10.42	17.99 +/- 1.03

The above data were plotted to give a graph of waistsize/(mm) versus Z/(m). The graph below (Figure 8.3.5) shows the plotted points with error bars. This was obtained after a polynomial regression fit to give a polynomial curve of second degree with the equation as shown.

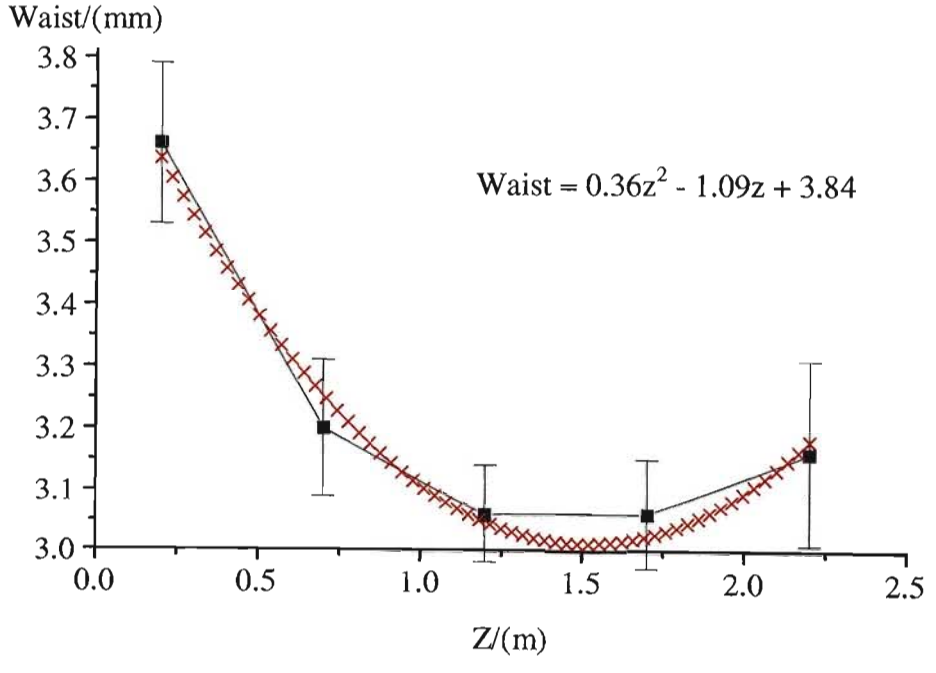

Figure (8.3.5): Graph showing the variation of waistsize with distance Z from focus.

As can be seen on the graph, the focus of the laser beam occurred at Z =1.517 m where the waistsize was 3.06 mm. Please note that measurements were taken approximately within1m from either side of the focus. In order to find the beam divergence at a longer distance from the focus, the energy of the laser was measured at a distance of 10.42 m from the focus. The values are tabulated in table (8.3.8) above. The waistsize at this distance was 17.99 mm.

From the above results, it was possible to calculate the theoretical and actual divergence. Hence, the M^2 value of the laser beam could be deduced. The theoretical beam divergence is given by:

$$\theta_{th} = (2 \times \lambda)/ \pi w_0$$

$$= (2 \times 10.6 \times 10^{-6})/ (\pi \times 3.06 \times 10^{-3})$$

$$= 2.24 \times 10^{-3} \text{ radians}$$

The actual beam divergence is given by

$$\theta_{act} = (2 \times w)/ D$$

$$= (2 \times 18 \times 10^{-3}) /10.42$$

$$= 3.455 \times 10^{-3} \text{ radians}$$

Thus the M^2 value is

$$\theta_{act}/\theta_{th} = (3.455 \times 10^{-3})/ (2.24 \times 10^{-3})$$

$$= 1.54$$

This value is close to the M^2 value of a gaussian beam which has a value of 1 but there can always be ways to produce a better beam quality than this one. The M^2 factor was plugged into a laser beam analysis software (Beam Cad) which allowed an analysis of the beam propagation along different sections of the laser chain. Referring to the graph in Figure (8.3.6), the waistsize was easily known at different points on the path of the laser beam due to which changes could be made to improve the beam quality. These changes could include replacing the concave mirrors with larger or smaller radius of curvature. The M^2 value could also be changed to see graphically its effect on the waistsize and the distance to waist since the software also allowed a graphical representation of the set-up by plotting a graph of beam diameter versus the distance the beam passes through. Figure (8.3.6) shows the graph of the beam propagation.

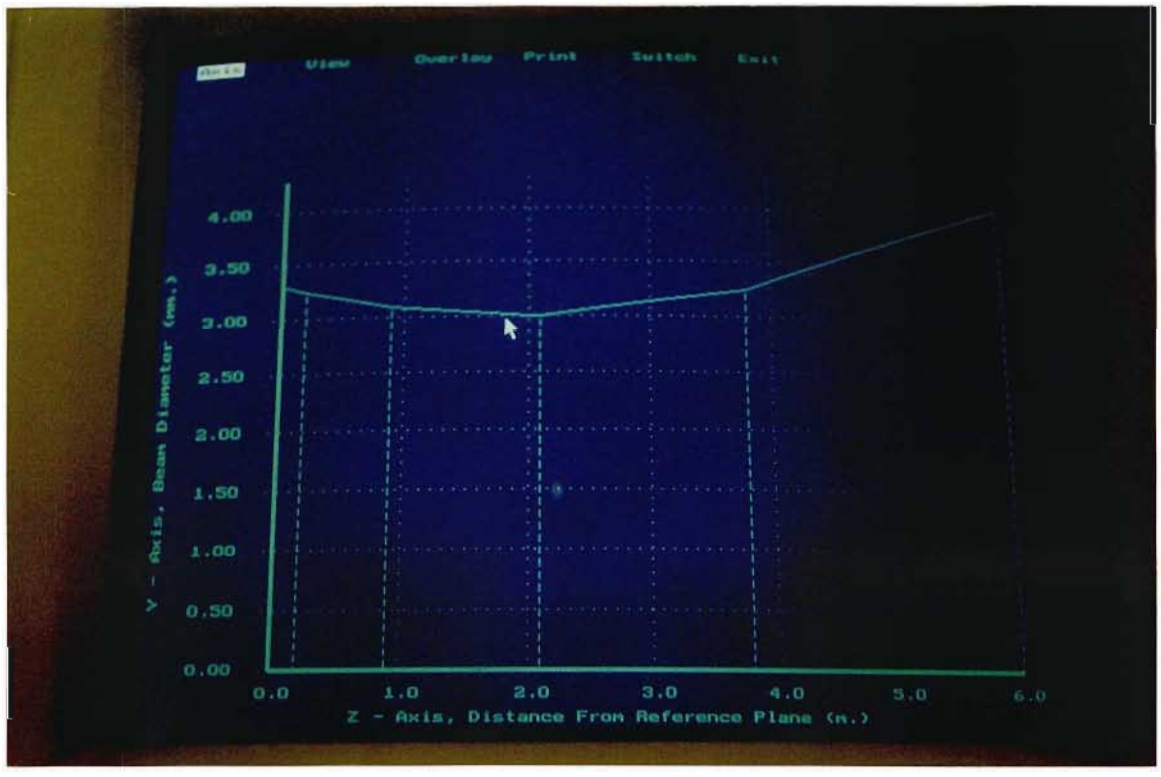

Figure (8.3.6): Graph showing the beam propagation.

The figure below shows a burn pattern on thermal paper at various distances from the focus. Since the original thermal paper with the burn pattern was not available, the following is a copy of it. The internal white zone in the burn patterns below is the deep burn and the black surround is the film exposure.

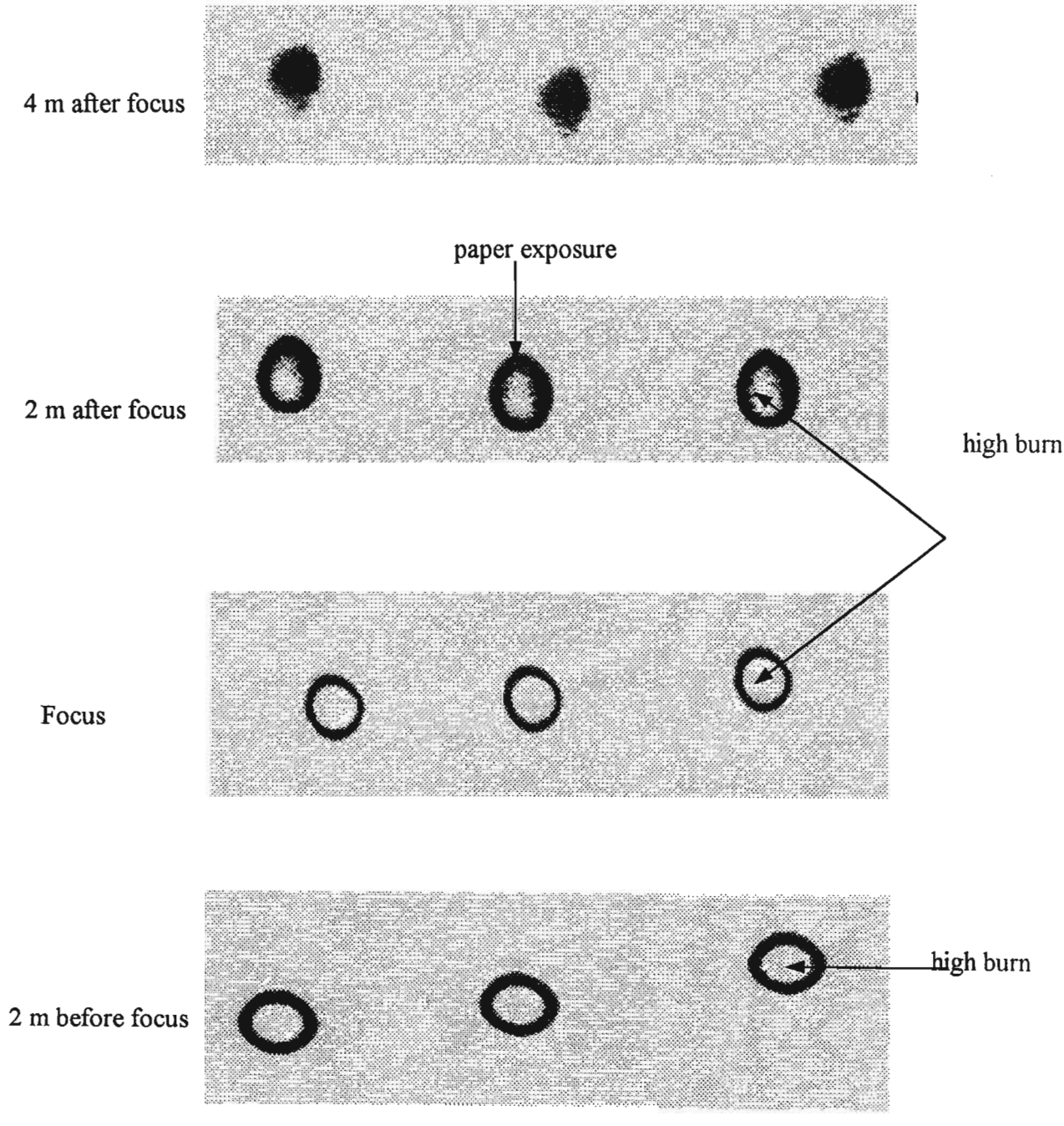

Figure (8.3.7): Burn patterns to show beam quality at several points from focus.

As can be seen from the burn patterns, the beam quality before focus was better and closer to a gaussian beam profile while those after the focus started to deteriorate. However, the burn pattern at 4 m was quite good and almost in the TEM_{oo} mode.

A burn pattern at a distance of 10.42 m was also done to observe the shape of the burn on thermal paper at different exposure times. The figure below shows the burn pattern for exposure times of 2, 3, 5, 7 s.

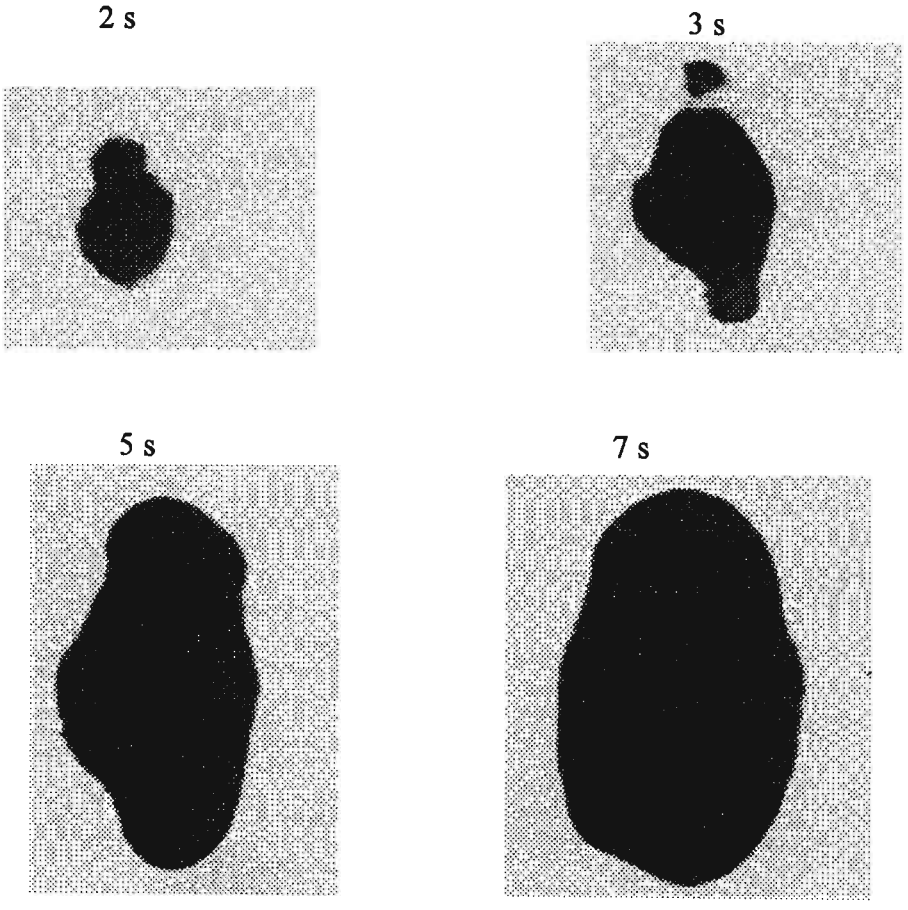

Figure (8.3.8): Burn patterns for different exposure times.

The burn pattern at an exposure time of 2 s shows a TEM_{01} mode which is expected at a distance of 10.42 m from the focus.

8.4 Experiment 2: Increasing Laser energy output

The aim of this experimental section was to try out possible ways to increase the energy output of the laser. The laser beam was made to pass through two amplifiers and the schematic diagram is shown in Figure (8.4.4. p 180). This experimental part was very tedious since the alignment was quite difficult. The laser beam passed through the optical axis of both amplifiers with the best possible alignment in order to have the lowest possible energy loss.

Figure (8.4.1, p.178) shows a picture of the amplifier.Tables (8.4.1 and (8.4.2) below show the variation of energy at different oscillator aperture sizes and in cases when amplifier 1 and amplifier 2 were either in the off or on mode. It also shows the percentage increase in energy output when the Amplifier 1 and Amplifier 2 were in the on/off modes.

Table (8.4.1): Table showing the variation of energy with aperture sizes.

Aperture/(mm) at Oscillator	**Energy/(mJ) (Amplifier 1 off)**	**Energy/(mJ) (Amplifier 2 on)**	**% increase**
10	202	541	62.66
9	177	502	64.74
8	140	436	67.89
7	98.1	342	71.32
no aperture	274	631	56.56

Table (8.4.2): Table showing the variation of energy with aperture sizes.

Aperture/(mm) at Oscillator	**Energy/(mJ) (Amplifier 1 and 2 off)**	**Energy/(mJ) (Amplifier 1 and 2 on)**	**% increase**
10	203	1099	81.53
9	178	972	81.69
8	144	866	83.37
7	105.6	743	85.79
no aperture	243	1202	79.78

The values in the above tables show that there was a very remarkable increase in the output energy when the amplifiers were switched on. There was approximately a 48 % increase in the laser energy output. Note that the values in table (8.4.1) show the output energy when being measured at the exit of Amplifier 1 and similarly the second table shows the values at the exit of Amplifier 2 passing through Amplifier 1 first. It can also be noted that the energy values in the second column of both tables are slightly different, especially the value at no aperture. The energy value after both Amplifier 1 and Amplifier 2 was actually less than that after Amplifier 1 only. This was due to energy losses in the optical components in the amplifiers, mirrors on the optical benches and diffraction losses. In section (8.6), an investigation was carried out by the author to find out the origin of these losses and ways to avoid or reduce them.

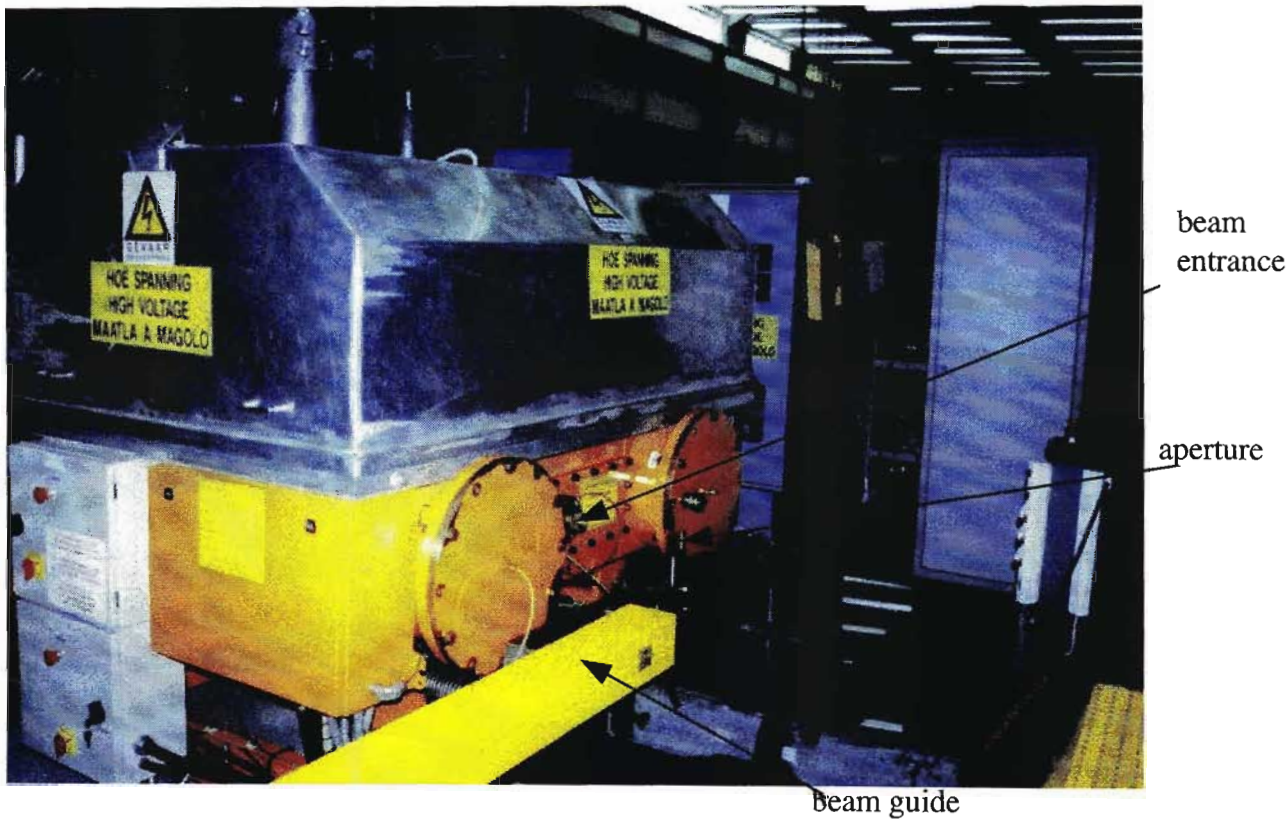

Figure (8.4.1): Picture of the amplifier.

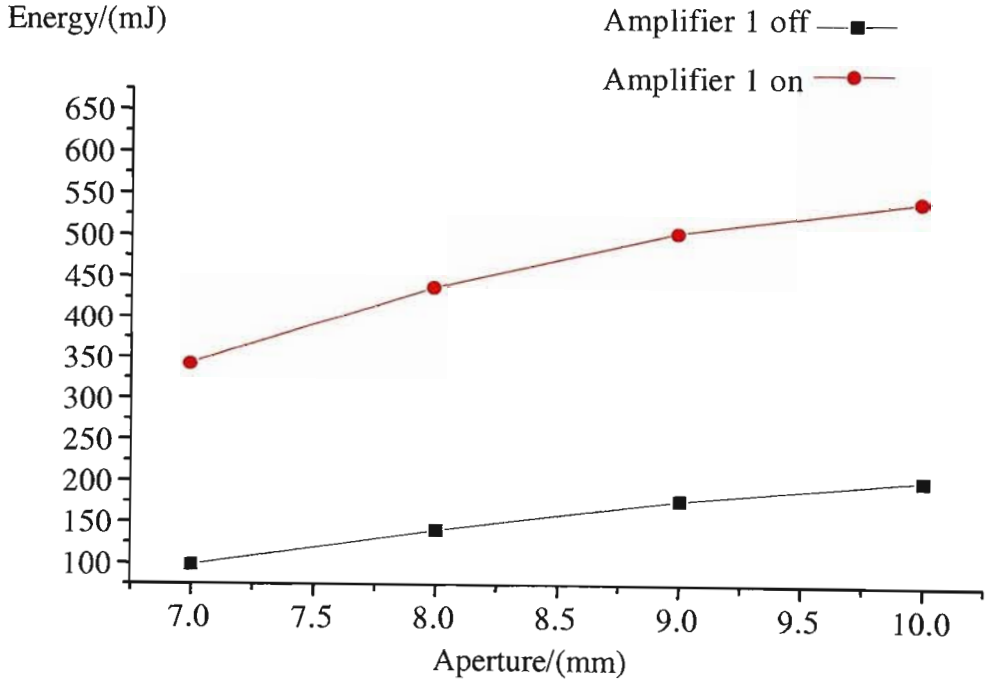

Figure (8.4.2): The variation of energy with aperture with Amplifier 1 switched on/off.

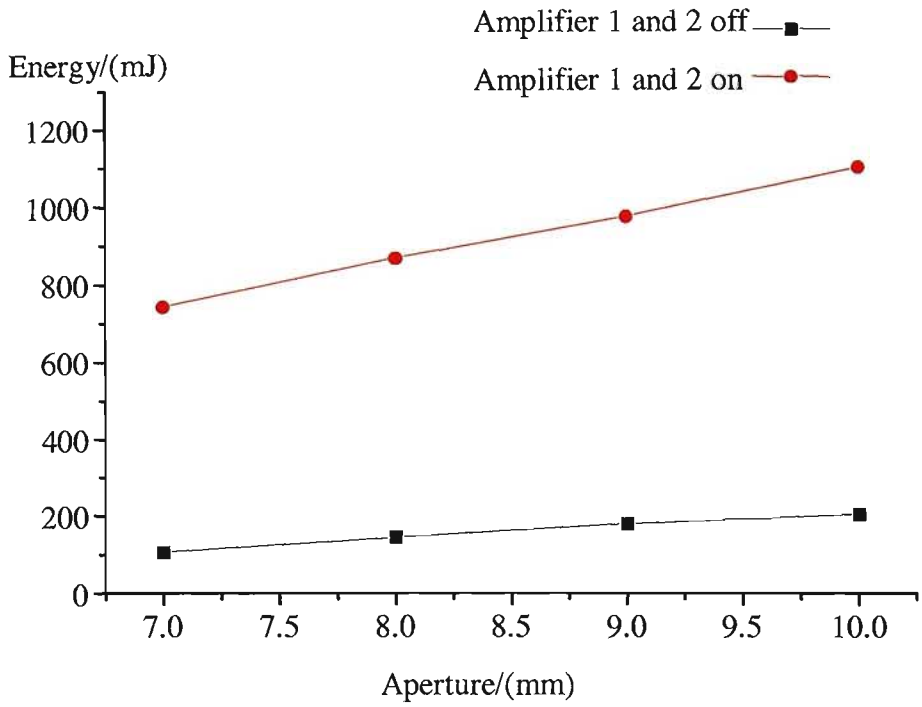

Figure (8.4.3): The variation of energy with aperture size with Amplifier 1 and 2 switched on/off.

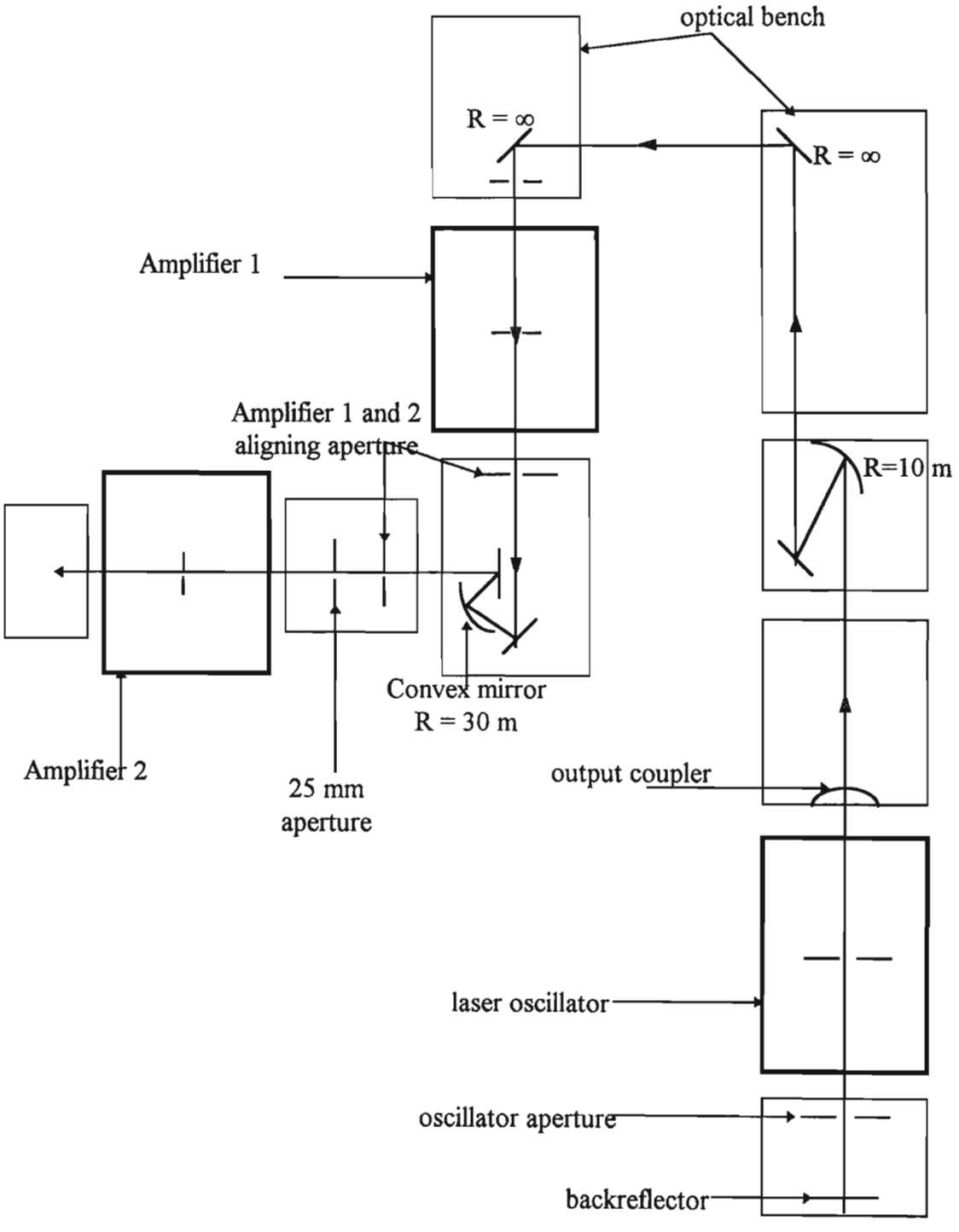

Figure (8.4.4): Schematic diagram showing the laser path through the amplifiers.

8.4.1 The Double Pass through Amplifier 1

In the previous section, we have seen one of the ways by which the output energy of the laser can be increased, i.e by passing the beam through two amplifiers.There was a significant increase in energy using this method. The output energy can also be increased by placing the two amplifiers in series and close to each other. This method eliminates losses from any optical components, especially mirrors which are used in transporting the beam from one amplifier to the next. By having the amplifiers close to each other, less mirrors would be used and hence a lower energy loss. However, this task would have required a drastic change in the actual set-up. Therefore, using the present set-up, the laser beam was made to double pass through Amplifier 1 and then the energy of the double passed laser beam was measured. This arrangement was actually a 'simulation' of the proper double pass and gave an idea about its viability in giving a higher energy output. Figure (8.4.1.1) below shows a picture of the Amplifier 1 in which the double pass was done. It also shows the reflecting mirror which reflected the beam back into the amplifier.

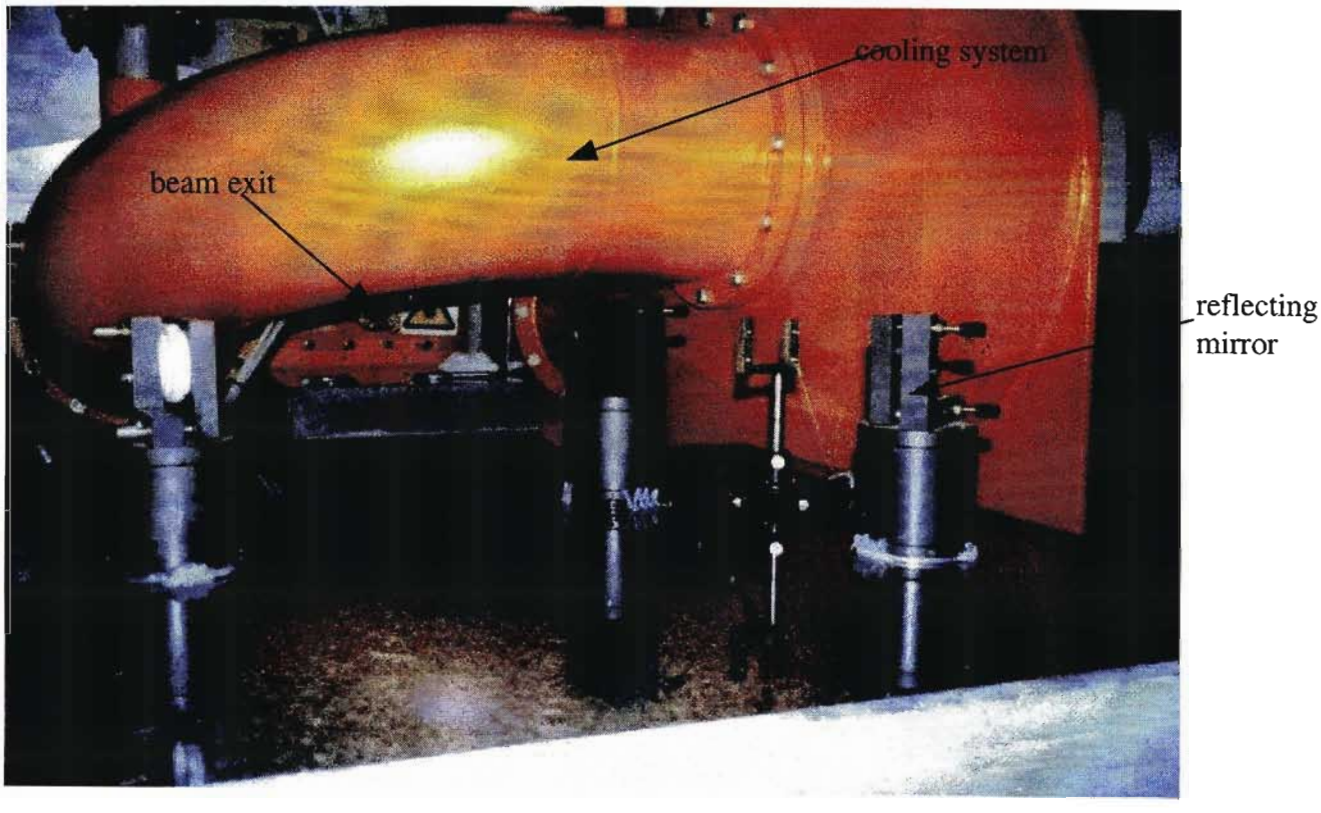

Figure (8.4.1.1): Picture showing Amplifier 1 for the double pass and the reflecting mirror.

The alignment for this experiment was quite tricky and time consuming. Again, the laser itself was used to aid the aligning. Figure (8.4.1.2) shows the schematic diagram of the set-up showing the path taken by the laser and as can be seen on it, mirrors A and B were used to deflect the beam by 90°. The beam was then made to pass through the optical axis of the Amplifier 1. An aperture mounted on its entry was used to guide the beam so that it coincided with the optical axis of the amplifier. The mirrors were fine adjusted until the beam was incident at the centre of aperture. A concave mirror of radius of curvature 20 m was placed at the exit of Amplifier 1 to reflect the beam back into the amplifier. Here, the best possible alignment was necessary, since it was very crucial that the reflected beam coincided with the optical axis of the amplifier.

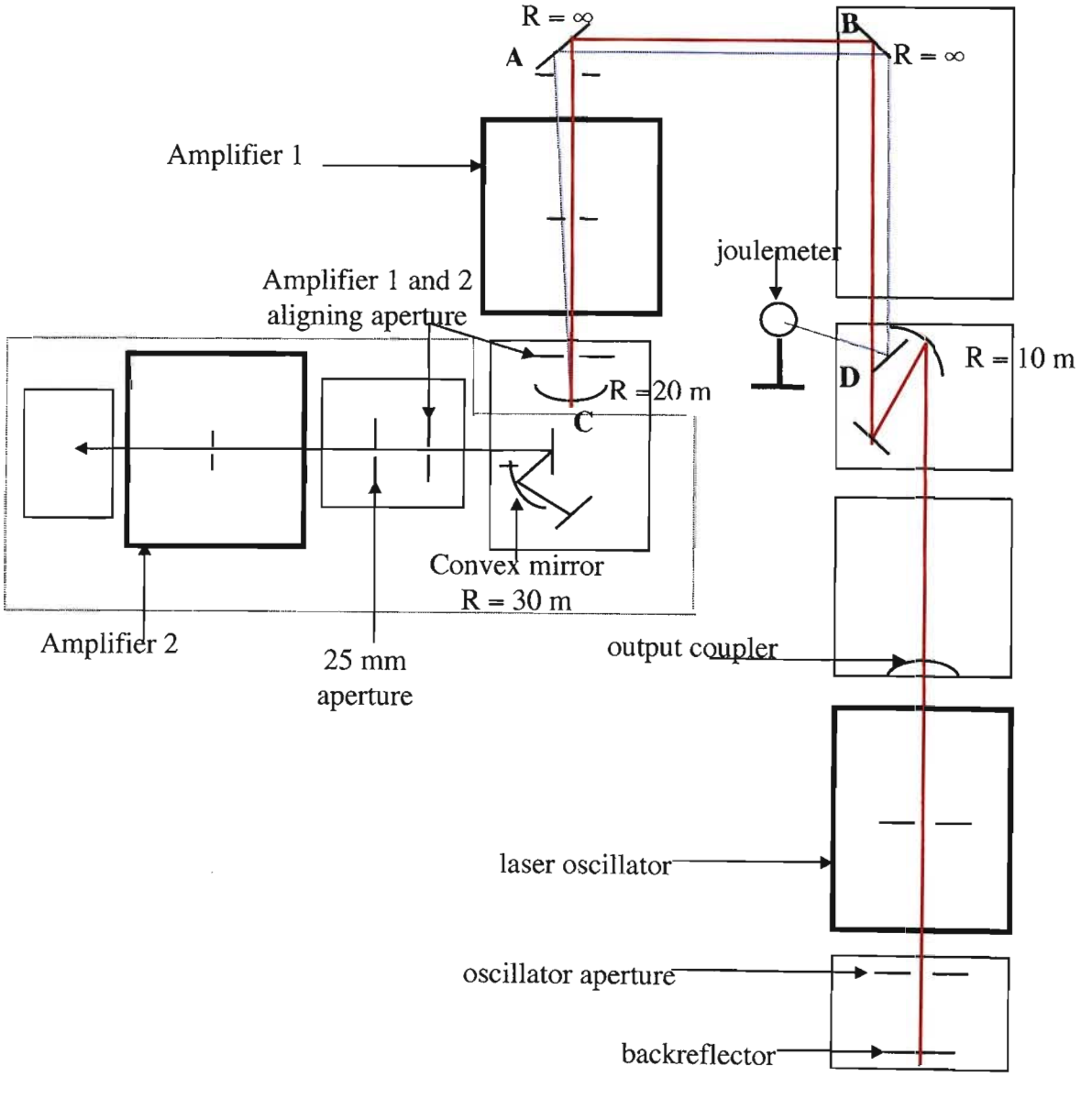

Figure (8.4.1.2): Schematic diagram showing the double pass through Amplifier 1.
[Note: The section enclosed in dark dotted lines was not used at that stage.]

It was also very important that the angle between the reflected and incident beam be optimum for a high gain and that the two beams do not coincide on the mirrors A and B. After reflection at mirror A and B, the beam hit the convex mirror which also acted as a focusing element. The beam was then reflected back to mirrors A and B which then guided the beam on the joule meter for energy measurements. The following table shows the laser energy values under different conditions.

Table (8.4.1.1): Table showing laser energy values at single and double pass.

Single pass

Energy/(mJ) (Oscillator only)	159.6
Energy/(mJ)(Oscillator and Amplifier)	550.0

Double pass

Energy/(mJ) (Oscillator only)	177
Energy/(mJ)(Oscillator and Amplifier)	614

The laser energy output as can be seen in the above tables is approximately 64 mJ more than that of the single pass which represents a 10 % increase. However, higher values than these were actually expected for the double pass. The low laser energy output could be due to laser not being properly aligned or to losses from the optical components. There would be losses if the laser did not pass closely on the optical axis of the amplifier during the double pass. The gas pressure inside the laser cavity could also have changed to a lower value. The gas mixture also is important since the required percentage of CO_2 is normally 34.4 %, N_2 is 24.15 % and He is 41.45 % at a temperature of 22 ° C. The distance or angle between the reflected and incident beam which should be as small as possible. However, to reduce the angle between these two beams was not an easy task since care had to be taken to avoid them coinciding. The smaller the angle between them, the lower the energy loss and the higher the gain.

The gas pressure in the laser cavity was measured as 92 kPa which was considered low and which could be one of the factors contributing to a low energy output. Therefore, the N_2 gas pressure was increased and the following table (8.4.1.2) shows the variation of energy output with nitrogen gas pressure and Figure (8.4.1.3) is a graph showing this tendency. The output energy was measured with the detector placed at the exit of the laser oscillator. Note that throughout the experiments the laser frequency was kept at 10 Hz.

Table (8.4.1.2): Table showing the variation of laser energy with N_2 gas pressure.

N_2 gas pressure/(kPa)	Energy/(mJ)
91.9	180.0
94.0	191.0
96.0	199.1
98.0	204.8
100.0	214.5

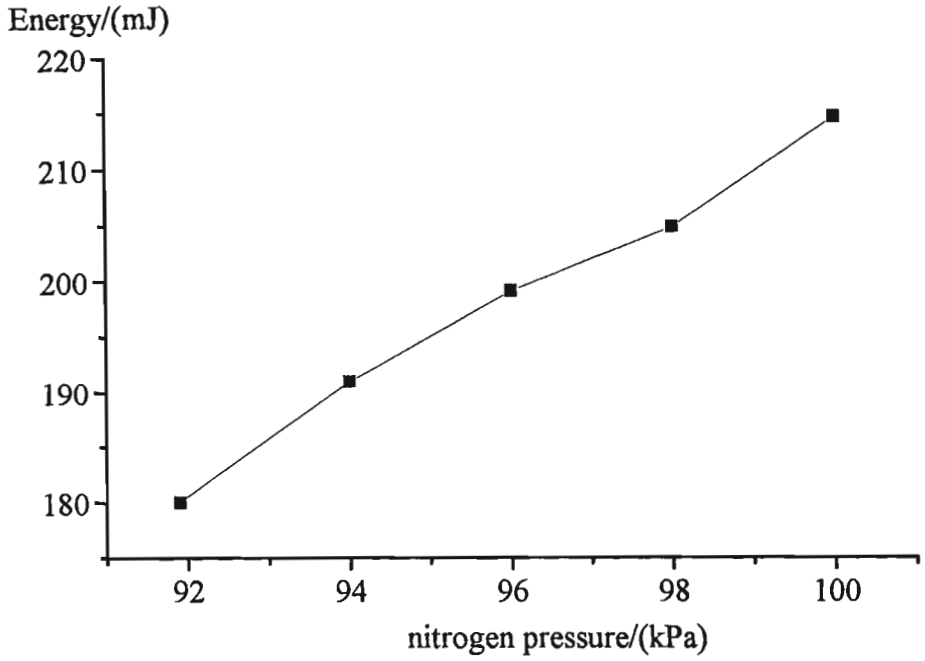

Figure (8.4.1.3): Graph showing the variation of laser energy with N_2 gas pressure.

The laser was then run with a N_2 gas pressure of 100 kPa and the beam was double passed through Amplifier 1 and the table below shows the results.

Table (8.4.1.3): Table showing the energy values at gas pressure of 100 kPa.

Energy/(mJ)(Oscillator only)	216.8
Energy/(mJ)(Oscillator + Amplifier)	687.0

Comparing the energy values of table (8.4.1.1) and table (8.4.1.2), there was an 18 % energy increase for the double pass. This shows an improvement in the energy output.

In other words, the output energy for a single pass was 550 mJ and for a double pass it was 687 mJ which represented an extra 137 mJ being extracted from this system.

As mentioned earlier, another way to increase the energy output was to reduce the angle between the reflected and incident beam. Before attempting to do this, the angle of separation between the two beams had be determined first. The distance from the double pass mirror C to mirror D (refer to Figure (8.4.1.2)) was approximately 8.06 m. The spot separation at mirror D, i.e after 8.06 m, was measured to be 11.1×10^{-3} m. The distance between the reflected and incident beams is given by

$$\theta = d/D$$

where: d is the separation distance between the reflected and incident beams

D is the distance from the double pass mirror C to mirror D

Thus,

$$\theta = (11.1 \times 10^{-3})/ 8.06 = 1.38 \times 10^{-3} \text{ radians}$$

By fine adjusting mirror B, the separation between the beams was reduced by a minute amount but this change had a remarkable effect on the output energy as we will see. Another change which was done in the actual set-up was to move the mirror C nearer to the window of the Amplifier 1. The laser was then run and the tables below show the results. The first table shows the energy values with a double pass but with no beam separation adjustment while the second one shows results with a reduced beam separation.

Table (8.4.1.4): Table showing energy outputs with unchanged beam separation.

Energy/(mJ)(Oscillator only)	203
Energy/(mJ)(Oscillator + Amplifier)	686

Table (8.4.1.5): Table showing energy outputs with reduced beam separation.

Energy/(mJ)(Oscillator only)	218
Energy/(mJ)(Oscillator + Amplifier)	736

There was therefore an extra 50 mJ extracted with a reduced beam separation. The maximum energy output which could be extracted from the double pass system was 736 mJ which is an extra 186 mJ. Therefore, there was a 25 % increase in the laser

Amplifier 1 was 550 mJ. At this point of the experiment, it was considered that this was the highest energy output that one could get from the double pass as most of the ways to increase the energy further had been attempted.

8.4. 2 Transporting the double passed beam through Amplifier 2

The second part of the double pass was to transport the beam to the second Amplifier 2 and then make energy measurements at its exit. Figure (8.4.2.1) shows the same set-up as before except that this time the beam after being reflected at mirror D reaches the concave mirror of 30 m radius curvature and finally is transmitted to the second amplifier after reflection with a plane mirror. In this experimental section, alignment was again the most difficult and time consuming. Before any energy measurement was made, the distance values were plugged in the laser software analysis to find out how the beam propagated through the actual system and especially to calculate the beam size at different sections of the laser chain. For this exercise, the distance between the optical components had to be known. In other words, for example the distance from the backreflector at the entry of the oscillator to the convex mirror, R = 10 m; the distance from the latter to the middle of Amplifier 1 had to be measured. These distance values together with the radius of curvature had to be known for the computer software program. Figure (8.4.2.2) is a schematic diagram showing the distance between the components.

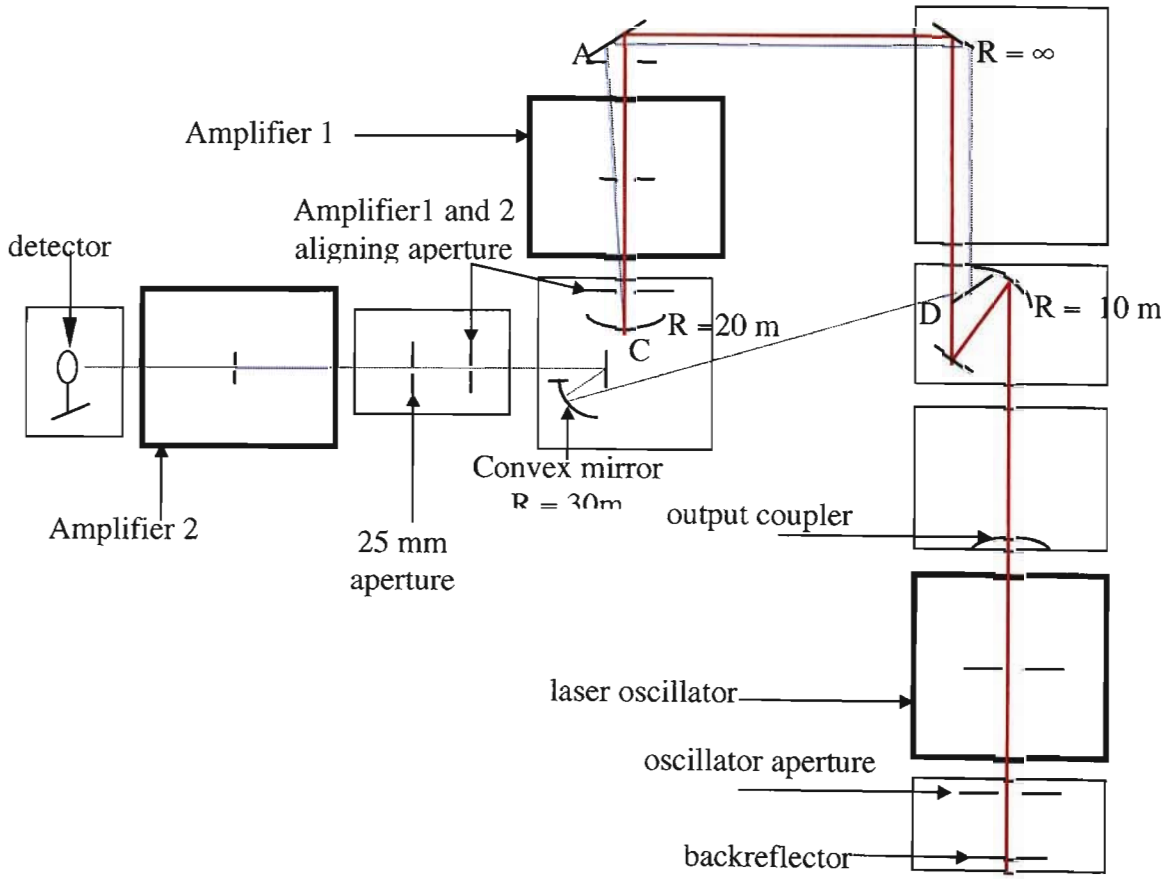

Figure (8.4.2.1): The laser set-up for the double pass through the amplifiers.

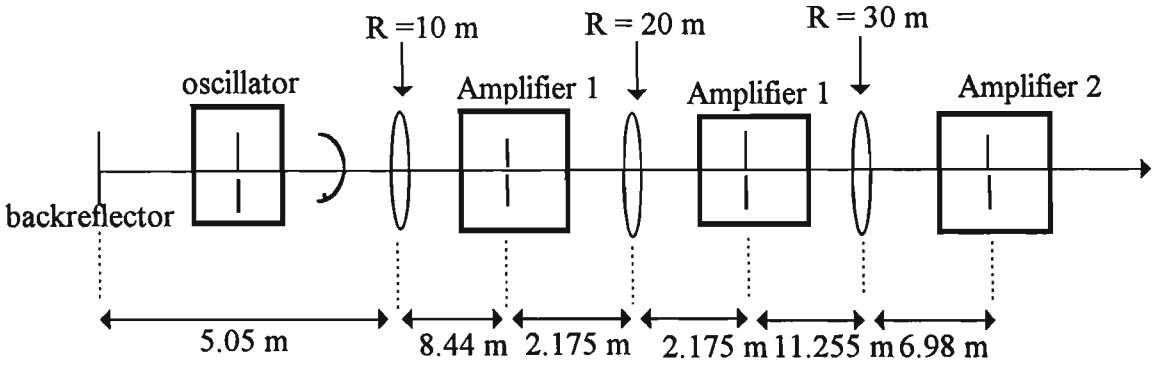

Figure (8.4.2.2): Schematic diagram showing the distances between components.

In the above diagram which is not to scale, there are two Amplifiers 1 drawn which signifies the double pass. This diagram is important since it gives a clearer picture of the beam propagation for the double pass. Figure (8.4.2.4) shows a picture of a plot of beam diameter against distance respectively taken from a computer screen.

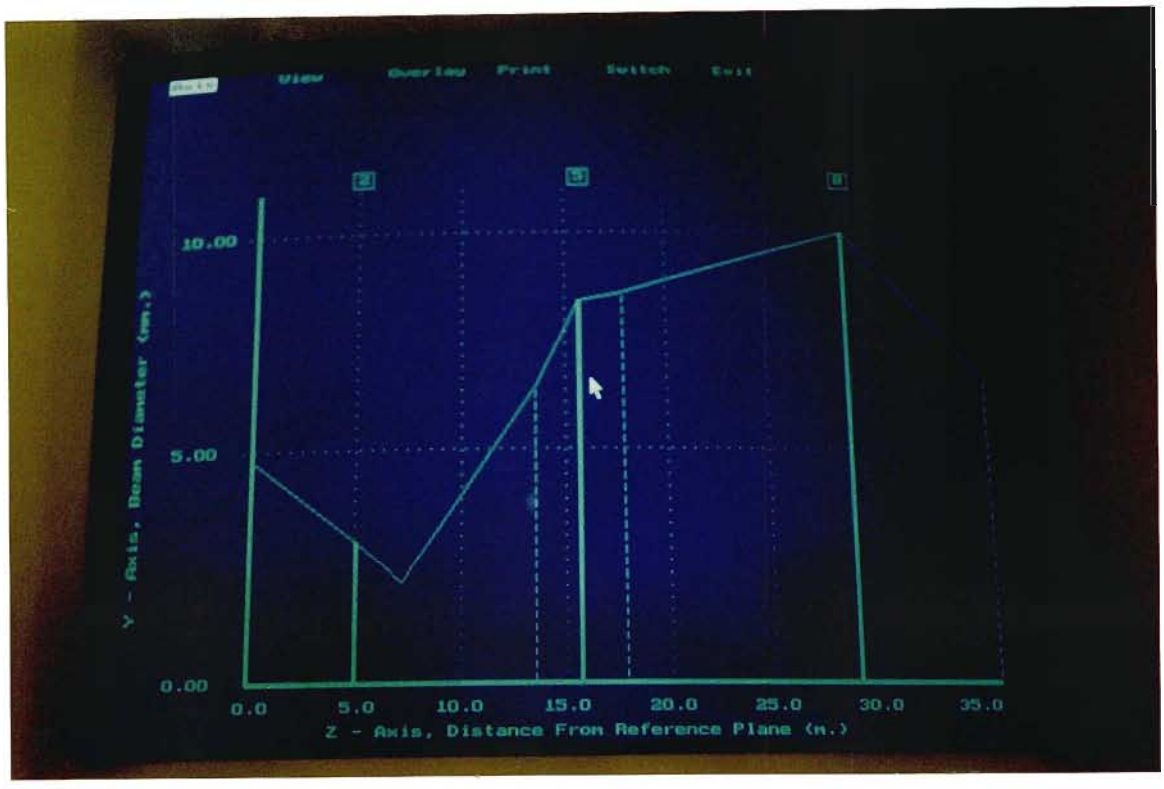

Figure (8.4.2.4): A graphical representation of the beam propagation.

The above graph shows the variation of the beam size with the propagation distance. From this graph, it is possible to know the beam waist at each of the components in the laser chain. For example, referring to the graph in Figure (8.4.2.4), the beam waist at the centre of the second Amplifier 2 is 6.7 mm which is a reasonable size. The graph allowed us to know how the beam is propagating and from this information, the optical component can be changed to see and predict how the beam will behave. As an

example, the concave mirror (R= 30 m) had to be changed to a 15 m radius of curvature in order to focus the beam better. This new value of radius of curvature gave a beam diameter of 6.7 mm at the centre of Amplifier 2.

8.5 Energy measurements along the laser chain

Since proper alignment of the beam was a very critical factor in getting the maximum output energy from the system, it was considered necessary to measure the energy at different points along the chain and then to adjust the alignment if required. Measurements such as the previous ones were also done to observe the effects on the energy outputs when Amplifier 1, Amplifier 2 and the double pass were on/off. Therefore, the following table shows the results of the energy outputs for several cases. As done previously, the energy at specific point was measured with varying aperture sizes and the aperture was placed infront of the joulemeter.

At a distance = 2.5 m before Amplifier 2 window and Amplifier 1 and 2 were switched off.

Table (8.5.1): Table showing the variation of energy/aperture size (distance=2.5m).

Aperture/(mm)	Energy/(mJ)
no aperture	200.7
5	40.8
6	58.1
7	75.5
8	94.3
9	113.4

The above values were plugged into the computer software program and the beam size at that point was found to be, $w = 7.19 \pm 0.17$ mm

At a distance = 0.4 m before Amplifier 2 window and Amplifier 1 and 2 were switched off.

Table (8.5.2): Table showing the variation of energy/aperture size(distance = 0.4m).

Aperture/(mm)	Energy/(mJ)
0	198.7
5	45.6
6	60.9
7	78.9
8	97.7
9	115.1

The calculated value of the waist size is 6.92 ± 0.07 mm. This means that the beam was focusing down at this point onwards and the beam diameter at the centre of the Amplifier 2 was less than this value. Comparing the energy outputs of table (8.5.1) and table (8.5.2), it is found that the energy outputs at a distance of 0.4 m from Amplifier 2 are slightly higher. This was due to the focusing down of the beam at that point. Figure (8.5.1) below shows a picture of the set-up for energy measurements after Amplifier 2.

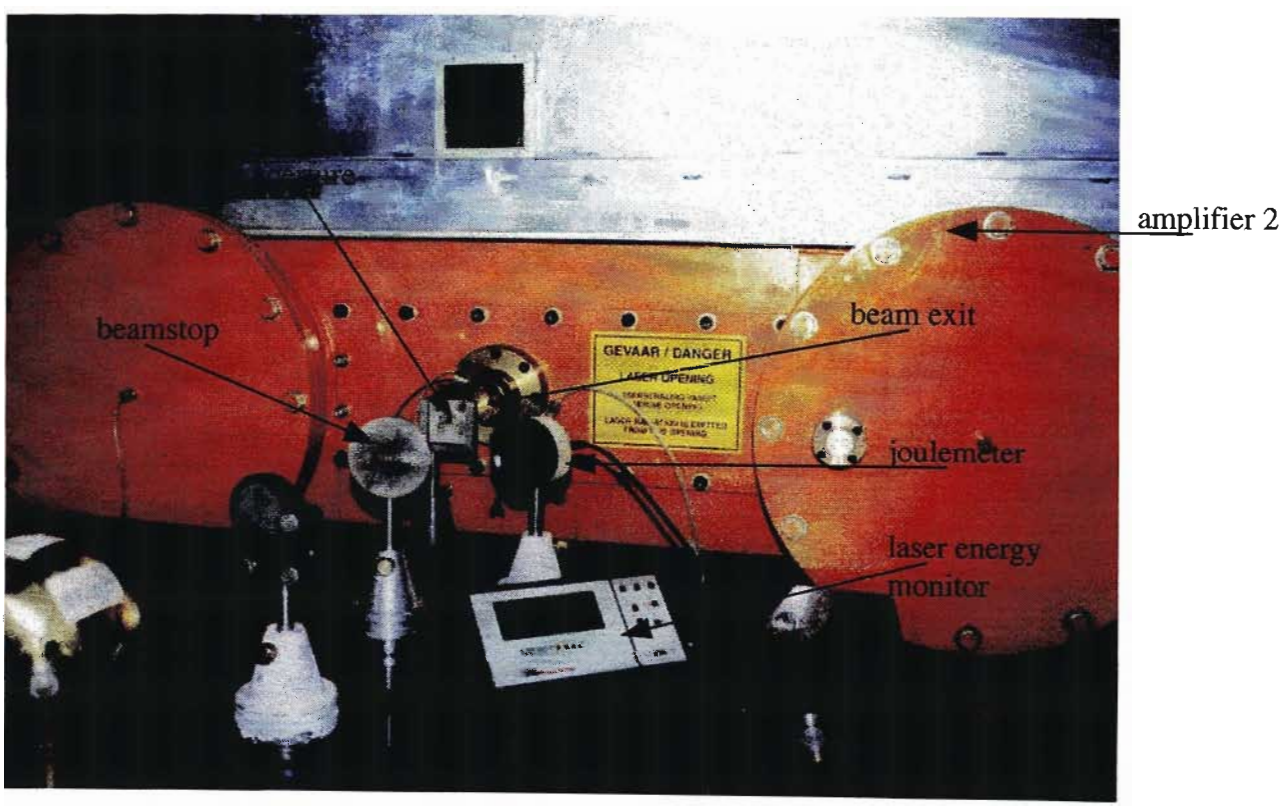

Figure (8.5.1): Picture showing the set-up for energy measurements.

The following table shows the laser energy outputs close to the exiting window of Amplifier 2 and under different conditions.

The following table shows the laser energy outputs close to the exiting window of Amplifier 2 and under different conditions.

Table (8.5.3): The variation of energy outputs under different conditions.

Conditions	Aperture/(mm)	Energy/(mJ)
Amplifier 1 and 2 off	no aperture	181.9
Amplifier 1 off and Amplifier 2 on	no aperture	498.0
Amplifier 1 and double pass on	no aperture	626.0
Amplifier1, Amplifier 2, double pass on	no aperture	1148.0

The energy output under the last condition when Amplifier 1, Amplifier 2 and the double pass were on was considered to be lower than expected and this was attributed to the diffractive losses in the optical components and the misalignment. In addition, a burn pattern was obtained on a piece of thermal paper and it was also found that the beam was not of good quality. In other words, it was not close to a gaussian beam profile. Figure (8.5.2) below shows the burn pattern. As can be seen, it was more in the TEM_{01} mode than in the TEM_{00} mode.

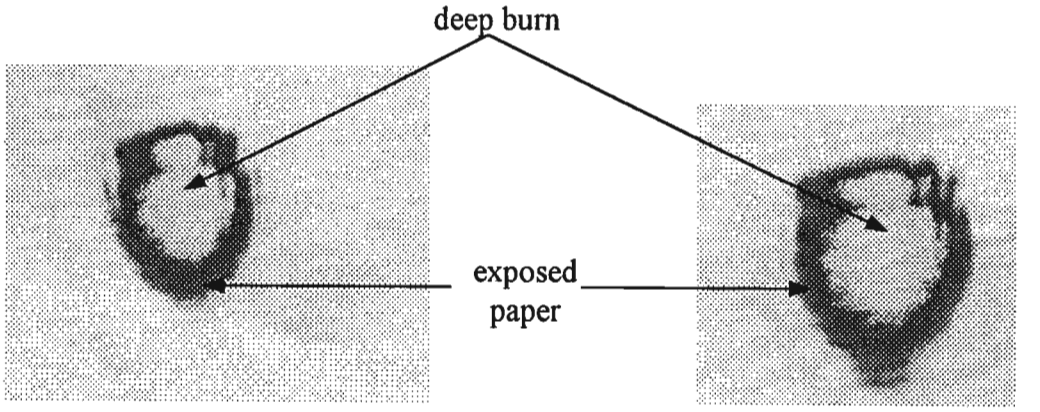

Figure (8.5.2): Picture showing the burn pattern of a poor quality beam.

At that stage of the experiment, it was suspected that the low energy output could be due to many factors which include misalignment, dirt, grease on mirrors, damaged or chipped windows. Therefore, before running the laser with the double pass again, a few fine adjustments had to be made. Firstly, the double pass mirror was fine tuned to move the reflected spot to the same horizontal level as the incident one. Great care and caution were taken not to interfere with other optical components which might disturb the alignment. The fine adjustment screw of the mirror was rotated through approximately 40°.

While inspecting the windows of the oscillator, it was found that the exiting window was chipped. There was a very minute crack approximately 2 mm from the centre of the window. This could be one of the main cause of a low energy output. The crack

could be caused when the laser was run at a very high repetition rates exceeding 300 Hz. The trivial steps were either to change the window or rotate the same window so that the beam did not pass through the damaged area. The latter would obviously be possible if the affected area was not right at the centre of the window as it was in our case. Before changing the window, the laser cavity had to be de-pressurised and the gases inside it had to be removed or recycled. Then, the window was removed, cleaned and placed back but rotated through 180°. The cavity was then filled with the appropriate gases until the pressure inside reached 98 kPa. The above operation did disturb the system as a result of which the alignment had to be checked and the necessary adjustments were made. Table (8.5.4) shows the energy results under different conditions.

Table (8.5.4): Table showing the energy outputs variation under different conditions.

Conditions	Energy/(mJ)
Amplifier 1 and Amplifier 2 off	185
Amplifier 2 on only	490
Amplifier 1 on only	624
Amplifier1, Amplifier 2, double pass on	1160

After several adjustments made in order to obtain a higher energy outputs, it was found as the above table shows that an extra energy of 12 mJ only could be obtained. As shown in the table above, the maximum energy output that could be extracted from the double pass through Amplifier 1 and then through Amplifier 2 was 1160 mJ. It was believed that there were many optical losses in the mirrors and windows. Therefore, the next experimental section deals with calculating the percentage loss from all the optical components.

8.6 Determining the percentage loss from optical components

All the mirrors were cleaned to make sure that they were free from dust and grease. Here again, great caution had to be taken not to disturb the alignment by moving any optical components of the set-up. Then, a transmission check was carried out by the author at different sections of the laser chain by measuring the energy output and calculating the percentage loss due the optics. The following table (8.6.1) shows the energy results after and before the Amplifiers 1 and 2 and the laser oscillator together with the percentage energy loss. Each one of these laser energy outputs represents the average of energy of 50 shots. For this particular experiment, both the amplifiers were switched off and only the laser oscillator was running at 10 Hz.

Table (8.6.1): Table showing the total percentage loss along the laser chain.

Location	Energy/(mJ)	Percentage Energy loss (%)
after Amplifier 2	39.0	-
before Amplifier 2	44.9	13.1
after Amplifier 1	46.1	2.6
before Amplifier 1	46.7	1.3
after Oscillator	57.2	18.4
	Total % loss	35.4

There was a 35.4 % loss along the laser chain and the highest energy loss (18.4 %) was from the section between the exit window of the oscillator and the entry window of the first Amplifier 1. A 35.4 % energy loss meant that we were losing approximately 410 mJ of energy which was quite a significant amount.

Table (8.6.2): Table showing the percentage energy losses of the optics.

Location	Energy/(mJ)	Percentage energy loss (%)
after Oscillator	59.7	-
after R = 10 m	52.8	11.6
after R = ∞	49.0	7.2
after R = ∞	49.3	0
after R = ∞	47.7	3.2
	Total energy loss	22

The quality of optics between the oscillator and Amplifier 1 was poor. As a result a more accurate transmission check was carried out along this section to determine the specific optical components of low optical quality. The table (8.6.2) above shows the laser energy outputs with the percentage energy losses after each optical component.

As one can see in the above table, the highest energy loss was 22 % was contributed by the optics in that particular section. The mirror R = 10 m had the lowest optical quality with a percentage loss of 11.6 % and the R = ∞ mirror with an energy loss of 7.2 %. Figure (8.6.1) shows a simplified version of the previous set up which gives a better idea on the location of the optical components with their respective percentage energy losses.

Figure (8.6.2): Picture showing the damaged windows of the laser cavity. (The non circular lighter central region is the damaged area in the ZnSe).

8.7 The Three Element Beam Analyser

The three element detector is a device which measures the laser beam width, beam position and energy. It was developed by Wouter Klopper in 1996 at the AEC. It relies on the simultaneous measurement of the energy contained in three sections of the beam. This technique has a number of advantages compared to the existing techniques such as scanning slit, knife edge and variable aperture devices. Some of these advantages include single shot measurement, ability to measure shot to shot variation in total energy, beam radius and beam position simultaneously, three signals of comparable magnitude and high damage threshold. In addition, it is relatively insensitive to beam centring. The main disadvantage is that the method assumes a near Gaussian profile and is therefore not suitable for analysing the actual intensity distribution in a beam. The device uses the error function to deduce the beam radius. The beam is split into three sections and the energy contained in each is simultaneously measured. The middle section is a slit of known width. It is then possible to calculate the percentage of the pulse energy contained in the two sections on either sides of the slit. Using the standard normal distribution one can determine how many standard deviations of the normal distribution is contained in the middle section and from this beam radius and centre of the beam can be known. (Refer to appendix B)

The diagram below illustrates the theory of the Three Element Beam Analyser.

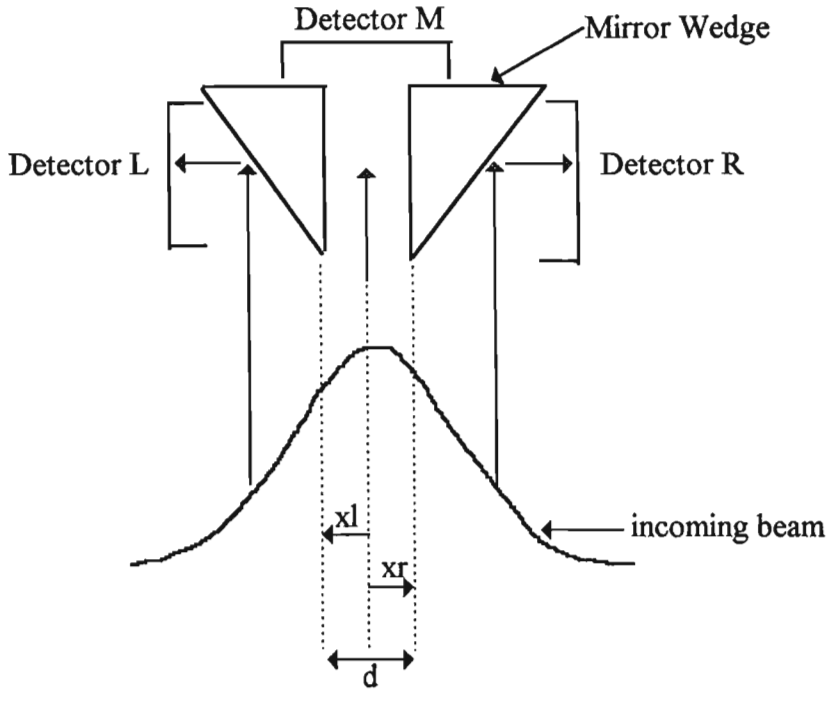

Figure (8.7.1): Diagram showing the components of the Three Element Analyser.

This device was used by the author at the AEC to characterise the existing TEA CO_2 lasers. A compact signal processing unit was developed to directly display energy, radius and position of the incoming laser beam. Integrated spheres with pyroelectric detectors were chosen instead of Joule meters, since the spheres are not easily damaged by high intensity, can tolerate high average power, is relatively insensitive to alignment and have a very large dynamic range. At high repetition rates and average power, the spheres can be cooled and the pyroelectric detectors replaced with power meters.

Figure (8.7.2) shows the schematic of the three element detector.

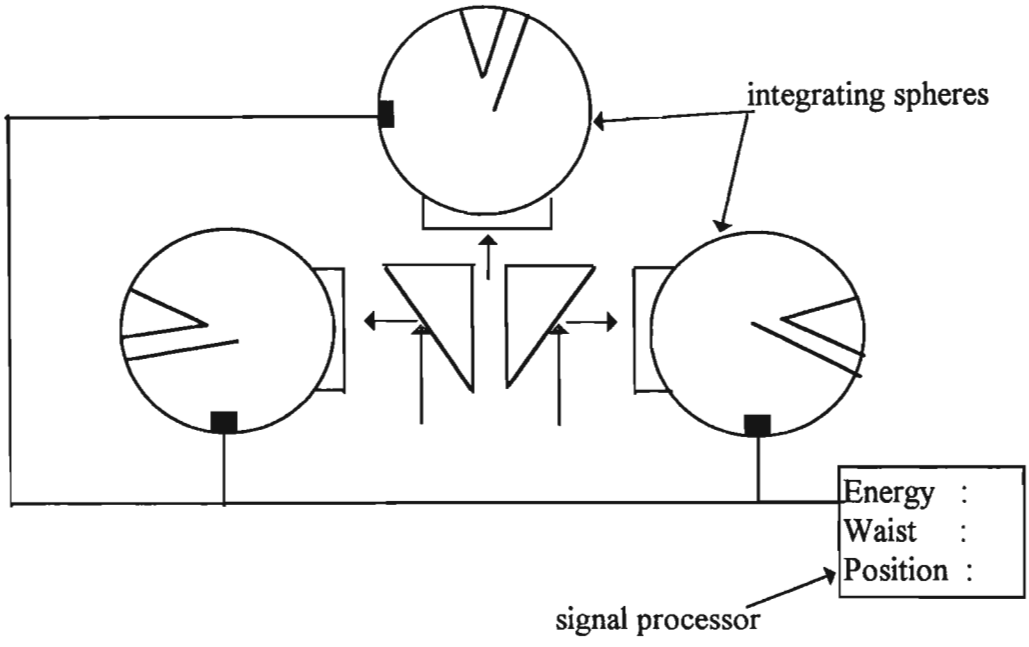

Figure (8.7.2): Schematic diagram of the Three Element Detector.

Some measurements were done with this device to obtain some beam diagnostics. The device was placed at the exit of the second amplifier A 2. Figure (8.7.3) shows a picture of the Three Element detector and table (8.7.1) shows the table of data obtained when the laser was running at 10 Hz. As shown in the picture there is a processing unit connected to the device and which can also be connected to a laptop or PC. The software to handle the data and graphics were designed by one of the member of the group there. $\mathbf{E_c}$ is the energy from the central part of the beam, $\mathbf{E_l}$ is the energy from the left part, $\mathbf{E_r}$ is from the right part and $\mathbf{E_t}$ is the total energy of the beam. The data shown below and in table (8.7.1) were obtained from the monitor of the device and they could be saved on the PC. They could then be run on Excel to obtain graphical illustrations of the data.

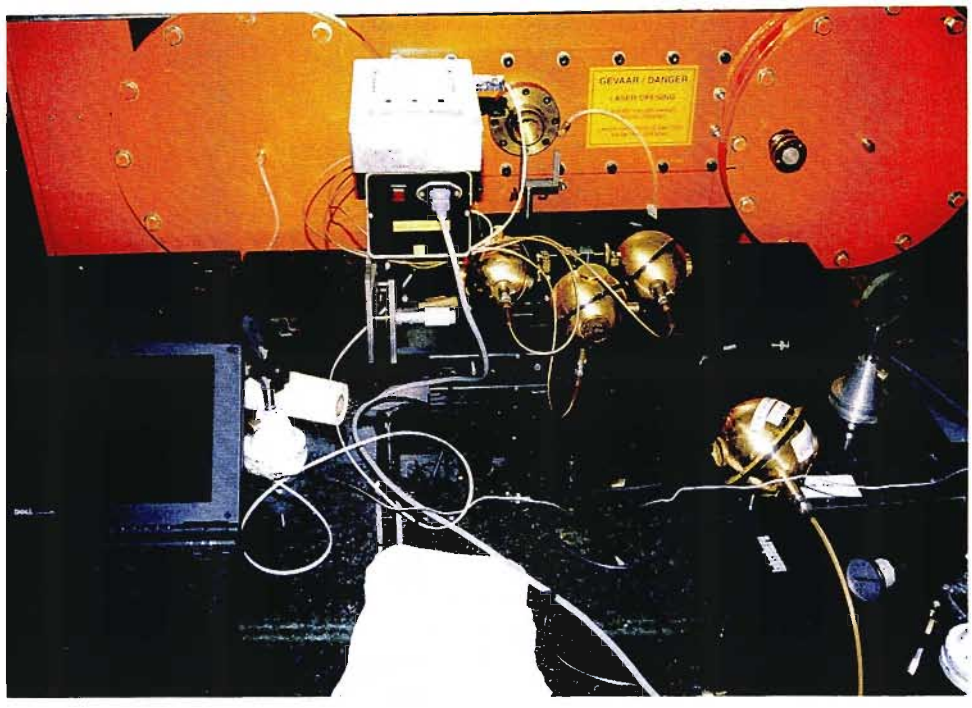

Figure (8.7.3): Picture showing the Three Element Detector.

The beam diagnostics results were:

The number of laser pulses = 800

E_c average = 156.6 mJ
E_l average = 143.5 mJ
Er average = 125.2 mJ
E_t average = 425.2 mJ E_t deviation = 347.5 mJ

Waist average = 6.33 mm Waist dev. = 1.62 mm
Position average = -0.11 mm Position dev. = 0.65 mm
(Note: The position is relative to the central axis of the beam.)

Table (8.7.1) shows only the results for 10 consecutive shots but the above energy results are for 800 shots. The laser at that stage was set at 10 Hz. However, one of the main reasons to use this device for energy measurements and beam diagnostics was to be able to run the laser at very high repetition rates in the order of 100 Hz.

No. of shots	E_c/(mJ)	E_i/(mJ)	E_r/(mJ)	E_t/(mJ)	Waist/(mm)	Position/(mm)
1	77	70.1	66.4	213.5	6.39	-0.07
2	75.2	67.6	65.7	208.5	6.38	-0.03
3	75.4	70.1	65.2	210.7	6.43	-0.1
4	74.5	69.1	64.8	208.4	6.43	-0.09
5	78.4	72.1	68.4	218.9	6.43	-0.07
6	78.9	71.4	66.5	218.7	6.37	-0.06
7	76.6	68.1	67.1	216.8	6.31	-0.1
8	77.5	69.9	68.1	211.8	6.35	-0.02
9	72.4	68.4	62.7	215.5	6.41	-0.03
10	78.9	71.4	69.5	203.5	6.45	-0.12

Table (8.7.1): Table showing the beam diagnostics for 10 consecutive shots.

Graphs of the energy, waist and displacement versus number of shots for 800 laser shots were plotted and are shown in Figures (8.7.4) to (8.7.6) respectively. In the figure below, for the sake of simplicity, the following abbreviations are used for the oscillator and amplifiers:

O-1: oscillator
A3-1: Amplifier 1
A3-2: Amplifier 2

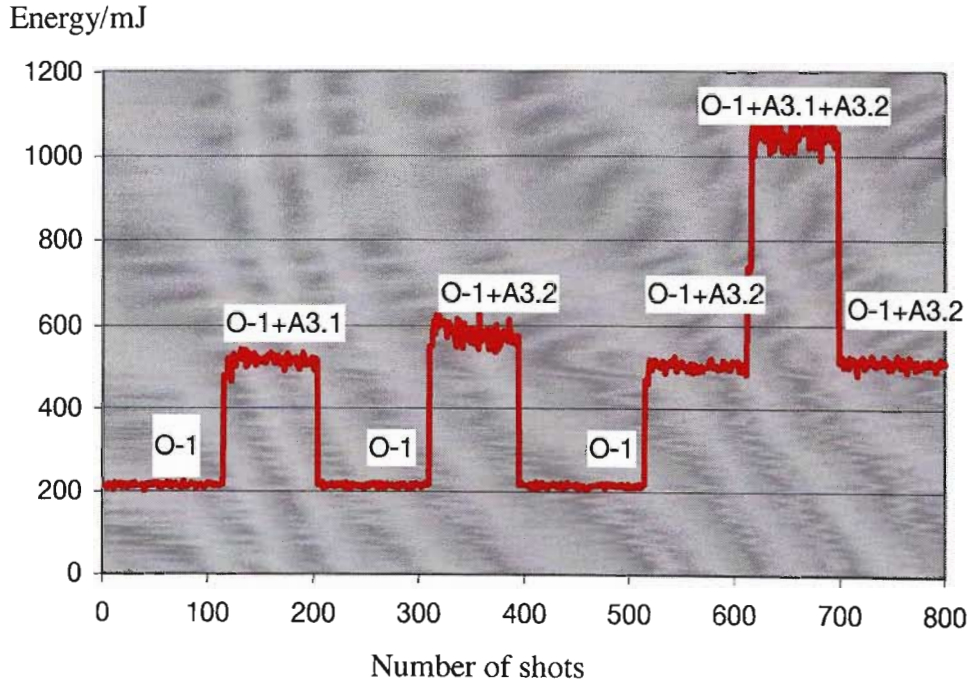

Figure (8.7.4): Variation of energy with no. of shots.

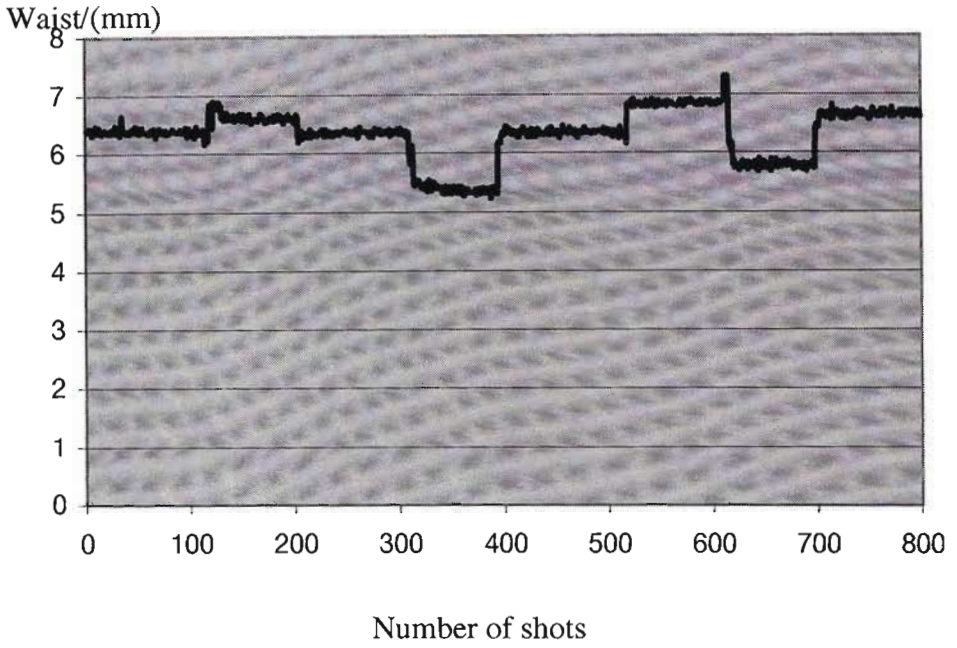

Figure (8.7.5): Variation of waist size with no. of shots

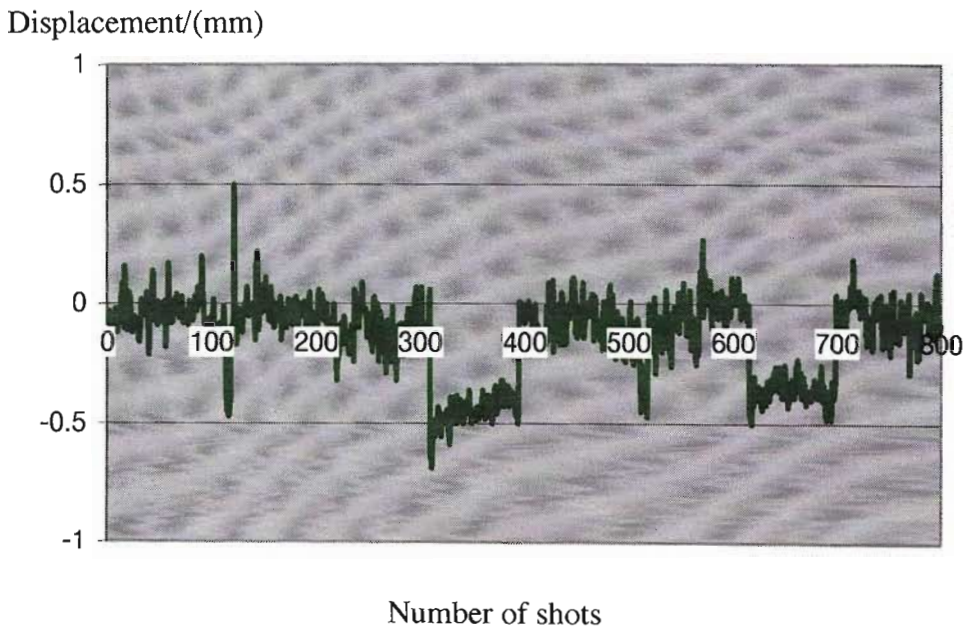

Figure (8.7.6): Variation of displacement with no. of shots

8.7.1 Discussion

From the above data, it was evident that the Three Element Detector provided a more qualitative analysis on the beam diagnostics of the CO_2 laser beams. From the values in table (8.7.1), it was found that the energy of the central section of the beam was the highest compared with the energy from the left or right section. This shows that the beam profile was very close to a gaussian one. The graph in Figure (8.7.1) shows that the maximum energy achieved was at approximately 1160 J and this occurred when the oscillator and both amplifiers were on. Referring to graph in Figure (8.7.5), we find that the beam waist remained relatively constant throughout the laser chain. However, as seen in the graph, there is a dip between the 300th and 400th shot and this occurred when the oscillator and amplifier A3.2 were on. This obviously implies that the beam was focusing down at that point. The same behaviour is observed between the 600th and 700th shot when the oscillator and both amplifiers were on. This occurrence would consequently have an effect on the displacement of the beam with respect to the origin which is the central axis of the beam and therefore shown in Figure (8.7.6). Therefore, by analysing the behaviour of the beam along the chain and between shots, it is possible to make the necessary adjustments to produce a higher energy beam with a close to gaussian profile.

Moreover, preliminary characterisation of the high power laser beams with the Three Element detector indicated good sensitivity, repeatability and ability to measure over a wide range of energies and lateral displacement. The Three Element detector is therefore able to provide a portable rapid means of determining beam radius, energy and relative position of laser beams. In addition, with such device, effects like thermal focusing and beam drift instability of high repetition rate lasers can be studied. In the future, the Three Element cw laser beams detectors could also be developed.

8.8 Conclusion

Carbon dioxide lasers have numerous industrial applications. The successful utilisation of these medium energy, high repetition rate TEA CO_2 largely depends on their beam quality. A near gaussian profile laser beam is required for most industrial applications. Moreover, high energy laser beams of the order of 1 to 10 J are necessary for various applications. Therefore, this chapter involves the investigation and analysis of the beam propagation of CO_2 laser beams.

From the experimental investigation, it was found the focus of the beam occurred at about 1.5 m from the exit window of the oscillator and the beam waist at that point was 3.06 mm. Referring to table (8.3.8) and the graph in Figure (8.3.4), it was noted that the beam focused and then from that point onwards, it became diverging. The beam waist at a distance of 10 m from the exit window of the oscillator was found to be 17.99 mm. An M^2 value of 1.54 was calculated while theoretically a value of 1 indicates a gaussian profile. However, a value of approximately 1.54 is good. The burn patterns further support the fact that the beam was close to a gaussian profile since a burn pattern at 4m after the focus gave a trace in almost a TEM_{00} mode.

In addition, several optimisation techniques such as improving the alignment, reducing diffractive losses and transmission loss, passing the beam through amplifiers and double passing were attempted successfully. Throughout the experiments, it was found that the energy output of the laser was greatly affected by misalignment. A greater energy output could be extracted from the best possible aligned laser system. The optical energy loss in this laser system was investigated and found to be approximately 38 % which represents a significant energy loss. High energy output could be achieved if energy losses from the separate optical components could be brought to a minimum. The double pass through the Amplifier 1 and then through the second Amplifier 2 gave a significant energy output. A maximum energy of 1160 mJ could be extracted from this laser system. If the optical energy loss of the system was reduced to the lowest value possible, a maximum energy of 1600 mJ could be extracted.

Finally, the Three Element detector provided accurate beam diagnostics of the CO_2 laser beam. The results obtained from this device were in agreement with that obtained from the joulemeter. Referring to the graphs and data where the results for the 800 laser shots were plotted, it was found that the highest energy output occurs at the 689th shot at an energy of 1100.7 mJ $\pm$ 347 mJ (the total energy deviation is $\pm$ 347 mJ). Hence, this device improved the beam diagnostics and thereby also the quality and the energy output of the carbon dioxide laser beam.

CHAPTER NINE

9.0 GENERAL CONCLUSION

This thesis has explored the various ways of improving the performance of pulsed molecular nitrogen lasers. The modified parabolic shape of the top plate of the laser showed a distinct improvement in beam quality and energy output. Several parameters such as the distance between the top and bottom plates, the area of the parabola, the flow speed of nitrogen gas and the electrode separation were varied to observe their effects on the laser energy output. A maximum energy output of 0.3 mJ per pulse was achieved with the laser with largest dimensions at an electrode separation of 2.5 mm. Nitrogen lasers made of aluminium foil are also promising. A multilayer nitrogen laser constructed with aluminium foil and mylar gave an average energy of 30 μJ per pulse. Future work could apply the multilayer scheme to the large laser and use cold nitrogen vapour as the lasing medium which should lead to much higher laser energy output. The provision of several layers on both plates of the laser could increase the energy further, possibly > 1 mJ.

The nitrogen lasers which were constructed and investigated in this thesis are affordable and suitable in the South-African context. As these devices can be built using cheap materials, they offer an appropriate direction for laser research in the developing South-Africa. Lasers made of aluminium foil could be used for educational purposes especially in schools to stimulate the students' interests in laser technology. Lasers could even be operated by college students since they are inexpensive. An affordable power supply to charge these lasers could be constructed from cheap materials which include a car ignition coil. Transparencies could be used as the dielectric for the laser depending on the power supply used. Mylar could be used for voltages > 15 kV.

One major application of nitrogen lasers is the pumping of dye lasers. Simple, compact and inexpensive nitrogen lasers could make dye lasers more affordable. They can be constructed to a relatively small size and have a sealed-off laser tube that operates for a long lifetime. They can be combined with a compact dye laser system that includes a diffraction grating providing pulsed tunable laser output over the entire visible spectrum. In addition, like any other UV sources, N_2 lasers can be used to study fluorescence effects. Their short pulses make them valuable for time resolved measurements and for Raman Scattering observation. Nitrogen lasers can also measure particle size by light scattering. The high peak power of a focused beam allows the use of N_2 laser pulses in cell biology and microcutting. They can also cut thin films for making and correcting semiconductor wafers and ablate tiny samples. They can also be used for spark gap triggering and ultra-high speed photography.

Carbon dioxide lasers have numerous industrial applications. The Laser Group at the South African Atomic Energy Corporation, Pretoria are investigating the possible applications of their TEA CO_2 lasers which were once used in the MLIS (Molecular Laser Isotope Separation) programme. An investigation of the beam propagation and beam quality was carried out by the author as a gaussian beam profile is important for

certain applications. Some of the short term applications which are being investigated are paint removal, de-rusting and surface cleaning. Paint ablation by lasers is the result of simultaneous thermal, photochemical, and photomechanical phenomena. With the short pulses of TEA CO_2 lasers, these processes take place very quickly which leads to minimal thermal loading on the substrates. The 2 kW average power TEA CO_2 laser from Urenco is currently being used in a joint project between SLCR and Lufthansa to investigate aircraft paint stripping. The laser delivers 7 to 9 J pulses and is capable of a repetition rate up to 300 Hz. The Urenco laser is also being used to investigate the removal of anti-corrosive coatings from the ends of brake lines before attachment. Layers of oxides need to be removed from a variety of metal surfaces. Chromium oxide has been successfully removed from stainless steel by laser ablation. The cleaning of synthetic rubber injection moulds, e.g, in tyre manufacturing is being investigated. Here, the long wavelength of the CO_2 laser is advantageous because it is strongly reflected by the metal mould. For an application such as this the AEC lasers would need to be made smaller and capable of being moved to the tool. The other medium to long term industrial applications of the existing CO_2 lasers which are being investigated are thin film deposition, nuclear decontamination, carbon isotope separation, welding and cutting of special materials.

Gas laser technology offers many exciting possibilities in industry. The South African laser community is presently endeavouring to set up a national laser facility. The present work would not have been possible without the type of co-operation envisaged for the facility. It is also hoped that it helped to keep laser research alive at the University of Natal.

APPENDIX A

Before the various parabolic lasers could be constructed, the parabolas had to be traced on graph papers together with the precise location of the focus and also with the right inclination angle of the laser channel. It would have been very tedious and time consuming to find the equations of the parabolas, their coordinates and the location of the focus. Therefore, the following is a computer software programme for calculating the coordinates, focus of the parabola with the right laser channel inclination angle. Moreover, it gives a graphical representation of the parabola. By entering parameters such as the size of the laser, the vertex of the parabola and the inclination angle, a parabola is drawn. A print out copy of the coordinates of the parabola and that of the focus are obtained. With these information, a parabola together with the precise location of the focus is drawn on graph paper.

This programme is called Tool Command Language/Tool Kit, abbreviated as TCL/TK. It is a programming system for developing and using graphical user interface(GUI) applications. The software was available from the net but the language and commands had to be learnt before the programme could be written.

```
#!/usr/bin/wish


set parc 0
set perm 4
global angle
global angled
global punti

proc par {} {
   global para parb parc
   global paraout parbout
   global xf xfout yf yfout
   global shadow
   global angle
   global xv xvout

   set dist 1.5

   set angler [expr $angle*3.1415/180.0]

   set yv [.vertex.yv get]

   set x3 [expr [.discharge.lenght get]*cos($angler)]
   set y3 [expr [.discharge.lenght get]*sin($angler)]

   set parb [expr 2.0*($yv+sqrt(($yv*$yv)-$yv*$y3))/$x3]
   set para [expr -1.0*($parb*$parb)/(4*$yv)]
```

```
    set xv [expr -1.0*$parb/(2*$para)]


 #  Calculates the focus of the parabola

    set xf $xv
    set ymin [expr $para*($xf*$xf)+$parb*$xf]
    set yf [expr $ymin+1.0/(4*$para)]

 #  Calculates the shadow at the focus

    set line1a [expr $yf/$xf]
    set line1b 0

    set line2a [expr ($yf-$y3)/($xf-$x3)]
    set line2b [expr $yf-$line2a*$xf]

    set alpha [expr atan($line1a)]
    set xs1 [expr $xf-$dist*(cos($alpha))]

    set alpha [expr atan(-1.0*$line2a)]
    set xs2 [expr $xf+$dist*(cos($alpha))]

    set shadow [expr ($xs2-$xs1)/$x3]

    set paraout [format "%2.3f" $para]
    set parbout [format "%2.3f" $parb]
    set xfout [format "%2.2f" $xf]
    set yfout [format "%2.2f" $yf]
    set xvout [format "%2.2f" $xv]
    set shadow [format "%1.3f" $shadow]

    laser

    return
 }

 proc angle { } {
    global angle
    global angled
    global perm
    set angle [expr asin(1.0/sqrt($perm))*(180.0/3.141592)]
    set angled [format "%3.2f" $angle]
 }

 proc write { } {
    global para parb
    global xf yf
```

```
    global angle

    set angler [expr $angle*3.1415/180.0]
    set x3 [expr [.discharge.lenght get]*cos($angler)]
    set y3 [expr $para*($x3*$x3)+$parb*$x3]

    set f [open /aju/progs/tcl/aju1.txt w]

    puts $f a=$para
    puts $f b=$parb
    puts $f xf=$xf
    puts $f yf=$yf

    for {set x 0} {$x<=$x3} {set x [expr $x+.5]} {
        set y [expr $para*($x*$x)+$parb*$x]
        puts $f $x,$y
    }
    puts $f $x3,$y3

    close $f
}

proc laser { } {
    global para parb
    global angle
    global punti
    global conversion
    global xf yf
    .draw.laser delete all
    drawcoordinates
    set punti 0
    unset punti

    set angler [expr $angle*3.1415/180.0]
    set x3 [expr [.discharge.lenght get]*cos($angler)]


    set xold .1
    set yold 20

    for {set x 0} {$x<=$x3} {set x [expr $x+.1]} {
        set yd [expr 20-$conversion*($para*($x*$x)+$parb*$x)]
        set xd [expr 0.1+$x*$conversion]
        .draw.laser create line ${xold}c ${yold}c ${xd}c ${yd}c
        set xold $xd
        set yold $yd
    }
    .draw.laser create line ${xd}c 20c ${xd}c ${yd}c
    .draw.laser create line .1c 20c ${xd}c ${yd}c
```

```
    set c1x [expr .1+($xf-1)*$conversion]
    set c1y [expr 20-($yf-1)*$conversion]
    set c2x [expr .1+($xf+1)*$conversion]
    set c2y [expr 20-($yf+1)*$conversion]

    .draw.laser create oval ${c1x}c ${c1y}c ${c2x}c ${c2y}c

}

proc drawcoordinates {} {
    global angle
    global conversion
    global xf yf
    set angler [expr $angle*3.1415/180.0]

    set x3 [expr [.discharge.length get]*cos($angler)]

    set xscale [expr $x3+5]

    set conversion [expr 15.0/int($xscale)]

    .draw.laser create line 0.1c 20c 15.1c 20c -width 2
   .draw.laser create line 0.1c 0c 0.1c 20c -width 2

    for {set x 0} {$x<=[expr int($xscale)]} {incr x} {
        set xd [expr .1+$x*$conversion]

        set test [expr int($x/10)-$x/10]

#       if {$test=0} {
#
   set up 19.8}
#
        .draw.laser create line ${xd}c 20c ${xd}c 19.9c
        }

    set yl [expr 20/$conversion]

    for {set y 0} {$y<=$yl} {incr y} {
        set yd [expr 20-$y*$conversion]
        .draw.laser create line 0.1c ${yd}c .2c ${yd}c
    }
}
set draw .draw


toplevel .$draw
```

```
wm title . "Parameters"
wm geometry . 400x400
wm resizable . 0 0

wm title $draw "Nitrogen Laser"
wm geometry $draw 550x650
wm resizable $draw 0 0

canvas .draw.laser -width 16c -height 21c
pack .draw.laser -pady 5 -padx 5


button .exit -text Exit -relief sunken -command exit
pack .exit -pady 10 -side bottom

button .write -text Write -relief sunken -command write
pack .write -pady 10 -side bottom

set yv 40

frame .vertex
pack .vertex -side top -pady 10

label .vertex.lab -text Vertex
label .vertex.lx -width 5 -text "Xv cm" -justify right
label .vertex.ly -width 5 -text "Yv cm" -justify left
label .vertex.xv -width 5 -textvariable xvout -relief sunken
entry .vertex.yv -width 5 -textvariable yv

bind .vertex.yv <Return> par

place .vertex -x 0 -y 0 -bordermode outside
grid .vertex.lab -row 0
grid .vertex.lx -row 1 -column 0
grid .vertex.ly -row 1 -column 1
grid .vertex.xv -row 2 -column 0
grid .vertex.yv -row 2 -column 1

set lenght 35.0

frame .discharge
pack .discharge -side top -pady 10

label .discharge.lab -text Discharge
label .discharge.lenl -width 5 -text Lenght -justify right
label .discharge.perml -width 5 -text Perm. -justify left
entry .discharge.lenght -width 5 -textvariable lenght
entry .discharge.perm -width 5 -textvariable perm
```

```
label .discharge.anglel -width 5 -text Angle -justify right
label .discharge.angle -width 5 -textvariable angled -justify left -relief sunken

bind .discharge.lenght <Return> par
bind .discharge.perm <Return> angle
bind .discharge.perm <Return> +par


place .discharge -x 100 -y 0 -bordermode outside
grid .discharge.lab -row 0
grid .discharge.lenl -row 1 -column 0
grid .discharge.perml -row 1 -column 1
grid .discharge.anglel -row 1 -column 2
grid .discharge.lenght -row 2 -column 0
grid .discharge.perm -row 2 -column 1
grid .discharge.angle -row 2 -column 2


set voltage 20

frame .volt
pack .volt -side top -pady 10
label .volt.voltl -text "Voltage kV"
entry .volt.voltage -widt 5 -textvariable voltage

place .volt -x 270 -y 20
grid .volt.voltl -row 5
grid .volt.voltage -row 6

label .results -text results:
place .results -y 100


frame .parabola
pack .parabola -side top -pady 10

label .parabola.lab -text Parabola
label .parabola.focus -text Focus
label .parabola.shadowl -text Shadow
label .parabola.al -width 5 -text a
label .parabola.bl -width 5 -text b
label .parabola.cl -width 5 -text c
label .parabola.xfl -width 5 -text xf
label .parabola.yfl -width 5 -text yf
label .parabola.a -width 5 -textvariable paraout
label .parabola.b -width 5 -textvariable parbout
label .parabola.c -width 5 -textvariable parc
label .parabola.xf -width 5 -textvariable xfout
label .parabola.yf -width 5 -textvariable yfout
```

```
label .parabola.shadow -width 5 -textvariable shadow

place .parabola -y 125
grid .parabola.lab -row 0 -column 0
grid .parabola.focus -row 0 -column 3
grid .parabola.al -row 1 -column 0
grid .parabola.bl -row 1 -column 1
grid .parabola.cl -row 1 -column 2
grid .parabola.xfl -row 1 -column 3
grid .parabola.yfl -row 1 -column 4
grid .parabola.shadowl -row 1 -column 5
grid .parabola.a -row 2 -column 0
grid .parabola.b -row 2 -column 1
grid .parabola.c -row 2 -column 2
grid .parabola.xf -row 2 -column 3
grid .parabola.yf -row 2 -column 4
grid .parabola.shadow -row 2 -column 5

angle
par
laser
```

APPENDIX B

The Three Element Detector

The following describes the mathematical technique used in calculating the middle(M), left(L) and right(R) sections of the laser beam (Wouter Klopper, 1996). First, the total energy contained in the beam is determined by summing the reading of the three detectors,

$$T = L + M + R$$

and then the percentage energy in each wing is calculated,

$$P_l = L/T$$

$$P_r = R/T$$

These percentages may be regarded as areas in the wings of a standard normal curve. We know that the total area under the standard normal curve is one and up to an arbitrary point x, the area is given by the error function(see Figure A.1).

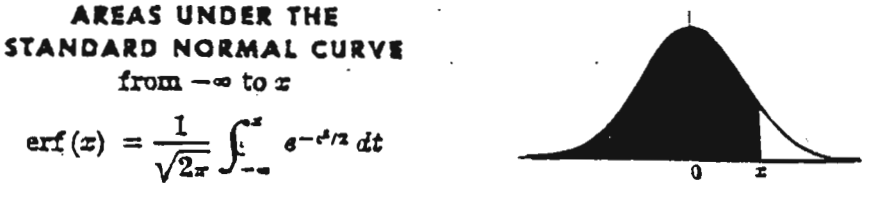

Figure (A.1): Area under Standard Normal curve.

with $x = (z - \mu) / \sigma$

Here x is the standard score, the number of standard deviations, σ, that a given point z in a Gaussian distribution is removed from its mean μ.

The measured percentages of P_l and P_r are in fact values of the complementary error function

erfc(x) = 1 - erf(x).

Knowing *erfc(x),* the unshaded area in Figure (A.1), the value of x may be obtained from tables or by numerical integration. Hence, having $P_l = erfc(x)$ and $P_r = erfc(x_r)$ for each wing, standard scores x_l and x_r may be found as indicated in Figure(A.1). The physical meaning of these values is this:

The edge of the left wedge is x_l standard deviations to the left of the centre of the beam and the edge of the right wedge is x_r standard deviations to the right of the centre of the beam. The distance between the wedges, *d,* is therefore equal to $(x_l + x_r)$ standard deviations of the Gaussian. It follows that the standard deviation(in distance units) is given by

$$\sigma = d/(x_l + x_r)$$

and it can be easily shown that the beam radius, the distance from the beam centre where the intensity falls to $1/e^2$ of its peak value, is simply

$$w = 2\sigma$$

The peak position can be specified relative to the edge of the left wedge as

$$y = x_l \sigma$$

This technique of determining the beam radius and centre position should be fairly insensitive to the alignment of the device relative to the actual beam centre, as long as the intensity distribution approximates a Gaussian closely enough. Should the beam centre fall on either of the wedges and not in the centre section, either P_l or P_r will be greater than 0.5. The only modification necessary in the above analysis is that the standard score, x_l or x_r, corresponding to the wedge on which the beam falls, should be made negative. This situation is easily catered for in computer code.

REFERENCES

Akins R.P. and Lin S.C, *Time behaviour of second positive emissions from a fast-discharge N_2 lasers*, *Applied Physics Letters*, **28**, 221-223(1976).

Ali A.W. *et al., Theory of pulsed molecular nitrogen laser*, Applied Optics, **6**, 2115-2119(1976).

Ali A.W., *A study of nitrogen pulsed power density and some design considerations*, Applied Optics, **8**, 993-9969(1969).

Armandillo A.J., *High power nitrogen laser*, Applied Physics Letters, **41**, 7(1982).

Basting D. *et al., A simple high power nitrogen laser*, Opto-electronics, **4**, 43-49(1972).

Beesley, M.J., *Lasers and their applications*, Taylor and Francis Ltd(1976).

Bergmann Ernest.E., *UV TEA laser with 760-Torr N_2*, Applied Physics Letters, 28, 84-85(1976).

Bergmann Ernest.E., *Coherent uv from a TEA N_2 laser system*, Applied Physics Letters, 31, 661-662(1977).

Bergmann H.M.Von, *Sealed-off, miniature high power N_2 lasers*, Journal of Physics, Sci. Inst., **10**, 1210-1212(1977).

Bergmann H.M.Von *et al., Gain, Fluorescence, energy extraction characteristics of photostabilized atmospheric pressure uv nitrogen lasers*, J. of Physics **D**: Applied Physics, 2341-2351(1978).

Bergmann H.M.Von and Penderis A.J, *Miniaturised atmospheric pressure nitrogen laser*, J. of Physics(1977).

Bergmann *et al., Effective glow discharge excitation of nitrogen lasers at gas pressures ranging from 0 to 5 bar*, Applied Physics Letters, **28**,17-18(1975).

Bergmann H.M. Von *et al., Travelling-wave corona excitation of high-power uv nitrogen lasers operating at gas pressures ranging from 0 to 3 bar*, J. of Applied Physics, **47**, 4532-4534(1976).

Bergmann H.M.Von *et al., Pulsed corona excitation of high- power uv nitrogen lasers at pressures of 0-3 bar*, Applied Physics Letters, 27,553-554(1975).

Bergmann H.M.Von, Nel J.B *et al., Applications for High Repetition Rate TEA CO_2 and Excimer Lasers*, Cogema/AEC Joint Venture(1998).

Bergmann H.M.Von, *Photo-preionization Stabilized High pressure glow discharge lasers,* Thesis 1980.

Bertolloti M., *Masers and Lasers, An Historical Approach*, Adam Hilger Ltd, Bristol(1983).

Bhagwandin N., *Laser diagnostics of plasmas and flames*, Master's Thesis(1983).

Bor Z., *Amplified spontaneous emission from N_2 laser pumped dye lasers*, Optics Communication(1981).

Cosmelli M. and Asselberg T., *Simple fast-discharge device for exciting a high power pulsed nitrogen laser*, http://www.geocities.com/Research Triangle/facility/2502.(1998).

Chalmers I.D., *The transient glow discharge in N_2 and dry air*, J. of Physics, **D**, **4**, 1147-1151(1971).

Chalmers I.D *et al.*, *The mechanism of spark breakdown in N_2, O_2 and Sulphur*, Proc.R. Society, London, **A329**, 171-191(1972).

Colin W.S. and Litynski D.M., *Power increase of N_2 uv and ir lasers by addition of SF_6*, Applied Physics Letters, **Vol. 26**, 188-120(1975).

Cosmelli M. and Asselbergs T., *Simple fast-discharge device for exciting a high power pulsed nitrogen laser*, Review of Laser Technology, **V2**(1998).

Cubeddu R. and Curry S.M., *A simple high power pulsed N_2 laser*, IEEE, J. of Quantum Electronics, **QE-9**, 499-500(1973).

Csele M., *Homebuilt Lasers*, Http://technology.niagarac.on.ca/people/mcsele/lasers.htm

Daniel T.N and Harris F.M., *The spatial growth of ionisation currents in N_2 at voltages up to 500kV*, J. of Physics B: Atomic Molecular Physics, 3, 363-368(1970).

Duarte F.J and Hillman L.W, *Dye Laser Principles*, Academic NY Press(1990).

Dunford H., *Elements of Diatomic Molecular Spectra*, Addison-Wesley, Massa

Eastham D., *Atomic Physics of Lasers*, Taylor and Francis(1986).

Eisberg R. and Resnick R., Quantum Physics of atoms, molecules, solids, nuclei and particles, New York Press(1974).

Fletcher R.C., *Impulse breakdown in the 10^{-9} sec. range of air at atmospheric pressure*, Physical Review, **76**, 1501-1511(1949).

Frantz L.M and Nidvik.J.S., *Theory of pulse propagation in laser amplifier*, J. of Applied Physics, 34, 2346-2349(1963).

Frungel F.B.A., *High speed pulse technology*, Academic Press NY, VII(1965).

Godard B., *A simple high-power large efficiency N_2 Ultraviolet Laser*, IEEE Journal of Quantum Electronics, **10**,147-153(1974).

Geller M *et al.*, *Some considerations in the design of a high power, pulsed N_2 laser*, Applied Optics, 7, 2232-2237(1968).

Gerry E.T., *Pulsed molecular nitrogen laser theory*, Applied Physics Letters,7, 6-8(1965).

Hecht E., *Optics*, 2nd Edition, Addison-Wesley Publishing Co.(1987).

Herden W., *Compact high power subnanosecond nitrogen and open air laser at 760 torr,* Physics Letters, 54A, 96-98(1975).

Herden W. and Bloss W.H., *N_2 laser(I bar) induced micro metal plasma capable of igniting combustible mixtures*, Applied Physics Letters, **31**, 66-67(1977).

Itani J.K. and Kimura Y., *Intense laser emission at 357.7 nm using N_2- SF_6 mixture*, Applied Physics Letters, **27**, 503-504(1975).

Jenkins A.F and White E.H, *Fundamentals of Optics*, 4th edition, Mc Graw-Hill Book Co.(1985).

Kline L.E and Denes L.J, *Investigations of glow discharge formation with volume preionization*, Journal of Applied Physics, **46**,1567-1563(1975).

Laser Science, Inc, *The Nitrogen Laser-Pumped Dye Laser*, http://itl.chem.ufl.edu/4411L_f96/i2_trf/dye_laser.html, 1-3(1999).

Maillard R. and Millet A., *Geometrie, Class de Mathematiques*, Classiques Hachette(1945).

Milonni W.P and Eberly H.J, *Lasers*, Wiley and sons, Inc(1988).

Moeller G. and Rigden J.D, *High power laser action in CO_2-He mixtures*, Applied Physics Letters, **Vol. 7,** 274(1965).

Myer J.A *et al.*, *Dye stimulation with a pulsed N_2 laser line at 3371A*, Applied Physics Letters, **Vol 16**, 3(1970).

Patel C.K.N., *Continuous-Wave Laser action on vibrational rotational transitions of CO_2*, Physics Review, **Vol. 136 A**, 1187(1964).

Patel C.K.N., *Continuous-wave high power N_2 and CO_2 laser*, Applied Physics Letters, **Vol.7**, 15(1974).

Polanyi J.C., *Proposal for an infrared maser dependent on vibrational excitation*, Journal of Chemistry and Physics, **Vol. 34**, 347(1961).

Sakai.Y. *et al.*, *High-speed camera investigation of CO_2 TEA laser discharges*, Applied Physics Letters, **31**,796-797(1977).

Siegman A.E, *Lasers*, University Science Books(1986).

Silfvast T.W, *Laser fundamentals*, Cambridge University Press(1996).

Svelto Orazio, *Principle of Lasers*, Plenum Press NY(1982).

Tary R., *Pulsed nitrogen laser at high repetition rate*, IEEE Journal of Quantum Electronics, **QE-8**, 726(1972).

Wadhwa C.L., *High Voltage Engineering*, Wiley Eastern Ltd(1994).

Wilson J., *Nitrogen laser action in a supersonic flow*, Applied Physics Letters, 8, 159-161(1966).

Willet C.E and Litynski D.M, *Power increase of N_2 UV and IR lasers by addition of SF_6*, Apllied Physics Letters,26, 118-120(1975).

Webb C.E., *The fundamental discharge physics of atomic gas lasers, High power gas lasers*, Institute of Physics conference series, 29(1976).

White H.E, *Introduction to atomic spectra*, 1st edition, Mc Graw-Hill Book Co.(1934).

Whitehouse D.R., *Understanding CO_2 lasers, Laser Advanced Development Center,* http://www.laserk.com/whiteCO.htm, 1-9(1999).

Woodward B.W *et al.*, *A reliable, repetitive pulsed, high power nitrogen laser*, Rev. Sci. Instrum., **44**, 882-887(1973).